ProQuest LLC.
789 East Eisenhower Parkway
P.O. Box 1346
Ann Arbor, MI 48106 – 1346

THE GENERATION OF THERMAL STRESS AND STRAIN DURING QUENCHING

by

A. B. SOOMRO

A THESIS SUBMITTED TO THE
COUNCIL FOR NATIONAL ACADEMIC
AWARDS IN PARTIAL FULFILMENT
FOR THE DEGREE OF
DOCTOR OF PHILOSOPHY

COLLABORATING ESTABLISHMENT:-

Tube Investments Limited,
Hinxton Hall
Hinxton,
Cambridge
England.

SPONSORING ESTABLISHMENT:-

Department of Metals and
Materials Engineering,
Sheffield City Polytechnic,
Sheffield
England.

March 1986.

PREFACE

All the work reported in this thesis was carried out at the Sheffield City Polytechnic during the period for which the candidate was registered for a higher degree.

The candidate has not, during the period of registration for the CNAA degree of PhD, been a registered candidate for any other CNAA award or for any university degree.

The results presented in the thesis are, as far as is known, original except where reference has been made to previous work.

In accordance with the regulations for the PhD in Industrial Metallurgy, the relevant part of the M.Sc in Metallurgical process and Management was successfully completed. The candidate's performance during this course was assessed by means of written examinations and continuous assessment of specific assignments. The details of the course are given below:-

MODULE - I

1. Process Metallurgy.
2. Mechanical Metallurgy.
3. Applied Thermodynamics.

MODULE - II

1. Accountancy.
2. Economic Analysis and Financial Control.
3. Numerical Methods and Programming.
4. Operational Research.

MODULE - III

1. Corrosion Resistant and High Temperature Metals and Alloys.
2. Stainless Steels.
3. Powder Metallurgy.
4. Heat Treatment and Transformations.
5. Automatic and Computer-Aided Control of Metallurgical Operations.
6. Quality Assurance.

MODULE - IV

Three Industrial Case Studies.

One of the Case Studies, which is related to the current research work, is presented with this thesis, as Appendix III.

Beside this, International Symposium on the Calculation of Internal Stresses in the Heat Treatment of Metallic Materials (Linkoping, Sweden 1984) and The First National Conference on Production Research (Nottingham, England 1985), were attended.

In addition, seven research papers have been written and to date five have been accepted for publication. The details of these papers is as under:-

1. "The Effect of Martempering on Thermal Stress and Strain". By F. Abbasi, A.J. Fletcher and A.B. Soomro. Proceedings of the First National Conference on Production Research, The University of Nottingham, September 1985. To be Published.

2. "The Effect of Stress Relaxation Rate on the Generation of Thermal Stress and Strain". By A.J. Fletcher and A.B. Soomro. To be published in "Materials Science and Engineering", Elseviern, Oxford.

3. "The Effect of Transformation Temperature Range on the Generation of Thermal Stress and Strain". By A.J. Fletcher and A.B. Soomro. To be published in "Materials Science and Technology" , London.

4. "The Effect of Plate Thickness on the Generation of Thermal Stress and Strain in Quenched Steel of High Hardenability". By A.J. Fletcher and A.B. Soomro. To be published in "Steel Research" (Achiv für das Eisenhüttervessen), Dusseldorf.

5. "Aspects of the Generation of Stress and Strain in Quenched Steel Plates". By F.S. Allen, A.J. Fletcher and A.B. Soomro. To be presented at "International Conference on Residual Stresses", October 1986, Garmish-Partenkirehen.

ACKNOWLEDGEMENTS

Praise be to God the Almighty

I would like to pay my deepest gratitude to Dr. A.J. Fletcher, for his inspirational guidance and excellent supervision and encouragement throughout the duration of the work. Thanks are also due to Dr. R.F. Price of T.I. Laboratories, Hinxton Hall, for his continuous support and advice during the course of my study.

Grateful appreiciation is also expressed to the other teaching and non-teaching staff of the Department of Metals and Materials Engineering, for their co-operation and help. Department of Mechanical and Production Engineering is especially acknowledged for the use of metrology facilities.

I would also like to express my sincere thanks to Dr. A.W.D. Hills, Head of Department of Metals and Materials Engineering, for providing the opportunity to undertake the work and the provision of facilities for the work.

I gratefully acknowledge the C.O.T. award of Government of Pakistan and the permission of my employers, Mehran University of Engineering and Technology, Sind, Pakistan, without which it would not have been possible to carry out this work.

Mrs. April Dawson is also to be thanked for her patience and excellent typing.

Finally, the support, encouragement and shear endurance of my wife and family deserve greater acknowledgement than words can express.

THE GENERATION OF THERMAL STRESS AND STRAIN DURING QUENCHING

A. B. Soomro

ABSTRACT

A visco-elastic-plastic mathematical model was used to calculate the thermal stress and strain generated during the quenching of an infinite plate of high hardenability steel (835M30) in water, oil and Polymer. In the present work the mathematical model was modified to include the effect of initial stress on the rate of stress relaxation, which has been found to be significant. The data required to incorporate this effect into the calculations, were obtained experimentally during the present investigation. The effect of an applied stress during transformation (transformation plasticity) was also introduced in the mathematical model. The new model produced a marked improvement in the degree of agreement between the calculated and experimental residual stress, although the corresponding level of agreement in the case of residual strain was less good. In particular, strains after water quenching agreed less well with experiment as a consequence of the change in the model, although this drawback was not found after oil and polymer quenching. The new mathematical model was used to investigate the effect of martempering, section size and transformation temperature range on the generation of thermal stress and strain. A salt bath treatment above the Ms temperature followed by air cooling prevented residual stress development, but an oil quench after the salt bath treatment generated a level of residual stress at the end of cooling that was similar to that obtained after a direct oil quench from 850^{o}C. Neither martempering process was successful in reducing residual strain. With an increase in section size a reduction in the residual stress and an increase in the distortions was obtained after a water quench. However, after oil quenching the overall effect of section size on residual stress and strain was small. The effect of variation in the transformation temperature range was found to be small in the case of residual stress but an increase in Ms temperature produced a significant increase in the level of residual strain.

NOMENCLATURE

A), B) = Parameters used in the standard linear solid equation.

A' = Constant used in equation 2.6.2.1.

C_N = Distance between the reference axis and position N on the plate at inclination.

ΔC_N = Correction factor for levelling at position N during through thickness measurement.

E = Young's modulus, MPa.

F = Yield function.

$F_{X,Y,Z}$ = body forces

FEM = Finite Element Method.

G = Shear modulus, MPa.

I), J) = Coordinates, used to define stress and strain components.

L = Length, mm.

N = Position number at which through thickness is obtained.

T_h = Thickness of plate in hardened condition, mm.

T_N = Thickness of plate at position N, mm.

T_s = Thickness of plate in softened condition, mm.

V_h = Volume in hardening condition, mm^3)

V_s = Volume in softened condition, mm^3) used in equation 4.4.4

$V\alpha$ = Volume fraction of martensite.

$V\gamma$ = Volume fraction of austenite.

$\%\Delta V$ = Percent volume change associated with the structure change from ferrite and carbide to martensite.

W = Strain hardening coefficient $(\frac{d\sigma_f}{d\varepsilon_p})$, MPa.

Y_h = Length of plate in hardened condition, mm.

Y_s = Length of plate in softened condition, mm.

$\%\Delta Y$ = Percent change in length.

a)
b) = Constants relating linear variation of E and ν with temperature, according to $E/(1-\nu) = a-b\theta$

e_{IJ} = Strain tensor.

h = Surface heat transfer coefficient, $Wm^{-2o}C$.

i = Node position subscript.

j = Number of elements in half thickness of plate.

m = Subscript used for mean stress or strain.

n = Node time subscript.

p)
q) = Thickness of plate at position 1 and 11 (figures 98 and 99).

S_{IJ} = Deviatoric stress tensor.

t = Time, s.

Δt = Time interval, s.

t^{n+1} = Total time elapsed in the n+1 interval.

αex = Coefficient of linear thermal expansion, $^{o}C^{-1}$.

αtd = Thermal diffusivity, m^2s^{-1}.

δ_{IJ} = Kronecker's delta.

ε = Strain.

$\dot{\varepsilon}$ = Strain rate, S^{-1}.

ε_{creep} = Creep Strain.

εe = Elastic Strain.

εp = Plastic strain.

ε_T = Total strain.

εtp = Transformation plasticity strain.

$\varepsilon_{thermal}$ = Strain due to thermal expansion and contraction only.

εve = Viscous strain.

εxx)
εyy)
εzz) = Strain in x, y and z direction.

η = Coefficient of viscosity of the mechanical model, MPa.s.

θ = Temperature, ^{o}C.

θA = Quenchant temperature, ^{o}C.

θo = Initial temperature of the plate before quenching, ^{o}C.

θs = Surface temperature of the plate.

λ = Thermal conductivity, $Wm^{-1}\ ^{o}C$.

ν = Poisson's ratio.

ℓ = Density, kg m^{-3}.

σ = Stress, MPa.

$\bar{\sigma}$ = Average stress level in half thickness of the plate, MPa.

σe = Equivalent stress, MPa.

σf = Flow stress with uniaxial stress system, MPa.

σ^{o} = Initial stress, MPa.

σ_t = Current stress, MPa.

$(\sigma)_r$ = Stress when edges of plate are restrained, MPa.

$\dot{\sigma}R$ = Rate of stress relaxation, MPa S^{-1}.

$(\Delta\sigma)$Rel: = Amount of stress relaxation in time Δt, MPa.

$\sigma xx)$
$\sigma yy)$ = Stress in x, y and z directions.
$\sigma zz)$

ϕ = Material parameter.

CONTENTS

1. INTRODUCTION

Thermal stress and strain induced during heat treatment is a substantial problem in the manufacturing of engineering components, particularly where the use of quenching operations is necessary to achieve optimum properties in a component. Generation of thermal stress as high as the flow stress of the material during quenching causes plastic flow of the material, which is retained in the component at the end of the treatment. The thermal stress and strain during the quenching may result in cracks during hardening or within a short period afterwards and may cause changes in dimensions above the allowable tolerances. Distortion and stress retained in the component make it difficult to achieve the critical dimensions of the component by machining and in some cases may result in the rejection of the component.

The traditional approach to the assessment and rectification of these problems has been an empirical one, based on previous experience and experimental trials. Unfortunately, such assessments are tedious, time consuming, costly and rarely yield completely satisfactory results. The unreliability of the empirical approach may be attributed to the large number of variables involved in the quenching process which contribute to the final stress distribution. Experimental determination of residual stress and strain is laborious and expensive; such costs can only be tolerated where large production runs are involved. These problems have led to increasing interest in an alternative approach which has led to the formation of theoretical models for the prediction of thermal stress and strain.

The use of realistic models has become possible with the arrival of high speed digital computers, which allow the possibility of extremely complex calculations. Simultaneously, progressively more detailed

investigations of the physical and mechanical properties required in these calculations have allowed a steady improvement in the accuracy of the results obtained.

The work described in this thesis is part of a long-term investigation whose object is the understanding and control of distortion and thermal stress in commercial steel components. The present calculation involves a visco-elastic-plastic model, which has been applied to an infinite plate of 835M30 steel. This has allowed the use of the simplifications associated with plane-stress conditions. Most of the physical and mechanical properties used have been obtained in earlier investigations, but the present work has included the determination of the effect of initial stress and prior deformation on stress relaxation rates, over the range of temperature involved in the quench. The basic mathematical model was also derived in an earlier investigation, but has been improved by the introduction of the data referred to above, as well as by an improvement to the equations used to represent the effect of applied stress on transformation strain (transformation plasticity).

The infinite plate used in the calculation produces a simple plane-stress system and so avoids the complications associated with more complex geometries. At the present time the level of agreement between calculation and experiment leaves much room for improvement, so the use of a simple shape is a sensible strategy until the present discrepancies have been erradicated. The use of a high hardenability steel confines the transformation effects to the austenite→martensite reaction and the wide range of quench severities tests the model over a wide range of cooling rates.

Although, the mathematical model has been used to follow the generation of thermal stress and strain in a wide range of quenchants,

most of the previous work connected with its development suffers from the limitations that only one plate thickness and one steel has been involved. Therefore, in the later stages of the investigation the thermal stress and strain generated in thicker sections and in steels with different Ms and Mf temperatures has been determined. This has indicated improvements to the mathematical model not evident in the work on the thin plates of 835M30 steel.

The model used in the present investigation, contains all the relevant properties of the material and the quenchants as well as transformation plasticity. Hence the results obtained from such a model should be realistic. The level of reliability obtained from the calculated results has been checked by experimental investigations of the residual stress and strain distributions at the end of the quench.

2. LITERATURE REVIEW

2.1 Introduction

In order to explain residual stresses several terms have been used, which include thermal stresses[1,2] and internal stresses[3,4,5]. Thermal stresses arise from two causes. In one case the application of a temperature gradient produces differential expansion or contraction of the component parts[6]. In the second an external constraint inhibits the free movement of a body as its temperature changes. Internal stresses refer to those stresses existing in bodies upon which no external forces are acting. They are also referred to as 'locked up' stresses[7]. The term residual stresses is best confined to stresses resulting from non-uniform temperatures, mechanical operation and metallurgical treatment that persist at the end of the operation. This obviously does not include all thermal and internal stresses.

The residual stresses are classified as either macro or micro stresses[7,8]. Macro stresses act over large distances within the body (therefore they are also known as body stresses) and affect long range properties and external dimensions. They may be due to external influences such as mechanical, chemical and thermal factors. Micro stresses are stresses that act over short microscopic distances and which occur at microstructural inhomogeneities in the material. The stresses around precipitates or inclusions after deformation and the stresses due to lattice defects are examples of micro stresses, which are also known as textural stresses[4,9] and tessellated stresses[5,10]. Measurement of macro stresses may be carried out by mechanical and x-ray diffraction techniques, whereas micro stress are measured by x-ray techniques[11].

The present work will principally be concerned with macro stresses and these will be referred to as thermal stresses.

2.2 Effect of Thermal Stresses

The state of thermal stresses during and after the quenching operation can lead to one or more of the following problems, depending upon the type of quenchant and the composition of material:-

(a) Quench cracks.

(b) Distortion of the component.

(c) Change in service properties.

(d) Distortion during machining.

The stress development during quenching may cause quench cracking, if it reaches the fracture stress of the material, but the precise levels of stress required for this to occur are generally unknown. The occurrence of such cracks has been found to be very erratic, and highly dependent upon the geometry of the component[12], which greatly influences the stresses. For example an assessment of quench crack occurrence was undertaken by Kobasko[13], who investigated the effect of cooling rate on the susceptibility of Si/Mn/S/P steels to quench cracking. A wide range of cooling rates was achieved by the use of quenchants of varying severities (Hot, Warm and Cold Water, Saturated Nacl Solution and a 12% NaoH Solution). The greatest tendency to cracking was found to be at a cooling rate of 300-350^{o}C/sec., whilst undergoing transformation, (see figure 1). In a later paper Kobasko[14] mentioned that surface cracking which appeared after the martensitic transformation has been completed, was due to the large tensile stresses which had developed at the surface of material.

The generation of stresses in a material during quenching will cause plastic distortion of the component when the magnitude of the stress developed rises above the elastic limit. Such distortions can cause great difficulty when critical dimensional tolerances are required.

The distortions which occur as a result of high level of stresses during quenching have been classified into three types by Sachs[15] viz:-

(i) Change in volume.

(ii) Change in shape.

(iii) Warping.

An important consequence, which has long been recognised, is the effect of residual stresses on the service properties of the component, particularly in corrosive environments. The surface tensile stress can contribute towards the susceptibility of stress-corrosion cracking, while a compressive residual stress will modify the magnitude of fatigue strength of the component[7].

Residual stresses within a component can cause warpage or even fracture of that component when it undergoes machining processes after the hardening operation[7]. This arises as the stresses are redistributed, following the loss of material during machining, to balance the forces and moments within the component.

It is evident that serious practical problems arise from the occurrence of thermal stress and strain during the quenching operation, and that their study is of considerable importance.

2.3 Factors Affecting the Development of Thermal Stress and Strain

From the earlier work of Scott[6] and others,[16-20] the later work of Denis et al[21] and recent work of Fletcher and Abbasi[22,23] and others[24-27], it was recognised that the development of thermal stress and strain during and after the quenching operation of steels is influenced by the following factors:-

(i) Geometry of the component.

(ii) Temperature gradients.

(iii) Thermal contraction due to cooling.

(iv) Expansion due to transformation of austenite to other phases.

(v) Viscous processes.

(vi) Transformation plasticity.

The geometry of the body has a marked influence on the generation of thermal stress and strain. Thermal residual stresses are self-equilibrating when the component is free of external constraint. The resulting stress pattern is usually symmetrical about the centre of the body as the cooling pattern tends to show this symmetry. In figure 2, the effect of specimen size on the residual stress in water quenched SAE1045 cylinders is shown. Bulher and Rose[28] have shown that the temperature gradients and residual stresses in a 10 mm cylinder were smaller to those in a 100 mm cylinder quenched under identical conditions. The complex effect of geometry on the thermal strain has been illustrated by Thelning[12] who used examples of dimensional changes that resulted from the hardening of plain carbon low alloy steel and high speed steels. The examples covered a wide range of engineering components and showed marked variation in behaviour.

The stress and strain pattern is not only dependent on the size and shape, but the influence of the edge of the component is of great importance, as the residual stress and strain in the plane of plate decays towards zero at a free surface. At the same time stresses and strains develop in the transverse direction[24]. These comments were first made by Saint Venant in 1885 and the later work of Horvay[19] and others[20,29] gave a theoretical foundation to Saint Venant's principle. The work of Horvay[19,20] gave an indication of how elastic

normal and shear stresses vary in the vicinity of an edge. The effect of the edge on the profile of quenched plates of 835M30 steel was investigated by Fletcher and Price[30], (Figure 3). It is evident from this figure, that consistent results were only obtained at distances greater than one plate thickness from the edge, and that the change in plate thickness was significant.

The effect of the free edge on the thermal stress has been predicted recently by Fletcher and Lewis[24], using a finite element technique. They have shown that the residual stresses developed in the interior of the plate began to fall at about 1.5 times the plate thickness from the free edge and became progressively smaller as the edge was approached, (see figure 4). This suggests a larger edge affected region than that suggested by Horvay or Saint Venant.

The temperature difference within the body during quenching is the root cause of thermal stress generation. The largest temperature gradient develops in the early stage of quench, but this gradually diminishes as the temperature of the body approaches that of the surroundings. The thermal gradients produced by different cooling rates are responsible for volume changes which produce thermal stresses. Andrews[7] and Rose and Hougardy[31] have illustrated the stress pattern developed by thermal contraction in the quenched cylinders. At the initial stage of quenching, the surface of the cylinder, which is in contact with the quenchant, cools and contracts more rapidly relative to the core of the cylinder. This means that the specific volume is greater in the core than in the surface region. The volume contraction in the surface is prevented by the higher specific volume in the core, so that a tensile stress is produced in the surface. As the forces within the material are in balance, a compensating compressive stress will arise in the centre. The nature and magnitude of these stresses vary

with time and the magnitude of the temperature gradient between surface and core. It is shown in figure 5, that the stress at any point reaches a maximum value when the temperature gradient reaches a maximum value, ('W' on curve). When the temperature difference between surface and core is reduced, unloading of these stresses will start as a consequence of a faster cooling rate in the core. If there has been any plastic flow within the material, a compressive residual stress at the surface and a tensile residual stress in the core will be left when the temperature reaches ambient throughout the body, (curve "b"). If there is only elastic deformation, then the stress in the surface follows curve "a" and once the temperature gradient has disappeared there will be no residual stress left in the body.

Thermal gradients and contraction in the quenched body are markedly influenced by quenchant severity and the thermal properties of the material: the higher the quench severity the higher is the temperature gradient, and the greater the deformation of the material. Numerous surveys have been carried out on the influence of different quenchants [32,33] and much of the data is available in the form of cooling curves. Water gives higher cooling rates than does oil and so produces a high level of stress, on account of the higher temperature gradients associated with water quenching [34].

The successive formation of transformation products (i.e. Ferrite, Pearlite, Bainite or Martensite) is connected with the expansion of the material. The magnitude of this effect depends upon the type of phase change; e.g. austenite→ferrite or pearlite, austenite→bainite or martensite, whereas the formation of transformation products depend on temperature and rate of cooling. In the case of an austenite→martensite transformation, a typical expansion is shown by the dialatometric curve in figure 6.

As mentioned before, the transformation processes are controlled by the temperature history, which is different for different points in the quenched body. During quenching, the surface reaches the transformation temperature earlier than the centre: this unequal transformation in different parts of the body will provide additional stress increments. The situation is well explained in figure 7[12]. At time t_1 the surface starts to transform and expand so that the thermal tensile stresses are counteracted. The stress reversal takes place earlier than would be the case if no phase transformation had occurred. At time t_2 the core starts to transform which causes another stress reversal. After cooling, transformation induced stresses dominate over the thermally induced stresses and finally, there will be a compressive stress at the core and a corresponding tensile stress at the surface.

In some circumstances, a steel component may transform to more than one phase, each of which have differing mechanical and physical properties, e.g. martensite in the surface region and bainite at the core, see figure 8. In addition to stress generation as a consequence of unequal transformation rates at different points, the presence of these phases will cause residual stresses within the component, on account of differences in specific volumes of the structures present before and after quenching. Even if no plastic deformation occurred during quenching, the misfit caused by the differences in specific volumes of structures present in the different parts of a component will cause residual stresses in the component after quenching.

The process of viscous flow may produce a significant effect on the generation of thermal stress and strain. This is because in such cases, stress relaxation and creep, which are dependent upon time, temperature and the level of stress may become significant. This occurs

even when the stress level is below the yield point of the material. In addition, it has been observed that if a phase transformation occurs in the presence of a stress, plastic strains may occur in excess of that expected from the associated volume expansion, even if the stress lies well below the overall elastic limit. This plastic strain is called transformation induced plasticity[35]. The plastic strain due to this type of induced plasticity greatly influences the development of thermal stresses and strains[23].

The effects of transformation plasticity and viscous flow on the generation of thermal stress and strain represent major aspects of the present programme. Therefore the earlier work concerning these two topics is discussed in greater detail in section 2.4 and 2.5.

2.4 Viscous Processes

In real solids, a linear relationship between stress and strain can be observed only at relatively low levels of stress and temperature. At high temperature and high stress levels, the material deviates from this elastic behaviour; and a more complex stress-strain relationship is observed. This behaviour is partly due to viscous properties of the material, i.e. creep and stress relaxation.

Creep is a temperature sensitive process which may be defined as the time-dependent inelastic flow of materials under constant stress, but it may also occur when the load is not constant. A schematic representation of a set of fundamental creep curves observed in a creep test is shown in figure 9. The shape of the curve depends upon both stress level and temperature. The four distinct stages of the curve can be distinguished on the time-strain rate.

Instantaneous strain occurs on loading followed by a decelerating

strain rate stage (primary and transient creep). This may be followed by a steady creep rate stage (secondary creep), which is finally followed by accelerating creep (tertiary creep) that ends in fracture. The precise sequence and the relative importance of each stage depends upon stress and temperature. Beside metallurgical influences, temperature time and stress level are the main factors that affect the creep behaviour of metals. All the stages described above may occur together in a single test if a suitable combination of these factors is available.

If a metallic component under load is prevented from changing it's shape, the load that it supports may decrease with time. The phenomenon is described as stress relaxation and experimental evidence conclusively shows that this process is thermally activated[36] at high temperatures ($> 0.4\ T_M$, where T_M is the melting point of alloy)[37]. At lower temperatures a smaller amount of stress relaxation occurs, which falls to zero after a certain length of time (see figure 10).

2.4.1 Models Involving Viscous Flow

Viscous flow may not be separated from the other types of deformation. Hence, the influence of this process has been described by three theories: i.e. the Elastic-Viscoplastic, the Viscoplastic and the Viscoelastic[38,39].

The Elastic-Viscoplastic theory has been reserved for those materials that show viscous properties in both the elastic and plastic regions. This theory assumes that the inelastic deformation is proportional to a function ϕ (F), where F is the yield function obtainable under conditions where viscous flow is absent[38]. The experimental conditions made it difficult to describe quantitatively the yield condition for an elastic-viscoplastic material. Therefore the theory has not yet been used to solve practically important problems.

The Viscoplastic theory has been described within the framework of strain rate and the loading path (i.e. static or dynamic)[38]. Such a theory considers viscous (time dependent) flow to occur in a material only in the plastic range, while it has only elastic properties before yielding. Although the theory has its foundation on certain assumptions which cannot always be satisfied in reality, the quantity of work that has been carried on this model is immense. Perzyna[39] proposed a viscoplastic constitutive equation for strain rate in the following form, in which the strain rate is resolved into an elastic and inelastic part.

$$\dot{\varepsilon}_{ij} = \frac{1}{2\mu}\dot{S}_{ij} + \frac{1-2\nu}{E}\dot{S}_{ij}\delta_{ij} + \gamma\,[\phi(F)]\,\frac{\partial F}{\partial \sigma_{ij}} \qquad \ldots\ldots 2.4.1$$

where, γ = coefficient of viscosity

F = yield function

μ = shear modulus of material.

In this equation the amount of time dependent flow that occurs at stresses below the yield point has been ignored on account of its small magnitude in comparison to that which accompanies plastic flow[39]. In order to make use of the constitutive equation 2.4.1 for inelastic flow it is necessary to know the form of $\phi[F]$, which controls the behaviour of the metal under viscoplastic conditions. The theory of viscoplasticity does not indicate what this function should be, so a variety of different functions have been chosen that allow the correct relationship between strain rate and yield stress. Power series with coefficients designed to give a curve of the required shape have been used to predict relationships between yield stress and strain rate that show the characteristic shape of the corresponding experimental curves.

It has been shown that the effect of strain rate had a negligible

effect on yield stress when the magnitude of the former was less than $40s^{-1}$. However the deformation rate relevant to the heat treatment of metallic parts is much smaller.

Recently Wang and Inoue[43] have considered the viscoplastic behaviour of material in the determination of the thermal stress generated during welding. The inclusion of the viscoplastic behaviour of material for welding processes may well be reasonable, as the material is heated beyond the melting point. In the case of the welding processes during the liquid → solid phase transformations the temperature is sufficiently high to include a substantial amount of viscous flow despite this short time interval. This is outside the normal range of heat treatment temperatures, where the lower temperatures do not produce such a large effect. Inoue and Wang also used[46] viscoplastic theory in a mechanical model to estimate the stresses developed in a semi-infinite body heated through the surface followed by cooling. The model used was complex, phase transformation, latent heat and kinematic hardening were included but not transformation plasticity. The results obtained in this case showed a smaller effect of viscous flow than that shown by the results obtained in the case of welded plates. This result was due to the model of viscoplasticity used, which assumed that viscous flow did not occur unless the yield surface was reached. Hence, the effect of viscous flow would not be expected when the temperature was low and yield stress high, in comparison to the case of welded plates. It was therefore, clear from the work of Inoue and Wang[43,46] that the use of the viscoplastic model can only be justified for the case where the temperatures are very close to or at melting point.

The main drawback to the viscoplastic theory is the absence of viscous flow when the level of stress is below the yield stress of the material. The stresses set up during quenching may be sufficient to

cause a significant rate of viscous flow, even though the level of stress is well below the flow stress. Therefore, there is a need for a theory that considers viscous flow in the elastic range.

The theory of viscoelasticity and its effect on the generation of thermal stresses had been described by many authors[22,40,41]. During the qualitative study of stress generation during the heat treatment of metallic materials, the high temperatures involved and the associated stress levels make it necessary to take into account the viscous properties of material such as creep and stress relaxation[22,42-45].

2.4.2 Relation Between Creep and Stress Relaxation

Creep can normally be observed when material is free to deform under a constant load, while in the case of thermal stress, the component is constrained at any instant to a particular size and shape. In a small time interval this constraint gives rise to a certain reduction in stress viz stress relaxation. The relaxation is normally characterised by the condition:

$$\varepsilon_T = \varepsilon e + \varepsilon p + \varepsilon ve = \text{Constant} \qquad \ldots\ldots 2.4.2$$

When a specimen is deformed to a given strain, part of this strain is elastic in origin and part is inelastic. Further, because of creep, some of the latter may be time dependent (viscous). Since the total strain εT is held constant in a stress relaxation test, the elastic strain εe must decrease with time to accommodate the increase in viscous strain εve. The elastic strain can decrease only if the applied stress becomes smaller. Hence, in stress relaxation, the viscous deformation gradually increases, accompanied by a decrease in elastic strain and the applied stress. Therefore, the stress relaxation test can also be described as a test of viscous flow but with a variable stress[42].

It follows from the above, that creep is related to the stress relaxation process and the conditions for stress relaxation process are present during the process of quenching of steel components. Both effects will have a significant effect on the generation of thermal stress and strain during the process. Hence, it is desirable to include the effect of stress relaxation in the mathematical models of thermal stress and strain generation during heat treatment.

Due to the lack of data which can be directly applied to the more complex situation of creep and stress relaxation, theoretical laws and the use of mechanical models have been made to simulate these effects during quenching. The results have been introduced into the mathematical models of the quenching process.

2.4.3 Viscous Flow and the Generation of Thermal Stresses

The influence of viscous flow on the generation of thermal stresses during quenching may be of great importance as, the components are subjected to very high temperatures and stresses during quenching. Although, the rate of quenching of components is rapid, there may be sufficient time for viscous processes to occur[22], particularly at the centre of thick sections.

Several workers have developed mathematical models of the generation of thermal stress and strain during quenching, but little consideration has been given to viscous processes. The published work that includes this effect is extremely small, probably because there has been a lack of appreciation of the extent to which stress relaxation can occur during quenching.

Perhaps the first, to incorporate viscoelasticity in a model of thermal stress generation was Landaue[47]. The viscoelasticity effect

was modelled by the Maxwell body, but his results suggested that the introduction of viscoelasticity had a negligible effect on the residual stresses. The results are suspect on several grounds, including lack of stress relaxation data, an absence of any consideration of phase transformations or the temperature dependence of mechanical properties.

Boyer and Bovin[48] presented a mathematical model for calculation of thermal stress with consideration of stress relaxation. This was modelled by considering the elastic-plastic extension and compression of stainless steel and aluminium infinite plates. They predicted that a significant amount of stress would be relaxed during plastic deformation in both the cases. However, the degree of relaxation would depend on the nature of the stress, as they observed low relaxation rates for compressive stresses in comparison with the results from tensile stress. They mentioned that an accurate prediction could be made for thermal stresses by the introduction of relaxation effects in the calculation model. Experimental stress relaxation results were only presented for aluminium plates in a state of tension, but good agreement was found in this case between experimental and calculated relaxation results. The way in which the experimental results were obtained was not fully described.

The work of Fletcher and Abbasi[22,41] introduced viscous properties in a realistic way. They demonstrated the effect of stress relaxation and creep on the predicted thermal stress and strain in 835M30 steel plates that had been quenched in water and oil. Visco-elastic behaviour of the metal was simulated by a mechanical model of viscoelastic processes in a standard linear solid. Theoretical equations for stress relaxation and creep were obtained from the behaviour of this model, and these were fitted to experimental stress relaxation data that had been obtained in an Instron testing machine at various

temperatures. At the upper end of the temperature range, creep tests were also carried out in a stress rupture testing machine. The introduction of viscous effects gave reasonable agreement between the calculated residual stresses and strains and those obtained by experiment in the case of oil, but when water quenching was used the agreement was not as good. They also concluded that the introduction of viscous effects in the mathematical model had a particularly great effect at temperatures just below the Ms temperature. A major criticism of this work is that it is based on stress relaxation data obtained at only one level of initial stress at each temperature. Although this stress was the best estimate available, coupling between stress, transformation and time rate brought these estimates into doubt.

2.5 Transformation Plasticity

It has been observed that when transformation takes place in a metal or alloy subjected to a non-zero stress state, strain occurs in excess of that expected from the dilatometry data obtained from stress-free specimen. This extra strain is plastic even though the level of stress lies well below the overall elastic limit of material[23,25,49,50]. This phenomenon is called 'Transformation Plasticity'.

Although, there is no direct evidence of this process, various suggestions have been made to explain the phenomenon associated with transformation plasticity. Attempts have been to describe this effect on a microscope scale in the case of transformation of iron and steel (i.e. $\gamma \leftrightharpoons \alpha$ transformation)[49]. The generation of this plasticity was explained by the suggestion that during transformation, atoms, located at the phase boundary diffuse preferentially in the stress direction with the result that extension occurs in the same direction as that of

stress. However, others[50,51] attribute the transformation plasticity in iron solely to the internal stresses set up by the change in volume. Bush and Bokros[35] suggested that the dislocations generated by the martensitic transformation under the influence of the stress affect significantly the transformation strain.

Porter and Rosenthal[52] have expressed the opinion that increased rates of nucleation of the product phase as a consequence of the applied stress created a number of dislocations, which piled up at coherent boundaries between austenite and martensite. When the nucleus looses its coherency with the austenite matrix the advancing interfaces act as sinks for the piled up dislocations and enhance the plastic deformation observed during transformation under the influence of stress.

The qualitative characterisitics of the phenomenon have been known for a very long time, although the implications for the calculations of thermal stress and strain generation during heat treatment has only been considered very recently[21,23,25,46,53,54]. Two methods have been used to introduce this into the calculation of thermal stress and strain.

(a) Reducing yield stress of the material during transformation.

(b) The use of an additional strain term during transformation.

The first approach was suggested by Sattler and Wessermann[49]. In this model the yield point, which must be exceeded when deformation is produced, is lowered sufficiently to produce such an effect for the duration of transformation only. However, this approach is not satisfactory since neither they nor any later investigators have found experimental evidence of an exceptionally low yield stress during transformation from austenite to martensite.

The second suggestion was developed by Greenwood and Johnson[50].

A rigid-ideal plastic model of the deformation was considered together with the assumption that all the plastic flow occurred within the region of the weaker phase. A range of transformations were considered including the $\gamma \rightarrow \alpha$ transformation in iron. Greenwood and Johnson suggested that an additional strain term could be calculated for a complete transformation in the presence of a uniaxial stress state. The quantity of such strain was obtained from the equation:

$$\varepsilon_{tp} \approx \frac{5}{6} \frac{(\Delta V/V)}{Y} \sigma z \qquad \ldots\ldots 2.5.1$$

where, ε_{tp} = Transformation plasticity strain.

$\frac{\Delta V}{V}$ = Transformation strain.

Y = Yield strength.

σz = Applied stress.

They described transformation-induced plasticity as an anisotropic effect which occurs only in the direction of stress and is proportional to the applied stress.

A reduction in yield stress was the first method used to simulate transformation plasticity during quenching of steel. Denis et al[21] incorporated the effect of transformation plasticity into thermal stress calculations by means of a decrease in the yield stress of the material during the martensitic transformation. Fletcher and Abbasi[23] have also introduced transformation plasticity in a mathematical model of thermal stress and strain by a reduction in the flow stress of 835M30 steel at temperatures between Ms and Mf. None of them have presented any experimental evidence of such a reduction in yield strength during transformation from austenite to martensite. In fact, Fletcher and Price[18,30] have found a steady increase in yield stress as martensite formed. The discrepancy between the experimental results and the data used for calculation might be justified if no transformation occurred

during the isothermal tensile test. If there was no transformation the yield stress obtained would not be reduced as a consequence of transformation plasticity. During continuous cooling, however the occurrence of the martensite transformation might be associated with unusually low yield stresses. Hence, the calculations that show a reduced yield stress during the martensitic transformation do not appear to be based on direct experimental measurements and are contrary to all the experimental data. It is probably the reason why this method has not been used extensively.

The reduced yield stress model of transformation plasticity has lost popularity in favour of the Greenwood and Johnson model because of its controversial nature to the experimental evidence and the unavailability of any data that could be used directly to model the effect of transformation plasticity by this method. The essential features of the equation proposed by Greenwood and Johnson are that the amount of transformation plasticity strain should be proportional to the applied stress and this suggestion is supported experimentally as well as theoretically by a large number of investigations[21,23,53-55].

Beck et al[53] have observed the transformation plasticity effect during the martensitic transformation as enhanced dilation when a specimen was transformed in the presence of a tensile stress. The amount of enhancement in the dilation was proportional to the applied stress, which supported the Greenwood and Johnson model.

Abrassart[55] proposed a linear relationship between applied stress and strain component during transformation plasticity that was consistent with the relationship established by Greenwood and Johnson. He suggested that the $\frac{5}{6}$ term in Greenwood and Johnson's equation should be $\frac{1}{4}$:

i.e.

$$\varepsilon_{tp} \approx \frac{1}{4} \frac{(\Delta V/V)}{Y} \sigma z \qquad \ldots\ldots 2.5.2$$

Both the relationships (2.5.1 and 2.5.2) are plotted in figure 11. It is evident that both the curves are identical in shape, but the strain values associated with transformation plasticity at a particular stress level are much smaller for the latter equation.

Experimental investigations of Denis et al[25] have shown the effect of a tensile stress up to 285 MPa during the martensitic transformation in a 0.57% carbon steel. The relationship obtained between the applied stress and the transformation plasticity was similar to those presented by other models (see figure 11). However, the amount of transformation plasticity associated with the applied stress was closest to that predicted by Greenwood and Johnson model.

The direction of applied stress under which transformation takes place influences the sign of the associated transformation plasticity strain. None of the above mentioned authors have examined the effect of compressive stress on the transformation characteristics. Recently Fletcher and Abbasi[23] and Desalos et al[54] have reported the effect of negative stress on the dilation produced during transformation. The presence of a compressive stress reduced the overall dilation during transformation and even contractions have been observed as the level of compressive stress was increased. A finite element analysis was carried out by Desalos et al[54], to demonstrate the effect of stress on transformation strain during transformation of an austenite grain to martensite. This work involved complex assumptions in the theoretical analysis and very low levels of stresses in the experimental investigations. However, a linear relation was established between transformation plasticity strain and the applied stress.

Recently, Fletcher and Abbasi[23] have conducted experimental investigations of transformation plasticity on 835M30 steel. They determined the relationship between dilatometer specimen length and temperature, when an austenitic specimen was cooled in the presence of either a negative or a positive stress. They have reported a decrease in transformation strain under the influence of a compressive stress, whereas, an enhanced expansion of the specimen has been observed during the formation of martensite in the presence of a tensile stress. They also suggested a linear relationship between applied stress and transformation plasticity, but the amount of plastic flow as a result of an applied stress during transformation was lower than that predicted by Denis model[25], (see figure 11). It may be that the small expansion during the formation of martensite in this case was due to the lower carbon content of the steel, in comparison to that used by Denis.

The linearity of the relationship between applied stress and transformation plasticity strain proposed by Greenwood and Johnson[50], was maintained in all the cases and usually there was no threshold stress below which transformation plasticity effect was not occurred. However, a threshold stress of about $\pm$ 40 MPa has been observed by Fletcher and Abbasi[23]: below this threshold stress no plastic flow occurred. They have also reported that all transformation plasticity effects occurred during the first 40^{o}C of transformation.

Most of the models discussed above have been used to demonstrate the effect of transformation-induced plasticity on the development of thermal stress and strain during quenching. This is discussed in the next section.

2.6 Prediction of Thermal Stress and Strain During Quenching

It has long been realized that martensite hardening can be accompanied by large thermal stresses and strains. They can be detrimental and cause quench cracking or distortion or they can be advantageous and improve the properties of the hardened steel. It is therefore natural that large efforts had been made to predict and understand thermal stress formation during the quenching process. The assessment of thermal stress and strain generation during quenching requires knowledge of the following important factors.

(i) Temperature distribution in the quenched component throughout the quenching process.

(ii) Phase transformation history of the material.

(iii) Temperature dependent thermal and mechanical properties of the material.

The first step in the prediction of residual stress and strain is the determination of the thermal history of the component during quenching. The temperature field of the quenched component is influenced by the severity of the quenching medium. High cooling rates will produce steeper overall temperature gradients, and hence greater thermal strains in the body. Conversely slow cooling quenchants will produce low thermal strain in the quenched body. The generation of thermal stresses at each temperature depends on the strain developed and also, when plastic flow is present, on the flow stress of the material at that temperature.

The complete history of the phase transformations has to be traced in parallel with the temperature history, if reliable calculation of thermal stress and strain is the object. Phase transformations are accompanied by volume changes and this affects the coefficient of thermal expansion. In an isotropic material both temperature changes and

transformation will cause only a uniform volume change in a body free to expand[33]. Hence, the coefficient of thermal expansion and volume changes due to transformation are modelled as a function of temperature.

In the course of the quenching process a large temperature range is involved and phase transformations proceed continuously with changing temperature. Both these circumstances make it necessary to take into account, the temperature dependent physical properties (thermal conductivity, specific heat and surface heat transfer coefficient) of the material. An accurate knowledge of temperature dependent mechanical properties (Young's modulus, Poisson's ratio, flow stress and strain hardening coefficient) of the material is also required if reliable thermal stress and strain calculations are to be carried out.

The calculation of thermal stress by analytical methods is well documented in standard texts[40,56], which usually involve simple shapes and simple temperature distribution, without consideration of any plastic flow. The avoidance of plastic flow made the mathematics of the problem more intractable[1]. The essential steps required in the prediction of thermal stresses have been described by Denton[8]. Initially, the temperature distribution within the body at different times during the quenching must be calculated. After this, the elastic stress distribution that arises from the change in the temperature distribution during each small time increment is calculated using elastic moduli and the coefficient of thermal expansion, with the assumption that the body is fully constrained by external loads and moments. Finally, the external forces and moments are removed to allow deformation of the body in such a way that there is complete compatibility and residual stresses are in equilibrium. This process is repeated after each time increment throughout the quench, and a complete history of stress and strain generation is obtained. The introduction of plastic

flow requires the use of a yield criterion and a rebalancing of the force on the section considered. This leads to a lengthy iterative process which is best handled by a numerical method.

2.6.1 Determination of Temperature Distribution

The determination of the temperature field in the quenched component is a fundamental prerequisite to the prediction of thermal stress and strain. The temperature distribution within a quenched steel component at all stages can be determined by the solution of the partial differential heat conduction equation[57]:

$$Cp\left[\rho \frac{\partial \theta}{\partial t}\right] = H + \frac{\partial}{\partial x}\left[\lambda \frac{\partial \theta}{\partial x}\right] + \frac{\partial}{\partial y}\left[\lambda \frac{\partial \theta}{\partial y}\right] + \frac{\partial}{\partial z}\left[\lambda \frac{\partial \theta}{\partial z}\right] \quad \ldots\ldots 2.6.1$$

This equation may be solved analytically[57,58] but the range of solutions is severely limited by the requirement of non-variant thermal properties. All the thermal properties described in equation 2.6.1 are temperature dependent during quenching and indeed vary markedly with temperature. In the case of analytical solutions, it is necessary that these thermal properties be invariable, or vary as some simple function of the variable concerned. Hence, analytical methods of solution in the present problem are not suitable.

Examples of numerical solutions are available in most of the heat transfer text books[59-62] and in many papers[63-68]. Solution by such methods allows the calculation of the temperature distribution with variable thermal properties. In the Finite Difference solution to the heat conduction equation given by Craft and Liley[59] and Dusinberre[60], the partial differential equation has been replaced by Finite Difference equations in terms of partial quotients, which are solved for the temperature at preselected discrete points within the body. The temperature at a certain point is taken as representative of a certain

region which includes the point, and the heat flow at a boundary is taken as the summation of the flows of heat from the appropriate regions.

The two types of Finite Difference solutions that are available may be divided into implicit and explicit formulations. In the case of uniaxial heat flow, the explicit form of the Finite Difference equation is given as[60,61]:-

$$\frac{\theta_i^{n+1} - \theta_i^n}{\Delta t} = \alpha td\left[\frac{\theta_{i+1}^n - 2\theta_i^n + \theta_{i-1}^n}{(\Delta x)^2}\right] \qquad \ldots\ldots 2.6.2$$

By maintaining the change in the Fourier number, $\frac{\alpha td \Delta t}{(\Delta x)^2} = \frac{1}{2}$, the solution of equation 2.6.2 simplifies to the Schmidt formulation as:

$$\theta_i^{n+1} = \left[\frac{\theta_{i+1}^n - \theta_{i-1}^n}{2}\right] \qquad \ldots\ldots 2.6.3$$

An equivalent implicit formulation of this problem is given by replacing the θ^n values on the right hand side of equation 2.6.2 by θ^{n+1} values. This is termed backward solution, as opposed to the forward, explicit solution. Another Finite Difference formulation available for determining temperature history in the specimen is known as the Crank-Nicolson method. This method works on central difference approximation and in the case of unidirection heat flow may be expressed as:

$$\theta_i^{n+1} - \theta_i^n = \frac{\alpha td\ \Delta t}{2(\Delta x)^2}\left[(\theta_{i+1}^{n+1} - 2\theta_i^{n+1} + \theta_{i-1}^{n+1}) + (\theta_{i+1}^n - 2\theta_i^n + \theta_{i-1}^n)\right] \ldots\ldots 2.6.4$$

The Crank-Nicolson solution provides efficiency and accuracy where the time accuracy is unimportant as the method is less accurate for short time intervals[69]. As the boundary conditions are varying rapidly with time during quenching, high accuracy and stability of the results will only be achieved by the use of small time steps.

Generally the derivation of Finite Difference formulation is obtained by the use of a Taylor series[70], but the convergence to a stable solution is dependent on the refinement of finite intervals (Δx), and the increase in number of finite time steps (Δt) over a given period. For both the explicit and Crank-Nicolson formulations the truncation error of Taylor series is of the order $(\Delta x)^2$, but in the case of the explicit formulation instability will not grow provided the Fourier's number is equal to or less than 0.5[62,70,71].

Much work has been undertaken on the calculation of temperature history during quenching steel components by the use of Finite Difference method with digital computers[17,34,63,64,72].

The model used by Hildenwall[17], for calculating the temperature field across infinite plates and long cylinders of three different steels quenched in oil involved a backward implicit Finite Difference method. Taking full account of the temperature-dependent properties of steels, all the input data was established by experimental investigations. Experiments have also been used to verify the calculated results, and the agreement between measured and calculated temperature gradients was often very good.

Sjöström[34] has calculated the temperature gradient in the infinite long cylinders of various steels during quenching in water and oil and iced water. He also used a backward implicit Finite Difference method. Temperature dependent properties were used, but instead of surface heat transfer coefficients the temperature dependence of the surface condition was expressed in terms of the heat flux. The effect of phase transformation was considered on the temperature distribution, but no experimental investigations were carried out to compare the calculated and experimental results.

Fletcher[63] predicted the thermal history of 835M30 steel plates quenched from 850°C by the use of a Finite Difference solution of Fick's law of transient heat conduction with both constant and variable heat transfer coefficients. He was able to complete the analysis using the Schmidt formulation equation (2.6.2) with the change in the Fourrier number of 0.5. Forty one elements were used to sub-divide the half plate thickness and many time steps were required to cover the whole quench. The calculated temperatures at any instant were not compared with the corresponding experimental values.

The heat transfer coefficient, used by Fletcher[63] was highly dependent on the experimental conditions. Therefore in the subsequent work by Price and Fletcher[64], surface heat transfer coefficients at various temperatures have been established for stainless steel plates quenched in water, oil and Polymers, before calculating the temperature profile. The values were used in conjunction with an explicit Finite Difference technique to calculate temperature profiles created during the quenching of low alloy steel plates. Predicted temperature profiles were checked against experimental results and a reasonably good correlation was found.

Archambault and Chevrier[72] have used an implicit Finite Difference method to calculate the temperature field in nickel cylinders quenched in boiling water. The thermal properties, except the surface heat transfer coefficients, were considered to be constant. Heat conduction was assumed to take place in two directions; radially through the surface of the cylinder as well as axially through its base. The calculated temperatures at the centre of the cylinder gave a very good correlation with those measured experimentally.

Several workers have used the Finite Element method to determine the temperature field in the quenched components[65-68]. A Finite Element method was first used by Inoue and Tanaka[65], to calculate the temperature profile in quenched 0.43% carbon steel cylinders of 60 mm diameter when quenched in water. Measured values of the temperature change at the surface and the centre of the cylinder were used as initial and boundary conditions. Heat generation due to phase transformation was ignored. The thermal diffusivity was taken to be 7.22 mm^2/sec. and assumed to be temperature dependent; no information was provided about other thermal properties.

Toshioka[66] has used a Finite Element technique, to calculate the transient temperature distribution in quenched steel bars. The effect of time on the temperature distribution was calculated using the data shown in table 1a, which was obtained from the literature. The subsequent results of the temperature field were used to predict distortions in the bars as a consequence of quenching.

A Finite Element method was used by Inoue et al[67] to determine the temperature distribution in a 12%Cr steel cylinder quenched in water. No description was given about the thermal property data used. A heat generation term was employed to incorporate the heat evolved due to the martensite transformation. By doing so, very large increases in the temperature were observed during the transformation, which temporarily halted the cooling process.

Recently, Jeanmart and Bouvaist[68], calculated the temperature gradient in quenched 70 mm square plates of high strength 7075 aluminium alloy using the MARC Finite Element programme assuming absence of thermomechanical coupling. To achieve an accurate thermal gradient in the plate a very fine mesh of very small elements with very small time increments was used. Thermo-physical properties used in the heat

conduction equation has not been determined but most of the data was taken from the literature; no information about heat transfer coefficients was provided. The plate was supposed to be infinitely long and large, with unidirectional heat flow through the thickness of plate. Temperature gradients developed within the specimens were different with different quenching severities and the temperature difference between surface and centre predicted for the quenchants of low severities was less than those for high severities. The accuracy of the results obtained has not been checked experimentally.

2.6.2 Calculation of Thermal Stress and Strain

The calculation of thermal stresses by analytical thermoelastic -plastic formulations is described in various texts[1,40,56] Benham and Hoyle[1] and Johns[56] have given solutions to the steady state thermo-elastic stress and transient temperature distributions, whereas Benham and Hoyle[1] have also given a method of solution to some problems of plastic flow. The most complete text covering the analytical solution for both the elastic and plastic deformation situation is by Boley and Weiner[40]. A range of elastic-plastic solutions was described and in some cases viscoelastic effects are taken into account. However, in most of the cases, the mechanical and thermal properties are assumed to be constant. Assuming that there would be no thermo—mechanical coupling and that the distribution of temperature across the body was known, the thermal stress-strain problems would be reduced to the following equations[40]:

Equilibrium Equations

$$\frac{\partial \sigma xx}{\partial x} + \frac{\partial \sigma xy}{\partial y} + \frac{\partial \sigma xz}{\partial z} + Fx = 0$$

$$\frac{\partial \sigma xy}{\partial x} + \frac{\partial \sigma yy}{\partial y} + \frac{\partial \sigma yz}{\partial z} + Fy = 0$$

$$\frac{\partial \sigma xz}{\partial x} + \frac{\partial \sigma yz}{\partial y} + \frac{\partial \sigma zz}{\partial z} + Fz = 0$$

Stress-strain relationships

$$\varepsilon xx = \frac{1}{E} [\sigma xx - \nu(\sigma yy + \sigma zz)] + \alpha ex:\theta$$

$$\varepsilon yy = \frac{1}{E} [\sigma yy - \nu(\sigma xx + \sigma zz)] + \alpha ex:\theta$$

$$\varepsilon zz = \frac{1}{E} [\sigma zz - \nu(\sigma xx + \sigma yy)] + \alpha ex:\theta$$

$$\varepsilon xy = \frac{1}{2G} \sigma xy$$

$$\varepsilon yz = \frac{1}{2G} \sigma yz$$

$$\varepsilon zx = \frac{1}{2G} \sigma zx$$

Strain displacement relations

$$\varepsilon xx = \frac{\partial u}{\partial x}$$

$$\varepsilon yy = \frac{\partial v}{\partial y}$$

$$\varepsilon zz = \frac{\partial w}{\partial z}$$

$$\varepsilon xy = \frac{1}{2} [\frac{\partial u}{\partial y} + \frac{\partial v}{\partial x}]$$

$$\varepsilon yz = \frac{1}{2} [\frac{\partial w}{\partial y} + \frac{\partial v}{\partial z}]$$

$$\varepsilon xz = \frac{1}{2} [\frac{\partial u}{\partial z} + \frac{\partial w}{\partial x}]$$

The solution of the above equations for a three dimensional problem would yield the following six stress, six strain and three displacement components, which must satisfy the above equations with prescribed boundary conditions.

6 stress components,

$\sigma xx, \sigma yy, \sigma zz, \sigma xy, \sigma yz, \sigma xz$

6 strain components,

$$\varepsilon xx,\ \varepsilon yy,\ \varepsilon zz,\ \varepsilon xy,\ \varepsilon yz,\ \varepsilon xz$$

3 displacement components,

$$u,\ v,\ w$$

Solutions of the above equations are only possible for a small number of cases when the geometry of the body allows the simplification of these equations. The required stress functions are extremely difficult to solve if such simplifications are not made. Only the plane stress and plane strain configurations have been subjected to rigorous study. Plastic flow, and phase transformation during the quenching process are additional complications. Application of a yield criterion is necessary to make an estimate of the position of the boundaries between the elastic and plastic zones. Estimation of the position of the elastic/plastic boundaries can be conducted by the use of Tresca or Von-Mises yield criterion, but the Von-Mises yield criterion has been the more popular, particularly for thermal stress calculations. This criterion states that deformation occurs when[73]:-

$$(\sigma xx - \sigma yy)^2 + (\sigma yy - \sigma zz)^2 + (\sigma zz - \sigma xx)^2 = 6GA' \qquad .....2.6.2.1$$

Strains are linearly related to the stresses in the elastic range, but in the plastic range a more complicated stress-strain relation arises. The solution for such a situation can be obtained from the Prandt-Reuss equation[74]:

$$d\varepsilon^p_{ij} = \frac{3}{2}\frac{d\varepsilon p}{\sigma e} Sij \qquad .....2.6.2.2$$

Boley[75] has described a solution of the two dimensional heat flow and thermal stress problem with a mathematical model that uses linear partial differential equations. He assumed both the modulus of elasticity and the coefficient of thermal expansion to be temperature dependent.

Hence he used dubious empirical relationships between each of these properties and temperature. The method of solution did not incorporate the effect of strain due to phase transformation on thermal stress generation, which is essential in the case of the quenching of steel components[76].

Symmetrically cooled plates were modelled by Landau[47], using elastic-plastic and viscoelastic effects based upon the Maxwell body, and the temperature dependent Von-Mises yield criterion. The viscous strain rate was obtained from the following equation, where the coefficient of viscosity was considered to be temperature dependent.

$$\dot{e}^{v}_{ij} = \frac{1}{2\eta} \dot{S}_{ij} \qquad \ldots\ldots 2.6.2.3$$

The temperature field across the plate was determined by a Finite Difference technique. The plate considered was thin enough to allow an assumption of plane-stress conditions. From the analysis of the results it was found that incorporating viscoelasticity into the model had a negligible effect on the residual stresses but the effect of temperature dependent yield stress was significant. The model was based on the equations that described the stresses developed by a slowly varying heat input, and no account was taken of phase transformations. This model also suffers from the drawback that it does not consider the temperature dependence of the physical and mechanical properties. Considerable doubt can be thrown on the correctness of the relationships between temperature and both flow stress and the coefficient of viscosity used in the Maxwell body. No attempt was made to verify the calculated results experimentally.

Fletcher[63] has studied thermal stress and strain in quenched plates of low alloy 835M30 steel, using various values of the surface

heat transfer coefficient. He proposed an explicit Finite Difference method for the analysis of the unidirectional temperature field. The choice of steel was such that it transformed completely to martensite during quenching. Heat transfer was assumed to take place only through the thickness of the plate, in order to produce plane-stress conditions. An approximately linear relationship between temperature and Young's modulus and the flow stress of material was considered whilst the material was in the austenite condition. The flow stress of martensite was assumed to be constant at 1200 N/mm^2. The transformation strain associated with the martensite reaction was assumed to be 1.5%: this reaction occurred between 310°C and 150°C. This information was used to calculate the stress arising from the combination of that due to temperature alone and that produced by the transformation of austenite to martensite. It was predicted that the type of residual stress distribution present at the end of quenching was dependent upon the cooling rate, so that, when high values of heat transfer coefficients (high quenching rates) were used in the calculations, the surface stresses produced were tensile, while the corresponding stress at the centre was compressive. However, the reverse pattern was produced with lowest values of heat transfer coefficients (slow quenching rates). Plastic deformation was produced during the quench and the onset of this phenomenon was determined by the use of the Von-Mises criterion, but no consideration was given to work hardening. The use of a heat transfer coefficient that was independent of temperature and the absence of work hardening and stress relaxation effects made the results doubtful, since the level of accuracy of the predicted results was not checked by experiment.

Fletcher and Price[18,30] followed up the above work by using improved mechanical and thermal property data of 835M30 steel. The

relationship between the surface heat transfer coefficient and surface temperature was established experimentally in the case of water, oil and polymer quenching. The cooling curve data was used to obtain the inverse solution to the explicit Finite Difference equation using the method of successive approximation. Modelling of the dilatometer curve by linear and polynomial relations was an important improvement to the model. Work hardening coefficients that depend on the temperature and previous plastic strain were established, and the flow stress of austenite at temperatures between 800°C and Ms was determined. The increase in flow stress due to the work hardening produced during each time increment was added to the flow stress at the end of each calculation and the Von-Mises yield criterion was applied to correct the stress value before using for the next step. The results obtained suggest that all the quenchants used produced plastic flow above the Ms temperature but no plasticity occurred during or after the transformation. The plastic flow above the Ms temperature gave rise to a complex residual stress distribution in the case of a water and polymer quench. Thus, there was a peak tensile stress predicted just below the surface with a compressive stress at the centre, as shown in figure 12a and 12b. This was reversed in the case of an oil quench, and stress levels were of a much smaller magnitude, as shown in figure 12c. The level of agreement with experiment was dependent on the type of quenchant used. This was good in the case of the predicted and measured results after a water quench (see figure 13a), whereas after a polymer quench the discrepancy between the two results was much greater (see figure 13b). As the severity of the quenchant was further reduced, the discrepancy became progressively worse, as can be seen from figure 13c, which indicates that the calculated and measured stress distributions after an oil quench were in conflict. It was suggested that the discrepancy in the case of oil quench may be due to stress relaxation effects, as cooling rates of oil

were low and a long cooling time would allow viscous flow to occur.

Toshioka et al[77] have developed a model for the determination of stresses induced during the quenching of 0.45%C steel cylinders. They estimated the temperature distribution by fitting a simple empirical equation, which gave a relationship between the measured central temperature and the temperature at any point from surface to centre. The total strains induced by the martensite and bainite transformation was introduced in the model as constants, but these had not been determined experimentally. The distribution of martensite and bainite after quenching was estimated by hardness measurements. The temperature dependence of the thermal expansion coefficient, Young's modulus and Poisson's ratio were ignored together with the effect of strain hardening. The yield strength of austenite was assumed to be zero while the material was in the austenite condition, but during the transformation the yield stress increased by an amount that was in proportion to the volume fraction of the martensite present. Hence, internal stresses were only produced after initiation of transformation at the surface. Stresses were calculated as a function of central temperature. The estimated residual stresses were compressive at the surface and tensile at centre with a low quenchant severity. However, with increased severity, the final surface stresses obtained were tensile in nature. Obvious criticisms of the model are the use of approximations such as the flow stress of austenite, the neglect of important temperature-dependent properties and the lack of experimental work in support of the model.

Fletcher and Abbasi[22,41] have recently proposed a numerical method for the determination of stress and strain in plates of a low alloy steel of high hardenability. They followed the work of Fletcher and Price[18,30] but included consideration of stress relaxation and creep effects by means of a standard linear solid mechanical model. The rest

of the input data for the model was the same as that used by Price[18] for water and oil quenching. In this case viscous flow was considered to be a function of temperature and time but not of initial stress, whereas all these three parameters have a significant effect on the relaxation behaviour of a metal. Hence, any model of viscous flow which ignore any of these parameters can not predict correctly viscous strain and the associated stress-relaxation. As Fletcher and Abbasi's model did not consider the effect of initial stress level on the viscous behaviour of material, this would affect the accuracy of the predicted results. Nevertheless, the inclusion of stress relaxation and creep effect significantly improved the degree of agreement between predicted and measured stress in the case of oil, but in the case of water a modest reduction in the corresponding level of agreement appeared. The discrepancy between predicted and experimental residual stresses after martempering was much improved when viscous flow was considered, compare figures 14a and 14b. They have also tried to incorporate transformation plasticity effects into the same model using stress-dilatometry data by either the concept of an additional transformation strain or by a reduction in flow stress between Ms and Mf temperatures[23]. The use of either method improved the degree of agreement between the calculated and experimentally determined residual stress and strain in case of an oil quench, although the level of correlation between the corresponding results after a water quench was poor.

Calculation of thermal stress and strain in quenched components have been performed on numerous occasions by the use of the Finite Element method[24,34,65-68,79,80]. This method, which has been described in several texts[81-84], involves the discretisation of the structure into an assemblage of elements. The elements are considered interconnected at a number of points, termed nodes. The force at each

nodal point is computed from the relevant displacements and the elastic properties of the material. Matrices of the required quantities in each element are incorporated into equations representing these relationships within each element. These are then merged into a single set of relationships for the whole structure with the strain energy of the structure minimised. The corresponding stresses and strains are then obtained from these results[84].

Toshioka[66] used the Finite Element method to analyse the distortion produced in steel bars of a 0.37%C steel (S38C) and 0.39%C, 1.7%Ni, 0.8%Cr, 0.17%Mo steel (SNCM8) when quenched in water. The calculations use temperature dependent thermal and mechanical property data (shown in table 1), which was obtained from previously published work. The effect of phase transformation was taken into account, but the contribution of viscous flow to the overall residual strain distribution was not included in the calculations, although the size of specimens used (200 mm diameter and 400 mm length) was such that the effect of creep strain is probably quite significant. The calculated results of residual strain were compared with those determined experimentally. Reasonable agreement was found in the case of diametral strain but discrepancies in the length changes were evident, as shown by figure 15.

Inoue and Tanaka[65] have used a Finite Element technique to perform the elastic-plastic stress analysis of a quenched 60 mm cylinder of a 0.43%C steel. The temperature field during the quenching process was also calculated by this method using experimentally determined surface and centre temperatures as boundary conditions. They have included the progress of phase transformation and the consequent specific volume changes, by modelling the coefficient of thermal expansion as a function of temperature and cooling rate. To model the thermal expansion coefficient they used the graphical relationships between temperature

and dilation pertaining at the relevant cooling rate. The flow stress and the work hardening coefficient were experimentally determined as a function of temperature. No consideration was given to the structure present during the determination of flow stress and work hardening coefficient. Hence, the use made of these results in the thermal stress calculation was sometimes inappropriate. The assumptions made for the effect of maximum cooling rate on the structural changes are treated in an oversimplified way and no attention was paid to CCT diagrams. Sach's boring out technique was used to measure residual stress distributions. The experimental values of residual stress distributions were in good correlation with predicted values (see figure 16) which is surprising in view of obvious omissions in the model.

In later work Inoue et al[67] have like-wise used the Finite Element method to determine the stress developed in a 12%Cr steel cylinder during water quenching. The specimen considered was of high hardenability and completely transformed to martensite. The temperature field was calculated by a Finite Element technique using the Crank-Nicolson method, but the information about the thermal property data used was not given. A heat generation term was used, to incorporate the heat evolved due to the martensite transformation. Strain hardening and the effect of the martensite transformation on the flow stress of the material was taken into account, but no description was provided about the method by which this was done. After hardening, cylinders were tempered and a reduction in residual stresses was obtained, (see figure 17). This was attributed to the viscous flow that occurred during the long time for which the specimen was held at the tempering temperature. The creep strain, as a result of stress relaxation during tempering time was represented as an empirical function of stress, time and temperature. The results of finite element calculations were compared

only with measured stresses at the surface of the cylinder where good agreement was found.

In a recent paper by Inoue et al[26], an investigation was made into the quenching stresses of carburized steel gears quenched in oil at 40°C from a temperature of 800°C. The aim of their investigation was to determine the effect of carburization on thermal stress generation and distribution of martensite during the quenching of steel gears. It was achieved by using carburized and uncarburized gears of 3.05%Ni, 1-0.75%Cr and 0.14%C steel (SNC815) and 0.44%C steel (S45C). The distribution of martensite and residual stresses in carburized and uncarburized gears were compared and it appeared that the two sets of results were very similar except near the edges of the teeth, where less martensite was formed. The information about the martensite distribution was obtained by hardness measurements. The residual stress pattern at the centre in both the cases was nearly the same, but high axial and tangential compressive stresses were predicted near the surface of the carburized gear, whereas, in the uncarburized component the level of these stresses were negligible. Radial stress was absent in both cases. X-ray difraction technique was used to measure the surface axial stress and it was found that both predicted and experimental results coincided in both the cases, see figure 18.

Fujio et al[85] used an elastic-plastic Finite Element method to calculate the stresses developed in a 50 mm diameter cylinder of a 0.45%C steel quenched in water. The transient temperature field within the cylinders was obtained by means of a classical method employing the constant physical properties of the material during the course of the quench. A constant heat transfer coefficient was obtained by comparing the calculated cooling curves with those obtained by experiment. Itteration

was continued until the current value of the heat transfer coefficient gave acceptable agreement between the calculated and measured temperatures. Due to the possibility of transformation products other than martensite, the volume fractions of martensite present at different depths below the surface were determined from hardness measurements. In figure 19, they have shown that, the form of dilatometer curve used to determine dimensional changes in calculation at a point in the specimen, depend on the fraction of martensite present at that point. The flow stress of the material was obtained by interpolation between a single value at high temperature and at room temperature in either the martensite or annealed conditions. A considerable effect of martensitic transformation on the residual stress distribution was observed. They have shown in figure 20, that the predicted stress distributions in the cylinder gave a close correlation with the experimental values, which were obtained using Sach's boring out method.

Fujio et al[86], extended the application of their model to obtain the residual stress distribution in a gear tooth. The temperature profile within the material obtained by the Finite Element technique was used in the subsequent stress and strain calculations. Predicted and experimental values of the distortions and residual stress distributions were in good agreement for the tooth profile, as shown in figure 21, but there were discrepancies between two results relating to diametral change of the cylinder at tip, and the tooth height.

Archambault et al[87,88] investigated the variation of internal stresses developed in aluminium alloy cylinders of 20-120 mm diameter during and after water quenching by the use of a Finite Element technique. In order to achieve the optimum conditions which could increase the strength of quenched components while minimising distortion,

various quenching severities were tested by altering the quenchant temperature, or by applying a conductive coating on the specimen before quenching. It was observed that high quenchant severity (fast cooling) produced more plastic flow, which resulted in large values of residual stresses at the end of the quench. When the severity of quenchant was low (slow cooling) less plastic flow and reduced levels of stresses were produced. Temperature distribution in the specimen during the course of the quench was calculated by an implicit Finite Difference method. At the end of their investigation, the Finite Element method was applied to very complex shapes.

Denis et al[21] have measured the effect of stress on the martensitic transformation, and their results were introduced into a model that calculated internal stresses in a 35 mm diameter, 105 mm long cylinder of tool steel (60NCD11), quenched in water at 20°C. A Finite Element programm MARC was used for stress analysis, with a thermo-elastic-plastic model and an approximation of the temperature dependent flow stress and work hardening parameters. Two effects of stress on the transformation were observed. Firstly, it displaced the Ms temperature to a higher value, secondly, it induced transformation plasticity. The effects were obtained during dilatation tests with various applied stresses and were introduced in the mathematical model by changing the Ms temperature by an appropriate amount and by reducing the apparent yield stress at temperatures just below this point, thus enhancing the plasticity obtained during the transformation. The level of predicted stresses at the surface and the centre was increased by the introduction of these effects. No experimental investigation was carried out in support of the predicted results and the effect of viscous flow on the stress pattern was also ignored.

Later, Denis et al[25] presented the above model with some modifications. Detailed studies were carried out to examine the effect of stress on the transformation interactions. They suggested that transformations are inhibited by the presence of high level hydrostatic stresses, but are promoted by monoaxial stresses (tensile or compressive). The effects were introduced into the model by the use of a positive shift in Ms temperature equal to the shift observed in dilation in the presence of a tensile or compressive stress, and a negative shift in the same property in the presence of high level hydrostatic stresses. Calculations were performed by the Finite Element method to determine the stress history during the quench. The effect of low level hydrostatic stresses was assumed to be negligible, but the effect of transformation plasticity was introduced as an additional strain. Calculated stresses were compared with those obtained experimentally by the use of Sach's method in the axial direction only. Experimental results are in reasonably good agreement with the calculated results when transformation interactions between stress and temperature are included, see figure 22.

Yu et al[89] have made a study of the generation of thermal stress during the quenching of steel cylinders, with and without transformation effects. They used a Finite Element programm for the calculation of both the temperature profile and the stress distribution in the specimen during the quenching process. All the physical and mechanical property data used was temperature dependent, but no information was provided in their paper about the source of this data. However, TTT diagrams for the materials investigated have been used to model the structural changes during the heat treatment process. A 50 mm diameter cylinder at a temperature of 600^{o}C was quenched in water at 0^{o}C with no consideration of phase changes. In addition, a 10 mm

diameter cylinder austenitised at 850°C for half an hour quenched in water at 20°C, was considered: this time transformation effects were included in the calculations. In this case, the structure transformed completely to martensite except in the centre of the specimen where 10% of the material transformed to phases other than martensite. In the case where no transformation occurred the calculation predicted compressive residual stresses at the surface and tensile stresses at the centre in the axial direction. These predicted residual stresses were reversed when transformation effects were taken into account. This Finite Element model was also applied to a butt welded axisymmetrical ring of plain carbon steel, and the state of stress in and near the weld was calculated. Experimental measurements of the residual stresses were made in the case of the welding process only by the x-ray diffraction technique and good agreement was observed between experimental and calculated results. Doubt may be expressed about the correlation between the experimental and the calculated results as the model used in the calculations did not consider the effect of viscous processes. In fact, the influence of viscous flow on the generation of stress and strain in welding process has been found to be significant[43]. Another drawback of the model used by Yu **et al** was the absence of any consideration of transformation plasticity.

Sjöström[34,90] has produced a mathematical model of the stress generation process based on Finite Element techniques whereas, for the temperature distribution Finite Difference methods has been used. The model includes transformation plasticity as well as isotropic and kinematic hardening effects. All the physical and mechanical properties used were temperature dependent and non-martensitic transformations have also been considered. Three steels (SA 1050, SIS 2511 and Ni steel with

various weight percentage of Ni) were investigated and the geometry of the specimen was cylindrical; the dimensions and quenchant have been chosen in such a way that direct comparison was possible with the experimental results available in the literature. This was necessary because Sjöström did not perform any experimental measurements of thermal stress. The results obtained from Sjöström's model indicated a significant level of discrepancy with experimental results obtained by others, but the inclusion of transformation plasticity has reduced this discrepancy. The calculated residual stresses at the surface in the axial direction were compressive. The level of these stresses fell in the interior of the specimen and finally they were reversed towards the centre. Hence, a maximum compressive stress at the surface and a maximum tensile stress in the centre were predicted. Sjöström has also examined the effect of the degree of memory of plastic history in the earlier stages of the quench on the stress generation process. He suggested a complete loss of this memory in the case of kinematic hardening and no loss in case of isotropic hardening. No experimental evidence of such a memory effect has been mentioned and the effect of viscous flow on the stress generation process was also not taken into consideration.

Boyer and Bovin[48] used a numerical method of elastic-plastic stress analysis to study the quenching of stainless steel and aluminium alloy infinite plates in water and air. It was assumed that the material was homogeneous, isotropic and single phase throughout the treatment. The mechanical and thermal properties used were temperature dependent, but the surface heat transfer coefficient was calculated for a series of time intervals and was considered as constant during that interval irrespective of the temperature change. The variation of mechanical properties with temperature, used in the model is shown in

figure 23. The surface heat transfer coefficient has been considered as time dependent instead of temperature dependent: furthermore the effect of transformation on the stress generation has been ignored and unverified assumptions were taken to incorporate stress relaxation effects in the model. Therefore, the results obtained from such a model can not be fully accepted. However, the authors have found good agreement between the calculated and experimental results, when the latter was obtained by the layer removal method with an electro chemical process.

Kamamoto et al[79] described a computer programm based on the Finite Element technique, developed for analysis of the quenching of large scale low alloy steel shafts with a diameter of 1310 mm. The model was used to calculate the complete stress history and the effect of transformation on the residual stress and distortions, during cooling of a shaft sprayed by water. The steel selected for investigation was transformed to bainite by the end of the quench. Heat generated during the transformation has been included in the temperature calculations, although the effect of such heat on the stress generation process was largely avoided by assuming very small amounts of such heat. Physical and mechanical properties used as input data for the model were considered temperature dependent, but no relations between these properties and temperature were given. Experimental investigations were carried out to obtain the values of the strain hardening coefficient and the yield strength of material only and no measurements of residual stress and strain were made. The effect of transformation on the generation of stress was small in comparison to the corresponding effect on strain. In figure 24, it has been indicated that transformation only affected the stress history at the beginning of transformation and

at the end of the process. A tensile stress in the centre and a compressive stress at the surface was predicted in both the cases considered, i.e. both, with and without transformation. The effect of transformation on the distortion is shown in figure 25. The intensity of the transient and residual strain was increased when the effect of transformation was introduced in the model. At the end of the quench, the residual strain in the axial and radial directions at the surface was 5.2×10^{-3} and -2.6×10^{-3} respectively when transformation was taken into account, but it was only 0.4×10^{-3} and -0.2×10^{-3} respectively if no transformation occurred. Hence it was predicted that residual stresses and distortions are strongly related to the transformation behaviour of the material. A doubt can be thrown on the results, as the effect of viscous flow has been ignored. It is very important here, as the shafts were cooled for a long time, and were subjected to various stress levels at high temperatures; all these conditions are quite sufficient for viscous flow to occur.

Mitter et al [80] have calculated, and experimentally measured the residual stresses developed in 50 mm diameter, 300 mm long pure iron cylinders quenched in ice water from 850°C. The stress analysis was effected by the use of the Finite Element method assuming plane-strain conditions. Experimental analysis was carried out by the boring-turning method, assuming pure elastic strain changes during this operation. Many of the thermal and mechanical properties used in the mathematical model were determined experimentally as a function of temperature, but thermal conductivity, specific heat and density values were taken from the literature. Cooling curves were obtained experimentally by setting thermocouples at the surface and centre of the specimen. These cooling curves were used as boundary conditions for calculations of temperature

history throughout the quenching process. This data was then used in the thermal stress and strain calculation. The calculated and the experiment results were compared, but the results differed significantly from one another. It was suggested that the reason for the difference was unwanted plastic deformation induced during measurement of the residual stresses which violates the assumption of elasticity on which these results were based. It should be pointed out that Mitter's material was very weak, so plastic deformation was possible at very low stresses. It may, therefore, not be applicable to harder carbon-containing steels.

Jeanmart and Bouvaist[68], performed Finite Element calculations for predicting thermal stress in aluminium alloy plates 70 mm thick, which had been quenched either in hot or cold water. Temperature gradients in the material were calculated by the Finite Element technique, thermomechanical problem was assumed to be uncoupled, and isotropic behaviour and temperature dependent properties were assumed. Some of the properties were determined experimentally; although the majority of the data was taken from the literature. However, no information about surface heat transfer coefficients has been described. The plate model and the assumptions were the same as those of Fletcher[63], except that 18 elements in the half thickness of plate were considered instead of 41. The flow stress considered was related to the strain history of the material. Tensile stresses at the centre and compressive stresses at the surface were predicted, but the level of stresses was higher for cold than hot water, as this was due to the high surface heat transfer coefficients for the former, which produced high plastic flow. The calculated results were checked experimentally, using the same experimental technique as adapted by Fletcher and Price[18,30]. Matching of the two sets of results (theoretical and experimental)

showed good agreement in the case of both the quenching conditions, see Figure 26.

2.7 Residual Stress and Strain Measurements

The measurement of residual stress is slow and difficult and requires great care if it is to be successful[7]. The accurate measurement of distortion is similarly a slow and laborious process and depends on the geometry of the component[12]. There are many reports of different experimental investigations of residual stress and strain measurement, which are reviewed below.

2.7.1 Residual Stress Measurements

There are two major techniques available for the measurement of residual stresses, namely mechanical and x-ray methods. Although, electrolyte and chemical etching, ultrasonic and hardness testing have been proposed for the determination of residual stresses, they all suffer from considerable limitations, which hinder their extensive use. Hence, in the present review reference is only made to the most widely used techniques.

2.7.1.1 Mechanical Methods

When an internal stress is removed from a part of a component the remaining internal stresses are redistributed within the body, to reestablish equilibrium. This causes a change in the dimensions of the component, the measurement of which allows the determination of the internal stress that has been removed. Such mechanical methods are destructive, involve only macro stresses and assume that the redistribution of stresses does not produce plastic flow. The removal of the stress may involve the complete destruction of the material that contains the internal stress by boring or grinding or else the stress

may be relieved by cutting. The boring or grinding techniques require the use of a strain gauge rosette at an appropriate point in the remaining structure, to measure the consequent surface displacement. It is essential that the metal removal process does not induce significant additional stresses or that the material is significantly hotter than ambient at the time the strain measurements are made.

The longitudinal, radial and tangential stress distribution along a radius can be determined by removing layers from the bore or from the surface. The method is also known as Sach's boring out method. In case of boring out procedures, the material is removed from the bore and strain changes are measured on the surface, preferably with strain gauges. In the case of turning, strain measurements are made on the inside bore and material is removed from the outer surface.

The precision of the boring and turning procedure is largely determined by the accuracy of the measurement of strain changes and the care taken in the layer removal techniques. It is also important to eliminate temperature gradients in the specimen and to maintain a constant temperature each time the strain readings are obtained. The length of the specimen should be more than three times its diameter.

Many workers have adapted boring and turning technique for experimental investigations[80,91-95]. Buhler and Buckholtz[91,92] conducted the earliest investigations that involved the Sach's boring out method. Work was carried out on plain carbon steel cylinders of various diameters and carbon content quenched in water and air. It was found that the radial stress varied in a complex manner with radial depth and a reduction in the maximum residual stress was achieved by replacement of a water quench by air cooling. In later work they measured residual

stresses by boring and turning procedure in hollow cylinders of 0.3%C steel.

Buhler and Rose[93] have also used Sach's method for experimental investigations of residual stresses in steel cylinders of different diameters and compositions. Their results from low alloy [0.13%C] high hardenability steel cylinders showed that an increase in the diameter or quench severity alter the nature of surface stress from tensile to compressive (see figure 27). But in the case of steel cylinders with carbon of 0.26% or more have only compressive surface stress which became more compressive as the diameter or quench severity is increased.

Recently Mitter et al[80] have used the boring and turning process to measure residual stresses in a 50 mm diameter pure iron cylinders that had been quenched in water. In order to check the accuracy of the experimental results, the experimental procedure was simulated using the Finite Element method. Stress distribution after each boring or turning step was calculated and compared to the experimental results for the corresponding boring or turning step. A comparison of the two results (experimental and calculated) showed discrepancies which were explained as being due to unwanted plastic deformations during the process. Therefore, the assumption of a pure elastic condition during the metal removal process was unreliable. However, the work of Price[18] and Abbasi[41] has shown that the induced stresses due to material removal were negligible. Abbasi[41] checked the level of induced stresses due to material removal by grinding a stress-free plate, and he found that experimental stresses induced were negligible. The discrepancy of the results with those of Mitter et al[80] is probably due to the low yield strength of the material used by the latter. Denis et al[25] and Fujio et al[86] checked their calculated results by comparison with

measured results obtained by Sach's boring out method and found good agreement.

The layer removal process is also useful for measuring residual stresses in flat plates or beams in which the stress varies through the thickness. The stress in a layer is determined by removing that layer and measuring the strain change in the remaining part. The thickness of the layer removed depends on the magnitude of the stress, the size of the component and the precision required. Preferrably the minimum possible should be used.

The published work in the field is small as few authors[18,30,41,68] have mentioned the layer removal method with respect to their investigations of residual thermal stresses in plates. The method proposed by Andrews[7] has been used by Price and Fletcher[18,30] to examine quenched 835M30 steel plates that had been quenched in water, oil and polymer. The level of agreement with those predicted by calculations was variable. In subsequent work Abbasi[41] followed the same procedure for oil and martempered plates. He also tested the reliability of the procedure by investigation of experimentally induced stresses in a stress_free plate: a negligible amount of stress was induced by the metal removal technique.

Recently Jeanmart and Bouvaist[68], used the layer removal method for measuring residual thermal stresses in aluminium alloy plates quenched in hot and cold water. Their experimental results were in satisfactory correlation with those obtained by calculation.

Beside the two above mentioned methods, several other mechanical methods (such as; centre hole drilling technique, sectioning, cutting deflection and chemical removal of material) have been developed for

different shapes and measurement requirements. However, they have not been much used to compare experimental and calculated residual stresses. They are therefore not disucssed here.

2.7.1.2 X-Ray Methods

There are several reviews[7,96-99] of the theoretical and practical aspects of residual stress measurements by x-ray techniques. If a metal is deformed the lattice planes become distorted. The change in the lattice parameter is determined by a back deflection technique; which is then used to calculate strain. From a knowledge of the strain, the stress may be calculated by the use of the elastic constants of the material. A single exposure method, where the x-ray beam is normal to the specimen surface, is used to determine the sum of the principal stresses[7]. However, if the magnitudes of individual principal stresses are required the two exposure method must be used[96]. In this technique two exposures are made. First, with the x-ray beam normal to the specimen surface and the second one with the beam at an oblique angle to the specimen surface. This technique is designed for the measurement of macro residual stresses but micro residual stresses can also be detected. It only measures surface stresses because, x-ray penetration is of the order 0.02 mm, but it is a completely non-destructive method. If the stress is to be measured at some point below the surface, material must be removed down to that point to expose a new surface for x-ray examination; the x-ray method then becomes destructive.

Nakagawa and Tamura[97] used the x-ray technique to measure the residual stresses in the surface of water and oil quenched 20 mm thick, 50 mm square plates of plain carbon steel containing 0.08% to 1.0% carbon. Compressive surface stress was found in the steels containing up to 0.5%C. The level of stress was increased as the carbon content falls

from 0.5% to 0.08%. In steels containing more than 0.5% carbon the reverse behaviour was observed. They also used oil and water quenched low alloy steel plates of various carbon contents for their investigations, and in this case only tensile surface stresses were observed, irrespective of the quenched severity and carbon content.

Yu and Macherauch[89] have conducted an x-ray examination of a welded plain carbon steel ring, to determine the residual stress at the surface of the weld. A good correlation was found between their experimental and calculated results.

Recently, x-ray difraction techniques was used by Inoue et al[26], to measure the surface axial stress in carburized and uncarburized gears. Experimentally measured surface axial stresses in both the cases were in good agreement with that obtained theoretically.

Wenyu and Yohai[95] used x-ray techniques to measure residual stresses along a shaft diameter. After quenching the cylindrical surface of the shaft was removed layer after layer and the residual stresses in the newly exposed surfaces were measured successively. The layer removal process involved grinding followed by electric etching in order to eliminate grinding stresses.

In order to verify his calculated results Burnett[99] has measured residual stresses in carburized steel cylinders by x-ray diffraction methods. The material used for the experimental work was a 0.18%C steel before carburization. Oil and water were used as quenching media. In both cases a tangential compressive stress was found at the surface, which rose to a maximum at a depth of 0.0125 mm where the carbon was 0.5%. Measured stress values compared favourably to those calculated by the Finite Element method for both the quenchants (see figure 28).

2.7.2 Residual Strain Measurements

In addition to the development of thermal stresses and quench cracking, a quenching operation will also cause an overall geometrical distortion in the quenched components. These distortions are categorized into three types[15,100].

(i) Volume change.

(ii) Symmetrical changes involving modifications to the sectional profile.

(iii) Non-symmetrical change, such as warpage.

The volume changes are associated with transformation of the structure in the absence of a temperature gradient, but the remaining two are mainly due to thermal stresses.

Fletcher and Price and Abbasi[18,30,41] carried out distortion measurements on water and oil quenched and martempered plates, using a Societe Genvoise machine. Pre and post quenching measurements were made across the edges of the plate and lateral distortion was given by:

$$\%\Delta Y = \frac{Y_h - Y_s}{Y_s} \times 100$$

Measurements by this method are known to be affected by stress variation in the vicinity of the edge. By measuring the thickness of the plates between the centre of the faces, the average strain could be accurately determined. The plate profile after quenching also indicated the magnitude of the edge effect.

Liewellyn and Cook[101] have studied the distortions that occurred in the heat treatment of carburized components. In their investigations washer-like specimens made from various carburized steels were used.

The specimens were subjected to a carburising treatment followed by air cooling or water quenching or oil quenching. Variations in the dimensions were obtained by the use of the same procedure and equipment that were used by Fletcher and Price and Abbasi[18,30,41]. The dimensional change in any steel that occurred after air cooling was very small but after water quenching significant variations were observed. Whereas those produced by oil quenching were intermediate. They also recognised that the hardenability and the composition of the steel have a marked effect on distortions.

Novik et al[102], measured the distortion of rings of different shapes and sizes of a low alloy steel that had been quenched from 850°C into oil. They reported that distortions of rings were mainly dependent on the dimensions of the specimens. Thelning[12] has reported measured distortions in heat treated engineering components and the variation in distortional behaviour of material. He also reported the importance of the same factors, i.e. the size and shape of component.

Variation in the dimensions of gears, after heat treatment is a common problem in the automobile industry. Consequently a large amount of empirical work has been carried out on gear distortions[85,86,103]. The work of Fujio et al[85,86] on the distortion of gear teeth deserve special mention because it was associated with calculations of the thermal stress generated during the quench. Initially, they worked with cylindrical specimens[85], but later they applied their technique to distortions in gear teeth[86]. Measured distortions were compared with calculated results and discrepancies were found between the two results in the case of both the diametral change of the cylinder at the tip and the tooth height.

In more recent work Fujio[103] investigated the way in which spur gear distortions depend on the material and the criterion used to define gear distortion. Gears of different sizes and different materials were hardened by various heat treatment processes, and the effect of material, size and the conditions of heat treatment, on the gear distortions were studied. Dilation tests were carried out to investigate the influence of retained austenite on the dimensional change. It was predicted that the distortion produced by retained austenite was small, but gear distortion was related to the hardenability of material. The change in tip cylinder diameter was dependent on the face width and the material of the gear (see figure 29).

2.8 Conclusion from the Review of the Previous Work

Most effort has been concentrated in recent years on the development of modelling of the thermal stress generation process during quenching. In the early stages, some attempts had been made to calculate thermal stress and strain by classical calculus methods, using dubious assumptions concerning the thermal property data of the material and the quenching medium. An over simplified model used in the prediction of temperature distribution and stress-strain calculation, reduced the value of the results, as such equations did not allow the use of temperature dependent property data. The majority of the authors considered only elastic deformations during thermal stress generation. Few of the results obtained from such classical calculations had been correlated with experimental results, but some of these comparison related only to stresses at the surfaces of the components.

The subsequent introduction of mathematical models based on numerical analysis of thermal stress and strain allowed the use of temperature

dependent physical and mechanical property data. The use of accurate temperature distribution and thermal and mechanical property data, the introduction of plastic deformation and the phase transformation effect in the thermal stress and strain analysis improved the reliability of the results, but there remain some significant properties that have been ignored.

Two important aspects of the thermal stress generation process, viscous flow and transformation plasticity have been introduced very recently. Few authors[22,41,48] attempted to incorporate viscous flow effects in their models, which significantly improved the modelling of thermal stress generation process. However, viscous flow has been little studied in relation to stress and strain generation during quenching. There is obviously a need for more data on this topic.

In recent work[23,25,41,90] transformation plasticity has been introduced in the mathematical models of the thermal stress generation process. In some cases a significant improvement in the results has been observed, whereas some models did not show the importance of this effect. It is because the theory of transformation plasticity has not yet been fully developed and every author tried to handle the situation in its own way. The mechanism of transformation plasticity has not studied on metallurgical grounds.

The greater part of the development of the models has used experimental data from water quenched specimens to verify the model. Oil quenching is far more extensive commercially used and it would be interesting to know whether, the calculations can be equally well applied in the case of slower cooling rates. The work carried out on the prediction of distortion is very small, whereas this is too commercially important and difficult to carry out accurately by experiment.

3. VISCOELASTIC PROCESSES

3.1 Experimental Determination of Viscoelastic Process Effects

3.1.1 Experimental Method

This set of experiments is divided into three groups: firstly those that used the same test conditions as had been used in previous work by Abbasi[41], secondly those that investigated the effect of prior deformation on the rate of stress relaxation and thirdly those that investigated the effect of initial stress level on the stress relaxation behaviour of the material.

(a) Stress Relaxation Tests with one Stress at each Temperature

An Instron tensile testing machine was used to carry out the stress relaxation tests. The original arrangement of the machine limited the level of temperature obtainable, so a resistance wound furnace was installed on the front pannel, as shown in plate 1. The furnace used was moveable in two directions (i.e. vertically and horizontally) to facilitate the location of the hot zone of the furnace and the insertion of the specimen into the grips.

A cylindrical screw-end tensile specimen was inserted into the grips at a point between the load cell and a moving cross head. The readings from the load cell were recorded automatically on a chart recorder. The strain rate was controlled by the speed of the cross head, which would be varied from 0.005 cm/min to 50 cm/min. All tests were carried out at the cross head speed of 0.5 cm/min i.e. at the strain rate of $3.3014 \times 10^{-3} s^{-1}$, which was within the limits of strain rate noted during the quenching experiments of Price[18] and Fletcher[63].

In order to control the specimen temperature and to compensate for the heat losses, the furnace was coupled to a variable transformer and

was packed with Kaol wool at the top and bottom. Before starting the tests, the furnace was calibrated to obtain both the location of the hot zone in the furnace and the position of the thermocouple to give optimum transformer control. The time required to heat the furnace to the desired temperature was also obtained. The hot zone was located by moving the furnace up and down when the specimen was in position. The relationship between temperature and the transformer control position and also the heating curve of the furnace with the furnace fixed at the desired position, are shown in figures 30 and 31.

A cylindrical tensile specimen with screw threads as shown in figure 32, was selected from BS 3500. The specimen was coated with a solution of Berkatekt 304 in trichloro-ethane to prevent oxidation of the surface while at high temperature. To verify the oxidation protective capacity of the Berkatekt, metallographic inspection of the surface of the specimen was carried out after conducting the first test on the Berkatekt coated specimen. In plate 2, the result of metallographic inspection is shown and it is evident from this plate that no traces of surface oxidation are present in the surface of the specimen. Therefore, Berkatekt was found to be a satisfactory coating.

The specimen screwed between the grips was austenitised for 15 minutes at 850^{o}C in the furnace mounted on the Instron machine. A Chromel-Alumel thermocouple was attached to the specimen surface to monitor the specimen temperature. A temperature variation of $\pm$ 5^{o}C was observed at 850^{o}C, which was within the specified British Standard[104]. After completion of the austenitisation of the specimen, it was cooled to the test temperature by a stream of argon at ambient. In order to avoid the possibility of transformation of the austenite to bainite during this process, a cooling rate of about 30^{o}C/second was used.

This allowed the specimen to cool from 850°C to 150°C in 24 seconds, which was within the limits required to prevent decomposition to anything other than martensite, (see figure 33). The current in the furnace windings was reduced to that required at the test temperature. Although it was possible to cool the specimen to the test temperature very quickly by the use of the stream of argon, the furnace and grips cooled much more slowly. Therefore, once the specimen temperature had fallen to the required value the gas stream was directed towards the hotter parts of the assembly. Even so, it took up to 15 minutes to produce the required temperature distribution in the furnace when the lowest test temperature (150°C) was used. At high temperatures when the decomposition of the austenite by non-martensitic transformation was possible stabilisation was achieved in a much shorter time (4 minutes) which was sufficiently short to avoid spurious transformations.

Another difficulty during the heating and cooling process was the loading of the specimen. This was overcome by adjusting the cross head throughout the heating and cooling process, so that no load was generated on the specimen at any time.

After cooling to the test temperature, the specimen was stressed to the desired level at the specified strain rate, after which the strain was held constant. This was achieved by maintaining the cross head of the Instron machine at a fixed point. The reduction in the stress with time was recorded by the chart recorder. The stress data obtained was then expressed as a fraction of the initial stress i.e. $\sigma t/\sigma^{o}$.

Using the arrangements described above, stress relaxation tests were conducted at temperatures in the range between 850°C and 150°C. The hard martensite formed by rapid cooling to below 150°C, reduced the

stress relaxation rate to a negligible level and a test carried out below 100°C resulted in the brittle fracture of the specimen.

Every test was conducted 2 to 3 times to verify the results and to check the reproducibility of tests. The results obtained showed minor variations which were insignificant.

(b) Effect of Strain Hardening on the Stress Relaxation Process

In the first set of stress relaxation tests the specimens used were free of any deformation prior to the application of the load at the start of the test. However, in quenched plates the rate of stress relaxation might be affected by plastic deformation introduced in the early stages of the quench. To investigate the effect of such deformation, an appropriate amount of strain (0.5%) was introduced at various temperatures above that at which the stress relaxation tests were to be carried out. The same cooling procedure was used as in the original stress relaxation tests, both to obtain the intermediate temperature at which the initial deformation was to be introduced and to cool the specimen to the test temperature. The load was removed after the introduction of the plastic flow and then reapplied at the start of the stress relaxation test.

(c) Influence of Initial Stress on Stress Relaxation

There is coupling between the stress generated during quenching and the amount of viscous flow introduced by this stress. This arises because the flow causes stress relaxation, which in turn reduces the rate at which flow can occur. This means that it is not possible to predict from calculations that ignore viscous flow the appropriate initial stresses to be used in the stress relaxation tests. It is therefore necessary to carry out stress relaxation tests with a range of initial

stresses at each temperature, so that the effect of initial stress on the stress relaxation characteristics may be introduced into the calculations of thermal stress and strain. At least three different levels of initial stress have been used at each temperature, although the specific levels selected varied with temperature. This was necessary, because the flow stress of the material also varied with temperature and there was a general correspondence between the effect of temperature on stress relaxation rate and the effect of the same factor on yield strength. The procedure used for these tests was the same as that described in section 3.1.1(a).

3.1.2 Results of the Stress Relaxation Tests

(a) Results of the Stress Relaxation Tests with One Initial Stress at each Temperature

Earlier work[22,41], which involved only a single initial stress at each temperature, was first checked by the use of repeat tests using identical test conditions (figure 34). Broad agreement with the earlier work was obtained except at 850°C. A constant rate of stress relaxation was observed after 24 seconds in all the tests, although this rate increased as the test temperature rose. Likewise the stress relaxation rate at the start of the test increased as the temperature increased. At 850°C the stress level reduced to 75% of its initial value after 3 seconds, but during the same time interval, it reduced to only 98% of its initial value at a temperature of 150°C.

(b) Results of Stress Relaxation Tests Considering the Previous History of the Specimen

The stress relaxation characteristics were investigated at temperatures of 400°C, 250°C, 225°C, 200°C, 175°C and 150°C by the procedure described in section 3.1.1(b). The prior deformation of these

specimens was carried out at temperatures of either 600°C or 400°C. All the results show an insignificant effect of the prior deformation up to 0.5% on the stress relaxation behaviour of 835M30 steel, figures 35a and 35b.

(c) Results of Stress Relaxation Tests Considering the Influence of Initial Stress

The results obtained from the stress relaxation tests described in section 3.1.1(c) are presented in figures 36(I-X). All the results showed a significant effect of initial stress level on the rate of stress relaxation. However, the stress relaxation rate at a particular time and with a particular initial stress level was also affected by the test temperature. Similarly, by comparing the results of two tests conducted at the same temperature but at different initial stress levels, it is seen that the higher the initial stress the higher was the stress relaxation rate and vise-versa. It was also evident that at the lower end of the test temperature range a threshold stress existed below which stress relaxation did not occur. This threshold stress decreased with increase in temperature (i.e. 270 MPa at 150°C and 10 MPa at 500°C).

3.2 Theoretical Model to Calculate the Viscoelastic Behaviour of 835M30 Steel

Metallic material stressed at levels below the yield stress at high temperatures exhibit both viscous and elastic behaviour. In the presence of both these effects a complex relationship between stress and strain occurs. The nature of this relationship may be represented by simple mechanical models composed of springs and dashpots[40], which are arranged in such a way that the model approximates to the observed mechanical behaviour of the real material. Three such models are shown in figure 37.

The mechanical models shown in figure 37 are extensively used to represent the viscous and elastic behaviour of metals and alloys. All the three models have been analysed to simulate the viscous behaviour of 835M30 steel and the Standard Linear Solid has been found to give the best agreement with the experimental results[22].

3.2.1 The Standard Linear Solid

The Standard Linear Solid is a three element model which contains the features of both the Kelvin and Maxwell model (compare figures 37a, 37b and 37c). One arm contains a perfectly elastic spring to simulate elastic deformation and a dashpot consisting of a perforated piston moving in a cylinder containing a viscous fluid, to simulate inelastic behaviour, while a second contains only a spring. The combination of spring and dashpot in the first arm allows stress relaxation to occur by the replacement of the elastic strain in the spring by viscous strain in the dashpot. The process is partially restricted by the spring in the second arm, and the stress relaxation process ceases at some finite level of stress in the same way as was observed during the experimental investigations of stress relaxation.

3.2.2 Theoretical Equations Representing Viscous Processes, Derived from the Behaviour of Standard Linear Solid

From the Standard Linear Solid, the relationship between stress and strain in terms of the stress and strain tensors have been suggested by Boley and Weiner[40] to be:

$$\dot{e}IJ + \phi eIJ = \frac{\dot{S}IJ}{2G} + \frac{SIJ}{2\eta} \qquad \ldots\ldots 3.2.1$$

But for unaxial conditions, equation 3.2.1 can be written as:

$$\dot{e}xx + \phi exx = \frac{\dot{S}xx}{2G} + \frac{Sxx}{2\eta} \qquad \ldots\ldots 3.2.2$$

The mean stress and strain, and the deviatric stress and strain tensors are given as:

$$\sigma m = \frac{\sigma IJ}{3}$$

$$\varepsilon m = \frac{\varepsilon IJ}{3}$$

$$SIJ = \sigma IJ - \delta IJ\ \sigma m$$

$$eIJ = \varepsilon IJ - \delta IJ\ \varepsilon m$$

And for Uniaxial conditions these equations can be written as:

$$\sigma m = \frac{\sigma xx}{3} \qquad \text{..... 3.2.3}$$

$$\varepsilon m = \frac{(1-2\nu)}{3} \varepsilon xx \qquad \text{..... 3.2.4}$$

$$Sxx = \sigma xx - \sigma m \qquad \text{..... 3.2.5}$$

$$exx = \varepsilon xx - \varepsilon m \qquad \text{..... 3.2.6}$$

Equations 3.2.5 and 3.2.6 can be rearranged as:

$$Sxx = \sigma xx - \frac{\sigma xx}{3} \qquad \text{..... 3.2.7}$$

$$exx = \varepsilon xx - \frac{(1-2\nu)}{3} \varepsilon xx \qquad \text{..... 3.2.8}$$

Similarly,

$$\dot{S}xx = \dot{\sigma}xx - \frac{\dot{\sigma}xx}{3} \qquad \text{..... 3.2.9}$$

$$\dot{e}xx = \dot{\varepsilon}xx - \frac{(1-2\nu)}{3}\ \dot{\varepsilon}xx \qquad \text{..... 3.2.10}$$

By substituting values in equation 3.2.2, the resulting equation will be:

$$\dot{\varepsilon}xx + \phi\varepsilon xx = \frac{\dot{\sigma}xx}{2G\ (1+\nu)} + \frac{\sigma xx}{2\eta\ (1+\nu)} \qquad \text{..... 3.2.11}$$

From the above equations, the following two expressions were derived (Appendix I) for stress relaxation and creep strain under uniaxial conditions:

$$\frac{\sigma t}{\sigma o} = (1-A)\ \text{Exp}\ (-Bt) + A \qquad \ldots\ldots\ 3.2.12$$

$$\varepsilon(\text{creep}) = \frac{\sigma^{o}}{E}\ (\frac{1}{A} - 1)[1-\text{Exp}(-\phi t)] \qquad \ldots\ldots\ 3.2.13$$

Where A and B are parameters containing various material properties viz:

$$A = \frac{2\phi\eta\ (1+\nu)}{E} \quad \text{and} \quad B = \frac{G}{\eta}$$

The values of the parameters A and B have been chosen (see table 2) to give the best possible fit with the experimental curves. However, both these constants can be determined experimentally by an independent experimental determination of material properties η, E, ν and G whereas ϕ can be revised at will to obtain the required fit.

3.2.3 The Calculation of the Stress Relaxation Behaviour of 835M30 Steel

Although the experimental stress relaxation data can be used directly on a purely empirical basis, this is inconvenient since the stress and temperature vary continuously. Therefore, the Standard Linear Solid has been used to represent the stress relaxation process, but with the factors A and B in equations 3.2.12 and 3.2.13 as functions of both initial stress and temperature. This procedure has the added advantage that the information obtained can be used also to determine the associated viscous strain.

It is evident that the values of A and B lie between 1 and O and both are linear functions of temperature (see figure 38). Value of A for each curve is equal to the limiting stress ($\sigma t/\sigma^{o}$) attained during the stress relaxation test, while the value of the parameter B governs the rate of decay and the shape of curve. Therefore, for low temperatures, values of A are high and the corresponding values of B are low. As the

temperature increase, the limiting stress will decrease, whereas the rate of decay will increase.

It is evident from figure 36 that the level of initial stress has a very significant effect on the rate of stress relaxation. In order to take full account of this effect in the calculations, the parameters A and B of the Standard Linear Solid equations 3.2.12 and 3.2.13 have been fitted to the stress relaxation curves (figure 36) throughout the temperature range under consideration. The values of A and B at each temperature can be fitted to a linear relationship with initial stress, but this was based on only three results for each case. Nevertheless, it did provide the necessary interpolation between stress levels with a reasonable level of accuracy (figure 39). The regression equations for both temperature and initial stress are:

$\theta > 800^{o}C$

$$A = 0.769578 - 5.566694 \times 10^{-3}\sigma^{o}$$

$$B = 2.568512 \times 10^{-3}\sigma^{o} + 0.153036$$

$800^{o}C \leqslant \theta > 700^{o}C$

$$A = 0.7643788 - 2.360563 \times 10^{-3}\sigma^{o}$$

$$B = 2.187736 \times 10^{-3}\sigma^{o} + 0.1082211$$

$700^{o}C \leqslant \theta > 600^{o}C$

$$A = 1.02354 - 5.190969 \times 10^{-3}\sigma^{o}$$

$$B = 4.362874 \times 10^{-3}\sigma^{o} + 3.95996 \times 10^{-2}$$

$600^{o}C \leqslant \theta > 500^{o}C$

$$A = 1.023954 - 3.588758 \times 10^{-3}\sigma^{o}$$

$$B = 1.979367 \times 10^{-3}\sigma^{o} + 0.1613068$$

$500^{o}C \leqslant \theta > 400^{o}C$

$$A = 1.026924 - 2.674023 \times 10^{-3}\sigma^{o}$$

$$B = 1.377904 \times 10^{-3}\sigma^{o} + 3.542605 \times 10^{-2}$$

$400^{\circ}C \leqslant \theta > 300^{\circ}C$

$$A = 1.032454 - 1.086488 \times 10^{-3}\sigma^{\circ}$$

$$B = 1.544713 \times 10^{-3}\sigma^{\circ} + 4.004329 \times 10^{-3}$$

$300^{\circ}C \leqslant \theta > 250^{\circ}C$

$$A = 1.044971 - 1.161335 \times 10^{-3}\sigma^{\circ}$$

$$B = 8.940692 \times 10^{-4}\sigma^{\circ} + 1.815382 \times 10^{-2}$$

$250^{\circ}C \leqslant \theta > 200^{\circ}C$

$$A = 1.008907 - 1.597031 \times 10^{-4}\sigma^{\circ}$$

$$B = 9.268924 \times 10^{-5}\sigma^{\circ} + 5.748372 \times 10^{-2}$$

$200^{\circ}C \leqslant \theta > 150^{\circ}C$

$$A = 1.026407 - 1.428195 \times 10^{-5}\sigma^{\circ}$$

$$B = 1.334527 \times 10^{-4}\sigma^{\circ} + 9.704584 \times 10^{-2}$$

$\theta \leqslant 150^{\circ}C$

$$A = 1.025554 - 9.759142 \times 10^{-5}\sigma^{\circ}$$

$$B = 2.465597 \times 10^{-4}\sigma^{\circ} - 4.123284 \times 10^{-2}$$

A set of stress relaxation curves was obtained by putting these values in the theoretical equation derived from Standard Linear Solid. Figure 40 shows a comparison of predicted stress relaxation curves with those obtained experimentally. The results were in a very good agreement at low temperatures, but at high temperature a small discrepancy between the two sets of results was observed. It is the values of stress relaxation obtained from the use of equation 3.2.12, by the use of these values of A and B and the associated viscous strain that has been used to represent viscous effects in the mathematical model of stress and strain generation during quenching (see Chapter 4).

4. THE DEVELOPMENT OF A MATHEMATICAL MODEL OF THE STRESS AND STRAIN GENERATION PROCESS DURING THE COOLING OF 835M30 STEEL IN QUENCHANTS WITH A RANGE OF QUENCHING POWERS

The calculation of thermal stress and strain was carried out by a technique based on the method described by Fletcher and Price[30,63]. This involved the use of an infinite plate model with unidirectional heat flow. The flow of heat was considered in a direction perpendicular to the longitudinal plane of the plate, (see figure 41), which allowed the assumption of plane-stress conditions with two equal principal stresses acting in direction parallel to the longitudinal plane of the plate. For the calculations of the temperature distribution between the surface and the mid-plane of the plate, the half thickness of the object was divided into 40 elements whereas, in the subsequent thermal stress and strain calculation the same space was represented by 10 elements. The temperature in an element used for the stress and strain calculations was the average temperature of the four small elements of which that element was composed. The time required for the complete quenching process was divided into a series of small time steps. The duration of the time interval was determined by assuming a change in Fourier Number equal to 0.5. This assumption gave a value of the time increment which was small enough to ensure the stability and accuracy of the results[30]. Thermal stress and strain was calculated after each time increment by using the following steps.

(I) Determination of the temperature profile through the thickness of the plate during each time interval, by an explicit Finite Difference technique.

(II) Determination of the change in thermal strain introduced in each element during each time step.

(III) Calculation of the elastic thermal stress associated with the thermal strain increment in stage II, assuming no restraint at the edges of the plate and elastic conditions in the material, (i.e. there is a zero net force boundary condition).

(IV) The estimated elastic stress at stage III was further modified to take into account the stress component associated with the strain generated as a consequence of transformation plasticity. At this stage the relationships between these quantities were assumed to be elastic.

(V) Subsequent modification of thermal stress for a free plate model.

(VI) Calculation of the amount of stress relaxed during each time step and modification of the elastic stresses as a consequence of the stress relaxation effect. The estimated elastic stresses were further modified for the zero net force boundary condition.

(VII) Application of the yield criterion to check for plastic flow, and modification of the thermal stresses if there has been any plastic flow. The free edge boundary condition is then reapplied so that the stresses are further modified. The yield criterion is then re-applied followed by the application of the boundary condition. Iteration continues until there is $\leqslant 0.1\ N/mm^2$ net stress, immediately after the application of the yield criterion.

(VIII) Modification of thermal strain as a result of the change in stress level due to the application of the boundary condition.

(IX) Determination of creep strain due to the stress relaxation effect introduced by stage VI, and subsequent modification of the thermal strain to take into account this creep strain.

(X) Final strain estimate considering the strain component associated with transformation plasticity. At this stage the additional strain used as an elastic component in stage IV was added on as a plastic strain.

Stage VI and IX were only required when the effect of the viscous flow processes was introduced in the calculations. Stage IV and X were only effective when the transformation plasticity was considered. For simplicity the details of the process are first described with these two aspects absent (section 4.1).

4.1 Thermal Stress and Strain Calculations Without Stress Relaxation and Transformation Plasticity

The temperature distribution within the plate was determined using the Finite Difference explicit formulation of transient heat conduction with the assumption that the change in Fourier Number was equal to ½. This allowed the reduction of the heat conduction equation to:

$$\theta_i^{n+1} = \frac{\theta_{i+1}^n + \theta_{i-1}^n}{2} \qquad \ldots\ldots 4.1.1$$

where, i = Node position.

n = Node time.

with the following boundary and initial conditions.

$$\frac{\partial\theta}{\partial x} = \frac{h}{\lambda}(\theta_s - \theta_A) \quad \ldots \text{ at the surface.}$$

$$\frac{\partial\theta}{\partial x}_{x\to o} = 0 \text{ (ie, } \theta_{j-1}^n = \theta_{j+1}^n) \ldots \text{ at the centre.}$$

And $\theta=\theta_o$ at all points within the body at time t=0.

When the plate was completely restrained and fully elastic conditions were assumed, the change in thermal stress experienced by

each element of the plate due to thermal contraction and transformation during quenching was[63]:

$$(\Delta\sigma_i^{n+1})_r = \frac{E}{1-\nu}\,\alpha ex:\ (\theta_i^n - \theta_i^{n+1}) \qquad \ldots\ldots 4.1.2$$

Young's Modulus and Poisson's ratio were considered to be temperature dependent. Thus,

$$\frac{E}{1-\nu} = a - b\theta \qquad \ldots\ldots 4.1.3$$

The values of a and b used are represented in table 3. The total stress at the new time was determined by:

$$(\sigma_i^{n+1})_r = \sigma_i^n + (\Delta\sigma_i^{n+1})_r \qquad \ldots\ldots 4.1.4$$

The modification of the thermal stresses was then carried out for free edge boundary conditions. The average value of $(\sigma_i^{n+1})_r$ was determined by the use of equation:-

$$(\bar{\sigma}^{n+1})_r = \sum_{i=1}^{i=j} \frac{(\sigma_i^{n+1})_r}{j} \qquad \ldots\ldots 4.1.5$$

where, j = Number of elements in half thickness of plate.

To obtain the free edge stresses, this stress was subtracted from the stress in each element viz:

$$\sigma_i^{n+1} = (\sigma_i^{n+1})_r - (\bar{\sigma}^{n+1})_r \qquad \ldots\ldots 4.1.6$$

In the next step, the Von-Mises yield criterion was applied to test whether yielding occurred during each time interval. As per this criterion, plastic flow in a uniaxial stress system can occur only if:

$$\sigma_i^{n+1} > \sigma_{fi}^{n+1} \qquad \ldots\ldots 4.1.7$$

If

$$\sigma_i^{n+1} > \sigma_{fi}^{n+1}$$

Then,

$$\sigma_i^{n+1} = \sigma_{fi}^{n+1}$$

And if,

$$\sigma_i^{n+1} < \sigma_{fi}^{n+1}$$

Then,

$$\sigma_i^{n+1} = \sigma_i^{n+1}$$

If plastic flow occurred in any element, the replacement of the elastic stress by a flow stress unbalanced the forces within the plate after the application of the yield criterion. It was therefore, necessary to establish a new stress distribution which produced zero net force in the plate. This was achieved by an efficient iteration process, in which, the elastic stresses were modified by a constant amount. Zero force was considered to have been attained when $\bar{\sigma}^{n+1} \leqslant 0.1$ MPa.

The increase in flow stress as a result of plastic flow made it necessary to take into account the work hardening effect. For this purpose, strain hardening coefficients were used to adjust the flow stresses. These coefficients were dependent upon the temperature and the previous plastic deformation, and were represented by strain hardening rates as:-

$$W_1 = \frac{d\sigma_f}{d\varepsilon_p}, \quad \varepsilon_p = 0 \rightarrow 0.5\%$$

$$W_2 = \frac{d\sigma_f}{d\varepsilon_p}, \quad \varepsilon_p = 0.5\% \rightarrow 1.0\%$$

The values of W_1 and W_2 used for thermal stress and strain calculation are represented in table 3.

The initial estimate of the strain increment produced during any time interval was used to determine the first estimate of the elastic stress, prior to the application of the yield criterion. During the iterative procedure used to modify the elastic stresses, as a consequence of plastic flow, the initial estimate of elastic stress was changed, until the overall forces on the plate became zero after the application of the yield criterion. This change in the elastic stress produced a corresponding change in the estimate of elastic strain, which was calculated by:

$$\Delta\varepsilon_i^{n+1} = \frac{\sigma_i^n}{a-b\theta_i^n} - \frac{\sigma_i^{n+1}}{a-b\theta_i^{n+1}} \qquad \ldots\ldots 4.1.8$$

The total strain in each element at the new time was:

$$\varepsilon_i^{n+1} = \varepsilon_i^n + \Delta\varepsilon_i^{n+1} \qquad \ldots\ldots 4.1.9$$

The procedure described here does not specifically include transformation strain. However, the use of a pseudo coefficient of expansion that include dimensional changes due to transformation allow the inclusion of such effect without necessitating any change to the procedure described.

4.2 Thermal Stress and Strain Calculations with Stress Relaxation and Creep

Since the thermal stresses generated during the quenching process were liable to be affected by stress relaxation; the procedure described in Section 4.1, which was used to calculate thermal stress and strain, was modified to incorporate the effect of this time dependent change in the stress and strain level. This required the use of the relevant data for stress relaxation and the associated creep strain.

The amount of stress relaxed and the associated creep strain was obtained from the Standard Linear Solid model (figure 37c), which gave the following equations for stress relaxation and creep strain for plane-stress conditions (derived in Appendix I).

$$\frac{(\sigma t)_i^{n+1}}{(\sigma^o)_i^{n+1}} = 0.8363A_i^{n+1} + [1-(0.8363A_i^{n+1})]\ \mathrm{Exp}(-B_i^{n+1}\Delta t) \qquad \ldots\ldots\ 4.2.1$$

$$[\varepsilon creep]_i^{n+1} = \frac{[\sigma^o]_i^{n+1}(1-0.8363A_i^{n+1})[1-\mathrm{Exp}(-0.8363A_i^{n+1}B_i^{n+1}\Delta t)]}{0.8363(a-b\theta_i^{n+1})A_i^{n+1}} \qquad \ldots\ldots\ 4.2.2$$

where,

$$A = \frac{2\phi\eta(1+\nu)}{E}, \quad B = \frac{G}{\eta}$$

Δt = Time increment.

The dependence of A and B on temperature and initial stress (σ^o) level has already been established in section 3.2.3 and is shown in figure 39 and table 2.

Stress relaxation and creep effects were introduced in the model at the point where the initial elastic stress estimate has been modified for the free edge:

viz: $$\sigma_i^{n+1} = (\sigma_i^{n+1})_r - (\bar{\sigma}^{n+1})_r \qquad \ldots\ldots\ 4.1.6$$

The initial stress during any time interval applicable to the stress relaxation process was obtained from the average stress during that time interval:

$$(\sigma_i^{n+1})_{av:} = \frac{\sigma_i^{n+1} + \sigma_i^n}{2} \qquad \ldots\ldots\ 4.2.3$$

And $$(\sigma^{o})_{i}^{n+1} = (\sigma_{i}^{n+1})_{av:}$$

This initial stress $(\sigma^{o})_{i}^{n+1}$ as a factor that affected the rate of stress relaxation has been introduced in the relationships described in section 3.2.3 to estimate the values of parameters A and B. The equation 4.2.1 was then used to obtain the final value $(\sigma t)_{i}^{n+1}$ that has not been relaxed during the time interval in question. A knowledge of $(\sigma^{o})_{i}^{n+1}$ and $(\sigma t)_{i}^{n+1}$ thus allowed the determination of the magnitude of the stress reduction introduced in time Δt:

$$(\Delta\sigma_{i}^{n+1})_{Rel:} = (\sigma^{o})_{i}^{n+1} - (\sigma t)_{i}^{n+1} \qquad \ldots\ldots 4.2.4$$

Due to the complex relationships between the viscous flow process, time, temperature and the stress level that occur during continuous cooling, two methods have been used to obtain the rate of stress relaxation and creep. They are discussed in the next section.

The elastic stress estimate given by equation 4.1.6 was then adjusted to take into account the amount of stress relaxation given by equation 4.2.4.

i.e. $$\sigma_{i}^{n+1} = \sigma_{i}^{n+1} - (\Delta\sigma_{i}^{n+1})_{Rel:} \qquad \ldots\ldots 4.2.5$$

The remaining steps in the calculation were the same as those described in section 4.1 until the elastic strain (equation 4.1.9) has been calculated. After this step, the creep strain associated with the stress relaxation process obtained from equation 4.2.2 was added to the strain calculated by equation 4.1.9 to give the new strain estimate.

$$\varepsilon_{i}^{n+1} = \varepsilon_{i}^{n+1} + (\varepsilon creep)_{i}^{n+1} \qquad \ldots\ldots 4.2.6$$

4.2.1 Methods used to Model the Viscous Flow Processes used in the Thermal Stress and Strain Calculations

The complex relationships between viscous flow processes, temperature, time and the stress level during quenching made it difficult to use directly the stress relaxation data obtained under isothermal conditions. The stress relaxation rates predicted by the standard linear solid model fell to zero after a short time, whereas in practice this is not the case. Furthermore, the relaxation rates may be influenced by the thermal and mechanical history of the material during the quenching process. These complexities and the absence of information about the use of isothermal data relating to the viscous flow in a continuous cooling situation, made it necessary to use two different methods, which covered the range of possibilities likely to be encountered in practice.

Method 1: Rate of stress relaxation and creep as a function of temperature and initial stress.

Method 2: Rate of stress relaxation and creep as a function of time, temperature and initial stress with a steady rate used after 20 seconds. [This corresponded to secondary creep].

In method one, it was considered that stress relaxation was a function of temperature and initial stress only, so that during a time interval Δt, the average rate of stress relaxation and creep from equations 4.2.1 and 4.2.2 was given by:

$$(\dot{\sigma}_R)_i^{n+1} = \frac{(\sigma^o)_i^{n+1}(1-0.8363A_i^{n+1})\,[1-\mathrm{Exp}(-B_i^{n+1}\Delta t)]}{\Delta t} \qquad \ldots\ldots\ 4.2.7$$

$$(\dot{\varepsilon}\mathrm{creep})_i^{n+1} = \frac{(\sigma^o)_i^{n+1}(1-0.8363A_i^{n+1})\,[1-\mathrm{Exp}(-0.8363A_i^{n+1}B_i^{n+1}\Delta t)]}{0.8363(a-b\theta_i^{n+1})A_i^{n+1}\Delta t} \qquad \ldots\ldots\ 4.2.8$$

This method gave high stress relaxation rates, although these gradually fell as the temperature was reduced until they finally reached zero at low temperatures and stresses. This was due to the very hard martensite present and the low temperature.

Method 2 included the work hardening effect until the time reached a value of 20 seconds. Thus, the average rate of stress relaxation and creep was allowed to reduce with time for the first 20 seconds, but the rate obtained after this time was that appropriate to a specimen held for 20 seconds at the current temperature. The rate of relaxation at times greater than 20 seconds represented steady state viscous flow, was in line with both the experimentally observed rate of stress relaxation at later times during the test and the steady state creep rate obtained by experiment[22,41]. These tests were conducted with the upper end of the temperature range, where the structure of the material was stable. It has been assumed that a similar effect occurred at all temperatures before 150°C. The rate of stress relaxation and creep for this method from equation 4.2.1 and 4.2.2 were:

$$(\dot{\sigma}_R)_i^{n+1} = \frac{(\sigma^o)_i^{n+1}(1-0.8363A_i^{n+1})\,[1-\mathrm{Exp}(-B_i^{n+1}t^{n+1})]}{t^{n+1}} \qquad \ldots\ldots 4.2.9$$

$$(\dot{\varepsilon}\mathrm{creep})_i^{n+1} = \frac{(\sigma^o)_i^{n+1}(1-0.8363A_i^{n+1})\,[1-\mathrm{Exp}(-0.8363A_i^{n+1}B_i^{n+1}t^{n+1})]}{0.8363A_i^{n+1}t^{n+1}(a-b\theta_i^{n+1})} \qquad \ldots\ldots 4.2.10$$

where $t^{n+1} \leqslant 20$ seconds.

4.3 Calculation of Thermal Stress and Strain with Transformation Plasticity

The presence of stress during a phase transformation affected the magnitude of the strain associated with this transformation. This effect,

which was due to the occurrence of transformation-induced plasticity, has been introduced into the mathematical model described in sections 4.1 and 4.2.

The value of the transformation strain used was obtained from the dilatometry data produced when specimens initially in an austenitic condition were cooled under stress-free conditions. This transformation strain was subtracted from the corresponding value obtained when the dilatometer specimen was cooled in the presence of a stress to give the strain due to transformation plasticity alone. At stresses below 40 MPa no transformation plasticity was detected, and at higher values the amount of such strain was proportional to the excess stress above 40 MPa[23].

Thus, Fletcher and Abbasi[23] used a quadratic relationship between the temperature reduction below Ms and the amount of transformation plasticity strain. This tends to produce very unstable results at temperatures very close to Ms. To avoid this a linear relationship replaced the quadratic one. In fact the experimental results can be represented just as well by this relationship as the original one used by Fletcher and Abbasi[23] and the improvement in the stability of the results was beneficial. The equation from which the transformation plasticity strain was obtained now became:

$$\varepsilon tp = 6.25 \times 10^{-7} \, (\sigma - 40)(300 - \theta) \qquad \ldots\ldots \; 4.3.1$$

for

$$-40 \text{ MPa} > \sigma > 40 \text{ MPa}$$

where,

σ = applied stress (MPa), εtp = transformation plasticity strain,

θ = temperature [^{o}C].

This is represented in figure 42.

At first it was found that the introduction of transformation plasticity could create unacceptable instability in the calculations. This was eliminated when the transformation plasticity strain was limited to that produced by an applied stress of 160 MPa. This stress equated approximately with the yield stress of austenite at the temperatures in question and so this limitation was in accordance with the physical situation.

The transformation plasticity strain produced during a particular time interval was introduced into the calculations of thermal stress and strain immediately after the addition of the elastic stress increment to the current stress. This elastic stress increment can be regarded as an inital estimate which equates with the actual elastic stress increment plus the transformation plasticity increment. Therefore the initial estimated elastic strain increment was reduced as a consequence of the introduction of the transformation plasticity strain. The elastic stress increment associated with the initial elastic strain increment was modified to take into account this change in the elastic strain.

$$\sigma_i^{n+1} = \sigma_i^{n} + [\Delta\sigma_i^{n+1}]_{\substack{\text{initial}\\\text{estimate}}} - \frac{E\Delta\varepsilon tp}{1-\nu} \qquad \ldots\ldots 4.3.2$$

where, $\Delta\varepsilon tp$ has been obtained from equation 4.3.1 until $\sigma_i^{n} \geqslant$ Abs: (40 MPa)

It is of course necessary to apply the zero net force boundary condition before continuing to the next stage of the calculation.

In figure 43, a flow chart of the computer programme for the complete thermal stress and strain calculation is shown.

4.4 Data Used in Mathematical Model of the Thermal Stress and Strain Generation Process

In order to carry out the thermal stress and strain calculations, it is necessary to have information about the following.

I. Temperature dependent thermal property data.

II. Dilatometric data of the material (stress free condition).

III. Temperature dependent mechanical property data.

IV. The overall volume change that accompanied the hardening of the material.

V. Stress relaxation and creep data.

VI. Dilatometric data of the material under stress.

4.4.1 Temperature Dependent Thermal Property Data of 835M30 Steel

It was necessary to know the effect of temperature on the thermal diffusivity, the thermal conductivity, and the surface heat transfer coefficient, in order to calculate the temperature distribution in the plate throughout the quenching process. The equation for the variation of thermal diffusivity and thermal conductivity with temperature are shown in table 4. The relationships between temperature and surface heat transfer coefficient used in the calculations are given in table 5. In the case of the salt bath, data was obtained by Cuicas[78] and in the case of water, oil and polymer by Price and Fletcher[64], whereas for the air cooling, the surface heat transfer coefficient was assumed to be 50 $W/m^2\ ^oC$.

4.4.2 Dilatometric Data of 835M30 Steel During Cooling from 850°C

Knowledge of the relationship between temperature and the length of a specimen of 835M30 steel during cooling from 850°C without any constraint, allowed the determination of the variation of the thermal

expansion coefficient of the material with temperature. A relation between temperature and the length of a dilatometer specimen of 835M30 steel during cooling from 850°C was determined by Fletcher and Price[30] and is shown in figure 44. The following relationships, based on their results, were used in the calculations:

$$\theta > 300^{\circ}C, \quad \varepsilon_{thermal} = 2.1407 \times 10^{-5}\theta - 0.01066$$

$$288^{\circ}C < \theta < 300^{\circ}C, \quad \varepsilon_{thermal} = -0.00422$$

$$90^{\circ}C < \theta < 288^{\circ}C, \quad \varepsilon_{thermal} = \frac{Y^1 - 1.4435}{581.23}$$

$$\theta < 90^{\circ}C, \quad \varepsilon_{thermal} = 0.6133 \times 10^{-5}\theta - 0.0015$$

(Includes transformation effects) ...4.4.1

where,

$$Y^1 = 1.0102 + 0.1804X^1 - 0.35024(X^1)^2 - 1.0244(X^1)^3 - 0.824(X^1)^4$$

$$X^1 = 0.0080193\theta + 1.3079$$

The values of the thermal expansion coefficients used in equation 4.1.2 were obtained from the following equation by the use of $\varepsilon_{thermal}$ values from the above relations at the appropriate temperature.

$$(\alpha ex:)_{\theta_i^n \rightarrow \theta_i^{n+1}} = \frac{[\varepsilon_{thermal}]_{\theta_i^n} - [\varepsilon_{thermal}]_{\theta_i^{n+1}}}{\theta_i^n - \theta_i^{n+1}} \qquad \ldots\ldots 4.4.2$$

The use of $\varepsilon_{thermal}$ values to obtain the thermal expansion coefficient at the appropriate temperature allowed the expansion due to martensitic transformation to be included in this property.

4.4.3 Temperature Dependent Mechanical Property Data of 835M30 Steel

Uniaxial tests were carried out to check the flow stresses of 835M30 steel against the values obtained by Abbasi[41] and Fletcher and Price[30]. These tests were conducted at temperatures of 600°C, 400°C

and 250°C on an Instron tensile testing machine as described in section 3.1.1. A good correlation was found with the results previously established by Abbasi[41] and Fletcher and Price[30], as shown in figure 45. Table 3, shows the relationship between austenite flow stress and temperature used in the present calculation.

Below the Ms temperature, both austenite and martensite are present, so the flow stress used at a temperature lower than Ms was a function of the volume fraction of both the structures present, and their respective flow stresses[30].

$$\sigma f = V\alpha \ (\sigma f)\alpha + V\gamma \ (\sigma f)\gamma \qquad \ldots\ldots 4.4.3$$

The volume fraction of the austenite and the martensite at various temperatures were obtained from figure 44. The flow stress for a 100% martensite structure was used as 1600 MPa, which was obtained from the published data relating to 835M30 steel[105].

The effect of temperature on Young's modulus and Poisson's ratio during a rapid cooling to produce a martensite structure in a low alloy steel was given by Aitkens et al[106]. The variation of $\frac{E}{1-\nu}$ with temperature, derived from the data given by Aitken et al[106] is presented in table 3.

The relationship between temperature and the strain hardening coefficients used for the calculations are already discussed in section 4.1, and are presented in table 3.

4.4.4 The Overall Volume Change that Accompanied the Hardening of the Material

The structure of the plate prior to hardening consisted of a mixture of ferrite and carbide, while after the austenitisation and quenching

operation the structure contained only martensite. This structural change was accompanied by a uniform expansion independent of any thermal strain introduced during the quench. The calculation procedure used for the present work considered only changes in the dimensions produced during cooling from the austenitisation temperature, so this overall volume change was not included. Thus, the change in dimensions produced by the change in structure from ferrite and carbide to martensite must be added to those results predicted by the present mathematical model if these results are to be comparable to experimental values.

To obtain a measure of the volume change involved in 835M30 steel, a plate of dimensions 120 mm x 120 mm x 20 mm was heat treated in the same way as that described in chapter 6, but it was directly cooled from 850^{o}C to room temperature in air. The rate of cooling was such that no residual stresses were developed and at the end of cooling a stress-free, fully martensitic plate was observed.

The dimensions of the plate were measured at various points (figure 97) as described in chapter 6, before and after hardening. The percentage net volume change at all the measurement locations was calculated by the use of the following equation:

$$\% \Delta V = \frac{100 (V_h - V_s)}{V_s} \qquad \ldots\ldots 4.4.4$$

Table 6, shows the volumes of the plate in the softened (i.e. with ferrite and cementite structure) and in hardened conditions together with the net volume changes associated with the transformation from one structure to the other. The net volume change was 0.3583%, which was equal to a linear isotropic change of 0.12%. This value was in good agreement with that obtained by Price[18].

Stress relaxation and creep data of 835M30 steel used for the present work has already been described in detail in chapter 3, whereas stress dialatometric data has been discussed in section 4.3.

4.5 Thermal Stresses and Strains Predicted by the Mathematical Model

The results of the calculations obtained from the mathematical model have been divided into:-

I. No consideration of stress relaxation and transformation plasticity.

II. With the inclusion of stress relaxation only, which have been further subdivided as:

   a. consideration of stress relaxation by method one

   b. consideration of stress relaxation by method two.

III. With the inclusion of stress relaxation and transformation plasticity.

IV. With the inclusion of transformation plasticity only.

Each calculation has been defined by the abbreviation described in table 7. The corresponding figure reference is also given in the same table.

4.5.1 Water Quenching

Calculation FP_1 was used to follow the generation of thermal stress and strain when a 20 mm thick plate of 835M30 steel was quenched in water, without consideration of the effect of stress relaxation and transformation plasticity on the development of thermal stress and strain. The relationships between stress and strain in the surface and the central elements of the plate during the quench are shown in figure 46. During the initial stages of the cooling process from 850^{o}C, a

tensile stress was developed at the surface as a result of a fast cooling rate in this portion of the plate in the early stages of quenching. This elastic tensile stress was balanced by a compressive stress towards the centre of the plate. As the specimen cooled the temperature gradient between surface and centre became greater, so the level of stresses at both the surface and the centre increased until they produced plastic flow. Further increase in these stresses occurred at a rate dependent on the change in flow stress as the temperature continued to fall. Eventually when the surface temperature had reached 388^{o}C, the stress began to unload as the cooling rate at the centre rose to a point at which it exceeded that at the surface. Both surface and centre stresses now reversed. The magnitude of the latter was high enough to cause plastic flow, since the temperature at this point was relatively high (567^{o}C) and the yield stress relatively low. The associated increase in compressive stress at the surface was intensified when the surface reached the Ms temperature. A maximum compressive stress of -1175 MPa was developed as the surface temperature fell to 244^{o}C. As the transformation front moved from the surface towards the elements near to the centre, an unloading of the surface compressive stress occurred. Transformation of austenite to martensite at the centre prevented further plastic flow in this part of the plate. At this stage, the cooling rate at the centre was higher than at the surface, which caused a small increase in the tensile stress at the centre. As the transformation products increased, the volume expansion associated with them caused the tensile stress to unload as the temperature reached 286^{o}C and to become compressive. Finally, at the end of the quench both the surface and the centre possessed a compressive stress of -50 MPa and -228 MPa respectively. The tensile stress required to balance the force on the plate occurred at the intermediate positions.

4.5.1.1 Water Quenching with Stress Relaxation

Figures 47 and 48 show the relationships between stress and strain predicted by calculations FP_2 and FP_3 at the surface and the centre of a water quenched 20 mm plate: in these calculations viscous flow was represented by method one and method two respectively. During the initial stages of the cooling process viscous flow had no significant effect on the relationships between stress and strain on account of the rapidity of the water quench. Therefore, the results were very similar to those predicted by calculation FP_1 (no viscous effect). However, the temperatures at which the unloading of the surface tensile stress occurred were high (compare Figures 46, 47 and 48). The unloading of surface stress due to the fast cooling rate at the centre was further intensified by the transformation of the surface at 300°C, which led to compressive stresses. The level of stress and the time period involved in the cooling to this temperature were sufficient to cause a significant stress relaxation effect. Hence, the maximum compressive stress predicted by both the calculations FP_2 and FP_3 was lower than that suggested by calculation FP_1 (-1175 MPa for FP_1, -869 MPa for FP_2 and -1100 MPa for FP_3). Unloading of the surface compressive stress now occurred as the martensitic transformation approached completion at the surface. At this stage, the stress, temperature and the time interval were high enough to produce viscous flow, which increased the slope of the curves showing the relationships between stress and strain during the second unloading of the surface stress. This unloading was followed by a stress reversal, which led to a tensile rather than a compressive surface stress. In the case of calculation FP_2 (stress relaxation method one) the presence of high rates of stress relaxation produced a further unloading of the surface stresses at a temperature of 130°C. This was the temperature at which the martensite transformation finally ceased.

4.5.1.2 Water Quenching with Stress Relaxation and Transformation Plasticity

The relationships between stress and strain predicted by calculations FP_4 and FP_5 (transformation plasticity and stress relaxation method 1 and 2 respectively) were identical to those predicted by calculations FP_2 and FP_3 (only stress relaxation method 1 and 2 respectively), until the surface reached the Ms temperature (compare Figures 49 and 50 with figures 47 and 48 respectively). The presence of transformation plasticity at this stage limited the level of compressive stress that was developed at the surface. However, once the temperature fell below 260°C there was no longer a negative plastic strain component due to transformation plasticity. Hence, the negative stress increased very rapidly until the transformation of the interior of the plate to martensite caused a reversal of this stress at the surface. The maximum compressive stress developed at the surface in the case of both the calculations was lower than that developed in the cases when transformation plasticity was not considered (calculations FP_2 and FP_3).

At the hot, weak centre, the tensile stress produced plastic flow as a consequence of the martensitic transformation at the surface. This process was continued until the centre was cooled to 300°C and even after this point had been passed, the transformation plasticity and the viscous effects caused some further plastic flow. However, this was now associated with a reducing stress, so that once the stress fell below 40 MPa all plastic flow ceased and the unloading process was continued, obeying Hooke's law. The centre stress then became compressive and when this reached an absolute value greater than 40 MPa, further plastic flow occurred. This continued until the temperature reached 260°C, where the transformation plasticity ceased. Of course, the sign of the

strain associated with transformation plasticity was now negative. Below 260°C the absolute stress increased rapidly, to be followed by a very small reduction after completion of the transformation.

4.5.1.3 Water Quenching with Transformation Plasticity

Figure 51 shows the relationships between stress and strain at the surface and the centre of a water quenched plate predicted by calculation FP_6, which included transformation plasticity but not stress relaxation. The initial part of the stress generation process (i.e. before transformation of the surface) was identical to that predicted by calculation FP_1, where transformation plasticity and stress relaxation was not present (compare figures 46 and 51). At the onset of the martensite transformation at the surface, plastic flow occurred until the temperature reached 260°C, at which stage transformation plasticity ceased. A rapid rise in the level of compressive stress now occurred due to the normal expansion associated with the martensite transformation. As the transformation front moved towards centre, unloading of the surface compressive stress began, which led to a slight tensile stress (8 MPa) at the surface at a temperature of 126°C. A reduction in this surface stress as a consequence of the reducing temperature gradient between surface and centre, left the surface in a state of compression at the end of quench. The results obtained at the centre were very similar to those suggested by the results of calculation FP_1 (no transformation plasticity, nor stress relaxation), except that there was a reduction in the extent of the second period of plastic flow and the presence of transformation plasticity between 300°C (Ms) and 260°C, which led to a change in residual strain at the end of quench.

4.5.1.4 Residual Stresses and Strains after Water Quenching

The residual stress and strain distributions across the plate determined by calculations FP_1 to FP_6 are presented in figures 52 and 53 respectively. All the curves showing residual stress distribution in the plate obtained from various calculations (figure 52), have generally a similar shape, except that the magnitude of the maximum tensile stress just below the surface depended upon the model used in the calculations. The presence of viscous flow in the absence of transformation plasticity produced a reduction in the level of this maximum stress, whereas the corresponding variations at the centre were not significant. However, the introduction of transformation plasticity in the same calculations produced a moderate increase in the level of residual stress just below the surface. However , the introduction of transformation plasticity without stress relaxation developed the highest peaks of absolute residual stresses at both the surface and the centre.

The residual stress distributions predicted by calculations FP_1 (without stress relaxation and transformation plasticity) and FP_6 (with transformation plasticity only) showed a compressive stress at the surface and centre whereas, the calculations FP_2 to FP_5 which incorporated both the stress relaxation and transformation plasticity, predicted a tensile stress at the surface and a compressive stress at the centre. However, the overall level of residual stress in the case of calculation FP_6 was higher than those predicted by other five calculations. The magnitudes of the residual stresses predicted by calculations other than FP_1 and FP_6 (no viscous flow) were dependent on the method used to represent stress relaxation. Thus, the greater the overall level of stress relaxation rate during quenching, the

lower was the residual stress at the end of the cooling process.

The general patterns of the residual strains obtained from all the calculations were similar i.e. the strains were always positive and highest at the surface. However , the level of residual strains predicted in the case of calculations FP_1 (no stress relaxation) and FP_3 (stress relaxation method two) were the highest. The strains produced when transformation plasticity was included (calculations FP_4 to FP_6) were much lower than those obtained when this effect was not considered. The level of residual strains predicted by calculation FP_2, which incorporate stress relaxation method one, was intermediate between these two extremes.

4.5.2 Oil Quenching

Calculation FP_7 simulated the thermal stress and strain generated during an oil quenching of a 15 mm thick plate of 835M30 steel without taking into account the effect of viscous flow and transformation plasticity. Figure 54 shows the relationships between stress and strain in the surface and the central regions obtained from this calculation. During the initial stage of the quench tensile and compressive stresses were developed at the surface and centre, respectively, and the magnitude of both increased until plastic flow occurred in both the surface and central elements. The amount of plastic flow was now smaller than that predicted in the case of water, on account of the low value of the heat transfer coefficient during this part of the quench. As the cooling rate at the centre exceeded that at the surface, the first unloading of the thermal stress began at the surface at 747^{o}C and at the centre at 810^{o}C. The reduction in the stresses at both the surface and the centre was continued until at 545^{o}C the surface stress became slightly compressive (-5 MPa). However, at this stage, a sharp increase in the surface heat

transfer coefficient, due to the onset of nucleate boiling, produced a steeper temperate gradient, which caused a further reversal of the surface stress. This now became tensile, while at the centre the stress became more compressive. The magnitude of the surface stress at a temperature of 481^{o}C was high enough to cause plastic flow, until the temperature had fallen to 441^{o}C. At this point, the maximum tensile stress of 136 MPa was produced at the surface, which was less than the flow stress of the material. Another unloading of the stress now occurred, to be followed by a stress reversal as the centre again began to cool at a faster rate than the surface. At the onset of the martensite transformation, the surface compressive stress rose, whereas the compressive stress at the centre further declined and eventually became tensile. A maximum compressive stress of -375 MPa was developed at the surface at a temperature of 271^{o}C, after which this stress was reduced as a consequence of the transformation towards the centre of the plate. The arrival of the transformation front at the centre caused the tensile stress to unload at a temperature of 286^{o}C. At the end of the cooling process the surface was subjected to a residual stress of - 175 MPa, while a tensile stress of 65 MPa was produced at the centre. The corresponding residual strain at the surface and the centre was 0.035% and 0.004%, respectively.

4.5.2.1 Oil Quenching with Stress Relaxation

The relationships between stress and strain predicted by calculations FP_8 and FP_9, with stress relaxation represented by method one and method two respectively, are shown in figures 55 and 56. The essential features of the thermal stress and strain generation process are the same as those obtained from calculation FP_7, which ignores stress relaxation. However, the presence of viscous effects caused some

significant changes to the sequence of the stress and strain relationships, which are, of course, dependent upon the stress relaxation method used. Calculation FP_8 (method one) produced the greatest amount of viscous flow, which led to an earlier unloading (at 778°C) of the surface stress than that predicted by method two, that is calculation FP_9 (at 771°C). Both these temperatures were a little higher than the corresponding temperature when no stress relaxation was included (FP_7), 747°C. The magnitude of the stress and the slow cooling rate during the vapour blanket stage caused a significant viscous flow to occur at both surface and centre. At the start of nucleate boiling at 545°C an immediate unloading of the compressive stress at the surface was brought about, to be followed by a tensile stress. Due to the high stress relaxation rates associated with method one (FP_8), the level of stress developed in this case was not high enough to cause plastic flow, as was the case during the same stage of calculation FP_9, which includes a lower rate of stress relaxation (see figures 55 and 56). The unloading of the tensile stress occurred as a consequence of a faster cooling rate in the interior of the plate. This unloading was continued until a stress reversal occurred, which was assisted later by the transformation of austenite to martensite at the surface. In the case of calculation FP_8 (method one) the effect of viscous flow was very apparent during this stage of the quench (at temperatures between 445°C and 300°C). This led to a significant departure from the elastic Hooke's Law relationship between stress and strain, particularly at the lower end of this temperature range.

A maximum compressive stress of -270 MPa was developed at the surface at 274°C, in the case of the inclusion of stress relaxation by method one (FP_8) before the unloading of these stresses occurred due to the

combined effect of a reducing temperature gradient and the martensite transformation towards the centre. However, in the case of calculation FP_9 (method two) the surface was subjected to a compressive stress of -342 MPa at the same stage. The unloading of surface stresses was aided by stress relaxation and in the case where viscous flow was most prominent (calculation FP_8), the surface stress changed from a compressive state into a tensile one. At the end of the quench, the surface was subjected to a tensile residual stress (21 MPa) in the case of calculation FP_8, while the final stress predicted by calculation FP_9 was compressive (-68 MPa). However, the magnitudes of these residual surface stresses were lower than that predicted by calculation FP_7, which ignored stress relaxation.

The corresponding relationships between stress and strain at the centre followed a sequence that was the reverse of that obtained at the surface. However, the temperature at which particular events occurred and the corresponding levels of stress and strain developed were also different from those pertaining to the surface. In the case where the viscous flow was greater, the stress relaxation effect reduced the stresses at the centre to very low values.

4.5.2.2 Oil Quenching with Stress Relaxation and Transformation Plasticity

Figures 57 and 58 shows the relationships between stress and strain predicted by calculations FP_{10} and FP_{11} respectively, at the surface and the centre of an oil quenched 15 mm plate: both calculations included stress relaxation and transformation plasticity. The inclusion of transformation plasticity only affected results below the Ms temperature, so in the early stages the results were the same as calculation FP_8 and FP_9 respectively, and the differences occurred after the martensite transformation has begun at the surface.

In case of calculation FP_{10} (stress relaxation method one and transformation plasticity) the surface, at the onset of transformation, was subjected to a stress of -91 MPa. At these temperature and stress levels, viscous flow and transformation plasticity combined to reduce gradually the level of stress, which introduced a considerable amount of non-linear strain. When the absolute stress fell below 40 MPa, transformation plasticity ceased, although viscous flow still produced a non-linear stress-strain curve. As the stress reversed viscous flow effectively ceased and from then on Hooke's Law was obeyed. During the remainder of the quench the surface stress became progressively more tensile, and reached a level of 142 MPa at the end of the cooling process. The relationships between stress and strain at the centre was essentially the reverse of the behaviour observed at the surface.

After the transformation to martensite had begun, the results obtained from calculations FP_{10} and FP_{11} were essentially the same. That is, the difference in the modelling of stress relaxation had no significant effect when transformation plasticity was occurring. The absolute stress present at the start of the transformation at the surface in the case of calculation FP_{11}, was high enough to produce significant transformation plasticity. The combination of the transformation plasticity with viscous flow produced a steady reduction in the surface compressive stress until at a temperature of 278^{o}C the compressive stress fell below 40 MPa and transformation plasticity ceased. Unloading of the surface compressive stress continued under the influence of transformation towards the central positions of the plate and the reducing temperature difference between surface and centre. Finally the surface was subjected to a tensile stress of 145 MPa at the end of quench. The sequence of stress and strain relationships at the centre was similar to that obtained at the surface.

4.5.2.3 Oil Quenching with Transformation Plasticity

Calculation FP_{12} incorporated transformation plasticity but did not include the effect of stress relaxation. Prior to transformation the predicted relationships between stress and strain at the surface and the centre were the same as those predicted by calculation FP_7 (figure 54). However, figure 59 shows that, at the start of the transformation, a compressive stress of -96 MPa was sufficient to create transformation plasticity at the surface, so there was no further build up in the compressive stresses at this stage. In fact a reduction was observed. This reduction was due to the movement of the transformation front towards the centre, since the associated compressive stress caused a balancing tensile component to be introduced at the surface. The small temperature gradient in oil quenched material means that the transformation front moved quickly, so that the compressive stress generated by the transformation at the surface was soon followed by unloading. Transformation plasticity of course limited the compressive component at temperatures between 300°C and 260°C. The transformation plasticity effect ceased when the magnitude of the surface stress dropped to -40 MPa. Elastic unloading of this stress was continued under the influence of the transformation in the interior of the plate but once the surface was subjected to a tensile stress of 40 MPa, the further development of the surface stress was curtailed by more transformation plasticity. Once the surface attained a temperature of 260°C, the tensile stress increased rapidly to be followed by a very small reduction, after completion of the martensite transformation at all points in the plate. At the end of the cooling process a tensile stress of 191 MPa and a very small compressive strain (-0.0067%) were predicted at the surface.

The presence of transformation plasticity limited the surface stresses in the early stages of the transformation. This had an effect on the stresses in the rest of the plate, and was responsible for a relativley small tensile stress at the centre when the Ms temperature was reached at this point. Only a small amount of anelastic flow occurred before this stress fell below 40 MPa, at which point transformation plasticity ceased. On further cooling the centre stress unloaded and finally reversed, to leave a final stress of -102 MPa at the end of the quench.

4.5.2.4 Residual Stresses and Strains after Oil Quenching

The residual stress and strain distributions across the oil quenched plate predicted from calculations FP_7 to FP_{12} are shown in figures 60 and 61 respectively. The range of models used to calculate the residual stresses after an oil quench produced a very wide variation in the results. They varied from a tensile stress at the centre and a compressive stress at the surface (no stress relaxation or transformation plasticity) to the exact opposite, in the case of all the results where transformation plasticity was included (FP_{10} to FP_{12}). In the absence of transformation plasticity the introduction of an increasing amount of stress relaxation produced a progressive reduction in the absolute level of stress at all points in the plate. However, stress relaxation had little effect in the presence of transformation plasticity. These results above all the others show the importance of transformation plasticity in calculations of this type.

The shapes of residual strain curves obtained from all the calculations (FP_7 to FP_{12}) were very similar. However, the magnitude of the predicted strains at both the surface and the centre were reduced slightly by the introduction of viscous effects (calculations

FP_8 and FP_9). A further small reduction in the residual strains was predicted when transformation plasticity was introduced in the calculations (FP_{10} to FP_{12}).

4.5.3 Polymer Quenching

The predicted relatinships between stress and strain at the surface and the centre of a 20 mm plate cooled in a polymer (25% AquaQuench 1250) quenchant were obtained from calculations FP_{13} to FP_{18} (see table 7). The predicted variations in thermal stress and strain were similar to those obtained in cases of water quenching. Thus, there was initially a tensile stress at the surface and compressive stress at the centre followed by a plastic flow (figures 62 to 67). However, the amount of plastic flow produced at both the surface and the centre was less than that predicted in the case of the water quench. Later, as the centre began to cool faster than the surface, the stresses at surface and centre unloaded and in the case of the former reversal occurred just after the martensite transformation began in this part of the plate. On further cooling, the surface region became compressive while the centre was subjected to tension. As soon as the magnitude of the tensile stress at the centre reached the flow stress of the material, a second period of plastic flow occurred which lasted until the start of the martensite transformation at the centre. The influence of stress relaxation during the first unloading at the surface was significant in the case of both of the stress relaxation models (figures 63 to 66). In both the cases the temperature, cooling time and the level of stress present were such as to produce significant viscous flow at this stage in the quench. The presence of transformation plasticity (calculations FP_{16} to FP_{18}) limited the development of negative stresses at the surface during the martensitic transformation until the temperature at the surface fall to

260°C. Below 260°C, the compressive stress increased rapidly, until the transformation of the interior of the plate caused another reversal of these stresses. The maximum compressive stresses developed in all the calculations were also lower than those predicted under the same conditions during water quenching. Continued reduction in the surface compressive stress as a consequence of the influence of viscous effects and transformation of the central elements, eventually produced a tensile surface stress at the end of quench in all the calculations except FP_{13}, which did not consider the effects of stress relaxation and transformation plasticity on the thermal stress generation process.

At the onset of transformation at the centre, the presence of transformation plasticity and creep caused both plastic flow and stress reduction, until the tensile stress fell below 40 MPa, the threshold stress below which transformation plasticity did not occur. The stress reversal at a temperature above 260°C produced further flow when the compressive stress reached a value in excess of 40 MPa. Now the sense of the plastic strain was negative. Below 260°C the compressive stress increased rapidly and at the completion of transformation, a compressive stress was predicted at the centre which was slightly reduced at the end of the quench.

4.5.3.1 Residual Stresses and Strains after Polymer Quenching

The residual stress and strain distributions at the end of the polymer quench obtained from all the calculations described in section 4.5.3, are presented in figures 68 and 69. All the calculations showed a tensile stress at the surface and a compressive stress at the centre except calculation FP_{13} (without stress relaxation and transformation plasticity), which predicted compressive stress at both the surface and the centre. The absolute levels of the maximum residual tensile stress

near the surface and the maximum residual compressive stress at the centre were reduced by the introduction of viscous flow into the calculations, either on its own or in association with transformation plasticity. The residual strains predicted from all the calculations were tensile at all points within the plate, although surface strain values were higher than those at the centre. Calculation FP_{13} showed the highest residual strain values across the section whereas, calculation FP_{18} (with transformation plasticity only) gave the lowest. The calculated residual strains obtained from calculation FP_{15} (stress relaxation method 2) were slightly lower than that has been predicted by calculation FP_{13} (no stress relaxation). The introduction of transformation plasticity into the calculations reduced the magnitude of the residual strains. Thus, all the three calculations (FP_{16} to FP_{18}), which incorporated transformation plasticity, predicted very low levels of this quantity, although all the calculations that ignored transformation plasticity produced relatively large residual strains. An increase in the rate of stress relaxation also reduced these strains.

5. THE APPLICATION OF THE MATHEMATICAL MODEL OF THE STRESS AND STRAIN GENERATION PROCESS DURING QUENCHING

The mathematical model developed during the present work now contained all the known characterisitics related to the quenching process. Therefore, it should be able to predict the generation of thermal stress and strain with a reasonable degree of accuracy in a wide range of quenching conditions. Hence, it was necessary to check the model by its application to a wide variety of quenching situations. This had already been done in the development of the model as far as standard quenchants and thin plates are concerned. However, it was desirable to check further the developed model in other situations, to see whether any further modifications are necessary. The three examples chosen are:

(i) Martempering, because it involves a large period of time at relatively high temperatures.

(ii) Section size, because viscous flow becomes progressively more important as the thickness increases.

(iii) Effect of Ms and Mf temperatures, because these affect the magnitude of transformation strain in the quenching process.

5.1 Martempering

5.1.1 Martempering (Salt bath treatment at 400°C followed by air cooling).

The predictions of thermal stress and strain within a plate during martempering (followed by air cooling) were obtained from calculations FP_{19} to FP_{21} and are shown in figures 70 to 72. The residual stress and strain distributions at the end of this treatment are shown in figures 73 and 74 respectively. Figure 70 shows the stress and strain relationships predicted without considering the effect of viscous flow

on the thermal stress and strain generation process (calculation FP_{19}). During the salt bath treatment, the surface was initially subjected to a tensile stress while, at the centre the sense of the stress was compressive. At the start of this quench the absence of a vapour blanket led to a high heat transfer coefficient that produced substantial plastic flow at both the surface and the centre. A maximum tensile stress of 75 MPa at the surface and a maximum compressive stress of -48 MPa at the centre was developed. At the end of the plastic flow, the surface was at a temperature of 711°C and, due to the fast cooling rate at this stage at the centre, unloading of the tensile stress occurred at the surface. The stress at the centre now became tensile and that at the surface compressive. The magnitude of the latter was high enough to cause plastic flow when it was at a temperature of 591°C. Once the surface temperature reached 465°C, the plate specimen was transferred from the salt bath to the atmosphere for air cooling. As the temperature of the air was at 20°C, there was an immediate increase in the temperature gradient between the surface and the centre, which caused a reduction in the compressive stress at the surface until the temperature at this point reached 418°C. At this point in the quench the centre was subjected to a faster cooling rate than the surface, which caused the compressive stress at the surface to increase. The martensitic transformation at the surface further increased the level of compressive stress at this point to a maximum value of -180 MPa, when the temperature has fallen to 284°C. Unloading of the surface compressive stress now occurred as the transformation moved towards the centre of the plate. The maximum tensile stress developed at the centre was 135 MPa. At the end of the cooling process, the surface was subjected to a residual stress of -154 MPa and a residual strain of 0.0377%, while the centre was

subjected to a residual stress of 120 MPa and a residual strain of -0.0318%.

The relationships between stress and strain at the surface and the centre in the presence of viscous effects, which were predicted by calculation FP_{20} (stress relaxation method one) and FP_{21} (stress relaxation method two) are shown in figures 71 and 72 respectively. These relationships show the significant effect of the stress relaxation process on the results obtained at both the surface and the centre. In both calculations the first unloading of the stresses at the surface and the centre occurred at an earlier stage than that predicted by calculation FP_{19} (no stress relaxation). The presence of a substantial amount of viscous flow during the salt bath treatment reduced substantially the level of residual stress and strain at the end of treatment.

In the case of calculation FP_{20} (method one) the viscous flow effect was more prominent in the later stages of the treatment in the salt bath, when the temperature at the surface lay between 737°C and 465°C, and the temperature at the centre lay between 822°C and 469°C. As the rate of cooling fell, the time involved in the treatment became sufficient to allow the generation of a considerable amount of viscous flow. This is shown in figure 71 by the non-linear curve representing the relationship between stress and strain at the surface at temperatures below 737°C. None of this anelastic flow was due to plasticity, since the stress never reached a point on the yield surface. In the later stages of the salt bath treatment the stress relaxation that accompanied the viscous flow predominated over stress generation and the absolute stresses fell at both surface and centre. At the end of the salt bath treatment the absolute stresses at both surface and centre were in

consequence small. Subsequent cooling of the specimen in the air created an increase in the temperature gradient in the specimen, which produced a reduction in the compressive stresses at the surface and in the tensile stresses at the centre. This unloading was not significant on account of the subsequent martensitic transformation at the surface, which increased the absolute level of the stresses at the surface and the centre. This increase in the stress level was very small, due to the modest cooling effect produced by air and the presence of stress relaxation. The stress at the surface began to unload again at 285^{o}C, because at this point austenite at the centre started to transform to martensite. The tensile stress at the centre also began to unload as a consequence of transformation and viscous flow. This unloading of the stresses at both the surface and the centre was continued and at the end of cooling process very low values of residual stresses were predicted at all points in the plate.

In case of calculation FP_{21} (stress relaxation method two) a maximum tensile stress of 74 MPa was produced at the surface before the first unloading of the stress, which resulted from the combined effects of viscous flow and the fast cooling rate at the centre. The low stress relaxation rates, pertinent to this calculation, produced the steep slopes of the curves that show the stress and strain relationships at the surface and the centre, (compare figures 71 and 72). After the first reversal of stress at the surface, when the temperature reached 562^{o}C in 20 seconds, the rate of stress relaxation was maintained at a constant level to represent steady state creep conditions. As the temperature fell to 535^{o}C, an unloading of the surface compressive stress was brought about by the fast cooling rate at the centre. The maximum compressive stress produced by this calculation (FP_{21}) was about

twice as high as that suggested by calculation FP_{20} (method one). The removal of the specimen from the salt bath to the air created an immediate increase in the temperature gradient in the specimen, which caused further reduction in the compressive stress that already existed at the surface. Once the surface reached 300°C, a stress of only -4 MPa was left at this point in the specimen. At this stage, the surface began to transform to martensite and the surface stress became more compressive, until the temperature reached a value of 285°C. The maximum level of compressive stress attained (-31 MPa) at this stage, was smaller than that predicted by calculation FP_{19} (no viscous flow), but higher than that predicted by calculation FP_{20} (method one). The subsequent unloading of the surface stress as a result of martensite formation at the centre, was continued until a stress reversal occurred, so that at 152°C, a tensile stress of 6 MPa had been generated. This was slightly reduced after completion of the martensite transformation at all the points in the plate.

The residual stress distributions across the plate are presented in figure 73, while the corresponding residual strain distributions obtained are presented in figure 74. In the absence of viscous flow (FP_{19}) the predicted residual stresses were compressive towards the surface and tensile towards the centre. The maximum tensile stress was 120 MPa and the maximum compressive stress was -154 MPa. In contrast the residual stresses predicted by both the models that includes viscous flow suggested very low values at all points in the plate. This means that the complete martempering operation was sufficiently long to allow the virtual complete relaxation of the thermal stress generated during cooling. The patterns of residual strains predicted by all the calculations were similar except that the level of residual strains predicted by calculation FP_{19} was slightly higher at the surface

and lower towards centre than the corresponding values predicted by the other calculations (FP_{20} and FP_{21}).

5.1.2 Martempering (Salt bath treatment at 400°C followed by an oil quench to 20°C).

Figures 75 to 79 show the relationships between stress and strain at the surface and the centre of a 15 mm plate subjected to Martempering, followed by oil quenching. During the salt bath treatment these relationships were identical to those predicted for the 15 mm martempered plate cooled in air (section 5.1.1).

Figure 75 shows the relevant relationship predicted by calculation FP_{22} which ignores the stress relaxation effect. When the temperature of the specimen reached 465°C, it was transferred to an oil bath at 20°C. This immediately created a high temperature gradient in the plate, which caused a reduction in the compressive stress that already existed at the surface. At 428°C this process reversed, on account of the increase in the cooling rate at the centre relative to that at the surface. The remaining relationships between stress and strain were similar to those predicted by calculation FP_7 (oil quench without stress relaxation), figure 54.

The relationships predicted by calculations FP_{23} and FP_{24} in the presence of stress relaxation method one and method two respectively, are presented in figures 76 and 77. The variations in the stresses and strains during the earlier part of the quench, up until the specimen left the salt bath, were identical to those obtained from calculations FP_{20} and FP_{21} (Figure 71 and 72). Subsequent oil quenching increased the temperature gradient in the plate, which caused the surface compressive stress and centre tensile stress to unload. In the case of calculation FP_{23} which incorporated a high rate of stress relaxation

(method one), stress reversal at both the surface and the centre occurred, although the subsequent transformation of the surface produced another reversal of these stresses. As a consequence of the combined effect of stress relaxation and the martensitic transformation of the surface, the development of the compressive stress at the surface and tensile stress at the centre was brought about. After this stage, the stress and strain relationships observed were very similar to those observed in the case of conventional oil quenching (compare figures 76 and 77 with figures 55 and 56 respectively).

The relationships between stress and strain at the surface and the centre obtained from calculations FP_{25} and FP_{26} in the presence of viscous flow and transformation plasticity are shown in figures 78 and 79. These relationships were found to follow the same sequences as those predicted by calculation FP_{23} and FP_{24} in the absence of transformation plasticity, until the surface temperature reached the Ms. After this, the results were very similar to those obtained during conventional oil quenching under the same conditions (calculations FP_{10} and FP_{11}), figures 57 and 58. However, the levels of stresses and strains at the end of the Martempering (followed by oil quenching) process were slightly lower than after an oil quench direct from 850°C.

The residual stress and strain distributions within the plate determined from calculations FP_{22} to FP_{26} are presented in figures 80 and 81 respectively. All these residual stress and strain distributions at the end of the oil quench from the salt bath were very similar to those obtained at the end of a conventional oil quench from 850°C (figures 60 and 61).

5.2 The Effect of Plate Thickness on the Generation of Thermal Stress and Strain

The effect of specimen size on the development of thermal stress and strain has been studied by means of the same mathematical model that was used to calculate thermal stress and strain during the quenching of a thin plate: i.e. calculations FP_5 and FP_{11} (stress relaxation method two and transformation plasticity). In this investigation all parameters other than plate thickness were kept constant. The transformation that took place in the thicker sections also remained the same, viz only austenite →martensite. This was possible because the hardenability of the steel 835M30 was sufficiently high to prevent diffusional decomposition of austenite during quenching in all but extremely thick sections.

Water Quenching

Five plate thicknesses from 20 mm to the maximum 60 mm were considered in the case of water quenching. Figure 82 shows the relationships between stress and strain at the surface of water quenched plates. These relationships followed the same sequence as that described in section 4.5.1.2, calculation FP_5. However, the increase in the plate thickness produced certain changes to the thermal stress and strain generation process. Thus, a drop occurred in the temperature at which the first unloading of the surface stress was produced. As a consequence, the amount of tensile plastic flow at the surface became greater as the thickness was increased. The amount of negative plastic flow during the early stages of the formation of martensite was reduced by the same amount. Since both these changes contribute to the final state of strain, the overall effect of an increase in plate thickness was a substantial increase in the tensile strain present at the surface at the end of quench. The amount of

viscous flow before and after the start of unloading of the compressive stress and the magnitude of unloading of the tensile stress after the completion of transformation at all points in the plate, were increased as the plate thickness increased. Hence, the final stress at the surface became lower as the plate thickness increased.

The corresponding relationships between stress and strain at the centre during water quenching are presented in figure 83. In the centre of the plate, the same sequence occurred as has been reported in the case of the 20 mm thick plate (section 4.5.1.2). In contrast to the results obtained at the surface, an increase was produced in the temperature at which the first unloading occurred as the thickness increased. An increase in section thickness produced an increase in the plastic flow at the centre in the earlier stage of the quench and also later during the transformation of the surface region. The increase in the magnitudes of these plastic flows were largely responsible for the progressive increase in the final tensile strain as the thickness increased. The amount of unloading of the compressive stress at the centre after the completion of transformation within the plate also increased progressively as the thickness increased, which reduced the level of compressive stress at the end of quench.

The predicted residual stress distributions within plates of various thicknesses are presented in figure 84. In all the cases a small tensile stress occurred near the surface and maximum tensile and compressive stresses were produced at dimensionless position ratios (x/L) of 0.75 and 0.0 respectively. The corresponding residual strain distributions are shown in figure 85. The increase in strain that was produced by an increase in plate thickness from 20 mm to 60 mm was slightly greater at the surface than that at the centre (0.23% and

0.15% respectively). The overall effect of an increase in plate thickness in the case of water quenching was a reduction in the residual stresses and an increase in the residual strains at all positions in the plate.

Oil Quenching

The plate thicknesses considered in the case of an oil quench were generally smaller than those subjected to a water quench, with the maximum limited to 30 mm. This was because of the longer cooling times involved at a particular thickness with an increased possibility of decomposition of the austenite by diffusional processes. Figure 86 represents the variations in the relationships between stress and strain at the surface of plate specimen during oil quenching when the plate thickness was increased from 10 mm to 25 mm. Although, the patterns of the curves are the same as those predicted in the case of calculation FP_{11} (oil quench with stress relaxation method two and transformation plasticity), some modifications were associated with the change in plate size. An increase in plate thickness greatly increased the amount of positive plastic strain introduced at the surface in the early stages of the quench, slightly reduced the temperatures at which the first and second unloading occurred at the surface and significantly increased the level of compressive stress present when the surface reached the Ms temperature. The amount of transformation plasticity subsequently introduced was also increased by this change in plate thickness. The overall effect of this modification to the plate dimensions was a progressive increase in the compressive residual strain at the end of the quench.

The corresponding relationships between stress and strain at the centre followed the same general sequence as that developed at the surface, but the sense of the stress at any particular stage was

reversed. Also, the temperatures at which particular events occurred were usually different from those pertaining to the surface. These changes have not been described in detail.

Figure 87 shows the effect of plate thickness on the calculated residual stress distribution at the end of an oil quench. The residual stresses at the surface were only slightly increased by an increase in the plate thickness but, at other points in the plate the effect was more marked, particularly at the centre. However, the overall change in the stress level was small. The influence of plate thickness on the residual strain distribution in the case of an oil quench was in contrast to that of the water quench. The average strain in the section decreased as the thickness was increased, (figure 88).

5.3 The Effect of Transformation Temperature Range on the Generation of Thermal Stress and Strain

Compositional variation within a low-alloy steel specification has a significant effect on the Ms and Mf temperatures[12]. These in turn have an effect on the distortion and thermal stress generated during quenching[101]. In order to study this aspect of the problem a second steel 709M40 (Table 11) has been used to examine the effect of variation of Ms and Mf temperature on the generation of thermal stress and strain. The physical and mechanical properties of the steel do not differ significantly from those used in the work on the 835M30 steel, so these have continued to be used in these further calculations.

Figure 89 represents the influence of an increase in the Ms temperature from 315°C to 350°C on the relationships between stress and strain at the surface of a water quenched plate. Although, the stress and strain generation process followed the same basic pattern

in each case, the increase in Ms temperature produced certain modifications to the details of the sequence. Thus, an increase in Ms temperature produced an increase in the tensile plastic flow, whereas, the transformation plasticity in compression after the initial stress reversal was reduced significantly. The difference in the maximum compressive stress developed was insignificant but the temperature at which the surface attained this compressive stress was increased as the Ms temperature increased. This was associated with an increase in the tensile stress and strain present at the surface at the end of the quench.

The sequence of events at the centre (figure 90) was similar to that described in section 4.5.1.2, calculation FP_5. The most significant effect of the increase in Ms temperature on the relationships between stress and strain at the centre of the plate was an increase in the amount of tensile plastic strain introduced before the Ms temperature was reached. As a consequence, there was a corresponding increase in the amount of tensile strain at the end of the quench, although the associated change in the final stress level was very small.

Figures 91 and 92 show the effect of Ms temperature on the residual stress and strain distributions within a plate after water quenching. The change in the residual stresses present at all points within the plate as a consequence of this change in Ms temperature is very small. In all cases a maximum tensile stress occurred at a point just below the surface, while, a maximum compressive stress always occurred at the centre. The influence of Ms temperature on the residual strains was much more significant. These rose in a reasonably uniform manner as the Ms temperature rose from 315^{o}C to 350^{o}C.

The effect of variations in the Ms temperature on the residual stresses obtained after an oil quench was very small (figure 93). The corresponding effect on the residual strains was likewise modest (figure 94), although, there was a small but uniform increase in the strains at all points in the plate as the Ms temperature rose from 315°C to 350°C.

6. EXPERIMENTAL INVESTIGATIONS OF RESIDUAL STRESSES AND STRAINS

Although a considerable amount of experimental measurements of residual stresses and strains had been carried out previously on plates quenched in water and oil, there was a need for additional information on polymer quenched and martempered specimens. The experimental work involved the measurement of residual stresses and strains in the plates of 835M30 steel after martempering and polymer quenching. The dimensions of the plates were 120 mm x 120 mm x 15 mm and 120 mm x 120 mm x 20 mm. To achieve the conditions of unidirectional heat flow, the edges of the plates were insulated with Kaol-Wool ceramic fibre insulation. The thickness of this insulation was not more than 6 mm and was lightly held in position by a band of stainless steel. The tension of the band was very low, so the constraining forces applied to the edges of the plates were not significant. To prevent the oxidation of the specimen surface during treatment, the plate specimens were electro-plated with a 0.05 mm layer of nickel.

The experimental procedure involved in the present work contained the following four stages.

i. Stress-relief and softening treatment.
ii. Hardening treatment.
iii. Residual strain measurements.
iv. Residual stress measurements.

6.1 Stress-Relief and Softening Treatment

Prior to the hardening operation, the plate specimens were subjected to this treatment to ensure that the material was in the ferritic and carbide condition and that any residual stresses from previous operations were removed. This was necessary to achieve the same initial situation

as that represented in the mathematical model i.e. stress-free and soft plate specimen. The softening and stress-relief process involved heat treatment at 630°C in a muffle furnace flushed with argon, for two hours, followed by a furnace cool to room temperature. The surfaces of the plates were then lightly cleaned with 400 grade silicon carbide paper, to obtain a constant surface condition. After this, the dimensions of the plates were measured (section 6.3) before quenching.

6.2 Hardening Treatment

After the softening operation, the edges of the plate were fitted with Kaol Wool insulation as described earlier. In the centre of one edge of the plate an eye bolt was screwed (see figure 95) to facilitate the shifting of the plate from furnace to quenching tank. The material used for the eye bolt was of the same material as the plate to prevent any localized stresses due to uneven expansion or contraction.

Prior to quenching, austenitisation of the plate was carried out at 850°C for 1.5 hours in the argon atmosphere. The furnace used for this purpose was the same as was used for the softening operation. The quenching was carried out in Polymer Solution or in molten salt bath. The quenching of the specimens was carried out in a tank, the dimensions of which are shown in figure 96. In order to ensure that the specimen was quenched edge wise (the same manner as had been used to determine the surface heat transfer coefficients[18]), a pair of channel guides was used (figure 96). For efficient cooling a fresh supply of the quenchant at the specimen surfaces throughout the cooling process was necessary, so the quenchant was agitated by means of two stirrers rotated at a speed of 50 rpm in the quenching tank. The temperature of the quenchant was always within $\pm$ 1°C of 20°C, owing to the large quantity of quenchant used and the continuous agitating effect.

In the case of martempering a standard pot type furnace-heated salt bath was used with a Nitrate-Nitrite salt of eutectic composition at a temperature of 400^{o}C. The dimensions of the pot were 200 mm diameter and 240 mm deep and the depth of the salt was 180 mm. The salt bath quenching time was 80 seconds, which was found to be the best compromise between a small temperature gradient and no decomposition of austenite (see figure 33). After 80 seconds, the specimen was transferred to the external atmosphere for air cooling.

Once the specimens had cooled to room temperature, they were thoroughly cleaned with soap and alcohol and were remeasured for dimensional changes, as described in the next section.

6.3 Residual Strain Measurements

The residual strain developed in the plates after heat treatment was obtained by measurements of the length, breadth and the thickness of each plate before and after the quenching operation. The plates were left in the metrology laboratory at least 24 hours to acclimatise to the laboratory conditions before any measurement was made. However, the remeasurement of the specimen after it had been hardened was made within 48 hours of the completion of hardening treatment.

6.3.1 Measurements Along the Length and Breadth of the Plates

The changes in the dimensions of the steel component after quenching were found to be very small [18,30] and to measure such small changes a very accurate measuring system was needed. To achieve maximum accuracy a Societe Genevoise Universal measuring machine (shown in plate 3) was used, since it gave an accuracy better than $\pm$ 0.0003 mm, which was considered to be sufficient for the changes involved.

The thickness and lengths of the plates were each divided into 5 equally spaced zones and subsequent dimension measurements were made at the junction of the zones (see figure 97). The distances between corresponding points on opposite edges of the plate were measured before and after the hardening treatment. The plate was laid on the bed of the machine with a supporting plate between the bed and one face of the plate. The bed of the machine was capable of moving laterly. A steel probe positioned above the bed was attached to a vertical head, capable of vertical and transverse movements, the positions of which were measured using an eyepiece with cross wires. The probe was brought into contact with each edge of the plate at the measuring position by the combined movement of the horizontal bed and the vertical head. At each of the positions A-K, measurements were made at 5 points intermediate between two faces of the plate, as shown in figure 97. The results obtained before and after the austenitisation and quenching treatments were used to calculate the percentage strain in the longitudinal direction using the expression:

$$\% \Delta Y = \left[\frac{Y_h - Y_s}{Y_s}\right] \times 100 \qquad \ldots\ldots 6.3.1$$

6.3.2 Measurements of the Thickness of the Plate

The Societe Genevoise Universal measuring machine could only measure the thickness of the plate near the edges, due to the probe position in the machine. These measurements were affected by the presence of plate edges[18,24,30] and provided only information of strain developed in the vicinity of the edge. In order to determine dimensional changes unaffected by the edge it was necessary to obtain information from measurement of the thickness near the centre of the plate. To obtain this information, a complicated technique was adapted from the standard

test used to check the flatness of a surface [107].

The equipment shown in plate 4 were used to measure the changes in the thickness of plates at various points along both the axes as shown in figure 98. The plate was divided into 11 equispaced positions (10 mm apart) along both the axes across the centre of both surfaces of the plate. The thickness of the plate at the first and last position (C_1 and C_{11} in figure 99) was obtained by the Societe Genevoise Universal machine, as both these positions were near to the edge. The plate was placed with its faces inclined (keeping the position 11 towards the highest edge) at a very small angle to a reference axis which was parallel to the surface on which the plate was placed. An electronic comparator (see plate 4 and figure 99) was traversed across an axis from one edge to another and a reading was obtained at each position. The level of the comparator was set at zero while at position 11.

Due to changes in thickness at various points, the plate surface was not parallel to the central plane of the plate. It was assumed that the variation in thickness was as represented in figure 99. Where (x-x) was the central axis of the plate, (O-O) was the line of measurement and (O'-O') was a line parallel to the central axis of the plate. From figure 99:

$$\Delta C' = C_1 - \left(\frac{P-q}{2}\right) \qquad \ldots\ldots 6.3.2$$

And

$$\Delta C_1 = C_1 - \Delta C' \qquad \ldots\ldots 6.3.3$$

Since point 11 was made to lie on the reference line (O'-O'), the half thickness at point 1 was given by:

$$\tfrac{1}{2}T_1 = \frac{P}{2} - \Delta C_1 \qquad \ldots\ldots 6.3.4$$

Thus, the corresponding half thicknesses at the intermediate points was given by:

$$\tfrac{1}{2}\, T_N = \frac{P}{2} - \Delta C_N \qquad \ldots\ldots 6.3.5$$

Consider a set of right angle triangles with common angle 'β' and with the right angle placed at one of the measurement points numbered 1 to 11 on line (O-O) in figure 99. By similarity of triangles, the values of ΔC_N in equation 6.3.5 at intermediate positions were related to the values of $\Delta C'$ by:

$$\Delta C_N = C_N - \left[\frac{11 - N}{10}\right] \Delta C' \qquad \ldots\ldots 6.3.6$$

In a similar way the half thicknesses at corresponding points were obtained from the other side of the plate and were added together to give the total thickness of the plate at those points. The thicknesses obtained, prior to and after the hardening operation were then used to determine the strain produced in the thickness direction using:

$$\%[\Delta \varepsilon zz] = \left(\frac{T_h - T_s}{T_s}\right) \times 100 \qquad \ldots\ldots 6.3.7$$

The results obtained from this equation gave experimental evidence of the extent of the edge effect, which influenced the final shape of the plate. All the measurements of the change in plate length and breadth were made across points of the specimen that included positions which were affected by the edge. Therefore, the strains obtained from these measurements were also influenced by this effect. Hence it was important to have some information about the strains at points where the edge exerted no influence i.e. towards the centre of the plate. As no stress existed in a direction perpendicular to the plane of the plate (plane-stress condition), the measurement of the change in thickness at

the points not influenced by the edge, were directly related to the mean change in length and breadth across the thickness at positions away from the edge affected regions. Therefore changes in thickness at the centre could be used to obtain values of the strain in the plane of the plate at points where the edge exerted no influence. However, only an average strain for the whole thickness was obtained by this method, although it was useful to compare the values so obtained with the average of the directly measured in-plane stresses, which were affected by the edge. The difference between the two results gave an indication of the magnitude of the edge effects.

In order to compare the two sets of strain values, the measured strains were adjusted for the volume change associated with a change from a ferrite + carbide structure to martensite, as the calculated results involved only those generated during cooling from the austenitisation temperature, viz:-

$$\varepsilon zz \text{ (measured)} = \varepsilon zz \text{ (calculated)} + \frac{\Delta V}{3}$$

And

$$\varepsilon xx \text{ (measured)} = \varepsilon xx \text{ (calculated)} + \frac{\Delta V}{3}$$

$$\varepsilon xx \text{ (calculated)} = -\tfrac{1}{2}\, \varepsilon zz \text{ (calculated)}$$

Therefore,

$$\varepsilon xx \text{ (measured)} - \frac{\Delta V}{3} = -\tfrac{1}{2}\left[\varepsilon zz \text{ (measured)} - \frac{\Delta V}{3}\right]$$

The experimental results were useful for comparison purpose with the theoretical results obtained from the mathematical model.

6.4 Residual Stress Measurements

A destructive, mechanical method was used to measure the residual stress distribution across the thickness of the plate. The method used consisted of the measurement of the change in strain at the centre of

one face of the plate when successive layers were removed from opposite face. The residual stress was calculated from the measured change in strain; using the procedure documented by Andrews[7] and modified by Price[18] (see Appendix II).

The strain-measuring device consisted of a strain gauge rosette (Tokyo Sokki Kenkynjoo FRA-6-11) with three arms, which was fixed at the centre of the plate surface, as shown in figure 100. All the measurements from the strain gauges were made using a FYLDE Bridge/Transducer Amplifier of the type FE-359-TA. The output from the amplifier was connected to a digital voltmeter, capable of reading 10 volts, which corresponded to a strain of 0.33. A control box with multiway toggle switch was used, which enabled the arms of the rosette to be connected to the Wheatstone bridge one at a time. The three inactive arms of the Wheatstone bridge were formed from a separate strain gauge rosette, fixed to a steel strip, with its arms connected in series (figure 101). This strip was placed on the grinding bed, alongside the plate, so as to be in a similar condition to the other gauges. To ensure the proper insulation of the strain gauges, they were coated with Polyurethene and wax.

A Burdett surface grinding machine was used to remove the layers from the plate. In order to eliminate the introduction of machining stresses, a very slow rate (1 mm per hour for a 20 mm plate and 0.75 mm per hour for a 15mm plate) of surface grinding was used. The material was removed by a series of cuts 0.05 mm deep, accompanied by the cooling of the specimen with large quantities of coolant. The strain gauge readings were made after the removal of a 1 mm thick layer in the case of 20 mm plate and a 0.75 mm layer in the case of 15 mm plate. Prior to any strain measurements, the plate was allowed to cool for 20 to 30 minutes, so that the small amount of heat generated by the grinding

operation was dissipated and the strain gauge reading had stabilized. The magnets of the clamp in the grinding machine were switched off during this period and when the bridge was zeroed. After every reading the grinding wheel was dressed before grinding was recommenced.

The readings obtained from each of the rosette arms were independent of the orientation of the device i.e. all the stresses in the plane of plate were equal at the plate's surface, so the mean of the results obtained from three arms was used in the subsequent calculation of stress. The oscillations of the bed of the grinding machine, the very long time period required to complete the stress determination and the presence of large quantities of the coolant in the vicinity of the strain gauges, all introduced spurious signals not connected with the strain in the plate. To ensure the elimination of such signals, another strain gauge was installed as a standard on the spacing plate used to support the main plate specimen. Both strain gauges were read each time a strain measurement was made and the difference between the two readings was used to calculate the residual stress present in the layer which had just been removed.

It was not possible to measure the stresses throughout the whole thickness of the plates, since grinding became impossible when the thickness fell below a critical minimum value. Therefore, stress measurements were made only over half the thickness of the plates and the results in the remaining part of the plates were obtained by interpolation and the use of the assumption of symmetry of stress and strain about the central plane of the plate.

It is known that the grinding technique used in the residual stress measurement can induce additional stresses into the component due to frictional heat and plastic deformation[80]. However, the previous

work[41] had proved that such stresses were negligible with the technique at present in use. As a further check, the determination of the residual stresses was conducted by this technique on a plate specimen in a stress relieved condition. This was the same specimen as has been used for the determination of the overall volume change associated with a change from a ferrite + carbide structure to martensite (section 4.4.4). The experimental residual stresses found in the plate were insig nificant, so it has been concluded that no stresses were induced in the plate as a consequence of the grinding operation.

6.5 Experimental Results of the Residual Stresses and Residual Strains Present in Quenched Plates

In the earlier investigations by Price[18], experimental data was obtained for residual stress and strain in Polymer, Oil and Water quenched plates. In a later investigation[41] the experiments on the oil quenched plates were repeated, since the earlier results did not compare well with calculation. Martempered plates cooled in oil from the salt bath were also included in this second investigation.

Although a considerable amount of work had been done on the determination of residual stresses in various quenched plates there is an obvious need for some additional information. It was desirable to repeat the experimental measurements on plates quenched in Polymer, since the results previously obtained, like those of oil quenched material, did not compare well with the calculated data. Also included were results from martempered plates cooled in air from the salt bath. These experimental results are given in figures 102 to 111: also included for comparison are the results obtained by Price[18] and Abbasi[41]. The complete set give all the experimental data required to verify the calculated residual stresses and strains obtained in the present investigation.

6.5.1 Polymer Quenched Plate

The polymer quenching of a 20 mm plate specimen was carried out in the manner described in section 6.2, using a 25% by volume aqueous solution of "Aquaquench 1250" at 20°C. Table 8 shows the distortions which were generated in the length and breadth of plate specimen between the reference points A to K on the opposite edges. Figure 108 shows the mean strains obtained from these measurements which were nearly symmetrical about the centre of the plate. However, a slight wrapage of the plate was reflected in a minor variation in the symmetrical appearance of the length changes shown in figure 108, but this was not significant. The average strain calculated from the change in thickness at the centre of the plate is also presented in figure 108 as a horizontal broken line. This strain value obtained from the change in thickness was unaffected by the edge effect and was high in comparison to the strain values obtained by direct measurement of the length and breadth, which were affected by the edge. The average distortions found in the plate after polymer quenching was 0.0521%.

The results of the residual stress distribution in the polymer quenched plate are shown in figure 109. These measurements were made at 11 points beneath the surface at an interval of 1 mm by the procedure described in section 6.4. In the remaining part of the plate stresses were evaluated from consideration of the symmetrical distribution of residual stresses about the centre of the plate. Experimental investigations showed a tensile stress of 190 MPa at the surface and a corresponding compressive stress of -137 MPa at the centre.

6.5.2 Martempered Plate (Air cooling after salt bath treatment)

Table 9 shows the distortions produced, when a 15 mm plate had been quenched in a nitrate-nitrite salt bath at 400°C with a holding time of

80 seconds, followed by air cooling to ambient. The quenching procedure was the same as that described in section 6.2. The salt bath treatment had affected the surface conditions of the plate, particularly at the edges. Therefore, prior to the making of the measurements the plate was thoroughly cleaned with a dilute soap solution and alcohol, to remove any residue left on the plate after the quenching treatment. The mean values of the distortions at position A to K (figure 97) are shown in figure 110 together with the average strain obtained from the change in thickness at the centre of the plate (shown as a horizontal broken line). The discrepancies between the average strain determined from the thickness measurement and the strains obtained from the length and breadth measurements were very small, which indicate that the effect of the edge on the overall distortions found in the length and breadth of the plate was minimal. The average strain found in the plate as a consequence of martempering treatment was 0.0554%.

The magnitude of the residual stress present after martempering and subsequent air cooling was very small at all the points in the plate. Experimentally measured values of this quantity between the surface and the centre of a 15 mm martempered plate are shown in figure 111. This residual stress distribution showed a slightly tensile stress of 28 MPa just below the surface, which became compressive towards the centre of the plate.

7. DISCUSSION

7.1 The General Characteristics of the Stress and Strain Generation Process During Quenching, as Predicted by the Mathematical Model

The mathematical model developed by Price, Fletcher and Abbasi [18, 22, 41] has been used as a basis for the present work. The characteristic stages of the stress and strain generation process predicted by this model are presented in figure 112, and are briefly discussed here. These stages are similar in all the cases involved although, the magnitude and relative importance of each stage is dependent of the severity of the quench. Initially, the surface cooled (from 850°C) more rapidly than the centre, and a tensile stress developed in the surface, which was balanced by a compressive stress in the centre. With an increase in the temperature gradient, the stress level at the surface and the centre reached the flow stress of the material and both the surface and the centre were subjected to plastic flow. When the cooling rate at the centre became faster that at the surface, an unloading of the surface tensile stress occurred which was followed by a stress reversal. Simultaneously unloading and subsequent reversal of the compressive stress occurred at the centre. Once the surface is cooled to the Ms temperature, this region began to transform into martensite, which was associated with an expansion of this part of the specimen. However, in the 40°C temperature range immediately below Ms, the transformation plasticity strain predominated, which restricted the further development of compressive stress. This transformation plasticity was associated with negative plastic flow. When the surface reached 260°C the transformation plasticity effect ceased. Subsequently there was a marked increase in the compressive stress. The centre, which was still untransformed and at a high temperature, was subjected simultaneously to tensile plastic flow. As the transformation front

moved into the interior of the plate, the compressive stress produced at the surface began to unload. The tensile plastic flow generated towards the centre of the plate was terminated by the start of the transformation of the centre to martensite, since the associated expansion of the material caused the tensile stress to unload. These effects led to the reversal of the stresses present at both surface and centre. Once the transformation was complete at all points in the plate a further unloading occurred to a very limited extent only. This was due to the elimination of the remaining temperature gradient as the plate temperature approached ambient. However, at the end of the cooling process, the surface was still subjected to a tensile stress, while the centre was in compression. The presence of viscous effects in the model changed the slope of the curves, in cases where the temperature and time was sufficient to cause this effect.

7.2 Modifications to the Mathematical Model

7.2.1 Viscous Flow; a Function of both Stress and Temperature

The stress relaxation data obtained during the earlier work[41] was a function of temperature and time, which had been obtained over the whole range of temperatures involved in the quench. The stress level was the same as that found by Price[18] to be appropriate at that particular point in the quench. However, Price did not include stress relaxation in his calculations. This is a dubious assumption since it is known that there is coupling between initial stress and the amount of viscous flow. Hence, the stress relaxation rate is not only affected by temperature and time, but also the level of initial stress, and it is apparent from the results of different stress relaxation tests conducted at the same temperature but at different initial stress levels, that the higher the initial stress level the higher is the rate of stress

relaxation and vice-versa. It was therefore, necessary to make the rate of stress relaxation a function of initial stress as well as time and temperature. Hence, a more extensive set of stress relaxation tests have been undertaken at different temperatures and at various initial stress levels, so that the effect of initial stress on the various processes may be included in the model. The stress relaxation rate and the associated viscous flow by the introduction of the initial stress effect in the present model, is smaller than had been suggested by the earlier work of Abbasi[41], who ignored the effect of initial stress.

The stress relaxation rates obtained at a particular stage in the cooling process may be influenced by the thermal and mechanical history of the specimen during the earlier stages of the quench. Therefore, two ways have been used to introduce viscous flow effects into the mathematical model of the stress generation process. This was necessary because of the uncertainty about the degree of "memory" of the early stages of the quench as the material cooled continuously and because of the gradual introduction of the thermal stress over a period of time, rather than instantanously, as in a stress relaxation test. During the present work, the results of experimental investigations of the effect of memory of plastic deformation at higher temperatures suggest very little effect of such deformation on the stress relaxation rate at lower temperatures. However, the time taken to cool the specimen from the deformation temperature to that test temperature was sufficient to cause the recovery process to be completed, which may not be true for the situation of a quenching process where the time period involved is very small. To deal with this situation it is necessary to consider different methods of modelling the isothermal stress relaxation data in a continuous cooling situation. These methods are:

Method One:

The stress relaxation rate produced at a particular temperature is that obtained from the initial slope of the stress relaxation test. In this case the effect of work hardening from the previous strain history has been ignored and the recovery processes are considered to be the dominating feature. This also represents the case where all the stress present has just been introduced into the specimen.

Method Two:

The rate of stress relaxation at a given point is the mean rate obtained during the quench to this time for the first 20 seconds, after which the rate obtained is maintained until the end of the quench. This simulates the steady flow rate found at high temperatures.

The introduction of the initial stress effect on the viscous processes in the original mathematical model of the thermal stress and strain generation process has been found to be very significant in both of the methods used to describe the viscous flow. A comparison of the relationships between stress and strain predicted by either of the present models with those predicted by the earlier work of Fletcher and Abbasi[22,41] (when viscous effects were considered to be independent of the initial stress) shows the very considerable effect of initial stress level (compare figures 55 and 113).

The stress generation process during the early stages of cooling was relatively unaffected by viscous flow in the case of all the quenching conditions (i.e. water, oil and polymer). This is because of the short time period involved during this part of the process. However, in the case of water and polymer quenching, the introduction of the effect of initial stress on stress relaxation produced an earlier unloading of the

surface and centre stresses than was the case in the calculations that used the earlier model[18,22,41]. The viscous effect was found to be significant at the surface during the greater part of the oil quench (figures 55 and 56). An appreciable amount of viscous flow occurred during the transformation of the surface to martensite, on account of the high level of compressive stress produced at this point in the water and polymer quench. However, the maximum compressive stress so obtained was itself affected by viscous flow and is lower in the present calculation than in any of the earlier work[18,41], (for instance, compare figures 47 and 114). In most cases the calculations predicted tensile stresses towards the surface at the end of the quench. The introduction of transformation plasticity accentuated this effect (see figures 49, 50, 57, 58, 65 and 66). The influence of viscous flow on the stress generation process at the centre is not very significant. This is mostly because of low level of stress present throughout the quench.

Overall it may be concluded that in comparison with the results predicted by the present model, the earlier work[22,41] tended to overestimate the importance of viscous flow in the stress generation process. The residual stresses and strains are discussed in more detail in section 7.3.

7.2.2 Transformation Plasticity

The enhanced dilation during the transformation of austenite to martensite in the presence of a stress (transformation plasticity) is modelled as an additional plastic strain, which is a linear function of stress and temperature. The data of Fletcher and Abbasi[23] was used for this purpose, but the expression that represents this data in the present work has been modified. Thus, the level of transformation

plasticity has been made proportional to the stress above 40 MPa up to an upper limit of 160 MPa. The upper limit of this stress corresponds approximately to the flow stress of austenite. The present modelling of transformation plasticity is a better approximation to the experimental data than that used by Fletcher and Abbasi[23].

The effect of the introduction of transformation plasticity into the calculations of thermal stress and strain is much more significant than the new models of viscous processes. The main consequences of transformation plasticity are the introduction of additional negative plastic strain components as the stress falls to -40 MPa and the simultaneous curtailment of the development of negative stress. This means that the maximum compressive stress developed later in the quench is reduced and the residual strains at the end of the quench are less positive. There is, however a subsidiary effect when the stress is still above 40 MPa when the Ms temperature is reached. This involves extra positive plastic strain during the early stages of the transformation, which counteracts the plastic compressive strain referred to above. This effect, which reduces the shift in residual strain to less positive values, is particularly likely to occur at the centre of the specimen, but could occur also at the surface in material with a high Ms temperature.

The introduction of transformation plasticity also has an interesting consequence for the effect of viscous flow on the stress generation process. The earlier models which did not include this effect suggested very significant stresses during the early stages of the transformation, which produced substantial viscous effects. The restriction in the stress levels, so that they are mainly $\pm$ 40 MPa during this stage in the process, led to a much smaller effect of viscous flow, since the magnitude of this flow is dependent on the level of absolute stress.

7.3 The Residual Stresses and Strains at the end of the Quench

The only way in which the various mathematical models under investigation can be tested is by comparison of the residual stresses and strains with those obtained by experiment and then corrected for the edge effect. Figures 115 to 122 give these comparisons for three different quenchants of widely different quenching powers (water, oil and polymer). All the residual stress distributions after a water quench follow the same form with a maximum just below the surface and a minimum at the centre. However, the introduction of viscous flow reduces the maximum tensile stress and the introduction of transformation plasticity counteracts this effect (viz. calculations FP_4 and FP_5). Figure 116 indicates that the best agreement with experiment is found when viscous flow is introduced by method two (i.e. steady state conditions after 20 seconds) and transformation plasticity is included.

Although all the residual strain distributions after a water quench are of a similar type (figure 117) with slightly greater positive values at the surface than the centre, the introduction of viscous flow displaced the residual strains to lower values. This was similar to the effect of viscous processes on residual stress, although in this case transformation plasticity substantially accentuated the displacement. The original model developed by Fletcher and Price[30] gave very good agreement with experiment and all the modifications introduced since have reduced this correlation. Thus viscous flow on its own is slightly detrimental (figure 117) and transformation plasticity produces extremely poor results. This deterioration is due to the introduction of the negative plastic strain component during the early stages of the transformation.

In contrast to the results obtained after a water quench the residual stresses obtained after an oil quench in the original Fletcher and Price model[30] compared very badly with the experimental values. In fact the results were not even in qualitative agreement, with experimental positive surface stresses and negative calculated stresses at the same point. It was this situation that has led to the subsequent search for an improved model and the introduction of viscous flow and transformation plasticity. Figure 118 shows that the introduction of the former on its own makes the surface stresses less negative while transformation plasticity produces the required change to positive surface stresses. All the models that included transformation plasticity produced very similar results with higher absolute stresses at any given point in the plate than was obtained by experiment. Nevertheless, the level of agreement between these calculations and the experimental results was reasonably good.

The changes produced to the residual strains by the modifications to the model were relatively small, but were beneficial. The inclusion of both transformation plasticity and viscous flow reduced the discrepancy between experiment and calculation to very small values (figure 119).

In the case of residual stress distributions after a polymer quench the introduction of viscous flow produced a general reduction in the absolute level of stress obtained at a particular point. This was similar to the effect produced in the case of a water quench; as was the presence of a maximum tensile stress just below the surface. The effect of transformation plasticity was small but the best agreement with the experimental results was obtained when this effect was included together with either of the viscous flow models (see figures 120 and 121).

Like the results obtained after a water quench the introduction of viscous flow and transformation plasticity produced a very marked reduction in the residual strains produced after the polymer quench. This was especially so in the case of transformation plasticity. The calculated results originally obtained by Fletcher and Price[30] were in very poor agreement with experiment. The reduction in calculated residual strains produced by the introduction of viscous flow and transformation plasticity was responsible for a very marked improvement in the level of agreement with the experimental results. Either the use of model two viscous flow or no viscous effect taken in conjunction with transformation plasticity produced a satisfactory level of agreement between experiment and calculation, (figure 122).

It is evident that the use of method two for the viscous flow processes, together with transformation plasticity (calculations FP_5, FP_{11} and FP_{17}) produced an overall improvement in the level of agreement between calculation and experiment. This improvement is summarised in qualitative terms below. Thus:

	Water	Oil	Polymer (25% Aquaquench)
Residual Stress	Excellent	Good	Excellent
Residual Strain	Poor	Good	Good

This is an obvious improvement over the results obtained by Fletcher and Price[30], i.e.:-

	Water	Oil	Polymer (25% Aquaquench)
Residual Stress	Good	Very Poor	Mediocre
Residual Strain	Good	Mediocre	Very Poor

Despite the improvement overall, the reduction in the level of agreement in the case of the strain after a water quench is a matter of concern.

The only known omission from the present mathematical model is the small increase in Ms and Mf temperatures produced by the presence of an applied stress. Consequently a study of this effect has been carried out in the later stage of the investigation, together with an examination of martempering and increased plate thickness. These latter are both cases where viscous effects are likely to be more important and therefore provide better assessment of the viscous flow model selected in the first part of the investigation.

7.4 Varification of the Model by Application to Various Quenching Situations

7.4.1 Martempering

(a) Martempering (followed by air cooling).

The relationships between stress and strain during the martempering operation are shown in figures 70 to 72, which include the results obtained by the use of both the methods of stress relaxation. Transformation plasticity is not relevant in these calculations since the stress generated during transformation is not sufficient to cause

such an effect. In all cases the relationships between stress and strain show virtually the same amount of plastic flow as is produced by a conventional oil quench, despite the much smaller difference between the initial temperature of the specimen and that of the salt bath. The explanation of this lies in the characteristics of the salt bath, which does not produce a vapour blanket around the specimen during cooling from 850°C. Thus, nucleate boiling occurs at the onset of the quench, with a consequent high surface heat transfer coefficient at the time when the yield stress of the material is very low. However, during the later stages of such a treatment there is a considerable reduction in the surface heat transfer coefficients, with a consequent drop in the rate of cooling of the specimen, which in turn causes a stress reversal. This also allows sufficient time for a significant amount of viscous flow to be produced (figures 71 and 72) and most of the stress developed is removed as a consequence of stress relaxation by the time the specimen is transferred to ambient by air cooling. In contrast Abbasi[41] suggested the complete removal of all internal stress during this stage, as a consequence of enhanced viscous flow rates in the calculations.

The subsequent air cooling allowed the removal of most of the remaining stress and left the plate specimen slightly in compression before it began to transform to martensite at a temperature of 300°C. The slow cooling rate in air after the salt bath treatment, prevents the generation of a significant temperature gradient across the plate and allows the simultaneous formation of martensite at all points in the specimen. This significantly affected the stress generation process in the later stage of the cooling process and only a very small amount of compressive stress was generated as a result of transformation, which virtually relaxed to produce a stress-free plate at the end of the cooling process.

The corresponding thermal strain obtained at the end of the cooling is small in comparison to the maximum strain introduced during the early stages of quench. This is because the strains introduced before and after the stress reversal almost cancel each other.

In order to eliminate completely the temperature gradient across the specimen, a long salt bath treatment is required, which is undesirable on account of isothermal decomposition of the austenite. To ensure that no such transformations occur, a time of 80 seconds in the salt bath, at a temperature of 400^{o}C has been chosen, which reduces the temperature difference between the centre and the surface of the plate specimen to 3^{o}C. This is an insignificant temperature difference between the surface and the centre, so the time of 80 seconds for the salt bath treatment is a reasonable compromise between the need to reduce the temperature gradient and the necessity to prevent the formation of products other than martensite (see TTT diagram, Figure 33).

The experimentally measured residual stress distributions within a martempered plate show slight tensile stresses at the surface and small compressive stresses towards the centre. This is in reasonable agreement with the calculations of the mathematical model which incorporate stress relaxation process (see figure 123). In contrast the results of calculations that ignore the stress relaxation effect predict a significant amount of compressive stress at the surface and tensile stress towards the centre. The success of the model that includes viscous flow by means of method two, in predicting the residual stress distribution provides support for the accuracy of this model in circumstances where there is sufficient time for a significant amount of creep to occur at temperatures above 400^{o}C.

The experimental residual strain distributions which include 0.12% strain due to the change from the initial ferrite + carbide to the final martensite structure are shown in figure 124 along with the predicted distributions of strain within a martempered plate. It is evident that all the calculated strains are very similar and are not much different from the experimental results. However, a small discrepancy between experimental and calculated strains is present since the latter are slightly greater at all points in the plate. The level of agreement between calculated and experimental strains is virtually unaffected by viscous flow.

It is widely believed that martempering of steel components generally reduces the level of distortions produced in them at the end of quench[32]. However, in the present work, both the experimental and predicted results of residual strains obtained in the present investigation contradict this statement as both the results show a substantial amount of strain in the plate specimen at the end of the treatment. Furthermore, these strains are not significantly different from those produced by a direct oil quench from 850°C to ambient. There is, therefore, little point in using martempering to control distortion. This is because the additional distortions produced by the high surface heat transfer coefficient at the start of martempering negate completely the beneficial effect of the reduced difference in temperature between specimen and quenchant. However, the martempering operation successfully removes the thermal stress by the time the specimen has cooled to ambient. These results suggest that the value of the martempering operation is limited except in the case where it is essential to prevent build up of stress during the martensitic transformation.

(b) Martempering (followed by an oil quench)

There is no difference between the stress and strain generation processes in the salt bath stage of either martempering treatment, (compare figures 70 to 72 with figures 75 to 77). However, when an oil quench was used after the salt bath operation there was a substantial build up of stress during the later stage of the quench. This contrasts with the absences of such stresses during air cooling. The stresses set up in the oil quench during martempering were very similar to those produced in a conventional oil quench from 850°C, (compare figures 75 to 79 with figures 54 to 58).

A comparison of experimental and predicted residual stress distributions (figure 125) show excellent agreement, provided transformation plasticity is included in the mathematical model along with viscous processes modelled by method two. These results, which are similar to those obtained after an oil quench from 850°C, show a better level of agreement than that obtained by the calculations of Abbasi[41]. This further supported the improved accuracy of the present model. However, Abbasi obtained a good correlation between calculation and experiment when viscous flow effect was not considered into calculation after a temperature of 230°C.

The experimental and predicted residual strains are of the same magnitude as those found after an oil quench direct from 850°C (compare figures 119 and 126). It is evident from figure 126 that the experimental results are in good correlation with the calculated results provided transformation plasticity and viscous effects are taken into account. However, a small discrepancy remains, which is reduced towards the centre of the specimen. This discrepancy is very similar to that

found in material that had been subjected to a conventional oil quench from 850°C (figure 119).

The results obtained in the case of oil quenching from the salt bath show that in this case the residual stress and strain distributions are not greatly affected by the use of the intermediate salt bath treatment. There is, therefore, little point in using the extra treatment in the salt bath if the oil quenching is to be used subsequently.

7.4.2 The Effect of Specimen Thickness on the Generation of Thermal Stress and Strain

The increase in strain at the surface before the first stress reversal exceeds that obtained subsequently, while towards the centre the reverse is the case. As the section size increases from 20 mm to 60 mm the earlier strains increase at a greater rate than the later, so the net effect is an increase in the residual strain at all points. This is associated with an increase in the maximum temperature gradient in the plate, and is approximately in accordance with the experimental results. However, the general discrepancy between calculated and experimental results already discussed in the case of 20 mm thick water quenched plates remains in the thicker section, although the change obtained by the increase in section thickness is in good agreement with experimental results obtained from 20 mm and 40 mm thick plates, see figure 127.

The effect of an increase in section thickness, on the residual stress is in contrast to that found in the case of residual strain. An increase in the section size from 20 mm to 60 mm led to a reduction in the residual stress level, despite the increase in the maximum temperature difference between the surface and the centre. However, the

experimental results of Price[18] show an increase in the thermal stress at the end of the water quench, when the plate specimen thickness was increased from 20 mm to 40 mm. The most probable explanation for this discrepancy is an overestimate of the amount of stress relaxation present in the existing model during the later stages of the quench. The residual stress distribution is determined largely by the processes that occur in later stages of the quench, when the time period required to cool the central region of the thicker sections is considerably increased and the stress present is relatively high and quite sufficient to cause significant viscous flow at low temperatures. The large amount of stress relaxation after the completion of the martensitic transformation in thicker sections clearly show the influence of viscous processes. So it would appear that, it is the rate of viscous flow at longer times and low temperatures which is responsible for the existing discrepancy between experimental and predicted results of residual stresses after a water quench.

It also shows that present models of viscous flow overestimate the effect of this process at longer times and low temperatures. Model two assumes a constant rate of viscous flow after 20 seconds to simulate secondary creep, which is inconsistent with experimental data at 650^{o}C and above[41]. However, there is ample evidence that primary creep predominates in steels, at temperatures below 450^{o}C[37], so the present model probably overestimates creep beyond 20 seconds at these lower temperatures. In 20 mm thick plates this overestimate is unimportant, but in specimens 40 mm thick or greater the observed discrepancy between experiment and calculation is probably due to this limitation of the way in which viscous flow is included in the model.

In contrast to the results obtained in water quenched material, an increase in section thickness had little effect on either the residual stresses or residual strains after an oil quench. Although there was sufficient time for the error in the creep model referred to above to have an effect, the overall level of stress was lower, which substantially reduced the amount of viscous flow.

7.4.3 The Effect of the Transformation Temperature Range on the Generation of Thermal Stress and Strain

It has been suggested[101] that compositional variations within an alloy specification may well produce excessive variations in the amount of strains produced in quenched components of the alloy in question. This arises as a consequence of the effect of such changes in composition on the Ms temperature. The present work shows that the residual strain increases as the Ms temperature rises, although the corresponding effect on the residual stress is insignificant. It is evident from figure 89 that transformation strain is negative and smaller than the positive strain introduced at the surface during the earlier stages of the quench. As the Ms temperature increases, the transformation strain is reduced (see figures 89 and 128), while the tensile strain produced at the surface before the first stress reversal is increased (figure 89). Hence, the net effect of both these quantities at the end of quench is an increase in the residual strains as a result of a rise in Ms temperature.

The dilatometry curves that represent the change in dimensions of the martensite and austenite phases converge as the Ms temperature rises (figure 128). Hence, the displacement of the transformation temperature to higher values reduces the transformation strain. As the transformation temperature rises the incremental tensile strain at the

surface before the first stress reversal rises because of increased transformation plasticity before the reversal, (figure 89). This transformation plasticity must be positive and so must increase the total tensile strain introduced at the surface prior to the first stress reversal.

It is apparent from figure 129 that the calculated results obtained with progressively increasing Ms temperature move closer to the experimental results obtained from the 835M30 steel plates. In contrast, the effects of an increase in Ms temperature on the residual stresses and strains after an oil quench were small.

The magnitude of the effect of a relatively small change in the Ms temperature on the residual strain at the end of the quench has possible relevance to the level of agreement between the calculated and experimentally determined strains during the current work. There is some evidence that the Ms temperature rises about $10^{o}C$ in the presence of a stress[23] and Denis et al[25] have suggested that this could be rather higher. According to the present results, an increase in Ms of this magnitude would significantly increase the residual strains and this would significantly reduce the discrepancy between the experimental and calculated residual strains after a water quench. This would have been produced without affecting the existing good agreement between calculation and experiment in the case of residual stresses after a water quench and both residual stresses and strains after an oil quench. Hence, inclusion of such an effect in the mathematical model is of great potential value.

7.5 Overall Assessment of the Model

The mathematical model used in the present work was initially developed by Fletcher and Price[30] and then modified by Fletcher and Abbasi[22] to take viscous processes into consideration. It was apparent from the review of the previous model used by the latter that the approach used to model the viscous processes was not realistic. The effect of initial stress on the rate of stress relaxation and creep was not introduced in the model: instead the values of initial stress selected at each temperature were those that had been suggested by a non-viscous model of Fletcher and Price[30]. This has been found to be inappropriate on account of coupling between stress and viscous flow and the reduction in stress produced just below Ms by the simultaneous introduction of transformation plasticity. Although, transformation plasticity was taken into consideration by Fletcher and Abbasi[23], the equations used were not an exact representation of the experimental data and were prone to instability. The present model is a significant improvement in this respect. However, there is no doubt that the introduction of transformation plasticity, which was generally beneficial as far as agreement between experiment and calculation is concerned, has led to a reduction in the level of agreement between the experimental and calculated strains after a water quench.

The use of the visco-elastic model may be criticised in that it ignores the effect of viscous flow on the yield surface. This aspect of the problem has been considered by Perzyna[39] and Wang and Inoue[43]. However, both investigations used a visco-plastic model and ignored the visco-elastic contribution. This is equally invalid. To be strictly correct a model that takes into account both aspects is required, but this is a matter of extreme difficulty and has not yet been attempted.

The visco-plastic model is probably more correct at very high temperatures, during welding, but the visco-elastic model used here is probably more suitable at the temperatures encountered in quenching. The model used here does take into account viscous flow in both elastic and plastic conditions. It's deficiency is that it does not modify the yield surface in accordance with a combined elastic-visco-plastic model.

From a comparison between experimental and calculated results it is evident that the present model is a significant improvement over the previous models[18,41]. Thus a very good agreement between calculation and experiment is achieved in all cases except the residual strain after water quenching and the residual stress in thicker water quenched plates. The mathematical model was also tested by an investigation of the martempering process and the results obtained were in good correlation with experiment. This further supported the accuracy of the model.

All the results obtained from the existing model emphasise the importance of the inclusion of the effect of viscous processes and transformation plasticity in the calculations. Absence of any of these effects reduced the level of agreement. However, a significant discrepancy in the case of strain after a water quench and in the case of stress after the water quenching of thicker section remains. A possible source of this discrepancy is the effect of stress on the Ms temperature (which has not yet been introduced into the calculations) and a slight overestimation of viscous flow present in the existing model. In addition, the physical property data, particularly the surface heat transfer coefficient used in the calculations may be responsible for a part of this discrepancy, as it is this property that is most susceptible to the small changes in the conditions of the specimen surface and the quenching medium. In addition, the number of stress-dilatometers

installed in engineering laboratories are very few which has restricted the amount of data available on the magnitude of transformation plasticity. As more data becomes available it might be necessary to modify the existing relationships, with a possible improvement in the level of agreement between experiment and calculation.

8. CONCLUSIONS*

1. The level of initial stress in the isothermal stress-relaxation test markedly affected the relationships between dimensionless stress ($\sigma t/\sigma o$) and time at all the temperatures investigated. At the lower temperatures ($\leqslant 500^{o}C$) a threshold stress occurred, below which no significant stress-relaxation was possible. The threshold stress was a function of temperature.

2. The effect of memory of plastic deformation in the early stage of the quench has been experimentally investigated, and the results suggested an insignificant effect of the prior deformation up to 0.5% on the viscous properties of 835M30 steel.

3. The introduction into the calculations of the new stress-relaxation data without the inclusion of transformation plasticity significantly affected the level of agreement between the calculated and experimentally determined residual stress and strain at the end of each quench. A high level of agreement was obtained when a water or polymer quench was involved, but in the case of the oil quench the degree of agreement was still poor.

4. The inclusion of transformation plasticity in conjunction with the modifications to the way that viscous effects are introduced has led to excellent agreement between the calculated residual stress distributions and those determined by experiment after water, oil and polymer quenches. The level of agreement in the case of residual strains was also very good at the end of both the oil and polymer quenches, but after a water quench this agreement was poor.

5. The use of martempering does not reduce significantly the amount of distortion involved in a quenching operation, although air cooling subsequent to the salt bath treatment prevented a stress build-up during the formation of martensite. The poor performance of martempering with respect to the control of distortion may be attributed to the absence of a vapour blanket stage during cooling in the salt bath.

6. The use of an oil quench after the salt bath treatment was not beneficial, because the stresses produced during the transformation and at the end of quench were very similar to those produced by a conventional oil quench from the austenitising temperature.

7. An increase in the specimen thickness produced an increase in the residual strains and a decrease in the residual stress at the end of a water quench. The corresponding effect of an increase in the specimen size after an oil quench was small.

8. An increase in the Ms temperature increased the residual strains obtained at the end of a water quench. In contrast, the effect on residual stress after such a quench was insignificant. The corresponding effect of variation in the Ms temperature after an oil quench was small.

* N.B. All conclusions other than number 7 refer to plates no thicker than 20 mm.

9. RECOMMENDATIONS FOR FURTHER WORK

1. Further work is needed on the effect of stress on the transformation characteristics in steels of various compositions. This work should include diffusional decomposition of austenite as well as the formation of martensite. The extension of the range of transformations is important if processes such as carburising are to be considered.

2. The effect of memory of plastic deformation during the earlier stages of the quench, on the stress-relaxation rate obtained at later stages, should be investigated in more detail.

3. The effect of latent heat has not been included in the present work, although Inoue and Wang[46] suggested that the effect of this property on thermal stress and strain generation is small. It would nevertheless be of interest to include latent heat in the model.

4. Although the amount of strain introduced does not exceed about 0.7%, there will be some heat generated by the deformation process. This small effect could probably also be introduced into the model.

5. A point is now reached where the mathematical model is reasonably successful at the prediction of the thermal stress and strain in quenched plates. It would therefore, now be appropriate to extend the work to more complex geometries.

REFERENCES

1. Benham, P.P. and Hoyle, R., 'Thermal Stresses', Pitman, London, 1964.

2. Gatewood, B.E., 'Thermal Stresses', Mc Graw Hill, New York, 1957.

3. Barrett, S.C., Metals and Alloys, 1934, June, 5, (131).

4. Orowan, E., Proceedings of Symposium on Internal Stresses and Fatigue in Metals, Michigan U.S.A., 1958.

5. Orowan, E., Symposium on Internal Stresses, Inst. Metals London, 1948.

6. Scott, H., Scientific Papers Bureau of Standards, 1925 20, (399).

7. Andrews, K.W., 'Physical Metallurgy Techniques and Applications', Vol: II, George Allen and Unwin Ltd: 1973, (271).

8. Denton, A.A., Met. Rev., 1966, 11, 1, (101).

9. Dolan, T.J., Proceedings of Symposium on Internal Stresses and Fatigue in Metals, Michigan U.S.A., 1958.

10. Gensamer, M., Strength of Materials under Combined Stresses, Am. Soc. Metals, 1940.

11. Evans, W.P., Soc: Automotive Engineers n3, 1963.

12. Thelning, K., 'Steel and its Heat Treatment', IInd Edition, Butterworths, London, 1984.

13. Kobasko, N.I., Met. Soc. Heat Treatment, 1970, 11, (900).

14. Kobasko, N.I., Met. Soc. Heat Treatment, 1975, 4, (287).

15. Sachs, K., Metal Treatment and Drop Forging, July 1961, (281).

16. Inoue, T. et al, J. Mech. Phys. Solids 1978, 26, (187).

17. Hildenwall, B., Dissertation No. 39, Linkoping University Sweden, 1979.

18. Price, R.F., Ph.D. Thesis, 1980 Sheffield City Polytechnic Sheffield, U.K.

19. Horvay, G., J. Mech. Phys. of Solids, 1957, 5 (77).

20. Horvay, G. and Schenectady, N.Y., J. Appl. Mech., March 1953, (87).

21. Denis et al, Trans. I.S.I. Japan, 1982, 22, 7 (504).

22. Fletcher, A.J. and Abbasi, F., Materials Science and Technology 1985, I, (770).

23. Fletcher, A.J. and Abbasi, F., Materials Science and Technology, 1985, I, (830).

24. Fletcher, A.J. and Lewis, C., Materials Science and Technology, 1985, I, (780).

25. Denis et al, Materials Science and Technology, 1985, I, (805).

26. Inoue et al, Materials Science and Technology, 1985, I, (872).

27. Nelson et al, Soc. Auto. Eng. Fatigue Eval. Commt., Sept. 1969, 710283, (1-9).

28. Bulher, H., and Rose, A., Harterei Techn. Mitt., 1966, 21, 1, (1-6).

29. Goodier, J.N., Phil. Mag., 1937, 23, (607).

30. Fletcher, A.J. and Price, R.F., Metal Technology, 1981, 8, (427).

31. Rose, A. and Hougardy, H.P., Symposium Proceedings, Climax Molybdenum Company of Michigan, 1967, (155-167).

32. "Metals Handbook". 9th Edition, Vol. 4, A.S.M., 1981.

33. Dumont et al, Trait. Therm., 1975, 95, (67).

34. Sjöström, S., Dissertation No. 84, Linkoping University Sweden, 1982.

35. Bush, R.H. and Bokros, J.C., Acta Metal, 1964, 12, (102).

36. Odding, I.A., 'Creep and Stress Relaxation in Metals', Oliver and Boyd Ltd., London, 1965, (280).

37. Manjoine, M.J., J. Materials, 1971, 6, (519).

38. Perzyna, P., Advances in Applied Mechanics, 1966, 9, (243).

39. Perzyna, P., Proceedings of Vibration Problems Warsaw, 1963, 3, 4, (281-290).

40. Boley, B.A., and Weiner, J., 'Theory of Thermal Stresses', John Wiley and Sons Ltd., New York, 1960.

41. Abbasi, F., Ph.D. Thesis, Sheffield City Polytechnic, Sheffield, 1983.

42. Rotherham, L.A., 'Creep of Metals', London Inst. of Phys. 1951 (18).

43. Wang, Z., and Inoue, T., Materials Science and Technology, 1985, 1, (899).

44. Greenfield, P., 'Creep of Metals at High Temperatures', Mills and Boon Ltd., London, 1972.

45. Graffalo, F., 'Fundamental of Creep and Creep Rupture in Metals', McMillan Co., New York, 1966.

46. Inoue, T. and Wang, Z., Materials Science and Technology, 1985, 1, (845).

47. Landan, H.G. et al, J. Applied Mechanics, 1960, 27, (297).

48. Boyer, J.C. and Bovin, M., Materials Science and Technology, 1985, 1, (786).

49. Sattler, H.P. and Wesserman, G., J. Less. Com. Met., 1972, 28, (119).

50. Greenwood, G.W. and Johnson, R.M., Proc. Roy. Soc., 1965, 283A, (403).

51. Jong, M. de. and Rathenau, G.W., Acta Met., 10, 1961, 714, (881).

52. Porter, L.F. and Rosenthal, P.G., Acta Met., 1959, 7, (504).

53. Beck, G. et al., Int. Stress. Conf. Deutsch Gesellschaft Fur Metallkunde, 14th-16th April, 1983, Karlsruhe F.R.G.

54. Desalos et al, I.R.S.I.D., Report No. RE902 Saint German en Laye, May 1982.

55. Abrassart, F., Ph.D. Thesis, Nancy, 1972.

56. John, D.J., "Thermal Stress Analysis", Pergamon Press, London 1965.

57. Carslaw, H.S. and Jaegar, J.C., "Conduction of Heat in Solids", 2nd Edition, Oxford University Press, 1959.

58. Aparci, V.S., "Conduction Heat Transfer", Addison Wesley, Reading Mass, 1966.

59. Croft, D.R. and Lilley, D.G., "Heat Transfer Calculations using Finite Difference Equations", Applied Science Publishers, London, 1977.

60. Dusinberre, G.H., "Heat Transfer Calculations by Finite Difference", International, Scrantan, Pa. 1961.

61. Adams, J.A. and Rogers, D.F., "Computer Aided Heat Transfer Analyses" McGraw Hill, N.Y., 1973.

62. Ames, W.F., "Numerical Methods for PDE", Accedemic Press and Thomas Nelson and Sons, New York and London, 1977.

63. Fletcher, A.J., Metals Technology, 1977, 4, (307).

64. Price, R.F., and Fletcher, A.J., Metals Technology, 1980, 7, (203).

65. Inoue, T. and Tanaka, K., Int. J. Mech. Sci., 1975, 17, (361).

66. Toshioka, Y., Trans. I.S.I. Japan, 1976, 11, 13, (1756).

67. Inoue et al, Trans. I.S.I. Japan, 1978, 18, (11).

68. Jeanmart, P. and Bouvaist, J., Materials Science and Technology 1985, 1, (765).

69. Donea, J., International Journal for Numerical Methods in Engineering, 1974, 8,(103).

70. Milne, W.E., "Numerical Solutions of Differential Equations", John Wiley and Sons, New York, 1953.

71. McAdams, W.H., "Heat Transmission", IIIrd Edition, McGraw Hill Kogakusha, Ltd, 1954.

72. Archambault, P. and Chevrier, J.C., Int. J. Heat and Mass Transfer, 1977, 20, (1).

73. Rowe, G.E., "An Introduction to the Principles of Metal Working", Edward Arnold, London, 1965.

74. Mendelson, A., "Plasticity Theory and Application" McMillan Company New York, 1968.

75. Boley, B.A., J. Aeronautical Science, Jan. 1956,(67).

76. Russell, J.E., Proceeding of Symposium on Internal Stresses, Institute of Metals, 1974,(95).

77. Toshioka, Y., et al, Trans. I.S.I. Japan, 1972, 12,(6).

78. Cuicas, H., M.Sc. Dissertation, Sheffield City Polytechnic,1979.

79. Kamamoto, S. et al, Materials Science and Technology 1985, I, (798).

80. Mitter, W., et al, Materials Science and Technology 1985, I, (793).

81. Martin, H.C. and Carey, G.F., 'Introduction to Finite Element Analysis', Academic Press, New York, 1978.

82. Zeinkiewiez, O.C., 'The Finite Element Method in Engineering Science', McGraw Hill, New York, 1971.

83. Desai, C.S. and Abel, J.F., 'Introduction to Finite Element Method', Van Nostrand, Princeton, N.J.

84. Rockey, K.C., et al, 'The Finite Element Method', Crosby Lockwood Staples, London, 1975.

85. Fujio, H. et al, Bull. J.S.M.E., 1977, 20, 146, (1051).

86. Fujio, H. et al, Bull. J.S.M.E., 1977, 20, 150, (1655).

87. Archambault, P. et al, Mt. Sci. Eng. 1980, 43 (1).

88. Archambault, P., Thesis, C.N.R.S., Nancy, France, 1976.

89. Yu, H.J. and Macherauch, E. and Wolfstieg, Arch. Eisenhuttenwes 1978, 49, (499).

90. Sjöström, S., Materials Science and Technology, 1985, I, (823).

91. Buhler, H. and Buckholtz, H., Archiv. Fur das Esen., 1931, 5E, 8, (413).

92. Buhler, H. and Buckholtz, H., Archiv. Fur das Esen., 1933, 5E, 7, (315).

93. Buhler, H. and Rose, A., Archiv. Fur das Eisen., 1969, 40, (411).

94. Vannes, A., et al, Rev. Met. 1974, 71, 5, (307).

95. Wenyu, Z. and Yohai, Z., Proceedings of Int. Symp. on Thermal Stress Calculation, Linkoping, Sweden, 1984, (326).

96. Cullity, B.D., "Elements of X-ray Diffraction", IInd edition, Addison Wesley, 1978, (447).

97. Nakagawa, Y. and Tamura, T., J. Soc. Mat. Sci. Japan 1972, 231, (1099).

98. Breczko, T., Proceedings of Int. Symp. on Thermal Stress Calculation, Linkoping, Sweden, 1984, (513).

99. Burnett, J.A., Materials Science and Technology, 1985, I, (863).

100. Toshioka, Y. 'Materials Science and Technology, 1985, I, (883).

101. Liewellyn, D.T. and Cook, W.T., Metals Technology, 1977, 4, (265).

102. Novik, F.S. et al, Industrial Lab., 1975, 41, 5, (733).

103. Fujio, H., Proceedings of Int. Symp. on Thermal Stress Calculation, Linkoping Sweden, 1984, (388).

104. British Standards 3500.

105. Woolman, J. and Mottram, R.A., 'The Mechanical and Physical Properties of B.S. En Steels', Pergamon Press, London, 1966.

106. Aitkens et al, British Steel Corporation, Internal Report, 1973.

107. Sharp, K.W.B., "Practical Engineering Metrollogy", Pittman Press, 1970.

TABLE 1a: Thermal Property Data used by Toshioka[66]

Heat Transfer Coeff-icient, h ($W/m^2 °C$)	Water	°C	0	100	110	300	500	1000
		h	628	837	8793	8793	6280	209
	Oil	°C	0	200	750	1000		
		h	209	209	1884	1884		
Thermal Conduct-ivity, (W/m °C)	Ferrite Bainite) Martensite)	°C	0	200	400	800	1000	
			52.3	50.2	41.87	(27.2)	(14.7)	
	Austenite	°C	0	1000				
			14.65	27.2				
Specific Heat, Cp ($J/kg °C$)	Ferrite Bainite) Martensite)	°C	0	420	700	800	1000	
		Cp	460	628	837	1005	1885	
	Austenite	°C	0	500	1000			
		Cp	502	628	649			
Latent heat of Trans-formation (J/kg)	Austenite + Ferrite: 75,336							
	Austenite + Bainite: 75,336							
	Austenite + Martensite: 83,740							

TABLE 1b: Physical Property Data used by Toshioka[66]

Young's modulus, E (N/mm^2) x 10^5	^oC	0	400	550	700	1000
	E	2.107	1.842	1.646	1.372	0.588
Yield Strength (N/mm^2)	^oC		0	550	800	1000
	Austenite		196	98	49	29.4
	Ferrite		294	98	29.4	
	Bainite		392	343		
	Martensite		490	392		
Strain hardening coefficient ($d\sigma/d\varepsilon$)	Austenite	0.02 x E				
	Ferrite	0.08 x E				
	Bainite	0.5 x E				
	Martensite	0.6 x E				
Linear Thermal Expansion Coeff. α_{ex} ($^oC^{-1}$)	Austenite	$\alpha_{ex} = 11.9 \times 10^{-6} + 8.14 \times 10^{-9}\theta$				
	Ferrite	$\alpha_{ex} = 16.5 \times 10^{-6} + 7.06 \times 10^{-9}\theta$				
Linear Transformation Expansion, $\Delta\varepsilon$ (mm/mm)	$\Delta\varepsilon = 7.15 \times 10^{-3} - 0.460 \times 10^{-5}\theta_f + 0.540 \times 10^{-4}\theta_f^2$ (θ_f = Temperature of transformation finish)					
Poisson's ratio	0.3					

TABLE 2: Parameters A and B

Temperature °C	Initial Stress MPa	A	B	Temperature °C	Initial Stress MPa	A	B
150	934	0.935	0.17	500	128	0.69	0.19
	555	0.97	0.14		58	0.85	0.15
	270	1.0	0.0		35	0.95	0.12
					10	1.0	0.0
200	807	0.915	0.2	600	95	0.69	0.35
	553	0.94	0.18		56	0.8	0.27
	280	0.99	0.13		39	0.9	0.24
250	1025	0.852	0.15	700	49	0.77	0.25
	750	0.885	0.13		35	0.84	0.2
	550	0.91	0.11		24	0.9	0.14
	265	0.975	0.08				
300	153	0.86	0.16	800	56	0.64	0.23
	102	0.94	0.1		32	0.67	0.18
	42	0.99	0.06		15	0.74	0.14
400	158	0.83	0.26	850	42	0.54	0.27
	148	0.895	0.2		29	0.6	0.21
	70	0.98	0.16		15	0.69	0.2
	15	1.0	0.0				

TABLE 3: Mechanical Property Data used in the Thermal Stress and Strain Calculation

Property	Symbol	Temperature $\theta^{o}C$	Relationship used
(a) Austenite flow Stress[18,30]	$(\sigma_f)_\alpha$	< 850	40 MPa
		850 → 400	257.2-0.2556θ MPa
		< 400	155 MPa
(b) Martensite flow Stress	$(\sigma_f)_\gamma$	< 90	1600 MPa
(c) Flow stress below Ms[30]	σ_f	300 → 90	$V(\sigma_f)_\alpha + V(\sigma_f)_\gamma$
(d) Austenite strain hardening coefficient[18,30]	W_1	> 600	8950.0-7.75θ MPa
	W_1	< 600	4300.0 MPa
	W_2	> 600	10600.0-11.5θ MPa
	W_2	< 600	3700.0 MPa
(e) $\frac{E}{1-\nu}$ [106]		850 → 90	2.935×10^5-141.77θ MPa
(f) Dilatometer		850 → 90	See equations 4.4.1
(g) Transformation plasticity as an additional strain	ε_{tp}	300 → 260	See equations 4.3.1 and 4.3.2

TABLE 4: Variation of Thermal Diffusivity and Thermal Conductivity with Temperature [18,106]

Material	Temperature Range, $\theta^{o}C$	Thermal Diffusivity, αtd = (mm^2/s)
835M30 Steel	> 355	$4.0698 + 1.7802 \times 10^{-3}\theta$
	355 → 286	$0.03762\theta - 8.668$
	286 → 265	2.1
	265 → 164	$11.769 - 0.03644\theta$
	154 → 20	$7.357 - 0.00722\theta$
Material	$\theta^{o}C$	Thermal Conductivity, λ = ($W/m^{o}C$)
835M30 Steel	> 328	$20.1 + 8.29 \times 10^{-3}\theta$
	328 → 223	$33.152 - 3.143 \times 10^{-2}\theta$
	223 → 20	$25.521 - 2.726 \times 10^{-3}\theta$

N.B. From the above data, the average values between $850^{o}C$ and $100^{o}C$ were used in the calculations.

Viz:

$\alpha td = 0.5279 \times 10^{-3}\ mm^2/s$

$\lambda = 25.2\ W/m^{o}C.$

TABLE 5: Variation of Surface Heat Transfer Coefficient with Surface Temperature

Quenchant	θ(^{o}C)	h(W/m^{2}^{o}C)
(a) Oil (RDN175)[64]	$\geq$ 800	842
	800 → 542	1.191θ - 111
	542 → 470	11422 - 20.08θ
	470 → 434.4	1990
	434.4 → 308.3	11.34θ - 2937
	< 308.3	221 + 1.097θ
(b) Water[64]	> 826.8	1470
	826.8 → 381	23800 - 27.008θ
	381→ 275	3504 + 26.236θ
	275→ 93.75	51.584θ - 3466
	< 93.75	1370
(c) Polymer[64] 25% Aquaquench	> 792	700
	792 → 602	27933 - 34.47θ
	602 → 476	25.782θ - 8364
	476 → 276	7688 - 7.946θ
	276 → 134	31.786θ - 3282
	< 134	258 + 5.4θ
(d) Salt bath at 400^{o}C (Nitrate-Nitrite of eutectic composition)	850 → 530	14.463θ - 6660.043
	530 → 430	8.05θ - 3261.5
followed by Oil quench at 20^{o}C[78]	430 → 330	1242.75 - 2.425θ
	330 → 90	0.125θ + 401.25
followed by air cooling at 20^{o}C	<430	50.0

TABLE 6: Changes in Volume Accompanying the Hardening of 835M30 Steel Plate (120 mm x 120 mm x 20 m)

Measurement location	Average volume of plate before hardening Vs, mm^3	Average volume of plate after hardening Vh, mm^3	% Volume Change $\%\Delta V$
At Point,			
1	286968.70	287996.05	0.3580
2	286963.89	287967.40	0.3497
3	286948.31	287977.59	0.3587
4	286899.81	287915.15	0.3539
5	286981.46	288046.45	0.3711
		Mean Volume Change = 0.3583%	

$\therefore$ Linear Isotropic Change of Volume $= \frac{0.3583}{3}$

$= 0.11943\%$

approximately, 0.12%

Isotropic Volume Change calculated by Price[18] is 0.127%.

TABLE 7: Key to individual calculations of thermal stress and strain.

Calculation Number	Description	Relevant figure number
FP_1	Water quench without stress relaxation and transformation plasticity.	46,52,53
FP_2	Water quench with stress relaxation method one (dependence of parameters A and B on stress and temperature).	47,52,53
FP_3	Water quench with stress relaxation method two (dependence of parameters A and B on stress and temperature).	48,52,53
FP_4	Water quench, transformation plasticity as an additional plastic strain with stress relaxation method one (dependence of parameters A and B on stress and temperature).	49,52,53
FP_5	Water quench, transformation plasticity as an additional plastic strain with stress relaxation method two (dependence of parameters A and B on stress and temperature).	50,52,53
FP_6	Water quench, transformation plasticity as an additional plastic strain without stress relaxation.	51,52,53
FP_7	Oil quench, without stress relaxation and transformation plasticity.	54,60,61
FP_8	Oil quench with stress relaxation method one (dependence of parameters A and B on stress and temperature).	55,60,61
FP_9	Oil quench with stress relaxation method two (dependence of parameters A and B on stress and temperature).	56,60,61

TABLE 7: (Continued)..

Calculation Number	Description	Relevant Figure Number
FP_{10}	Oil quench, transformation plasticity as an additional plastic strain with stress relaxation method one (dependence of parameters A and B on stress and temperature).	57,60,61
FP_{11}	Oil quench, transformation plasticity as an additional plastic strain with stress relaxation method two (dependence of parameters A and B on stress and temperature).	58,60,61
FP_{12}	Oil quench, transformation plasticity as an additional plastic strain without stress relaxation.	59,60,61
FP_{13}	Polymer quench, without stress relaxation and transformation plasticity.	62,68,69
FP_{14}	Polymer quench, with stress relaxation method one (dependence of parameters A and B on stress and temperature).	63,68,69
FP_{15}	Polymer quench, with stress relaxation method two (dependence of parameters A and B on stress and temperature).	64,68,69
FP_{16}	Polymer quench, transformation plasticity as an additional plastic strain with stress relaxation method one (dependence of parameters A and B on stress and temperature).	65,68,69
FP_{17}	Polymer quench, transformation plasticity as an additional plastic strain, with stress relaxation method two (dependence of parameters A and B on stress and temperature).	66,68,69
FP_{18}	Polymer quench, transformation plasticity as an additional plastic strain, without stress relaxation.	67,68,69

TABLE 7: (Continued)..

Calculation Number	Description	Relevant Figure Number
FP_{19}	Martempering followed by air cooling without stress relaxation.	70,73,74
FP_{20}	Martempering followed by air cooling with stress relaxation method one (dependence of parameters A and B on stress and temperature).	71,73,74
FP_{21}	Martempering followed by air cooling with stress relaxation method two (dependence of parameters A and B on stress and temperature).	72,73,74
FP_{22}	Martempering followed by oil quench without stress relaxation.	75,80,81
FP_{23}	Martempering followed by oil quench with stress relaxation method one (dependence of parameters A and B on stress and temperature).	76,80,81
FP_{24}	Martempering followed by oil quench with stress relaxation method two (dependence of parameters A and B on stress and temperature).	77,80,81
FP_{25}	Martempering followed by oil quench, transformation plasticity as an additional plastic strain, with stress relaxation method one (dependence of parameters A and B on stress and temperature).	78,80,81
FP_{26}	Martempering followed by oil quench, transformation plasticity as an additional plastic strain, with stress relaxation method two (dependence of parameters A and B on stress and temperature).	79,80,81

TABLE 7: (Continued)..

Calculation Number	Description	Relevant Figure Number
FP_{27}	Effect of plate thickness on the generation of thermal stress and strain during quenching.	82,83,84 85,86,87 88
FP_{28}	Effect of transformation temperature range on the generation of thermal stress and strain during quenching.	89,90,91 92,93,94

TABLE 8: Experimental Results of Distortion of 20 mm Plate of 835M30 Steel after Polymer Quenching

Measurement Location	Change in Length Produced by Quench (ΔY)%	Measurement Location	Change in Length Produced by Quench (ΔY)%
1A	0.0599	3A	0.0303
1B	0.0592	3B	0.0295
1C	0.0713	3C	-
1D	0.0699	3D	0.0313
1E	0.0705	3E	0.0309
1F	0.0783	3F	0.0291
1G	0.112	3G	0.0296
1H	0.0781	3H	0.0307
1J	0.0743	3J	0.0308
1K	0.0711	3K	0.0318
Mean Value at Position 1	0.0677	Mean Value at Position 3	0.0274
2A	0.0479	4A	0.0563
2B	0.0464	4B	0.0579
2C	0.0484	4C	0.0569
2D	0.0514	4D	0.061
2E	0.0511	4E	0.062
2F	0.0587	4F	0.0867
2G	0.0616	4G	0.0604
2H	0.0532	4H	0.0601
2J	0.0506	4J	0.0599
2K	0.0484	4K	0.0548
Mean Value at Position 2	0.0471	Mean Value at Position 4	0.056
5A	0.0634	5H	0.068
5B	0.0653	5J	0.0729
5C	0.0689	5K	0.0694
5D	0.0689		
5E	0.0674	Mean Value at Position 5	0.0622
5F	0.0705		
5G	0.0691		

Average change in plate length calculated from change in thickness of plate (free from edge effect) = 0.0762%(calculated from 0.104% change in thickness).

TABLE 9: Experimental Results of Distortion of 15 mm Plate of 835M30 Steel after Martempering Treatment Followed by Air Cooling

Measurement Location	Change in Length Produced by Quench (ΔY)%	Measurement Location	Change in Length Produced by Quench (ΔY)%
1A	0.0314	3A	0.0318
1B	0.0302	3B	0.0271
1C	0.0235	3C	-
1D	0.0261	3D	0.0411
1E	0.0432	3E	0.0392
1F	0.0606	3F	0.0873
1G	0.0581	3G	0.0784
1H	0.0789	3H	0.0845
1J	0.0658	3J	0.0803
1K	0.0643	3K	0.0837
Mean Value at Position 1	0.0482	Mean Value at Position 3	0.0615
2A	0.0438	4A	0.0311
2B	0.0318	4B	0.0394
2C	0.0290	4C	0.0351
2D	0.0289	4D	0.0268
2E	0.0410	4E	0.0237
2F	0.0911	4F	0.0514
2G	0.0871	4G	0.0826
2H	0.0835	4H	0.0789
2J	0.0862	4J	0.0951
2K	0.0684	4K	0.0912
Mean Value at Position 2	0.0591	Mean Value at Position 4	0.0556
5A	0.0241	5H	0.0836
5B	0.0369	5J	0.0785
5C	0.0285	5K	0.0714
5D	0.0304		
5E	0.0392		
5F	0.0723	Mean Value at Position 5	0.0525
5G	0.0597		

Average change in plate length calculated from change in thickness of plate (free from edge effect) = 0.063% (calculated from 0.2342% change in thickness).

TABLE 10: Chemical Composition (wt.%) of 835M30 Steel

C	Mn	Si	Ni	Cr	Mo	Fe
0.30	0.72	0.42	4.83	1.25	0.28	Balance

TABLE 11: Chemical Compositional Range (wt.%) of 709M40 Steel

C	Mn	Mo	Cr	Ni	Fe
0.35-0.45	0.5-0.8	0.2-0.4	0.9-1.5	0.0-0.2	Balance

TABLE 12: Correction for edge effect[30]

Width of plate Y mm	Thickness of plate TH mm	Correction factor $\frac{Y}{Y-TH}$
120	20	1.2
120	15	1.14

$$\sigma_{actual} = \sigma_{measured} \times \frac{Y}{Y-TH}$$

FIGURE 1: Variation in probability of cracking with cooling rate. (After Kobasko)[13].

FIGURE 2: The effect of the size of component on the surface residual stresses in water quenched SAE 1045 cylinders. (After Nelson)[27].

FIGURE 3: The effect of the edge of the plate on the strain produced during quenching. (After Fletcher and Price)[30].

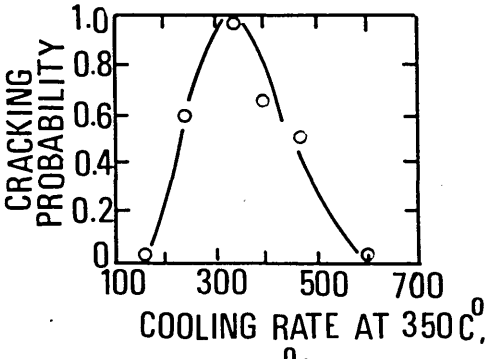
CRACKING PROBABILITY
1.0
0.8
0.6
0.4
0.2
0
100
300
500
700
COOLING RATE AT 350C°, C°/S

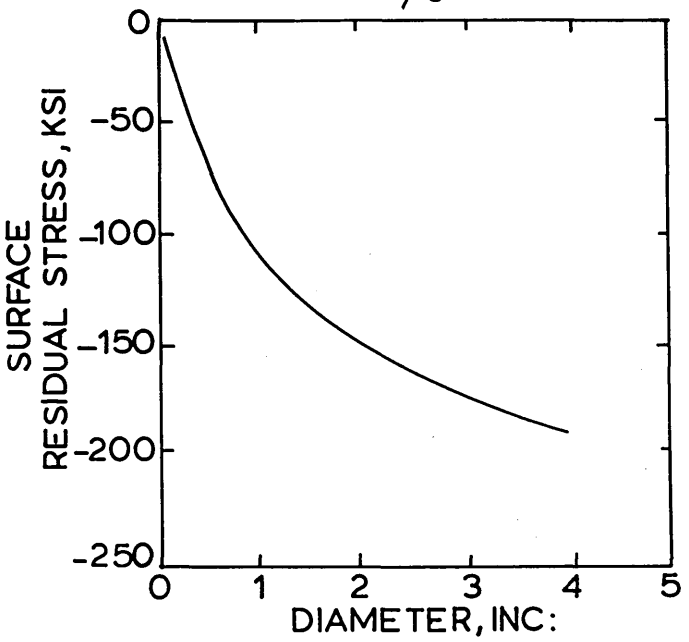
SURFACE RESIDUAL STRESS, KSI
0
-50
-100
-150
-200
-250
0
1
2
3
4
5
DIAMETER, INC:

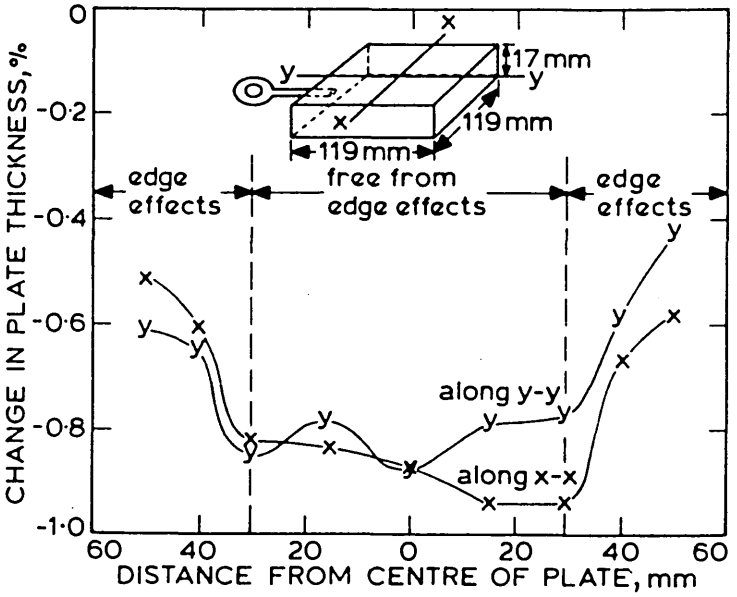
CHANGE IN PLATE THICKNESS, %
0
-0·2
-0·4
-0·6
-0·8
-1·0
17mm
119mm
119mm
edge effects
free from edge effects
edge effects
along y-y
along x-x
60
40
20
0
20
40
60
DISTANCE FROM CENTRE OF PLATE, mm

FIGURE 4: The effect of the edge of the plate on the stress generated during quenching. (After Fletcher and Lewis)[24].

FIGURE 5: Formation of thermal stresses on cooling.

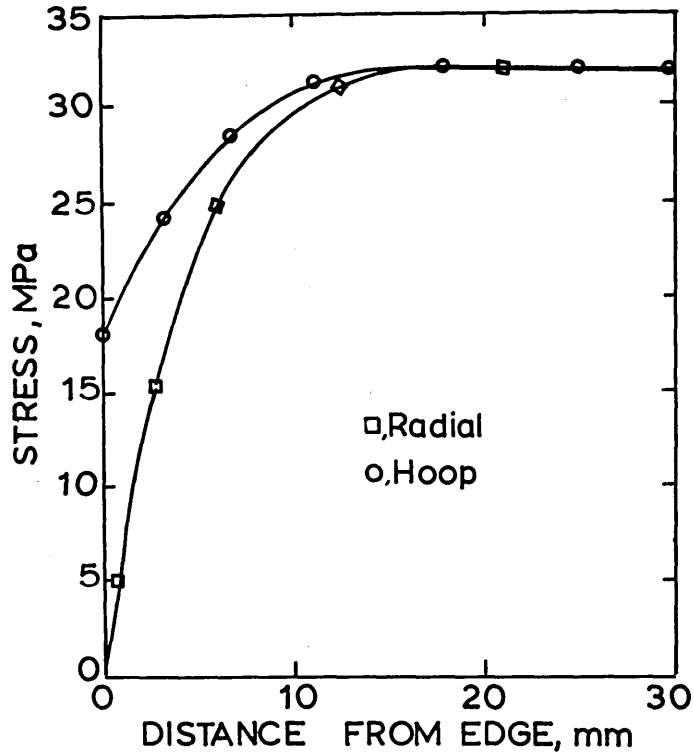
35
30
25
20
15
10
5
0
STRESS, MPa
□,Radial
o,Hoop
0
10
20
30
DISTANCE FROM EDGE, mm

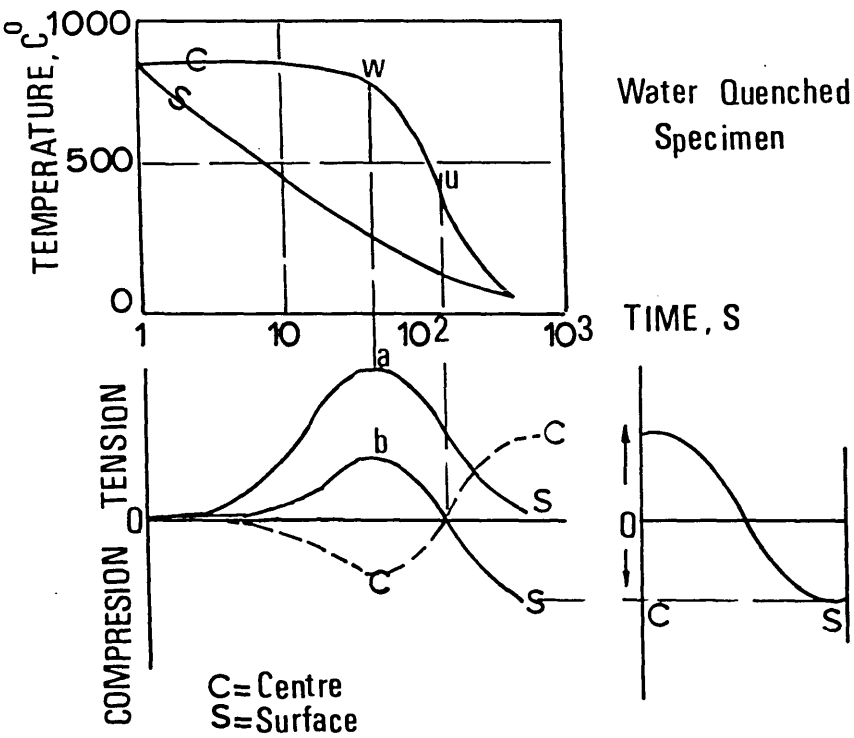
TEMPERATURE, C°
1000
500
0
C
S
W
u
1
10
10²
10³
TIME, S
Water Quenched
Specimen
a
b
C
S
C
S
TENSION
0
COMPRESION
C
S
C= Centre
S= Surface

FIGURE 6: Dilatometer curve for the austenite → martensite transformation in 835M30 steel. (After Price)[18].

FIGURE 7: Formation of residual stresses on cooling, steel specimens that undergo the austenite → martensite transformation. (After Thelning)[12].

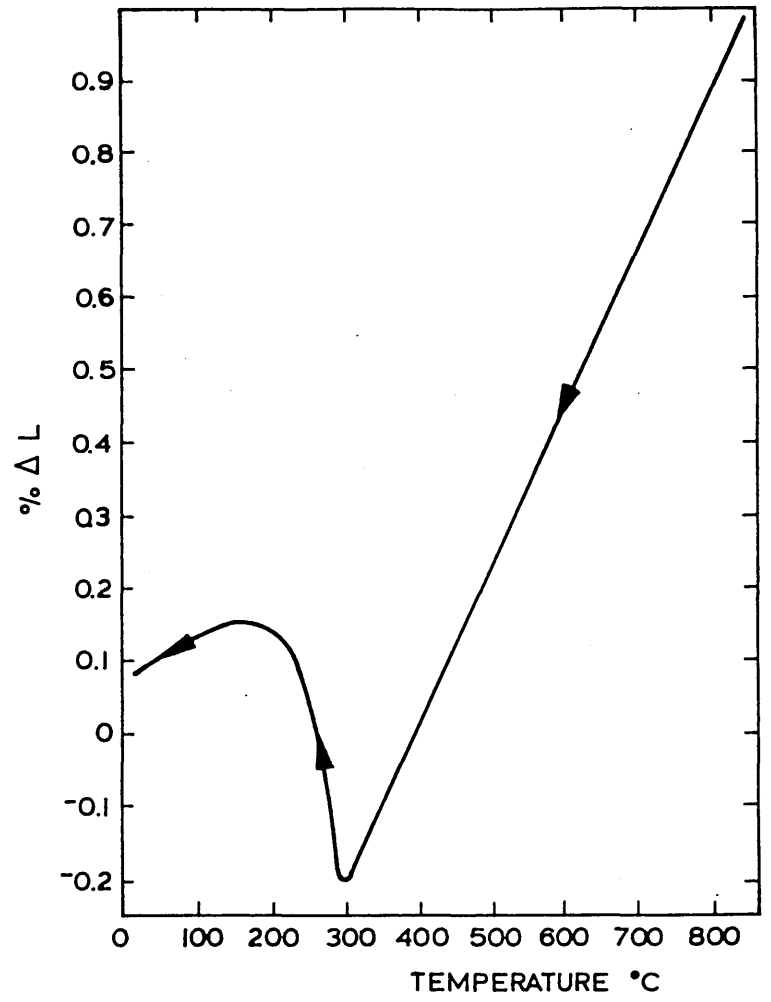
0.9
0.8
0.7
0.6
0.5
0.4
0.3
0.2
0.1
0
-0.1
-0.2
% Δ L
0 100 200 300 400 500 600 700 800
TEMPERATURE °C

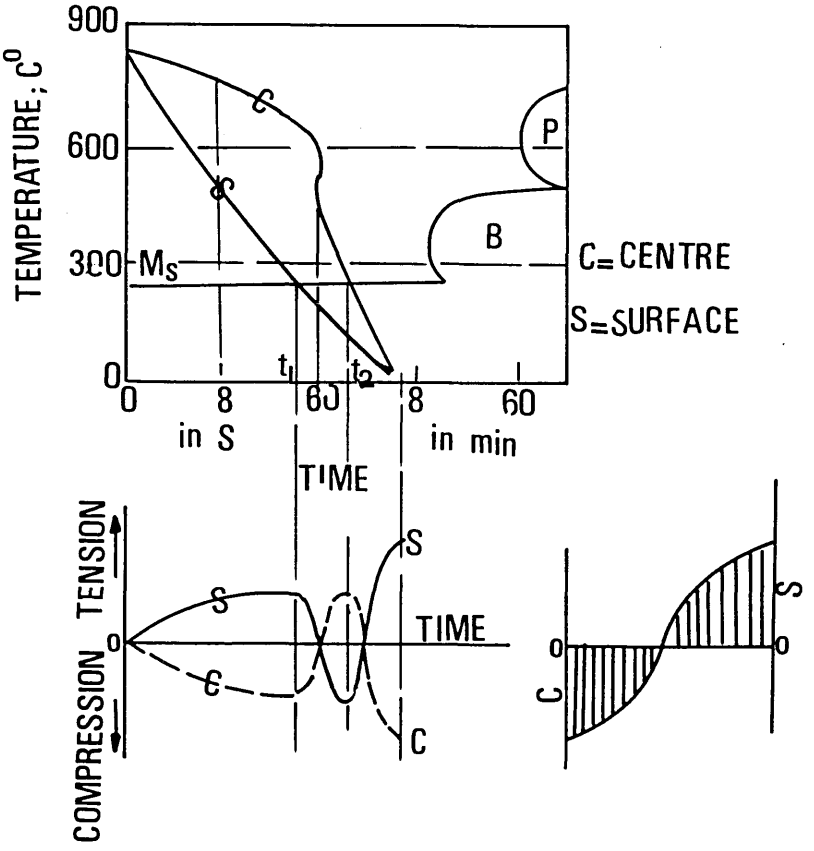
900
600
300
0
TEMPERATURE; C°
C
C
P
B
Ms
C= CENTRE
S=SURFACE
t1
t2
0 8 60 8 60
in S
in min
TIME
COMPRESSION TENSION
S
C
0
TIME
S
C
C
S
0
0

FIGURE 8: Transformation of austenite to various phases due to varying cooling rates at the surface and the centre.

FIGURE 9: A typical creep curve showing the different stages of creep.

FIGURE 10: A typical stress relaxation curve showing a reduction in stress with time and temperature.

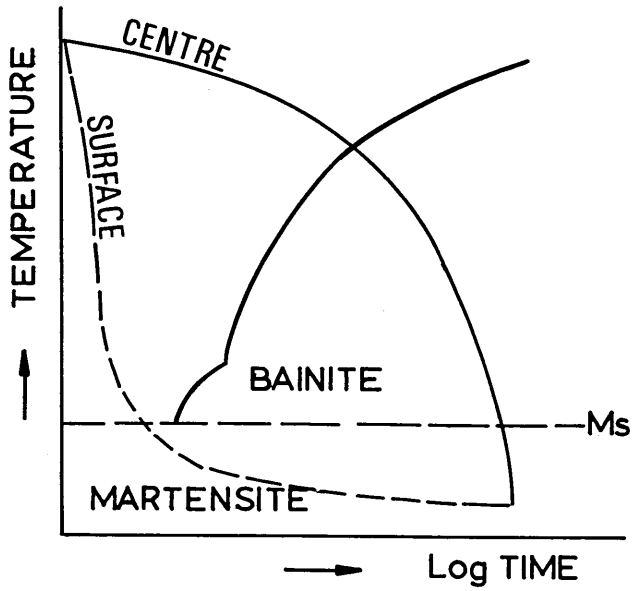
CENTRE
SURFACE
TEMPERATURE
BAINITE
Ms
MARTENSITE
Log TIME

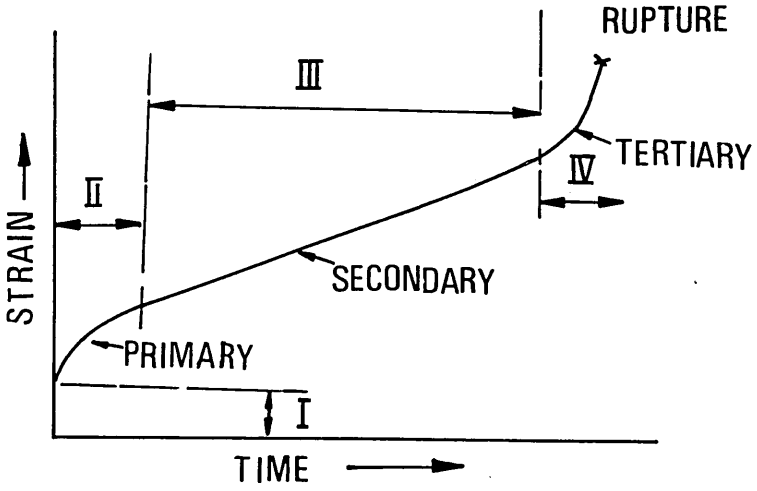
RUPTURE
III
TERTIARY
IV
II
STRAIN
SECONDARY
PRIMARY
I
TIME

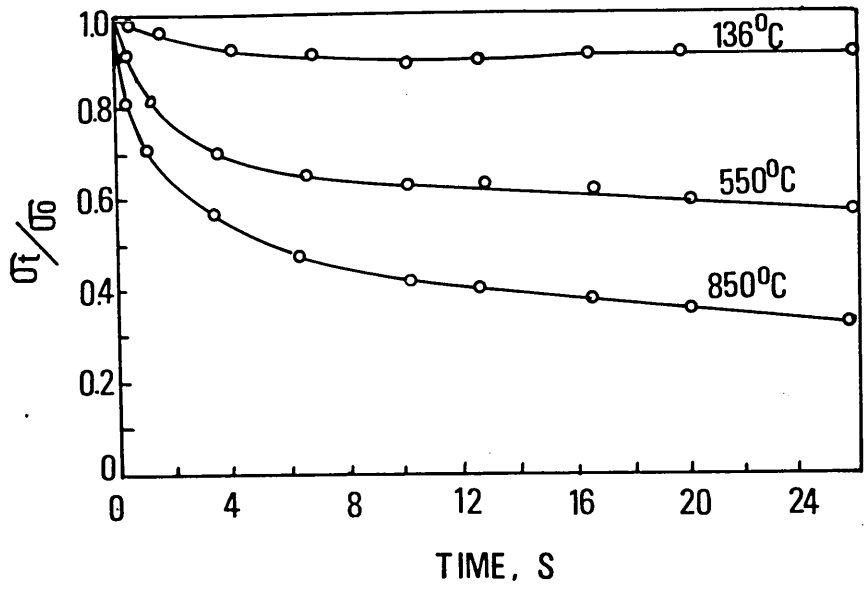
1.0
0.8
0.6
0.4
0.2
0
136°C
550°C
850°C
σt/σ0
0
4
8
12
16
20
24
TIME, S

FIGURE 11: Relationship between the absolute applied stress and the transformation plasticity strain.

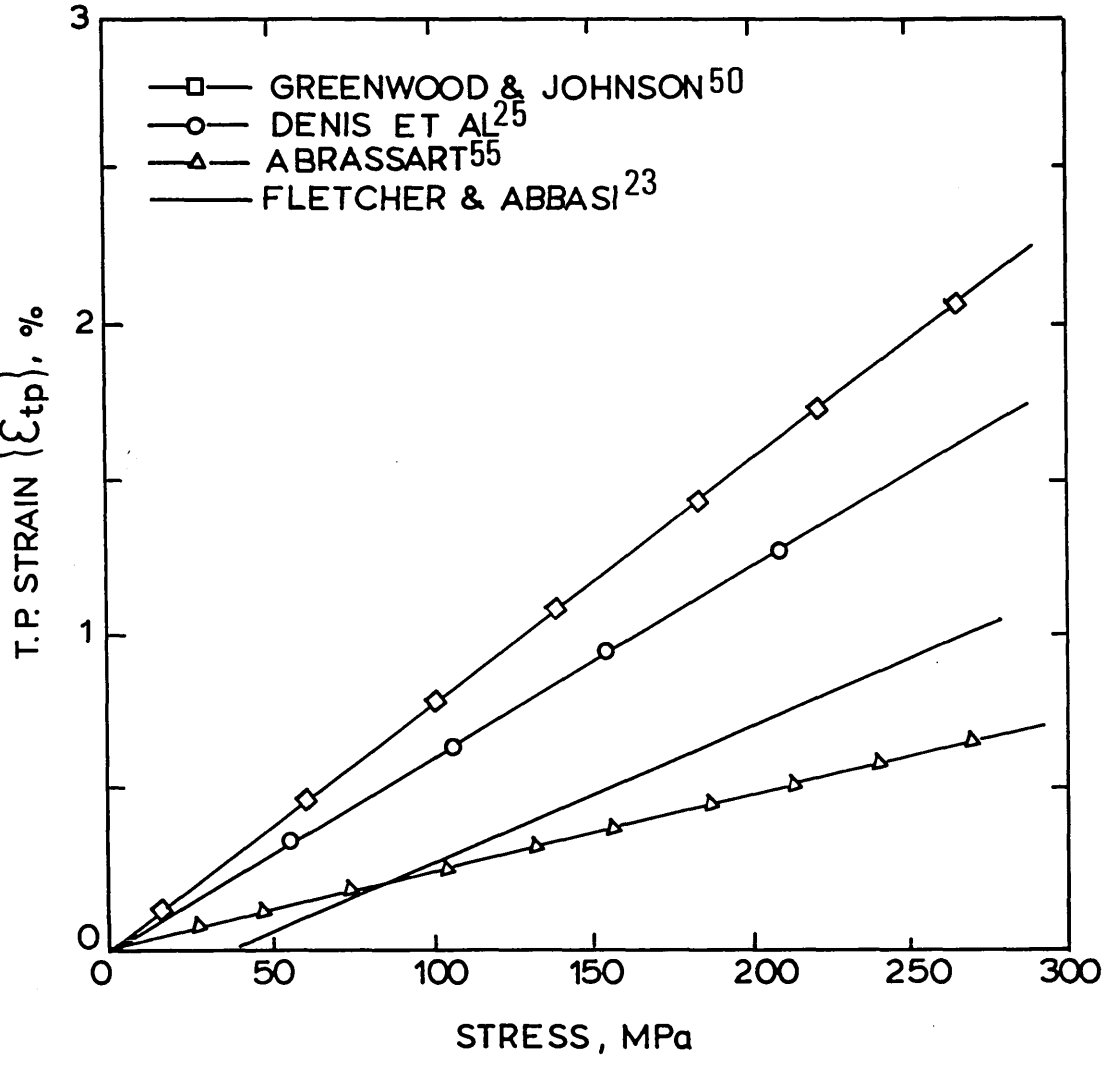
GREENWOOD & JOHNSON 50
DENIS ET AL 25
ABRASSART 55
FLETCHER & ABBASI 23
T.P. STRAIN (ε_{tp}), %
STRESS, MPa
0
1
2
3
0
50
100
150
200
250
300

FIGURE 12: Calculated residual stress distribution in a 20 mm thick plate after quenching in

(a) Water at 20°C
(b) Polymer at 20°C
(c) Oil at 20°C

(After Fletcher and Price).[30]

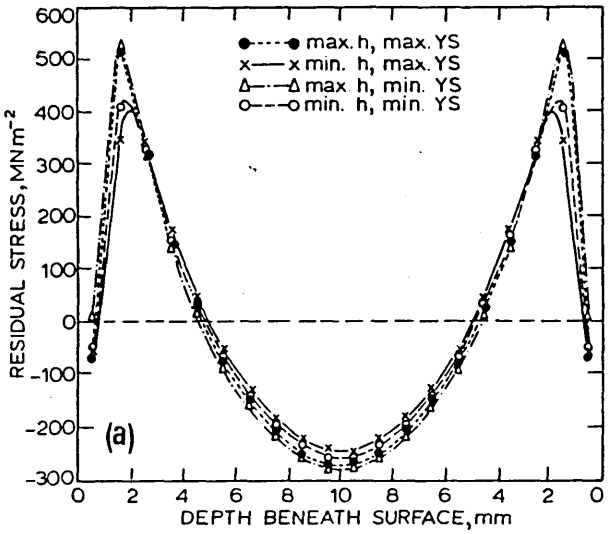
max. h, max. YS
min. h, max. YS
max. h, min. YS
min. h, min. YS
RESIDUAL STRESS, MNm⁻²
DEPTH BENEATH SURFACE, mm
(a)

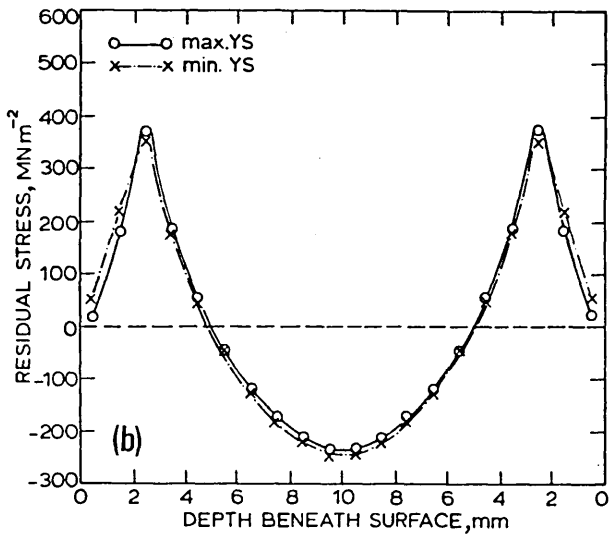
max.YS
min. YS
RESIDUAL STRESS, MNm⁻²
DEPTH BENEATH SURFACE, mm
(b)

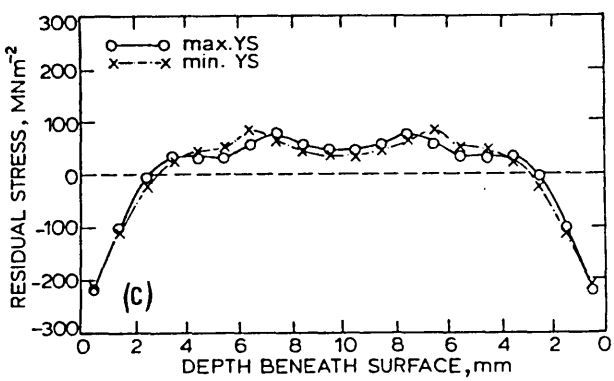
max.YS
min. YS
RESIDUAL STRESS, MNm⁻²
DEPTH BENEATH SURFACE, mm
(c)

FIGURE 13: Comparison of the experimental and the predicted residual stresses in 20 mm plate quenched in

(a) Water at 20°C
(b) Polymer at 20°C
(c) Oil at 20°C

(After Fletcher and Price).[30]

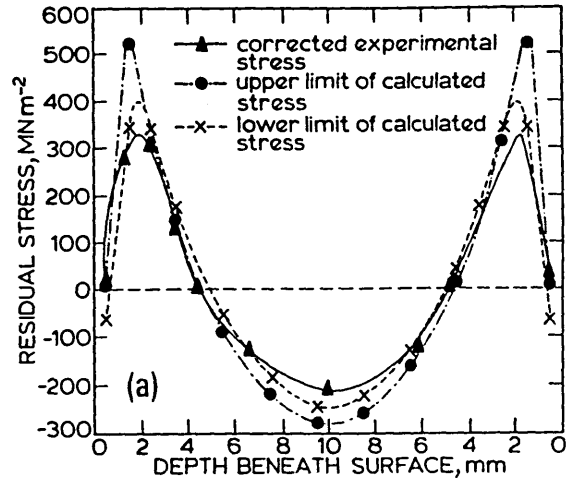
corrected experimental stress
upper limit of calculated stress
lower limit of calculated stress
RESIDUAL STRESS, MNm^{-2}
DEPTH BENEATH SURFACE, mm
(a)

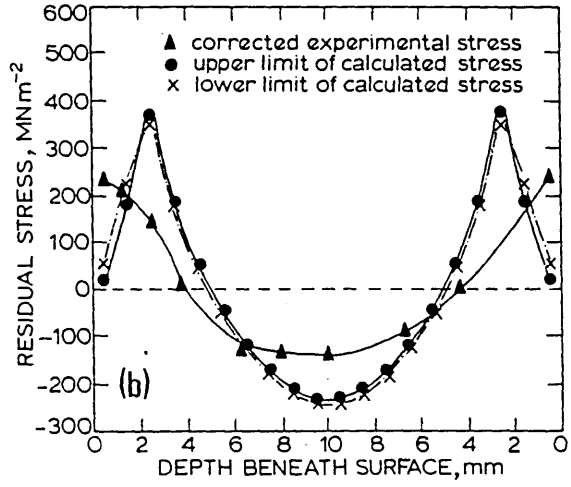
corrected experimental stress
upper limit of calculated stress
lower limit of calculated stress
RESIDUAL STRESS, MNm^{-2}
DEPTH BENEATH SURFACE, mm
(b)

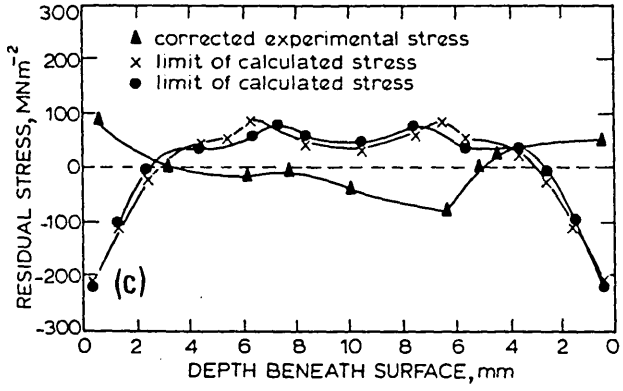
corrected experimental stress
limit of calculated stress
limit of calculated stress
RESIDUAL STRESS, MNm^{-2}
DEPTH BENEATH SURFACE, mm
(c)

FIGURE 14: Comparison of the experimental and the calculated residual stress distribution in a 15 mm plate after martempering followed by an oil quenching.

(a) Without viscous flow
(b) With viscous flow

(After Abbasi).[41]

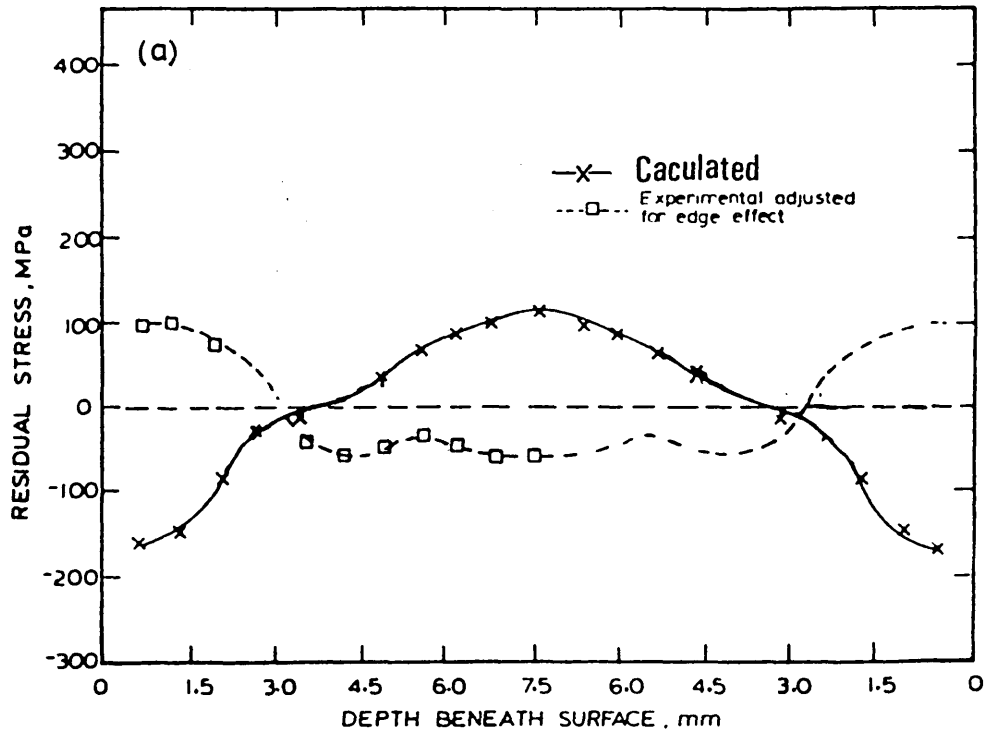
(a)
Caculated
Experimental adjusted for edge effect
RESIDUAL STRESS, MPa
400
300
200
100
0
-100
-200
-300
0
1.5
3.0
4.5
6.0
7.5
6.0
4.5
3.0
1.5
0
DEPTH BENEATH SURFACE, mm

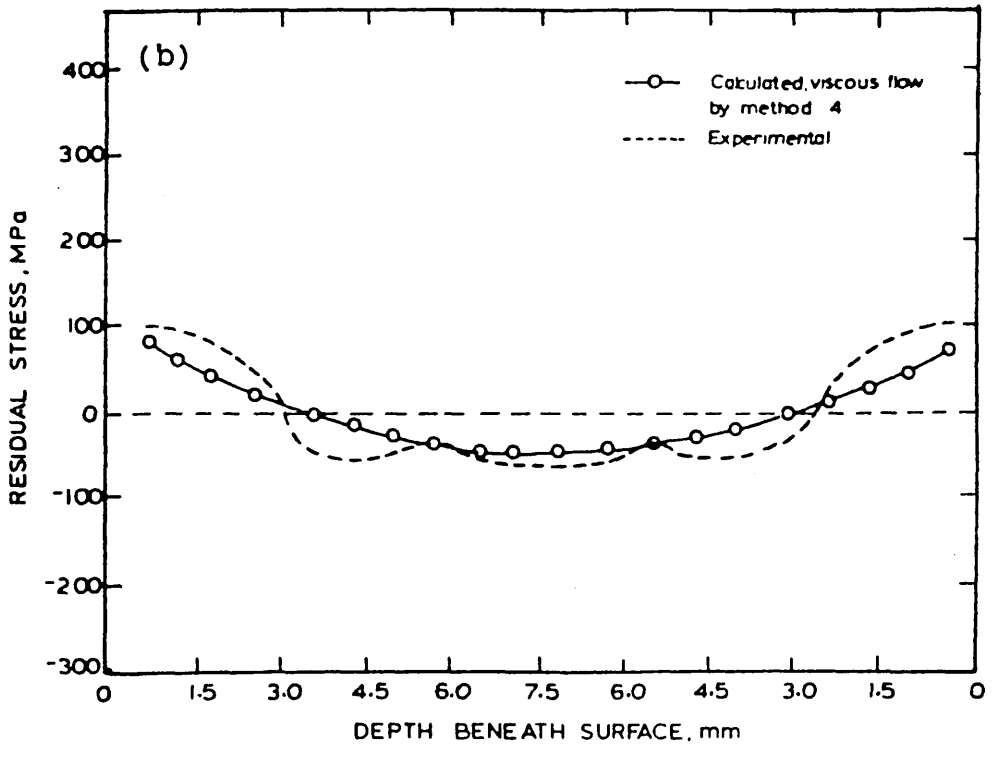
(b)
Calculated, viscous flow by method 4
Experimental
RESIDUAL STRESS, MPa
400
300
200
100
0
-100
-200
-300
0
1.5
3.0
4.5
6.0
7.5
6.0
4.5
3.0
1.5
0
DEPTH BENEATH SURFACE, mm

FIGURE 15: Comparison of the calculated and the experimentally determined distortions. (After Toshioka)[66].

FIGURE 16: Comparison of the experimental and the predicted residual stress distribution in 0.43%C steel cylinders quenched in water. (After Inoue and Tanaka)[65].

FIGURE 17: Reduction in residual stress levels after accounting for creep due to tempering of 12% Cr steel cylinders. (After Inoue et al)[67].

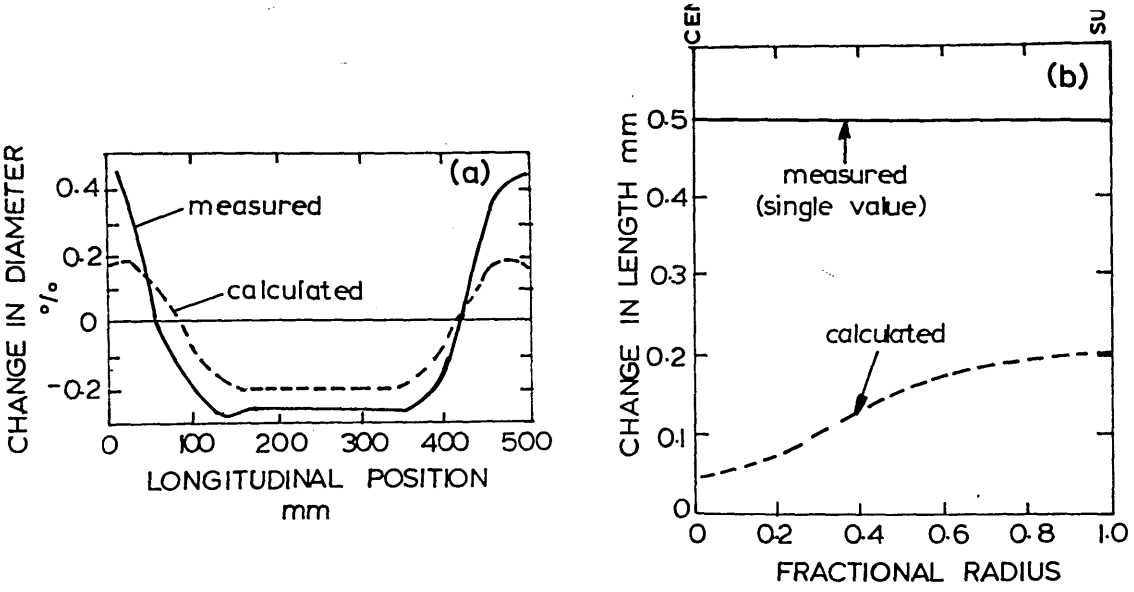
(a)
measured
calculated
CHANGE IN DIAMETER %
LONGITUDINAL POSITION mm
(b)
measured (single value)
calculated
CHANGE IN LENGTH mm
FRACTIONAL RADIUS

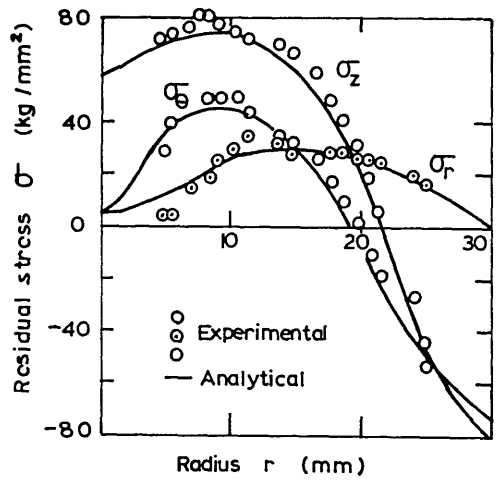
Residual stress σ (kg/mm²)
Radius r (mm)
Experimental
Analytical

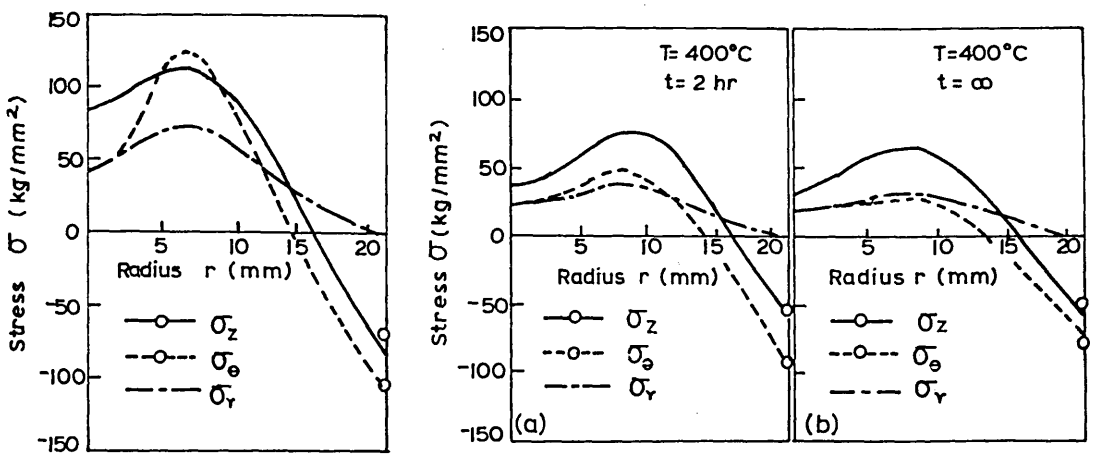
Stress σ (kg/mm²)
Radius r (mm)
T= 400°C
t= 2 hr
T=400°C
t= ∞
(a)
(b)

FIGURE 18: Comparison of the residual stress distribution in carburised and uncarburised steel gears quenched in oil at 40°C. (After Inoue et al)[26].

FIGURE 19: Variation of length of dilatometer specimen with temperature.

(a) Cooled to produce 0% martensite
(b) Cooled to produce 50% martensite
(c) Cooled to produce 100% martensite

(After Fujio et al)[85].

FIGURE 20: Comparison of the predicted and the experimental residual stress distribution in a 50 mm diameter cylinder of 0.45%C steel after quenching in water. (After Fujio et al)[85].

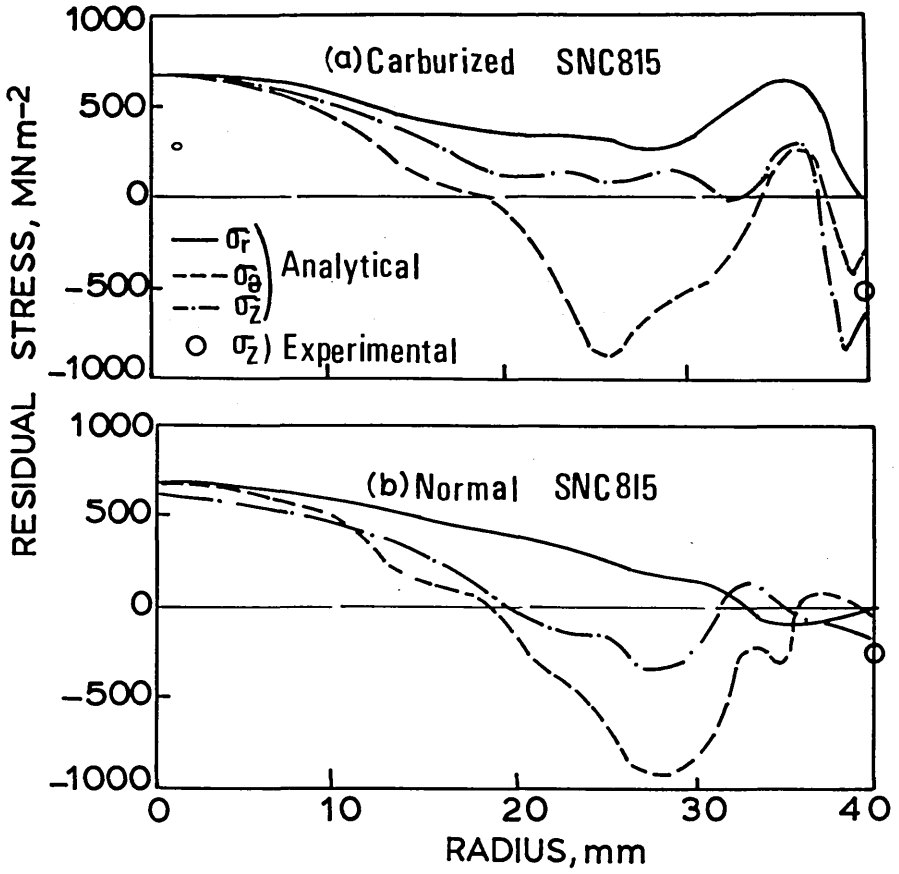
(a) Carburized SNC815
(b) Normal SNC815
RESIDUAL STRESS, MNm-2
1000
500
0
-500
-1000
σr
σθ
σz
Analytical
σz) Experimental
0
10
20
30
40
RADIUS, mm

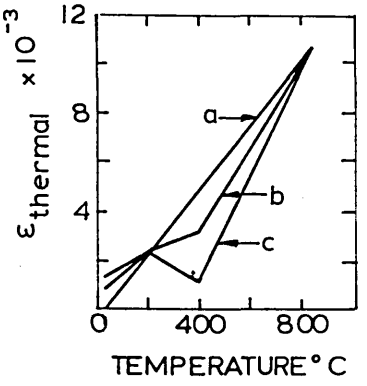
εthermal x10-3
12
8
4
a
b
c
0
400
800
TEMPERATURE °C

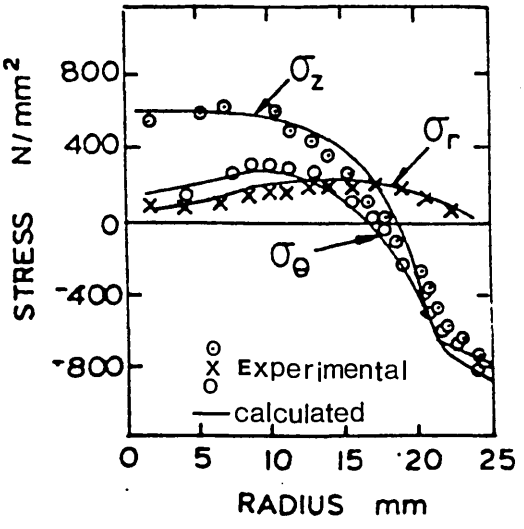
STRESS N/mm2
800
400
0
-400
-800
σz
σr
σθ
Experimental
calculated
0
5
10
15
20
25
RADIUS mm

FIGURE 21: Comparison of the measured and the predicted distortions of a gear tooth profile. (After Fujio et al)[86].

FIGURE 22: Comparison of the calculated and the experimental residual axial stress profiles.

----- Calculated without stress/transformation interactions.

——— Calculated with stress/transformation interactions.

— — — With transformation plasticity.

—·—·— With an effect of internal stress on the kinetics of martensite transformation alone.

(After Denis et al)[25].

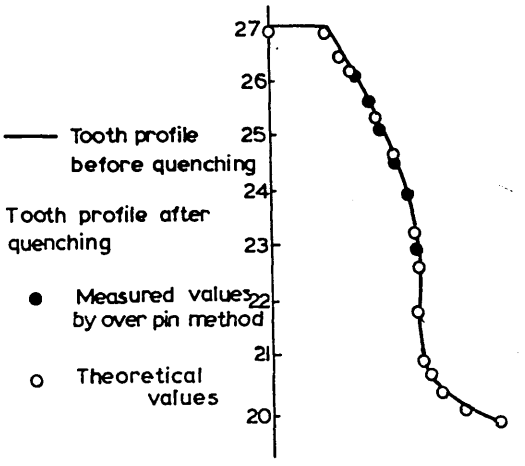
Tooth profile before quenching
Tooth profile after quenching
Measured values by over pin method
Theoretical values
27
26
25
24
23
22
21
20

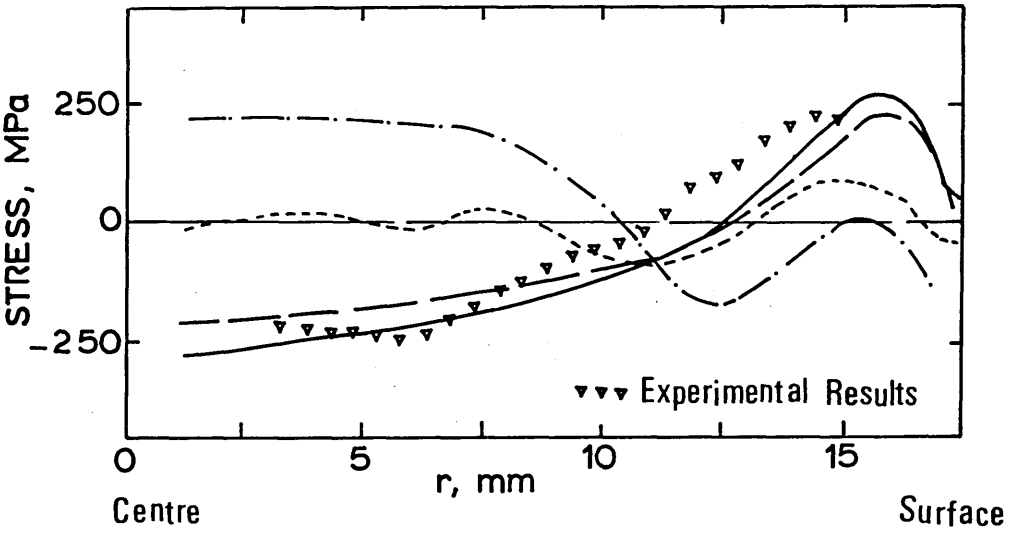
STRESS, MPa
250
0
-250
Experimental Results
0
5
10
15
r, mm
Centre
Surface

FIGURE 23: Variation of mechanical properties with temperature.

(a) Aluminium
(b) Stainless Steel

(After Boyer and Bovin)[48].

FIGURE 24: Generation of thermal stress in low alloy steel shafts during cooling by water spray.

(a) Without transformation
(b) With transformation

(After Kamamoto et al)[79].

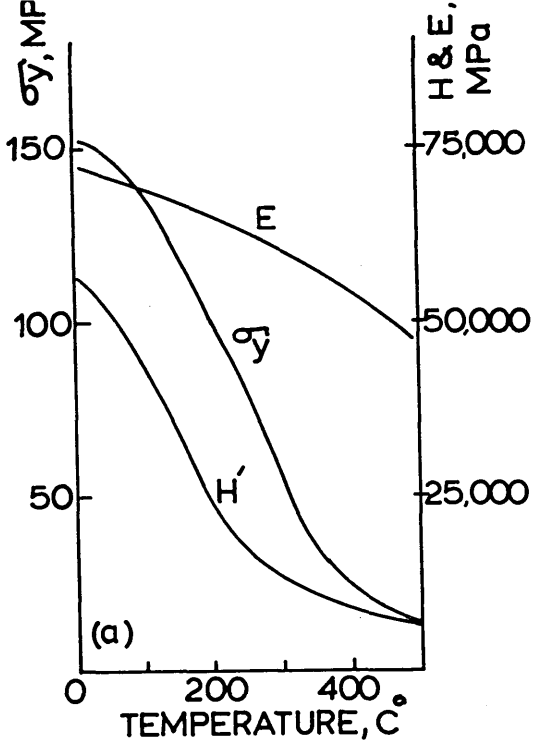
σy, MPa
H & E, MPa
150
100
50
75,000
50,000
25,000
E
σy
H'
(a)
0
200
400
TEMPERATURE, C°

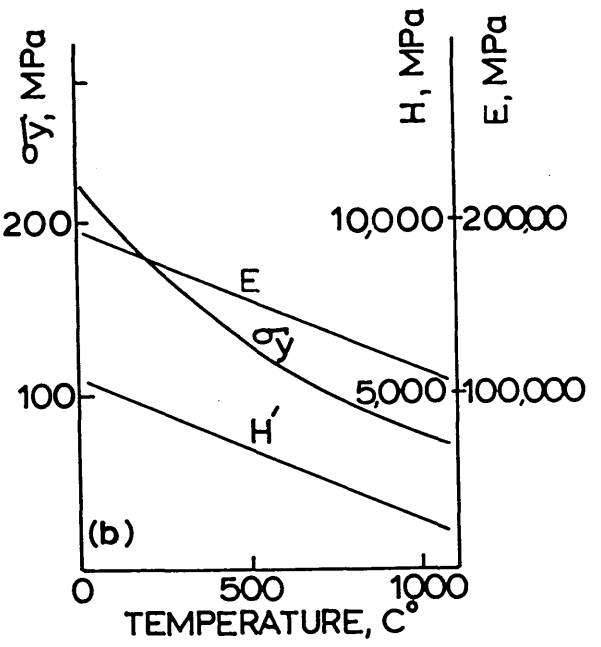
σy, MPa
H, MPa
E, MPa
200
100
10,000
5,000
20,000
100,000
E
σy
H'
(b)
0
500
1000
TEMPERATURE, C°

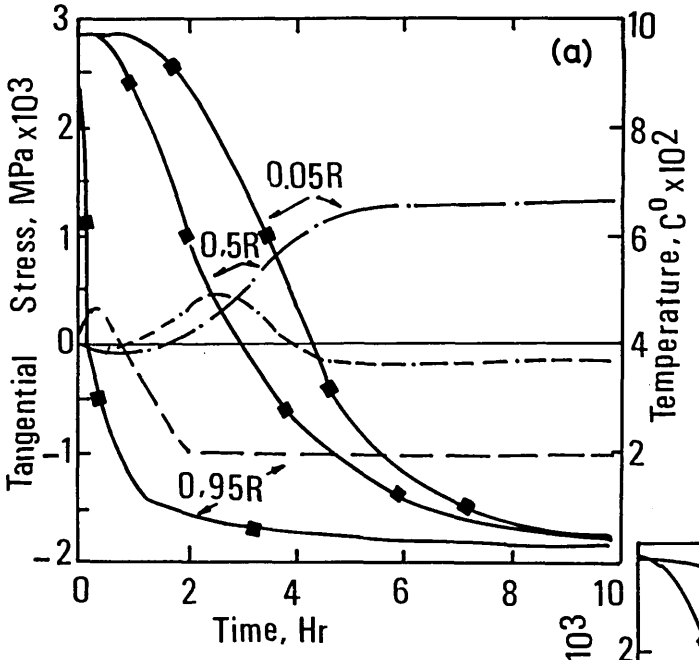
(a)
Tangential Stress, MPa x10³
Temperature, C° x10²
0.05R
0.5R
0.95R
Time, Hr
Temperature
Stress

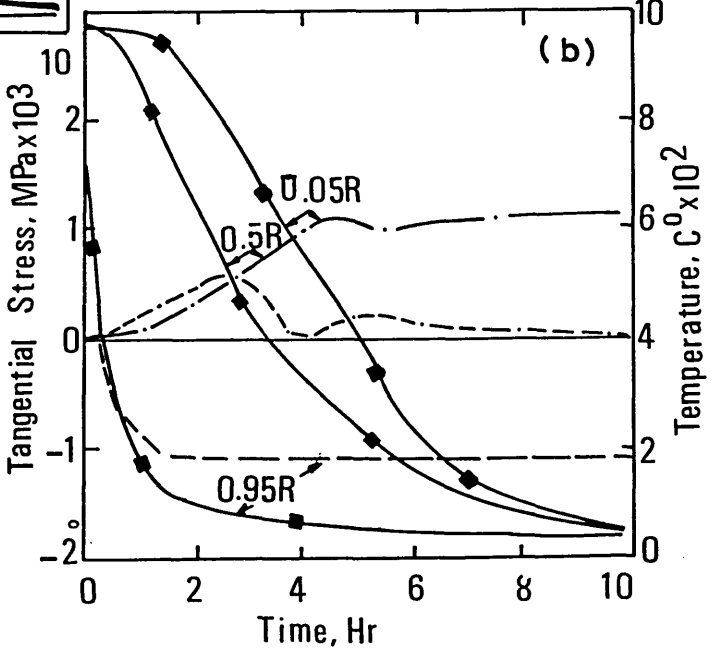
(b)
Tangential Stress, MPa x10³
Temperature, C° x10²
0.05R
0.5R
0.95R
Time, Hr

FIGURE 25: Distortions developed in low alloy steel shafts during cooling by water spray.

(a) Without transformation
(b) With transformation

(After Kamamoto et al)[79].

FIGURE 26: Comparison of the experimental and the calculated stress distribution in 70 mm thick aluminium plates quenched in

(a) Hot water at 80°C
(b) Cold Water at 20°C

(After Jeanmart and Bouvaist)[68].

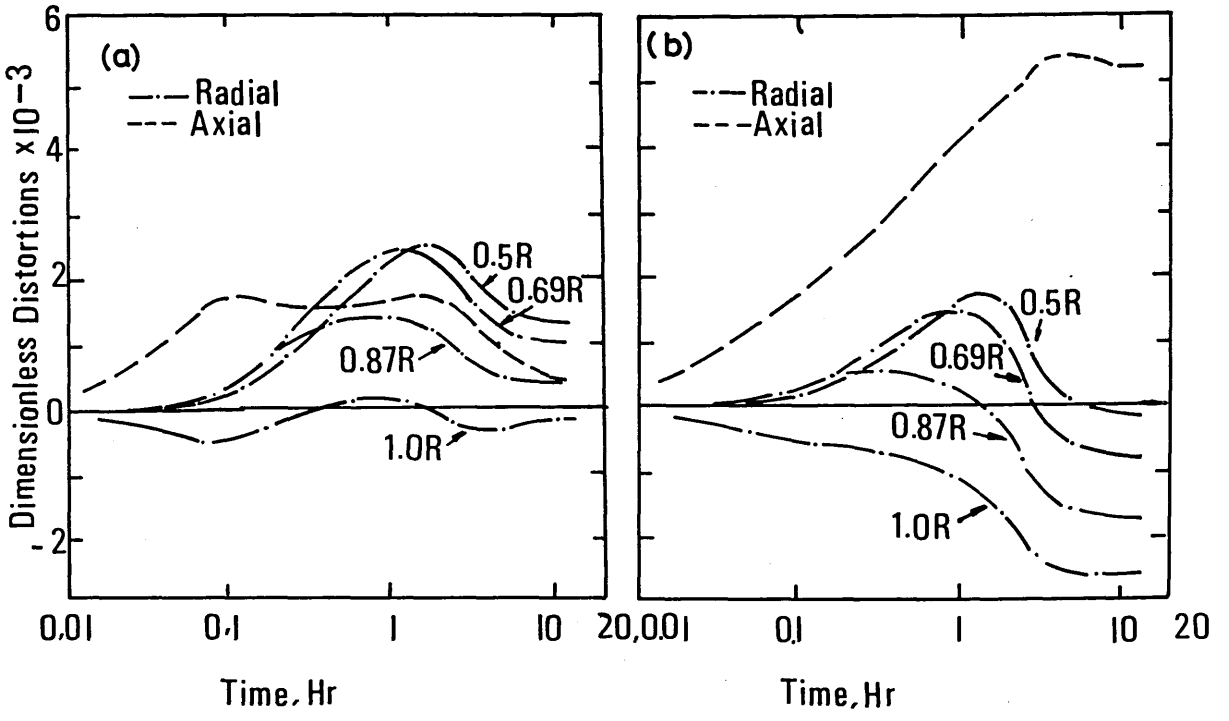
(a)
Radial
Axial
0.5R
0.69R
0.87R
1.0R
Dimensionless Distortions x10⁻³
6
4
2
0
-2
0.01
0.1
1
10
20
Time, Hr
(b)
Radial
Axial
0.5R
0.69R
0.87R
1.0R
0.01
0.1
1
10
20
Time, Hr

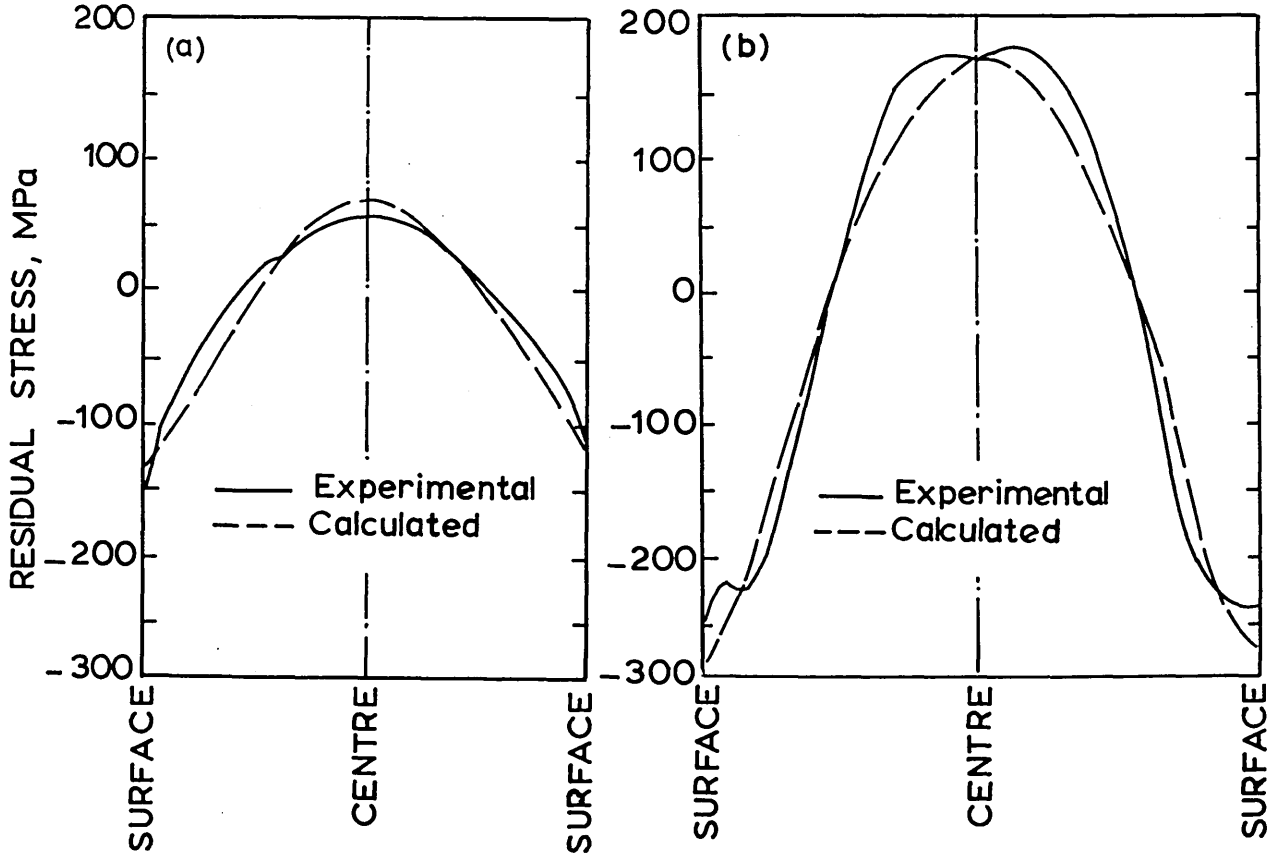
(a)
(b)
RESIDUAL STRESS, MPa
200
100
0
-100
-200
-300
Experimental
Calculated
SURFACE
CENTRE
SURFACE

FIGURE 27: Residual stress distribution in 0.5%C steel cylinders after quenching in water (solid line) and oil (broken line).

(a) 100 mm diameter
(b) 50 mm diameter
(c) 30 mm diameter
(d) 15 mm diameter

(After Buhler and Rose)[93].

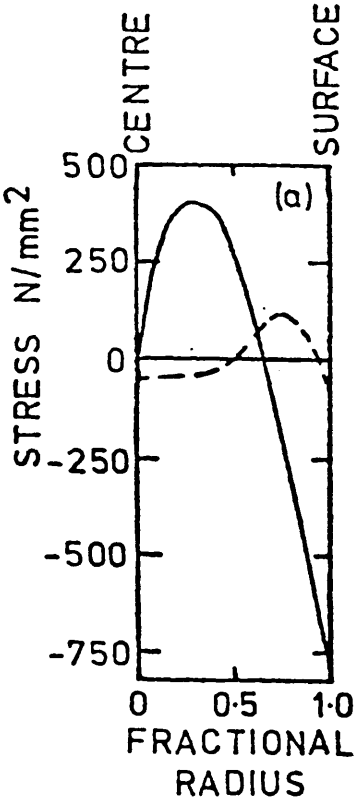
CENTRE
SURFACE
500
250
0
-250
-500
-750
STRESS N/mm2
(a)
0
0·5
1·0
FRACTIONAL
RADIUS

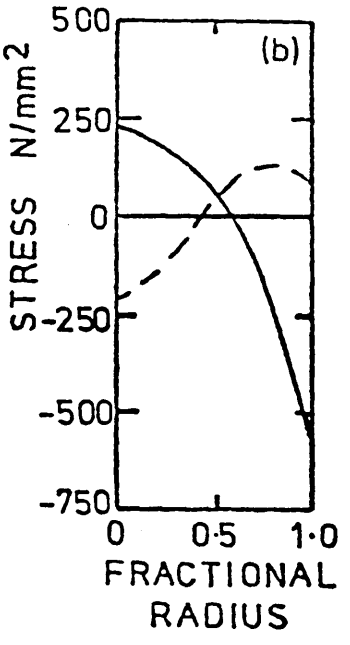
500
250
0
-250
-500
-750
STRESS N/mm2
(b)
0
0·5
1·0
FRACTIONAL
RADIUS

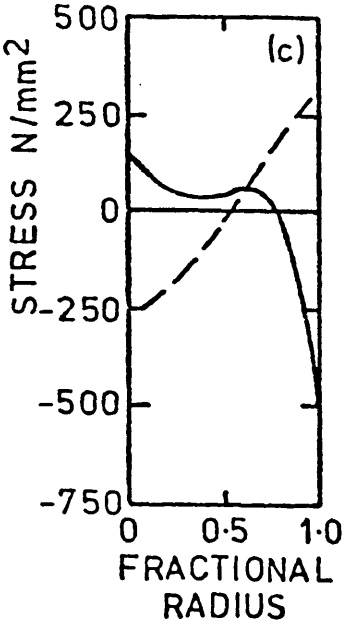
500
250
0
-250
-500
-750
STRESS N/mm2
(c)
0
0·5
1·0
FRACTIONAL
RADIUS

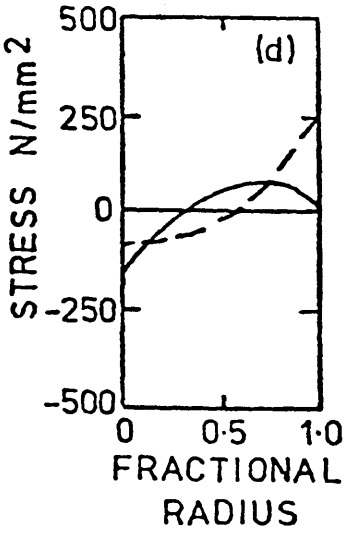
500
250
0
-250
-500
STRESS N/mm2
(d)
0
0·5
1·0
FRACTIONAL
RADIUS

FIGURE 28: Tangential stress determined by Finite Element analysis and X-ray diffraction.

(a) Water quenched cylinders
(b) Oil quenched cylinders

(After Burnett)[99].

FIGURE 29: Change of tip cylinder diameter of gears after hardening. (After Fujio)[103].

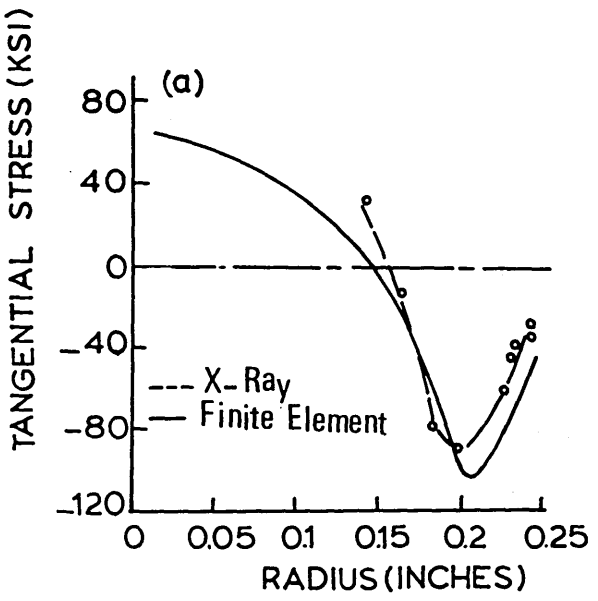
TANGENTIAL STRESS (KSI)
(a)
80
40
0
-40
-80
-120
--- X-Ray
— Finite Element
0
0.05
0.1
0.15
0.2
0.25
RADIUS (INCHES)

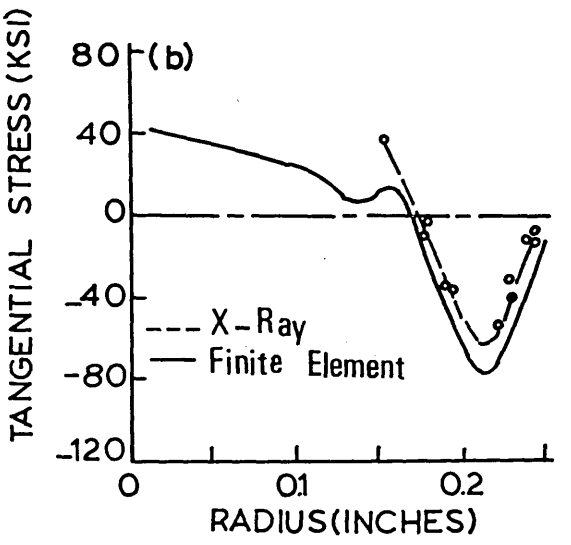
TANGENTIAL STRESS (KSI)
(b)
80
40
0
-40
-80
-120
--- X-Ray
— Finite Element
0
0.1
0.2
RADIUS (INCHES)

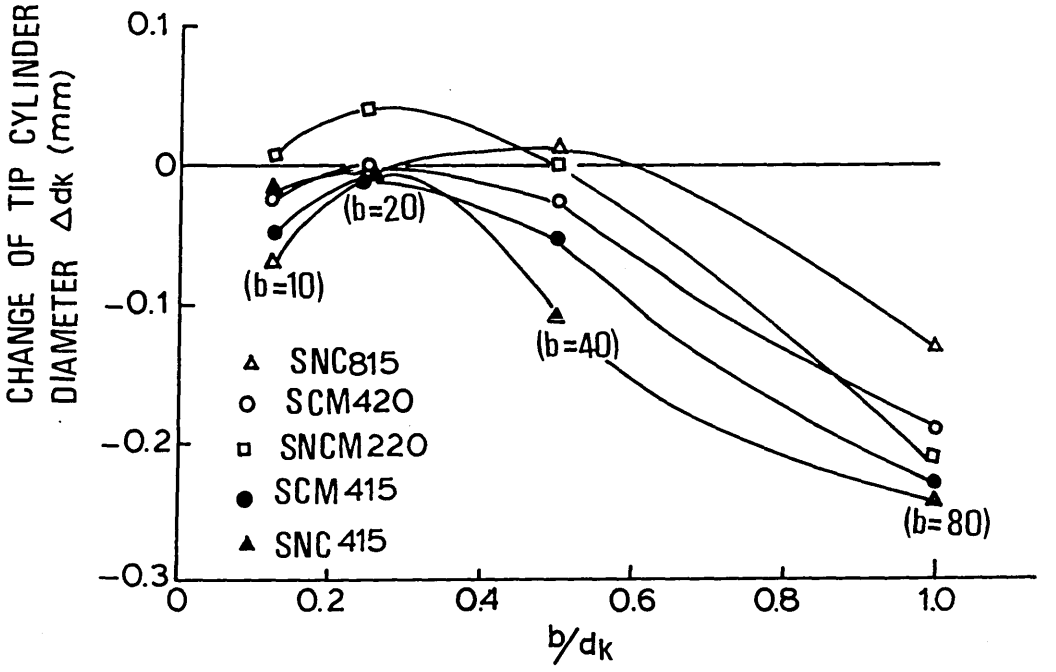
CHANGE OF TIP CYLINDER DIAMETER Δdk (mm)
0.1
0
-0.1
-0.2
-0.3
(b=10)
(b=20)
(b=40)
(b=80)
SNC815
SCM420
SNCM220
SCM415
SNC415
0
0.2
0.4
0.6
0.8
1.0
b/dk

FIGURE 30: Furnace calibration showing relationship between furnace temperature and transformer control position, when furnace was fixed at optimum position in the Instron machine.

FIGURE 31: Furnace calibration showing relationship between temperature and time, for heating and cooling the furnace, when furnace was fixed at optimum position in the Instron machine.

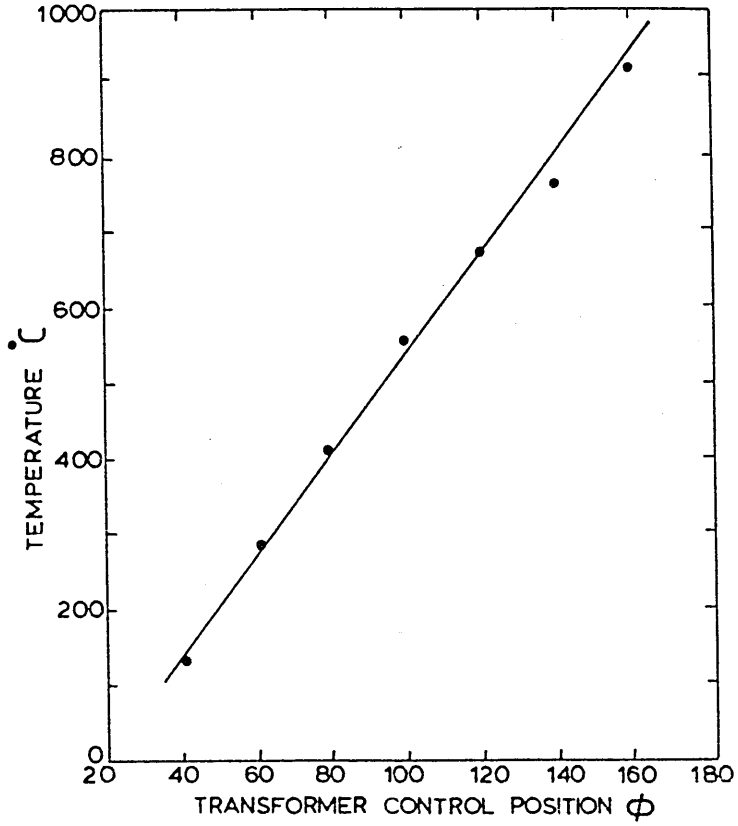
1000
800
600
400
200
0
TEMPERATURE °C
20
40
60
80
100
120
140
160
180
TRANSFORMER CONTROL POSITION Φ

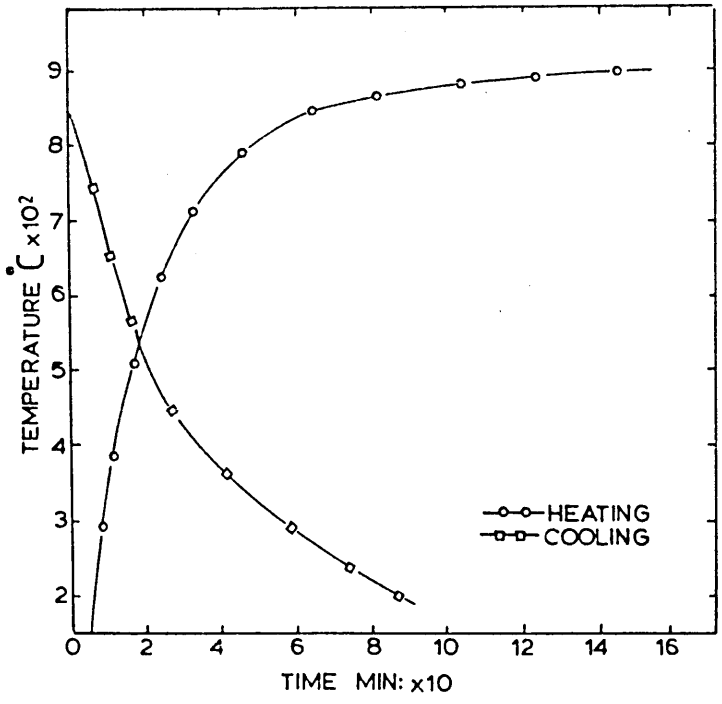
9
8
7
6
5
4
3
2
TEMPERATURE °C x10²
0
2
4
6
8
10
12
14
16
TIME MIN: x10
HEATING
COOLING

FIGURE 32: Dimensions of the screw-end cylindrical test specimen used for stress relaxation tests (BS 3500).

FIGURE 33: Time-temperature transformation diagram for 835M30 (EN30B) steel. (After Woolman and Mottram)[105].

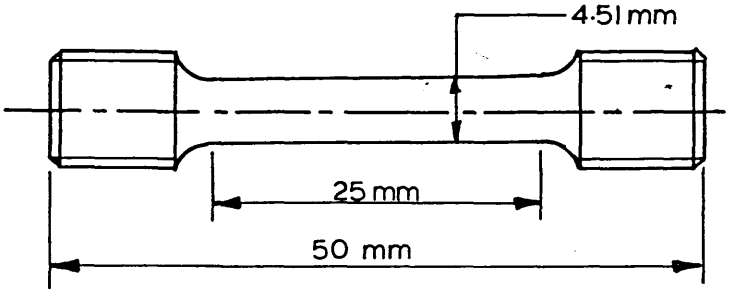
4·51 mm
25 mm
50 mm

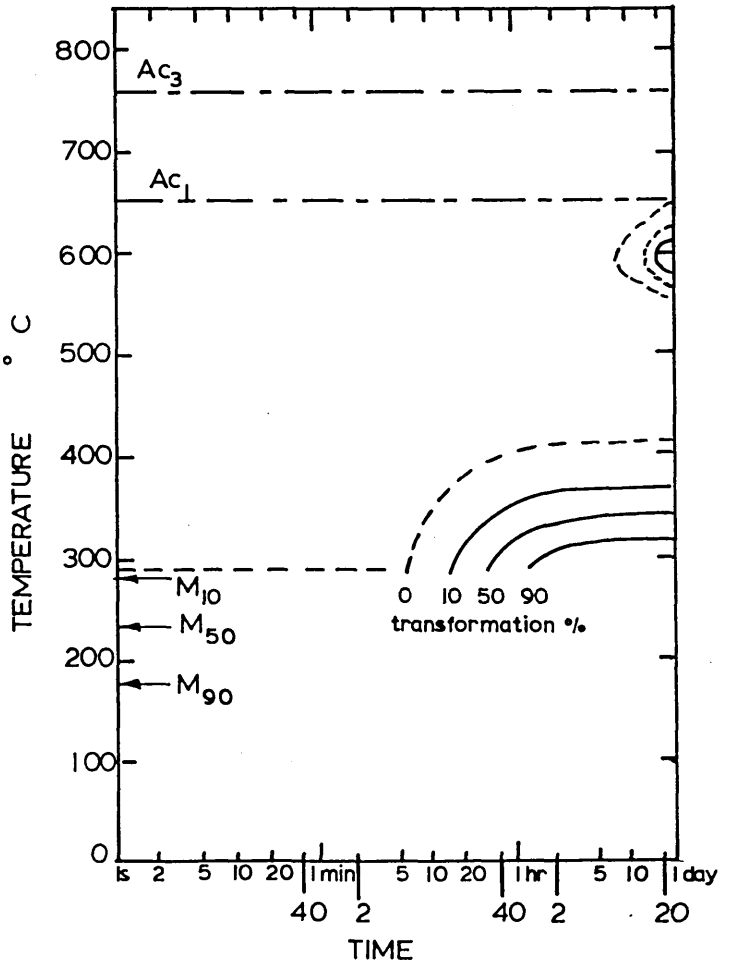
800
700
600
500
400
300
200
100
0
Ac3
Ac1
M10
M50
M90
0 10 50 90
transformation %
° C
TEMPERATURE
1s 2 5 10 20 1min 5 10 20 1hr 5 10 1day
40 2 40 2 20
TIME

FIGURE 34: Relationship between experimental stress relaxation and time for 835M30 steel specimen that had been austenitised at 850°C and tested at the appropriate test temperature.

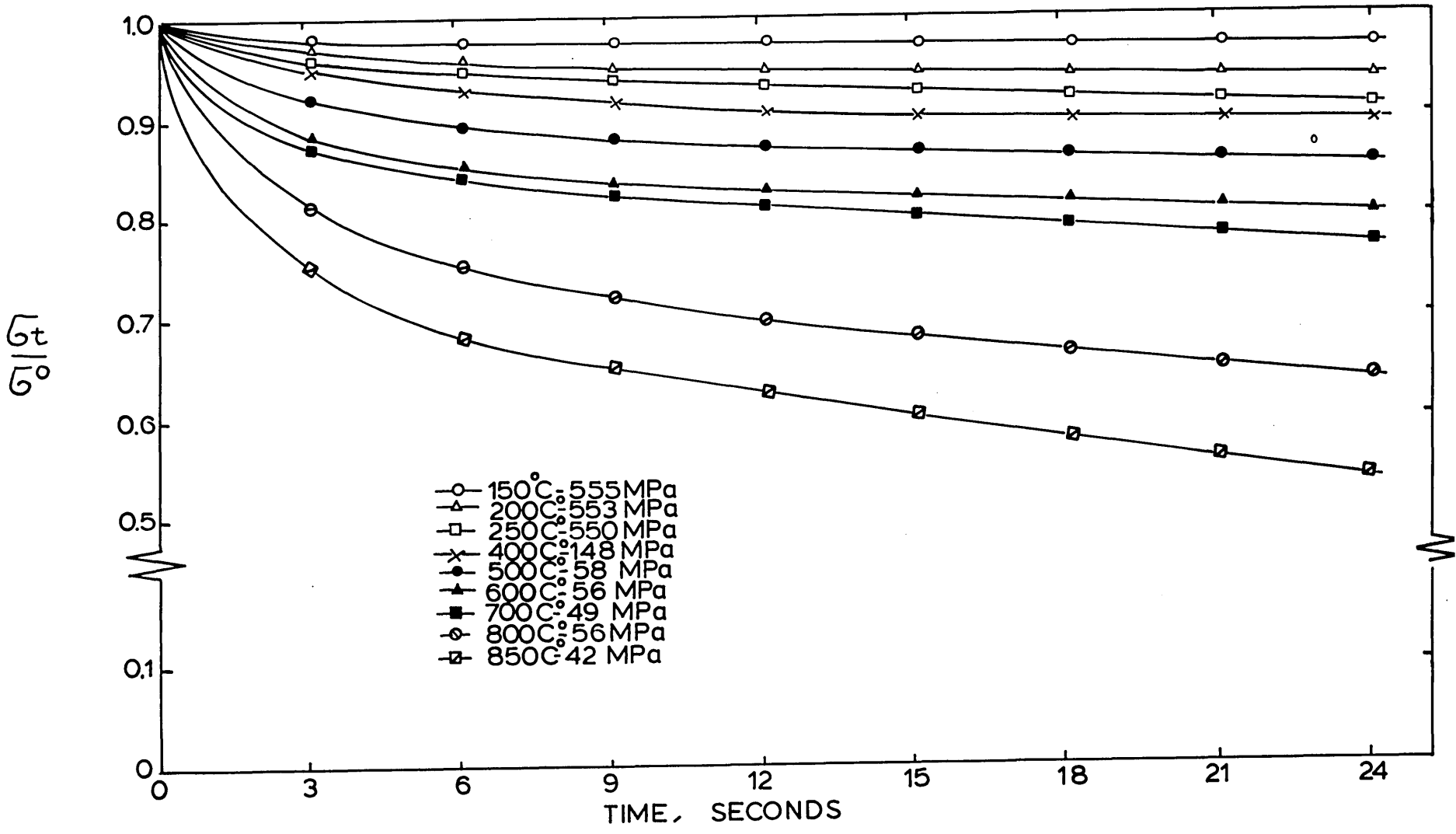
1.0
0.9
0.8
0.7
0.6
0.5
0.1
0
0
3
6
9
12
15
18
21
24
TIME, SECONDS
σt/σ°
150°C: 555 MPa
200°C: 553 MPa
250°C: 550 MPa
400°C: 148 MPa
500°C: 58 MPa
600°C: 56 MPa
700°C: 49 MPa
800°C: 56 MPa
850°C: 42 MPa

FIGURE 35a: Experimental results showing the effect of previous deformation of the specimen on the stress relaxation behaviour of 835M30 steel. Deformation temperature 600°C.

—O— strain free specimen

—Δ— specimen with 0.5% strain.

I,	Test Temperature	400°C
	Test Stress	158 MPa
II,	Test Temperature	250°C
	Test Stress	550 MPa
III,	Test Temperature	225°C
	Test Stress	540 MPa
IV,	Test Temperature	200°C
	Test Stress	548 MPa
V,	Test Temperature	175°C
	Test Stress	562 MPa
VI	Test Temperature	150°C
	Test Stress	555 MPa

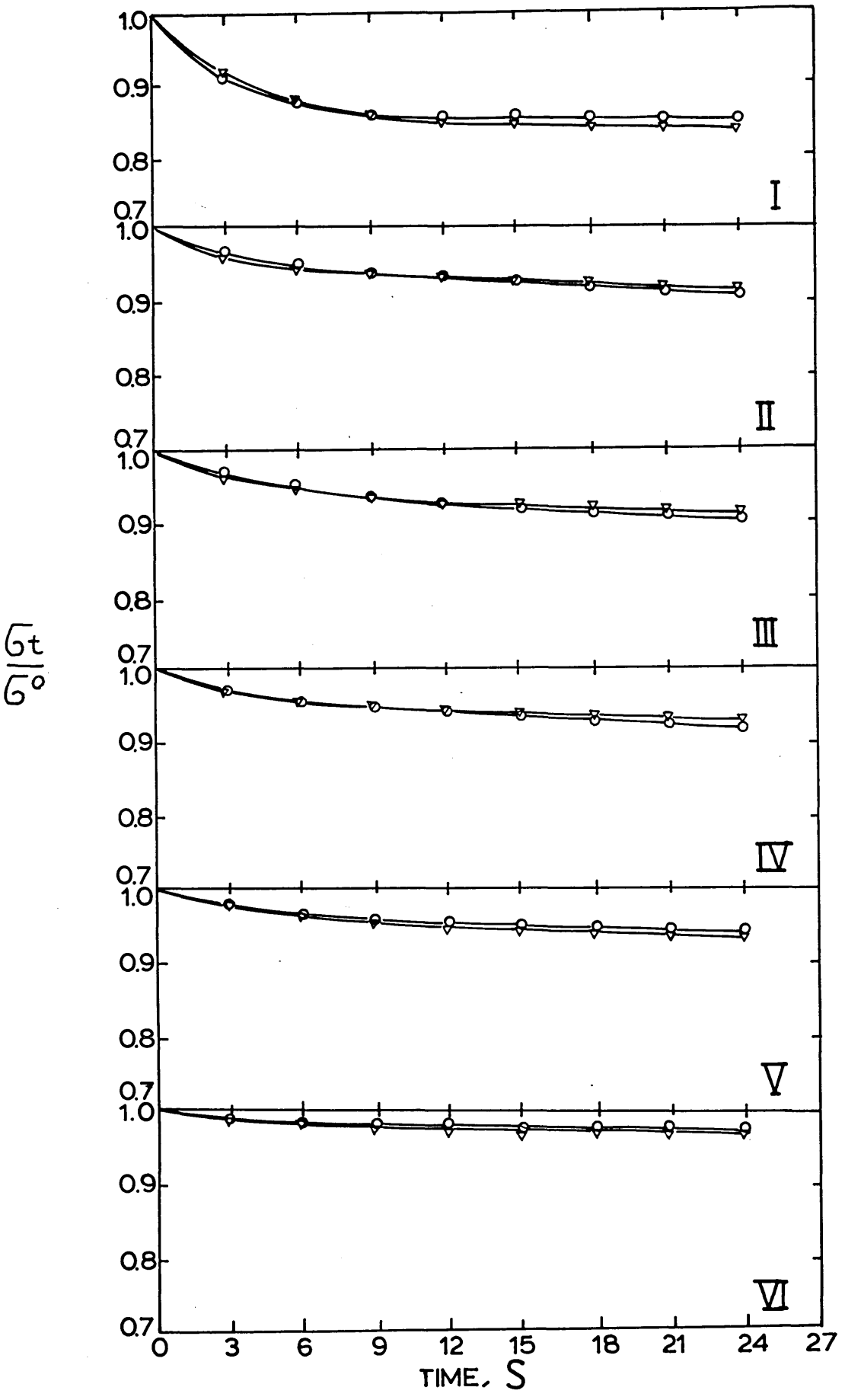
$\frac{\sigma_t}{\sigma^o}$
1.0
0.9
0.8
0.7
I
II
III
IV
V
VI
0
3
6
9
12
15
18
21
24
27
TIME, S

FIGURE 35b: Experimental results showing the effect of previous deformation of the specimen on the stress relaxation behaviour of 835M30 steel. Deformation temperature 400°C.

—O— strain free specimen

—△— specimen with 0.5% strain.

I,	Test Temperature	250°C
	Test Stress	550 MPa
II,	Test Temperature	225°C
	Test Stress	540 MPa
III,	Test Temperature	200°C
	Test Stress	548 MPa
IV,	Test Temperature	175°C
	Test Stress	562 MPa
V,	Test Temperature	150°C
	Test Stress	555 MPa

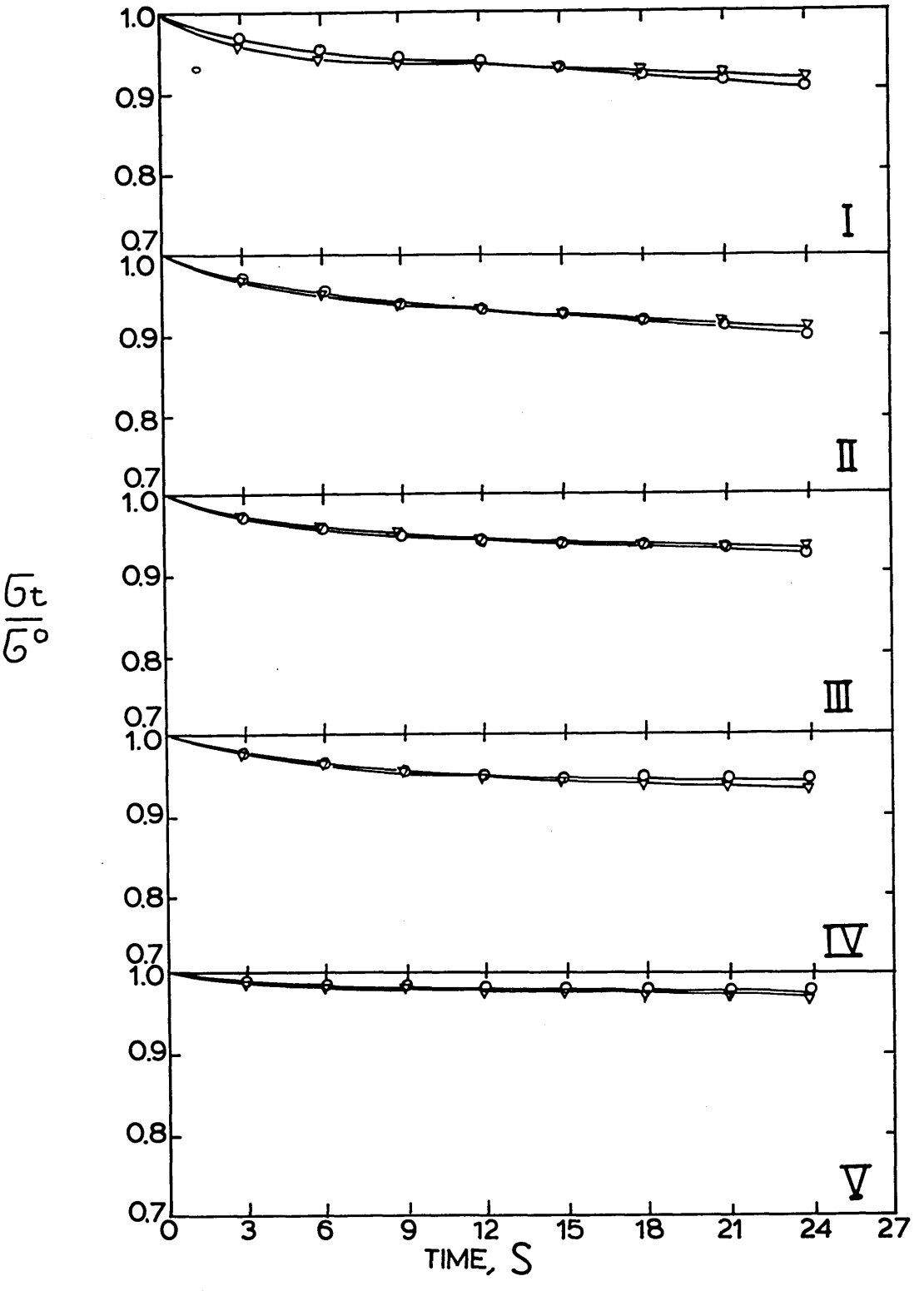
1.0
0.9
0.8
0.7
I
II
III
IV
V
0
3
6
9
12
15
18
21
24
27
TIME, S
σt/σ°

FIGURE 36: Experiment results showing the effect of initial stress [σ^{o}] on the stress relaxation rate.

I. Test Temperature = 850^{o}C

II. Test Temperature = 800^{o}C

III. Test Temperature = 700^{o}C

Continue:-

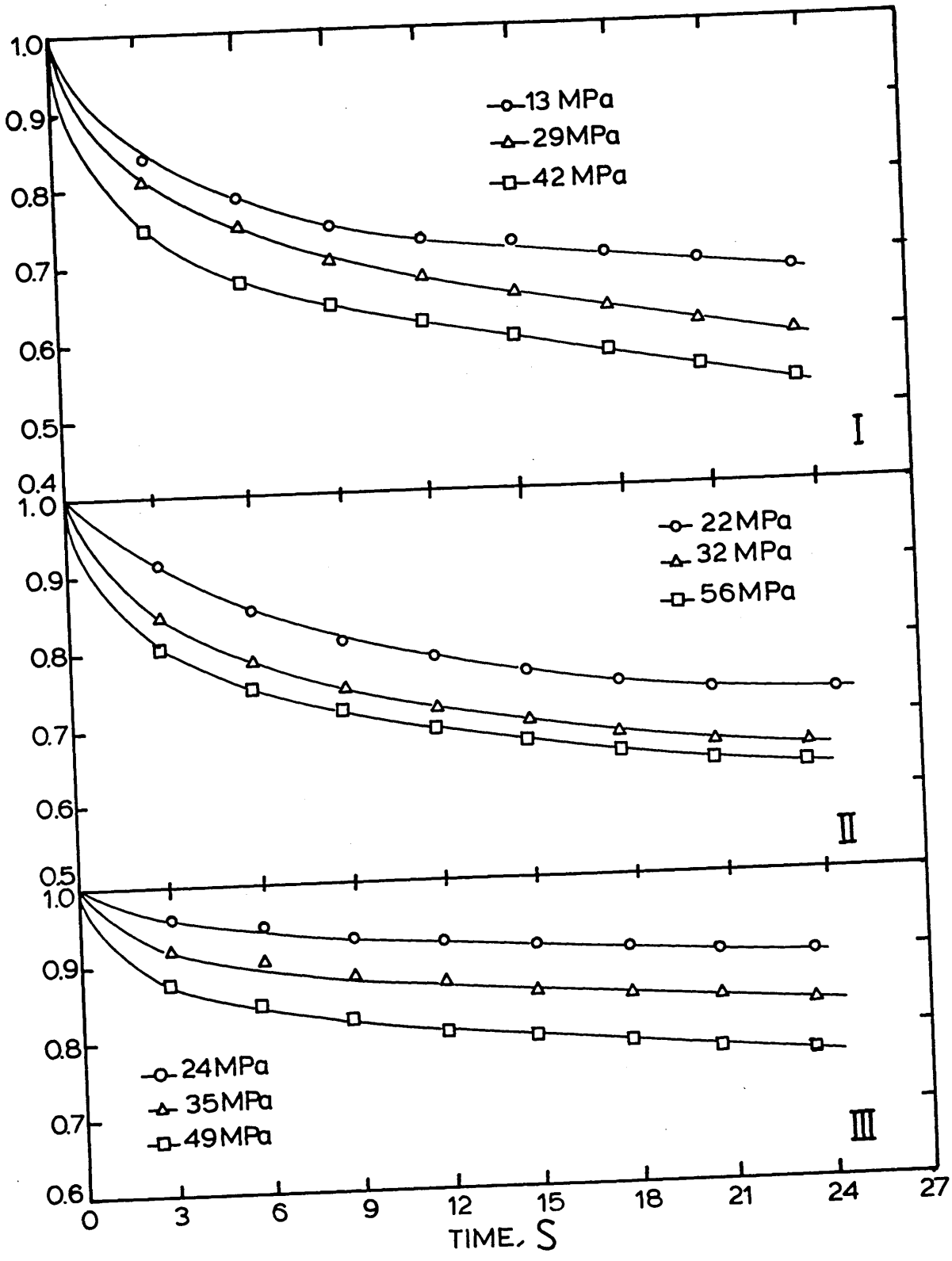

$\frac{\sigma t}{\sigma^{\circ}}$

Continue:-

FIGURE 36: Continued:

IV. Test Temperature 600°C

V. Test Temperature 500°C

VI. Test Temperature 400°C

Continue:-

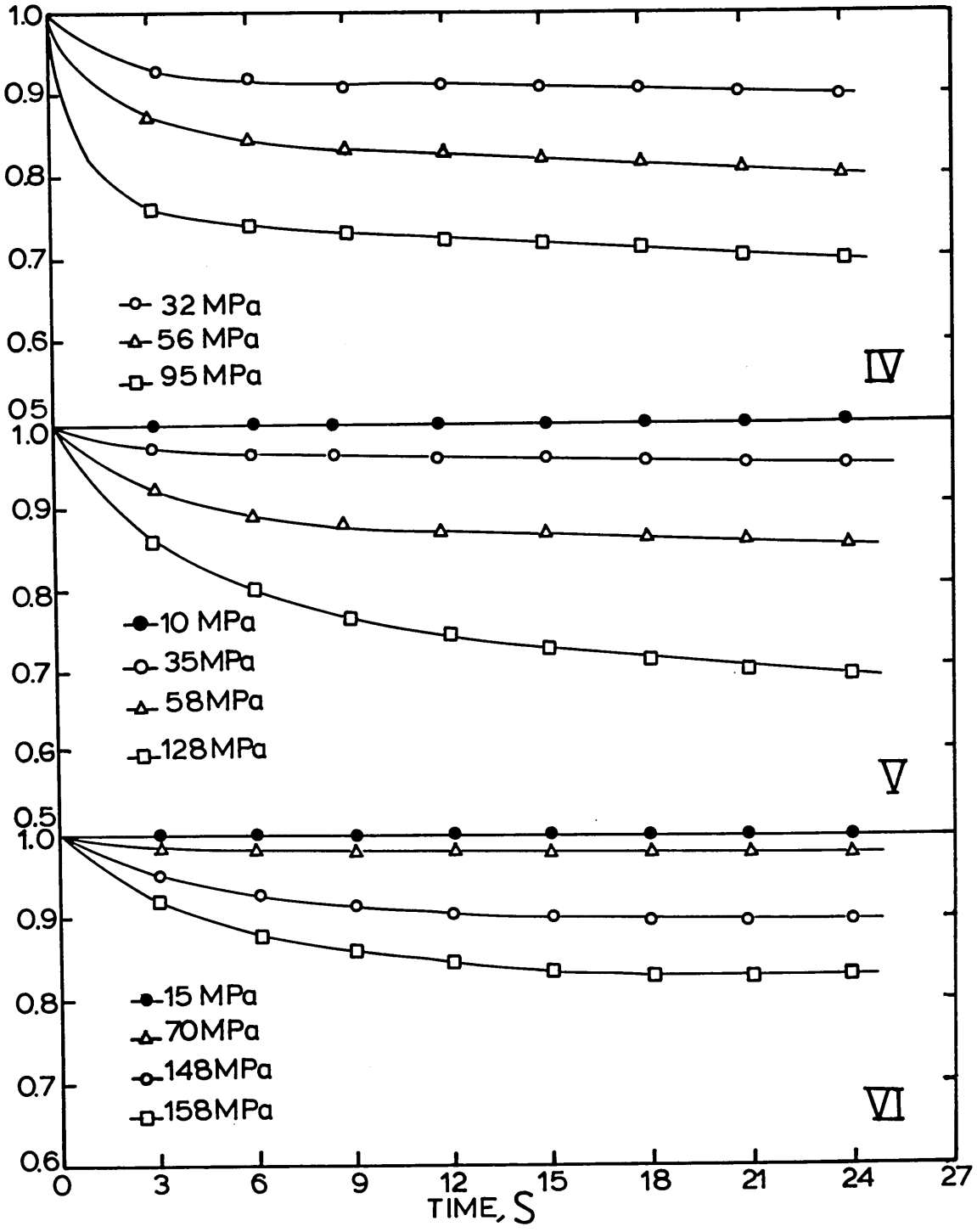

$\frac{\sigma t}{\sigma^{\circ}}$

Continue:-

FIGURE 36: Continued:

VII. Test Temperature 300°C

VIII. Test Temperature 250°C

IX. Test Temperature 200°C

X. Test Temperature 150°C

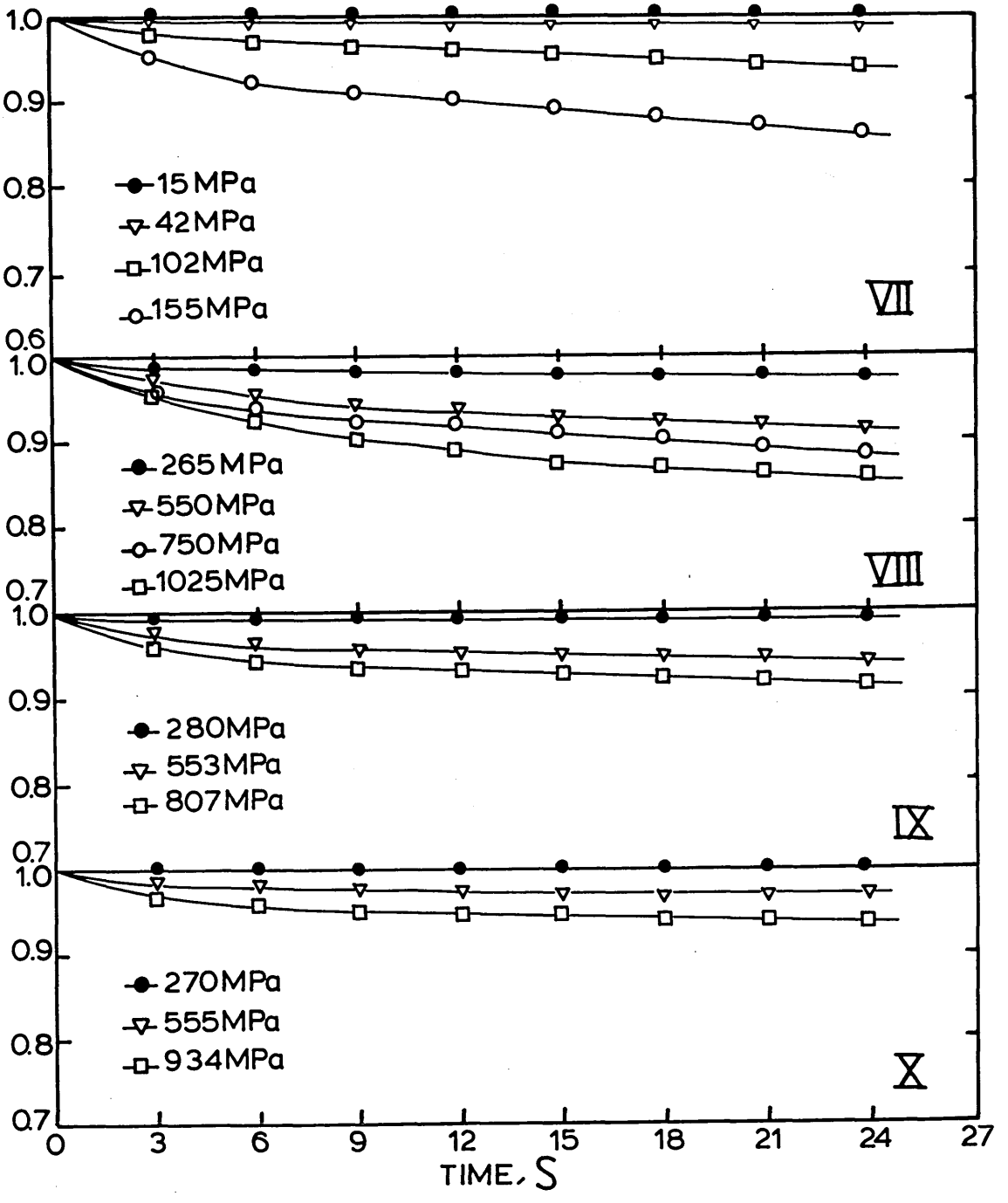
1.0
0.9
0.8
0.7
0.6
15 MPa
42 MPa
102 MPa
155 MPa
VII
265 MPa
550 MPa
750 MPa
1025 MPa
VIII
280 MPa
553 MPa
807 MPa
IX
270 MPa
555 MPa
934 MPa
X
0
3
6
9
12
15
18
21
24
27
TIME, S
σt/σ°

FIGURE 37: Mechanical models representing the viscoelastic behaviour of the material.

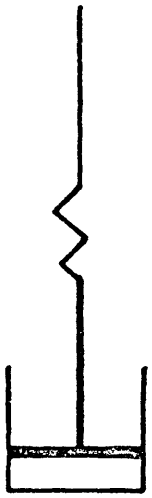

a) Maxwell body

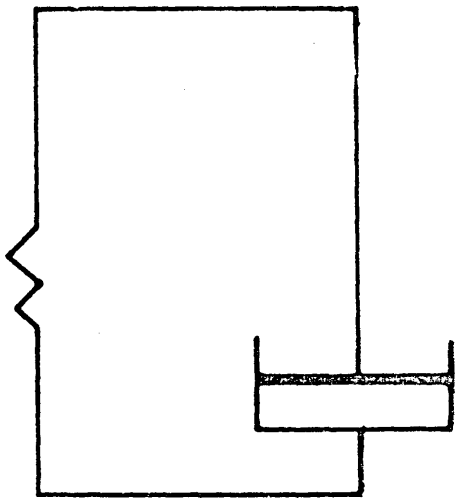

b) Kelvin body

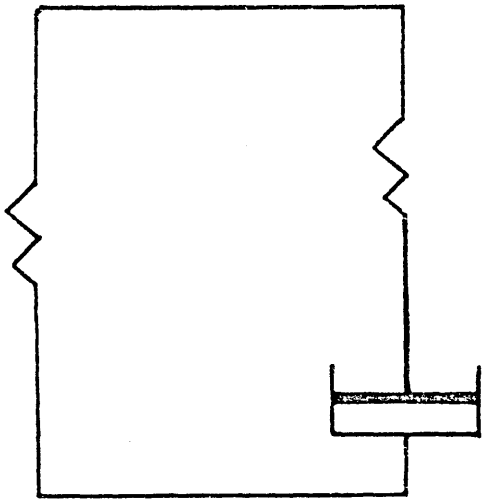

c) Standard linear solid

FIGURE 38: Variation of the Standard Linear Solid parameters A and B with temperature.

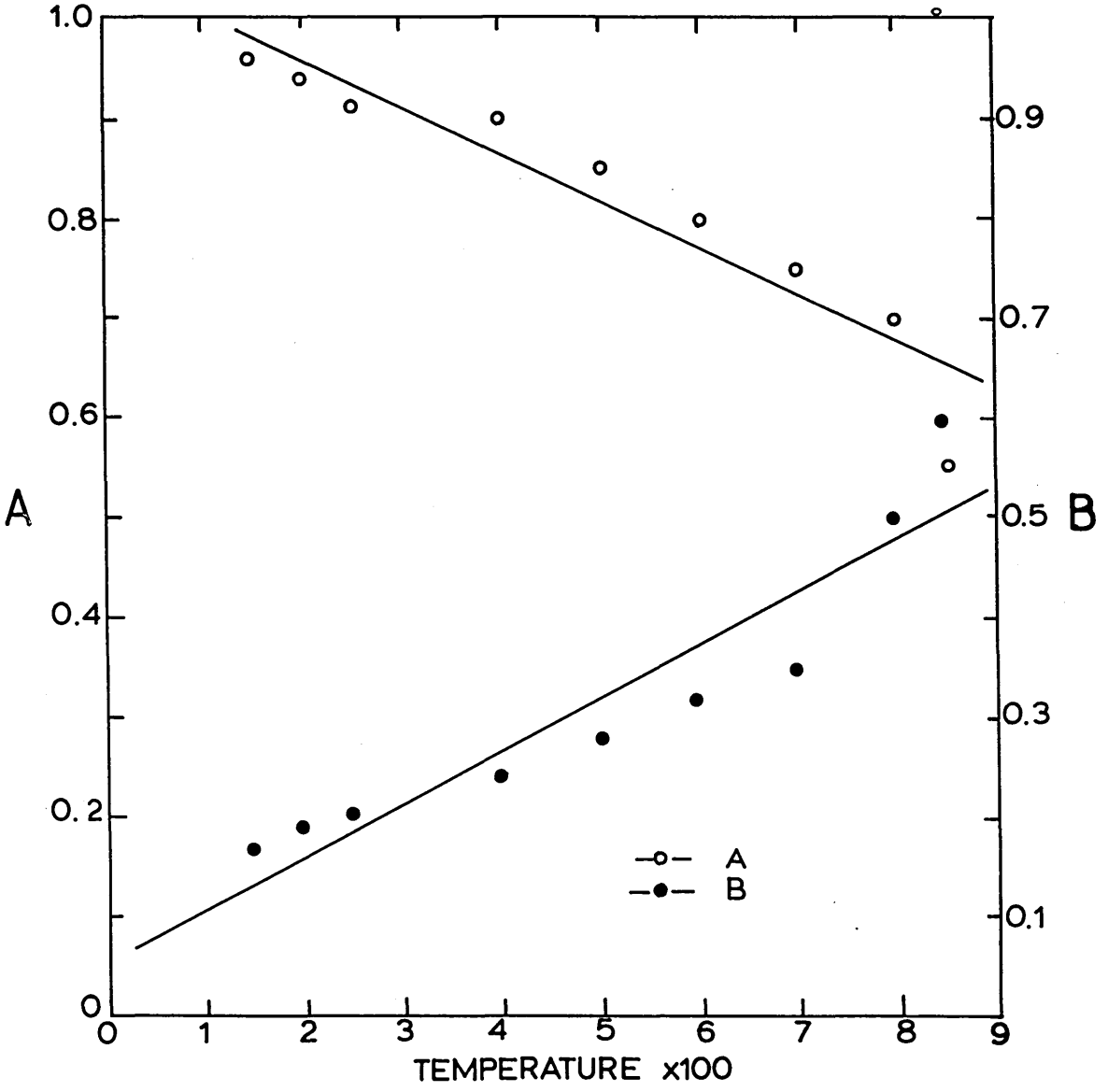
1.0
0.8
0.6
0.4
0.2
0
A
0.9
0.7
0.5
0.3
0.1
B
0
1
2
3
4
5
6
7
8
9
TEMPERATURE x100
A
B

FIGURE 39: Variation of the Standard Linear Solid parameters A and B with initial stress level [σ^o] for various temperature ranges.

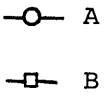

I. Test Temperature 850°C
II. Test Temperature 800°C
III. Test Temperature 700°C
IV. Test Temperature 600°C
V. Test Temperature 500°C

Continue:-

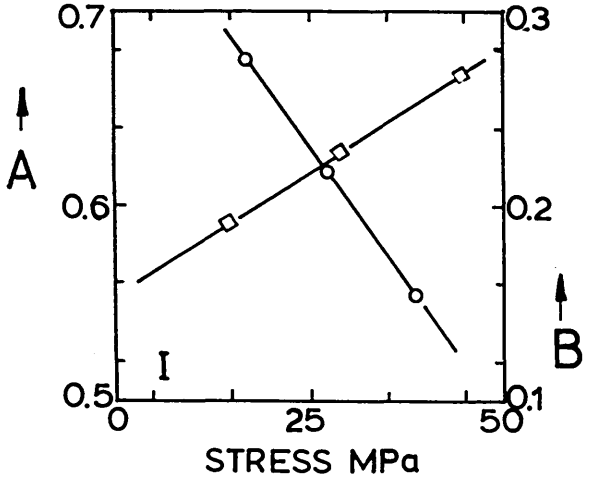
0.7
0.6
0.5
A
0.3
0.2
0.1
B
I
0
25
50
STRESS MPa

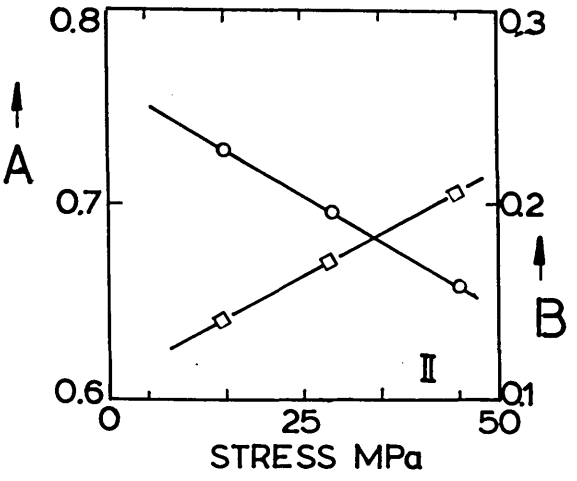
0.8
0.7
0.6
A
0.3
0.2
0.1
B
II
0
25
50
STRESS MPa

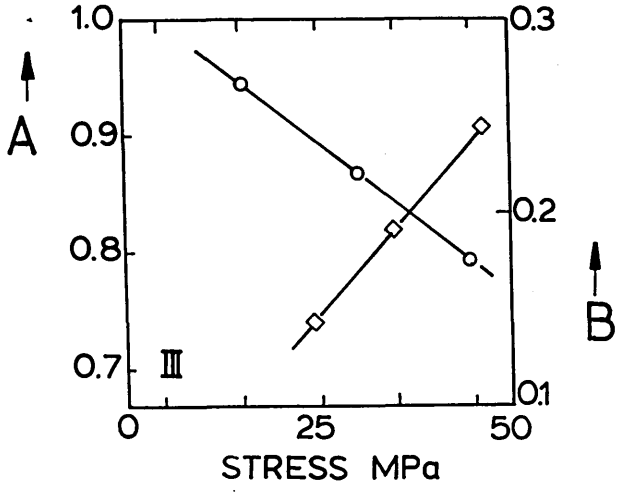
1.0
0.9
0.8
0.7
A
0.3
0.2
0.1
B
III
0
25
50
STRESS MPa

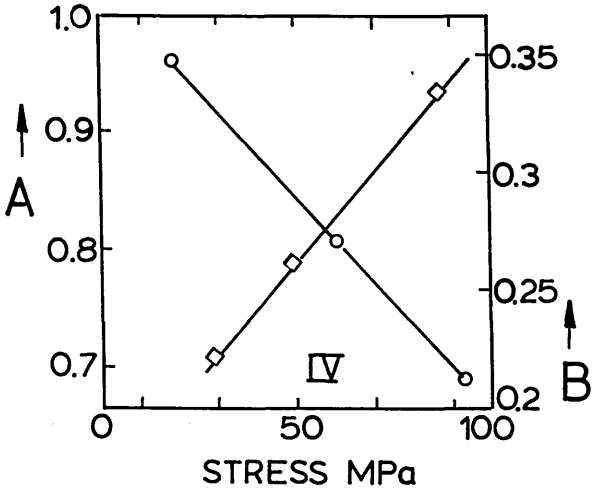
1.0
0.9
0.8
0.7
A
0.35
0.3
0.25
0.2
B
IV
0
50
100
STRESS MPa

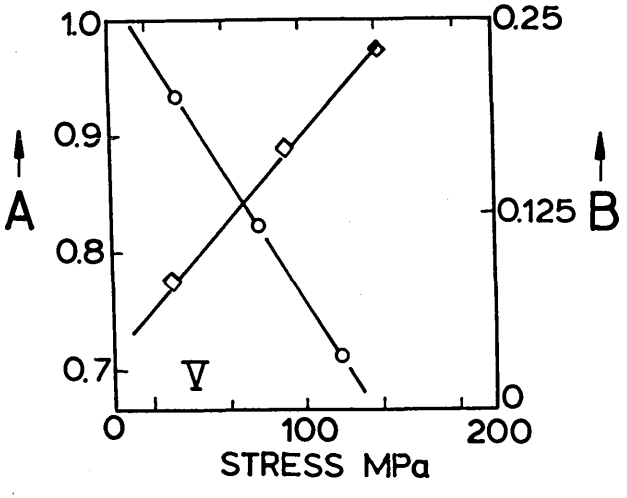
1.0
0.9
0.8
0.7
A
0.25
0.125
0
B
V
0
100
200
STRESS MPa

Continue:-

FIGURE 39: Continued:-

—○— A

—□— B

VI.	Test Temperature	400°C
VII.	Test Temperature	300°C
VIII.	Test Temperature	250°C
IX.	Test Temperature	200°C
X.	Test Temperature	150°C

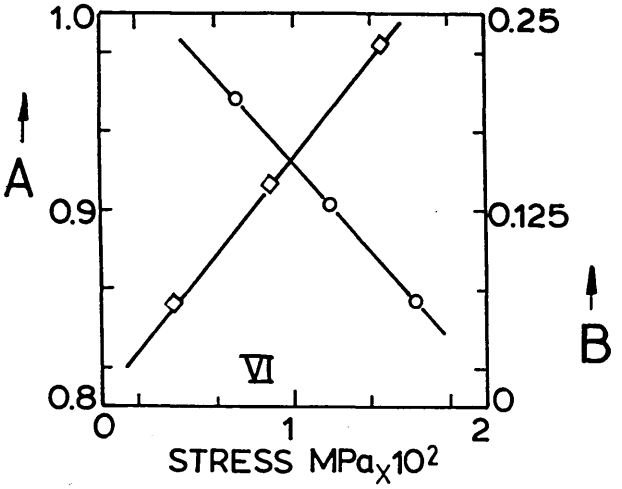
1.0
0.9
0.8
A
0.25
0.125
0
B
VI
0
1
2
STRESS MPa x 10²

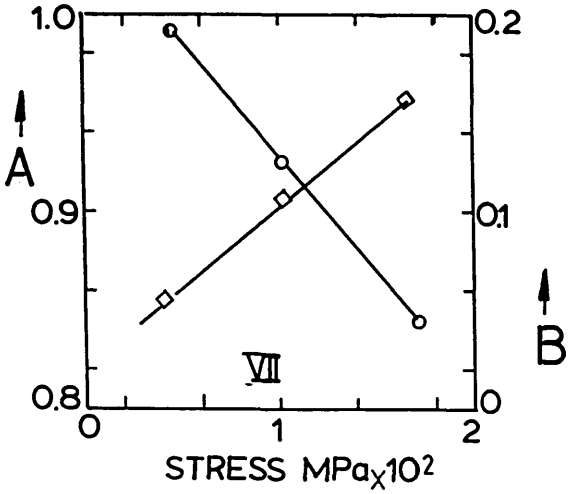
1.0
0.9
0.8
A
0.2
0.1
0
B
VII
0
1
2
STRESS MPa x 10²

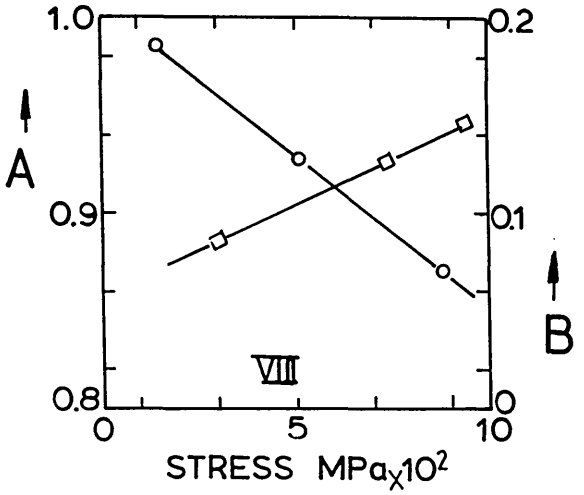
1.0
0.9
0.8
A
0.2
0.1
0
B
VIII
0
5
10
STRESS MPa x 10²

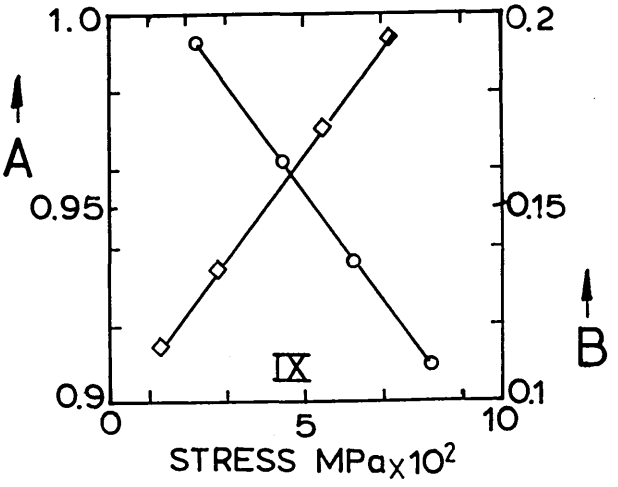
1.0
0.95
0.9
A
0.2
0.15
0.1
B
IX
0
5
10
STRESS MPa x 10²

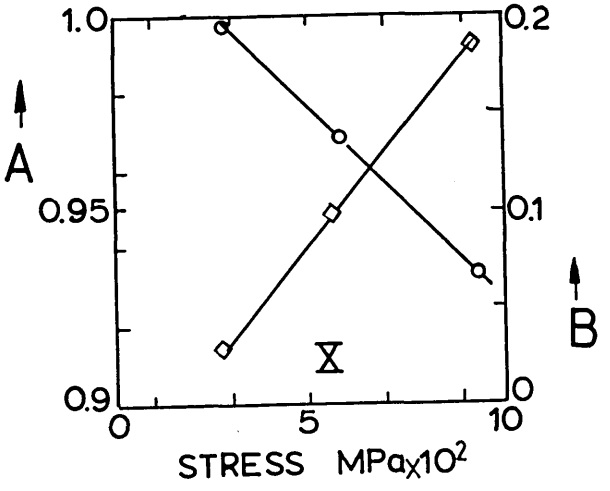
1.0
0.95
0.9
A
0.2
0.1
0
B
X
0
5
10
STRESS MPa x 10²

FIGURE 40: Comparison of experimental and calculated results of stress relaxation behaviour of 835M30 steel.

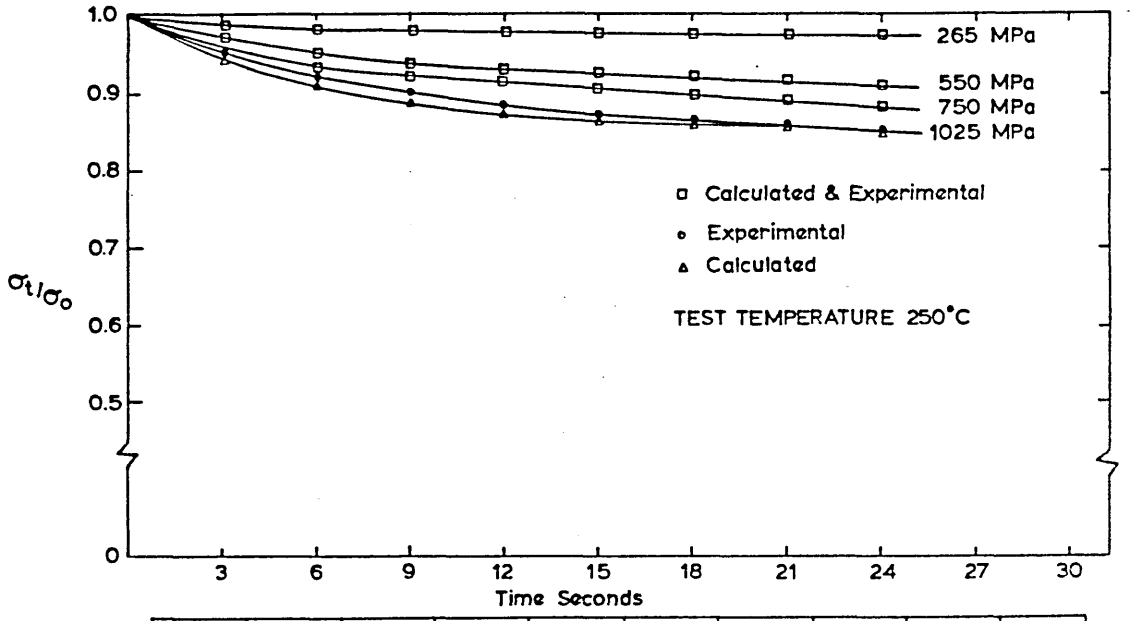
1.0
0.9
0.8
0.7
0.6
0.5
0
σ_t/σ_o
265 MPa
550 MPa
750 MPa
1025 MPa
Calculated & Experimental
Experimental
Calculated
TEST TEMPERATURE 250°C
3
6
9
12
15
18
21
24
27
30
Time Seconds

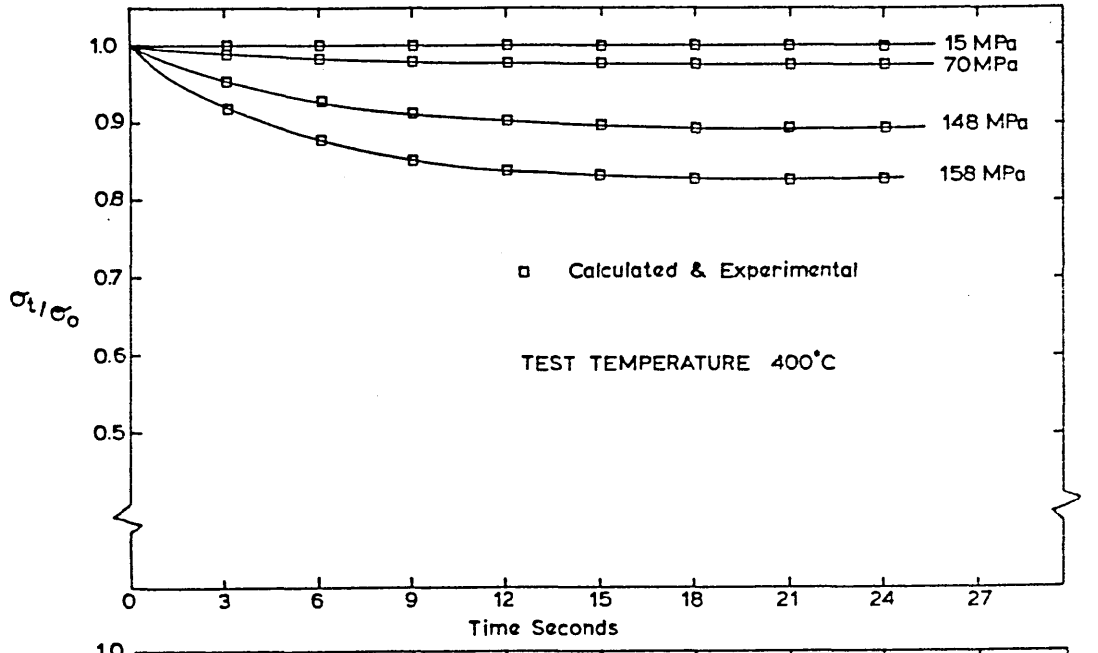
1.0
0.9
0.8
0.7
0.6
0.5
σ_t/σ_o
15 MPa
70 MPa
148 MPa
158 MPa
Calculated & Experimental
TEST TEMPERATURE 400°C
0
3
6
9
12
15
18
21
24
27
Time Seconds

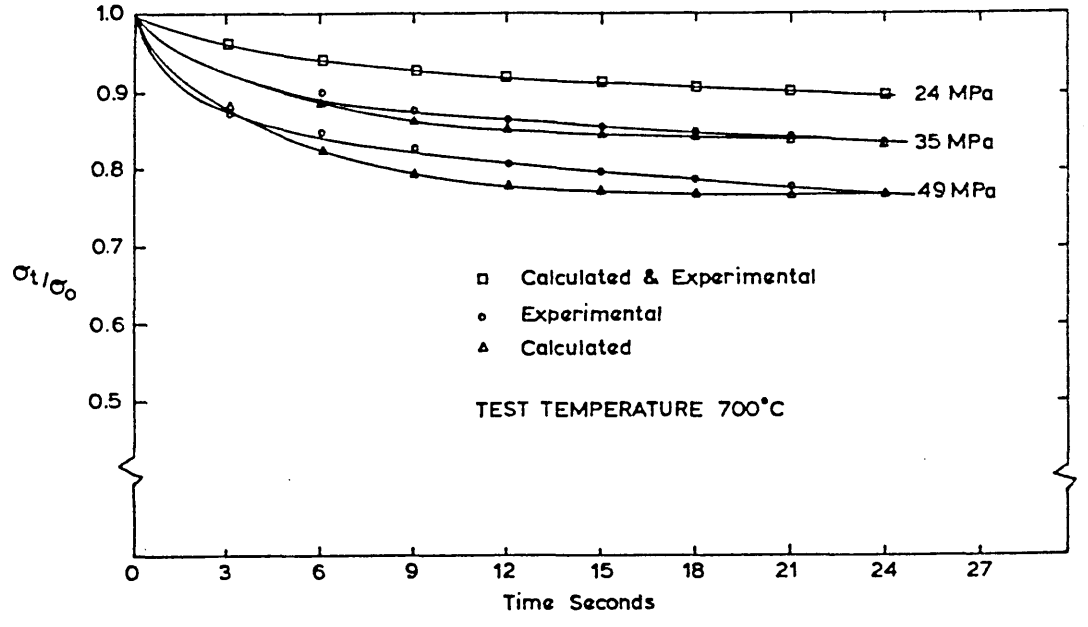
1.0
0.9
0.8
0.7
0.6
0.5
σ_t/σ_o
24 MPa
35 MPa
49 MPa
Calculated & Experimental
Experimental
Calculated
TEST TEMPERATURE 700°C
0
3
6
9
12
15
18
21
24
27
Time Seconds

FIGURE 41: Infinite plate model with plane stress acting in directions parallel to the longitudinal plane of plate.

FIGURE 42: Relationship between the absolute applied stress and the absolute change in strain produced in a dilatometer specimen at the end of the quench.

(After Fletcher and Abbasi)[23].

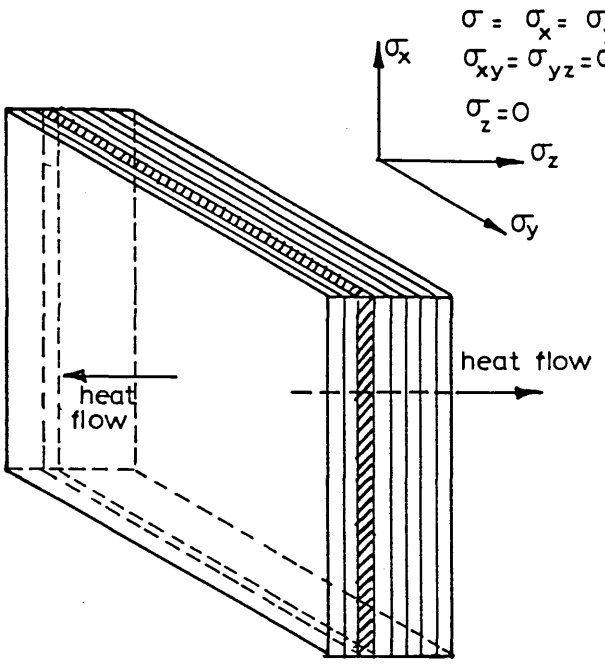
$\sigma = \sigma_x = \sigma_y$
$\sigma_{xy} = \sigma_{yz} = \sigma_{zx} = 0$
$\sigma_z = 0$
σ_x
σ_z
σ_y
heat flow
heat flow

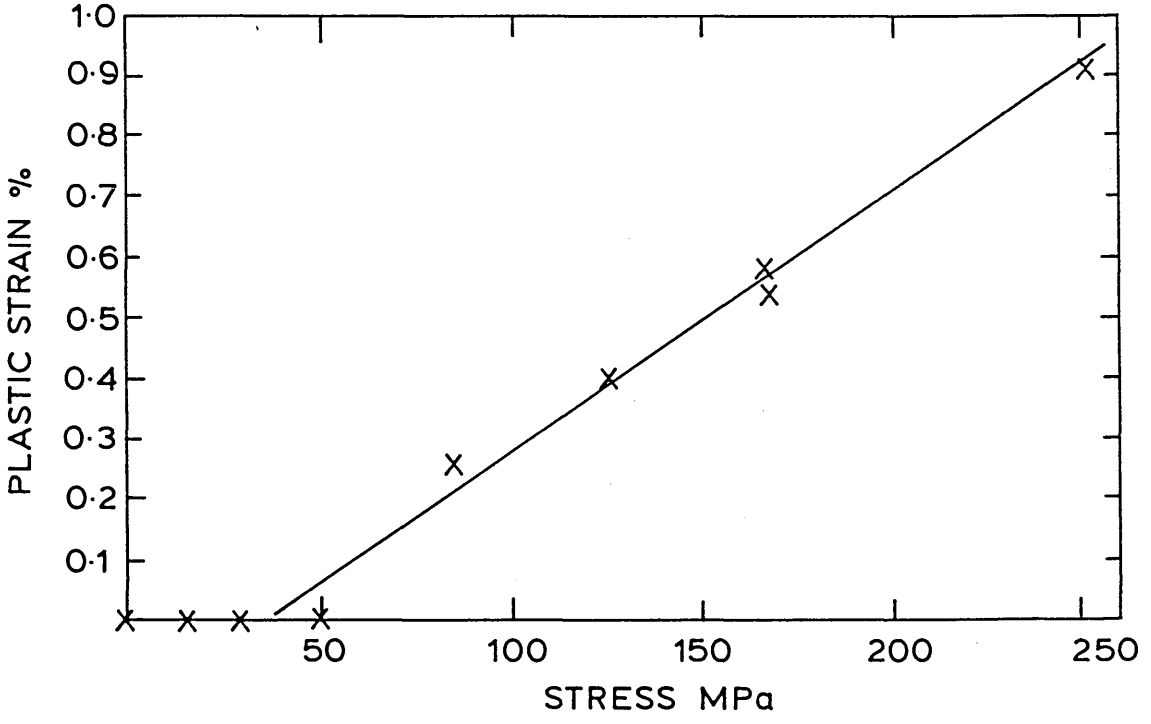
PLASTIC STRAIN %
1·0
0·9
0·8
0·7
0·6
0·5
0·4
0·3
0·2
0·1
50
100
150
200
250
STRESS MPa

FIGURE 43: Flow diagram of the computer programme, used for thermal stress and strain calculation.

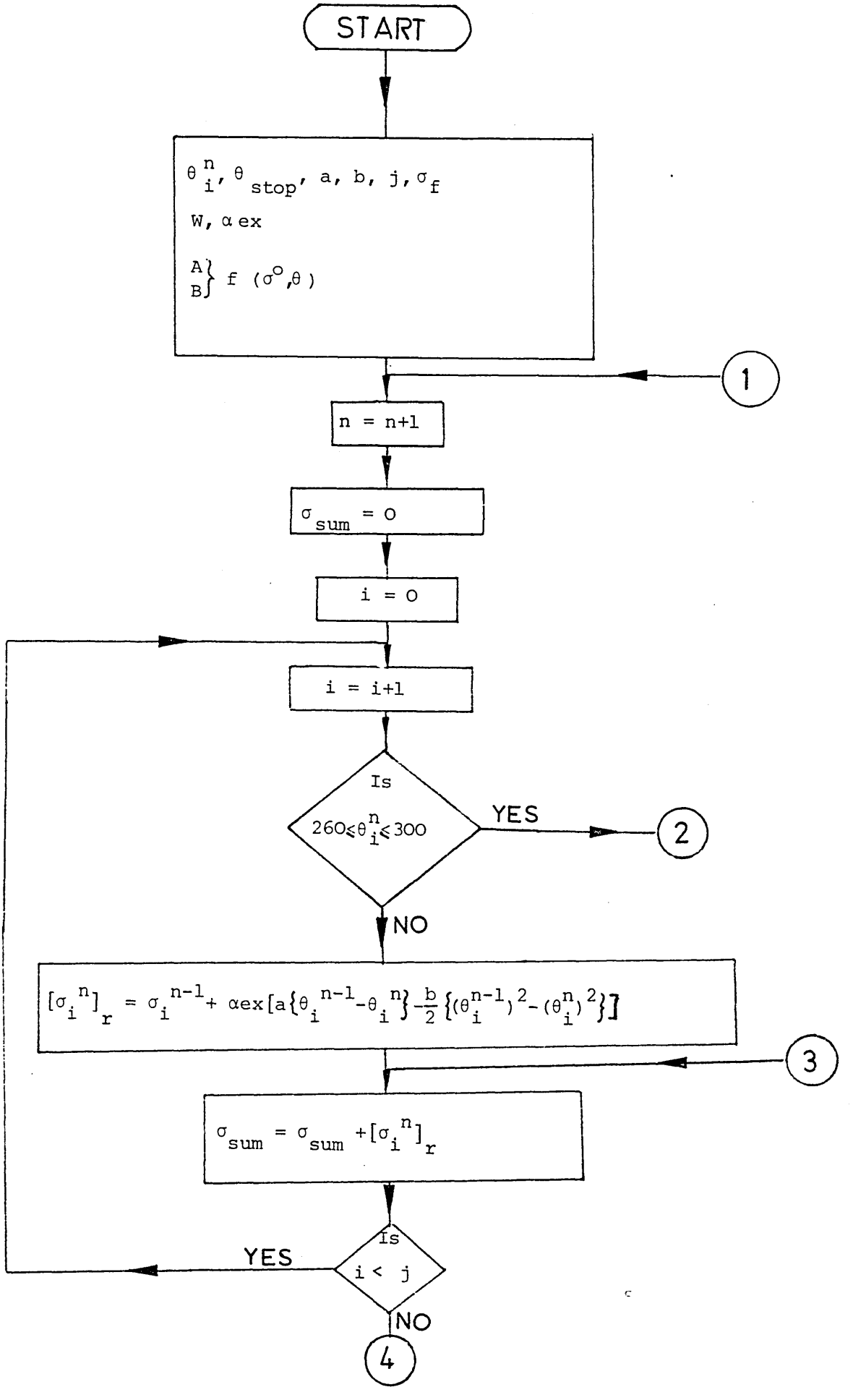
START
θ_i^n, θ_{stop}, a, b, j, σ_f
W, α ex
A, B } f (σ^o, θ)
1
n = n+1
σ_{sum} = 0
i = 0
i = i+1
Is
$260 \leq \theta_i^n \leq 300$
YES
2
NO
$[\sigma_i^n]_r = \sigma_i^{n-1} + \alpha ex[a\{\theta_i^{n-1} - \theta_i^n\} - \frac{b}{2}\{(\theta_i^{n-1})^2 - (\theta_i^n)^2\}]$
3
$\sigma_{sum} = \sigma_{sum} + [\sigma_i^n]_r$
Is
i < j
YES
NO
4

Continue:-

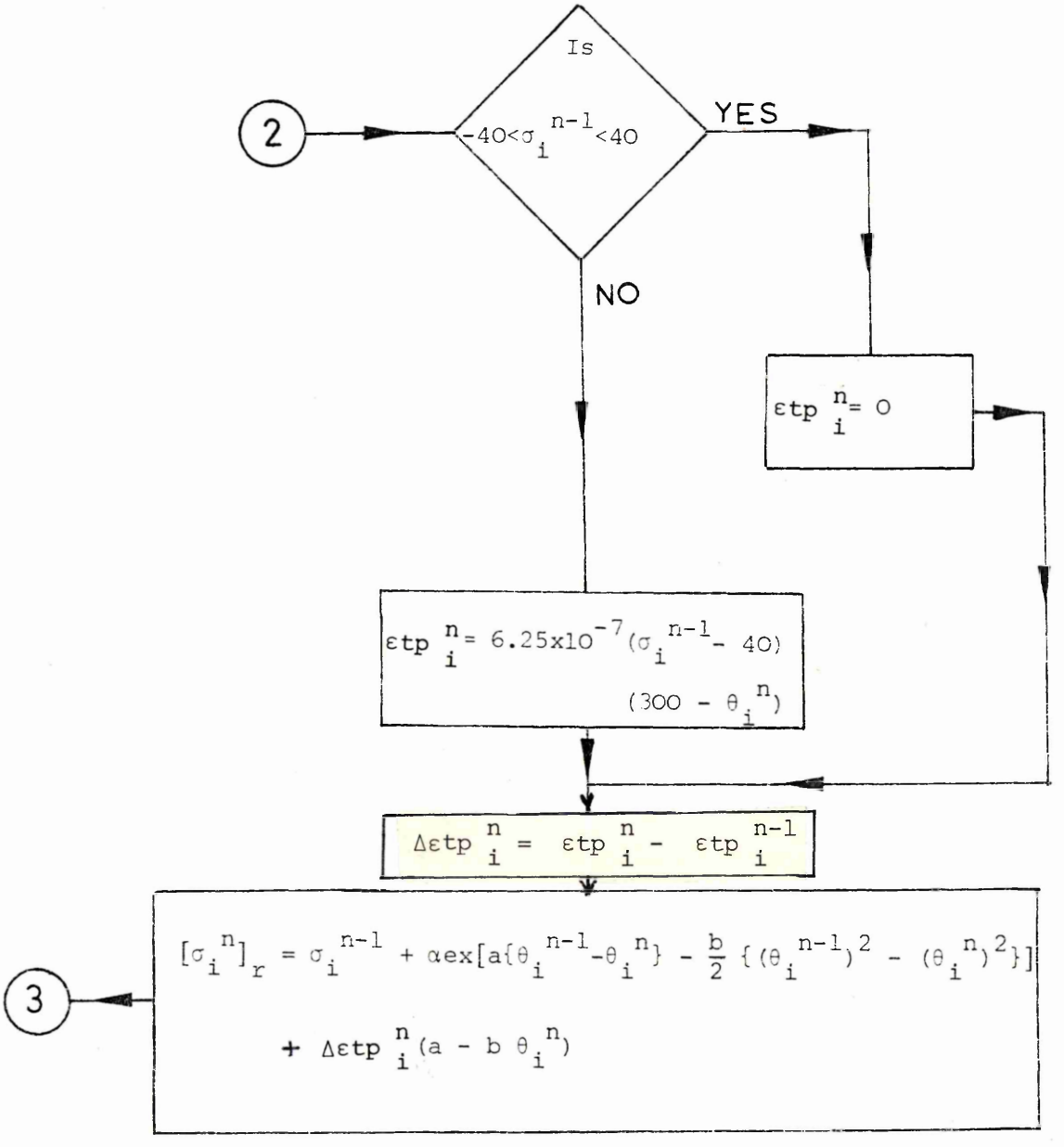
2
Is
$-40<\sigma_i^{n-1}<40$
YES
NO
$\varepsilon tp_i^n = 0$
$\varepsilon tp_i^n = 6.25 \times 10^{-7}(\sigma_i^{n-1} - 40)(300 - \theta_i^n)$
$\Delta\varepsilon tp_i^n = \varepsilon tp_i^n - \varepsilon tp_i^{n-1}$
$[\sigma_i^n]_r = \sigma_i^{n-1} + \alpha ex[a\{\theta_i^{n-1} - \theta_i^n\} - \frac{b}{2}\{(\theta_i^{n-1})^2 - (\theta_i^n)^2\}]$
$+ \Delta\varepsilon tp_i^n (a - b\,\theta_i^n)$
3

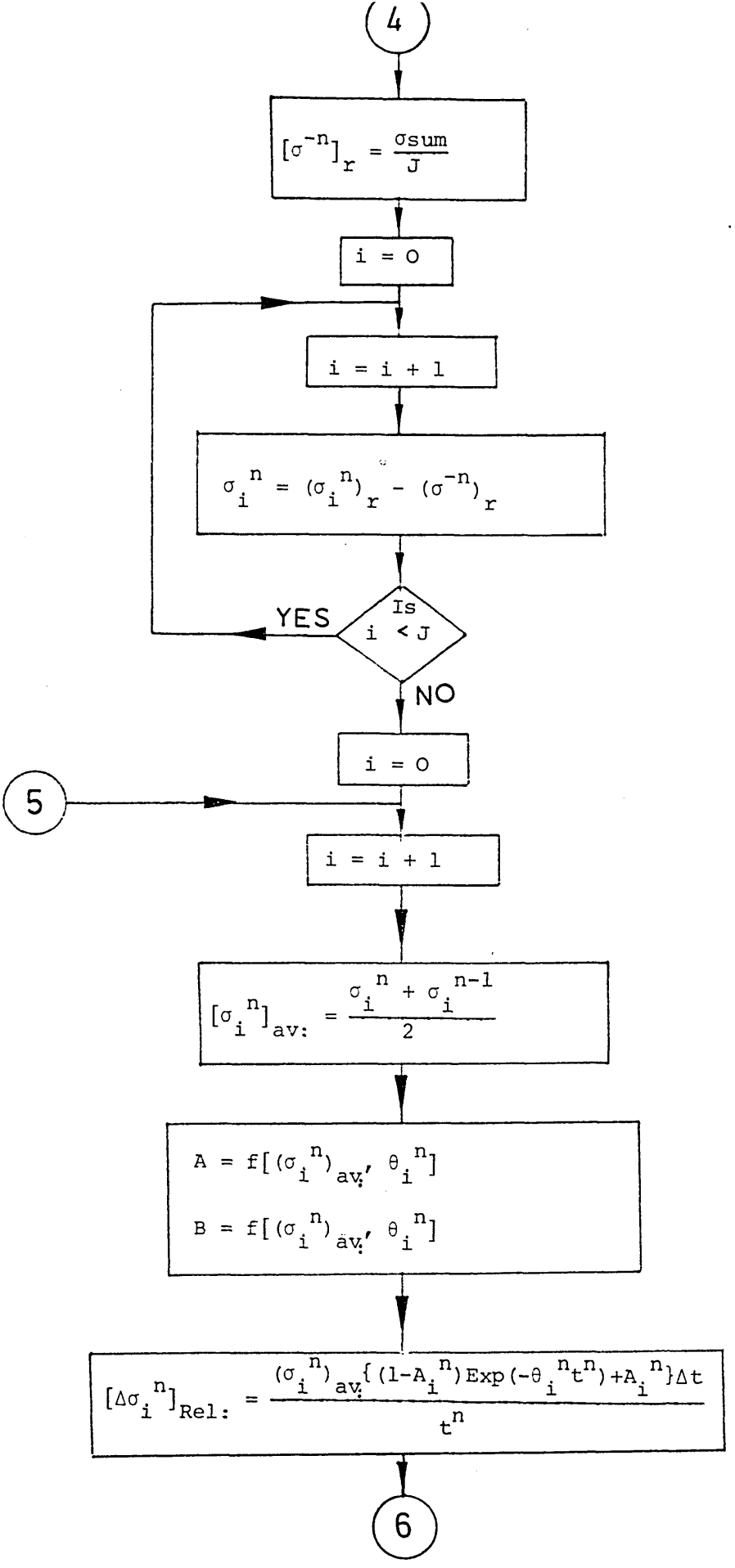
4
$[\sigma^{-n}]_r = \frac{\sigma sum}{J}$
i = O
i = i + 1
$\sigma_i^n = (\sigma_i^n)_r - (\sigma^{-n})_r$
Is i < J
YES
NO
i = O
5
i = i + 1
$[\sigma_i^n]_{av:} = \frac{\sigma_i^n + \sigma_i^{n-1}}{2}$
$A = f[(\sigma_i^n)_{av:}, \theta_i^n]$
$B = f[(\sigma_i^n)_{av:}, \theta_i^n]$
$[\Delta\sigma_i^n]_{Rel:} = \frac{(\sigma_i^n)_{av:}\{(1-A_i^n)Exp(-\theta_i^n t^n)+A_i^n\}\Delta t}{t^n}$
6

Continue:-

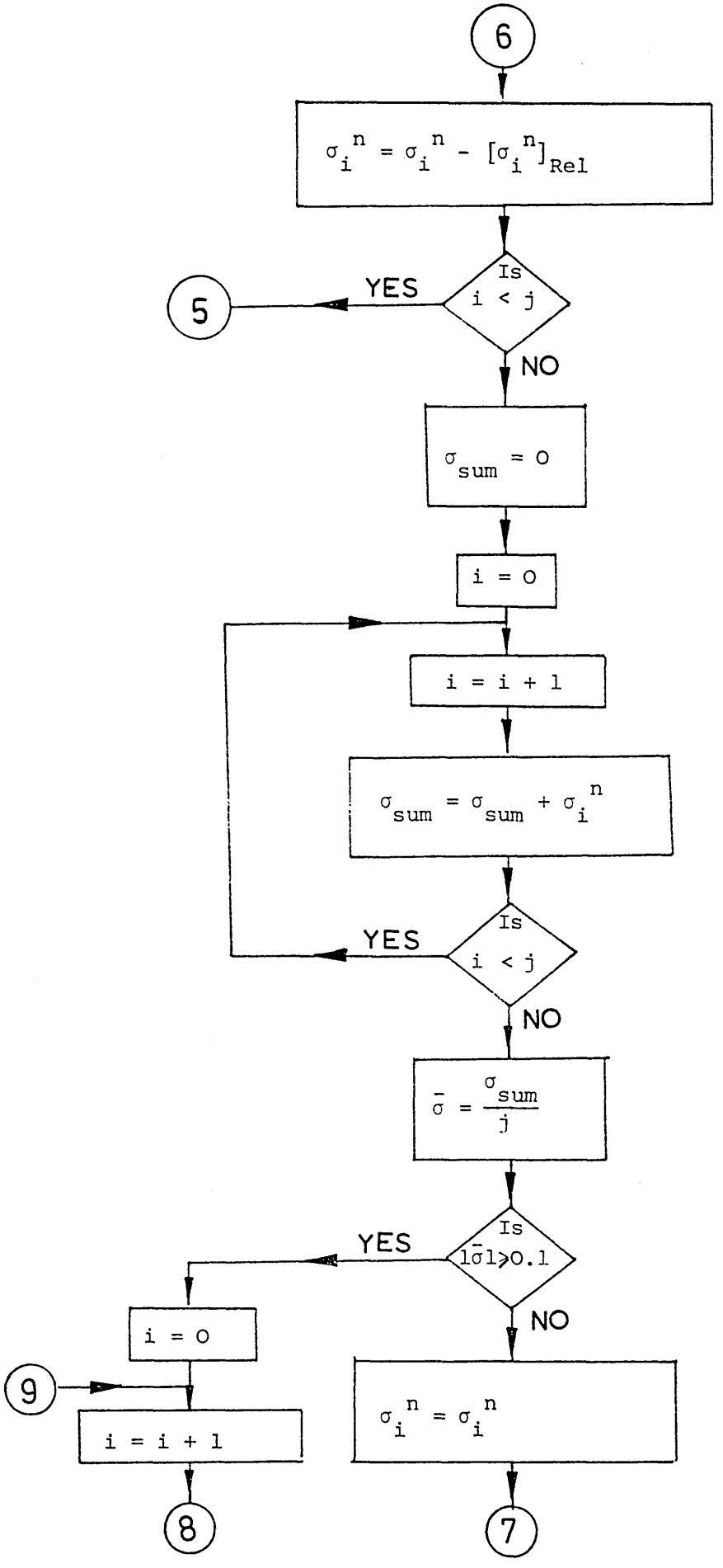
6
$\sigma_i^n = \sigma_i^n - [\sigma_i^n]_{Rel}$
Is
i < j
YES
5
NO
$\sigma_{sum} = 0$
i = 0
i = i + 1
$\sigma_{sum} = \sigma_{sum} + \sigma_i^n$
Is
i < j
YES
NO
$\bar{\sigma} = \frac{\sigma_{sum}}{j}$
Is
$|\bar{\sigma}| \geq 0.1$
YES
NO
i = 0
9
i = i + 1
$\sigma_i^n = \sigma_i^n$
8
7

Continue:-

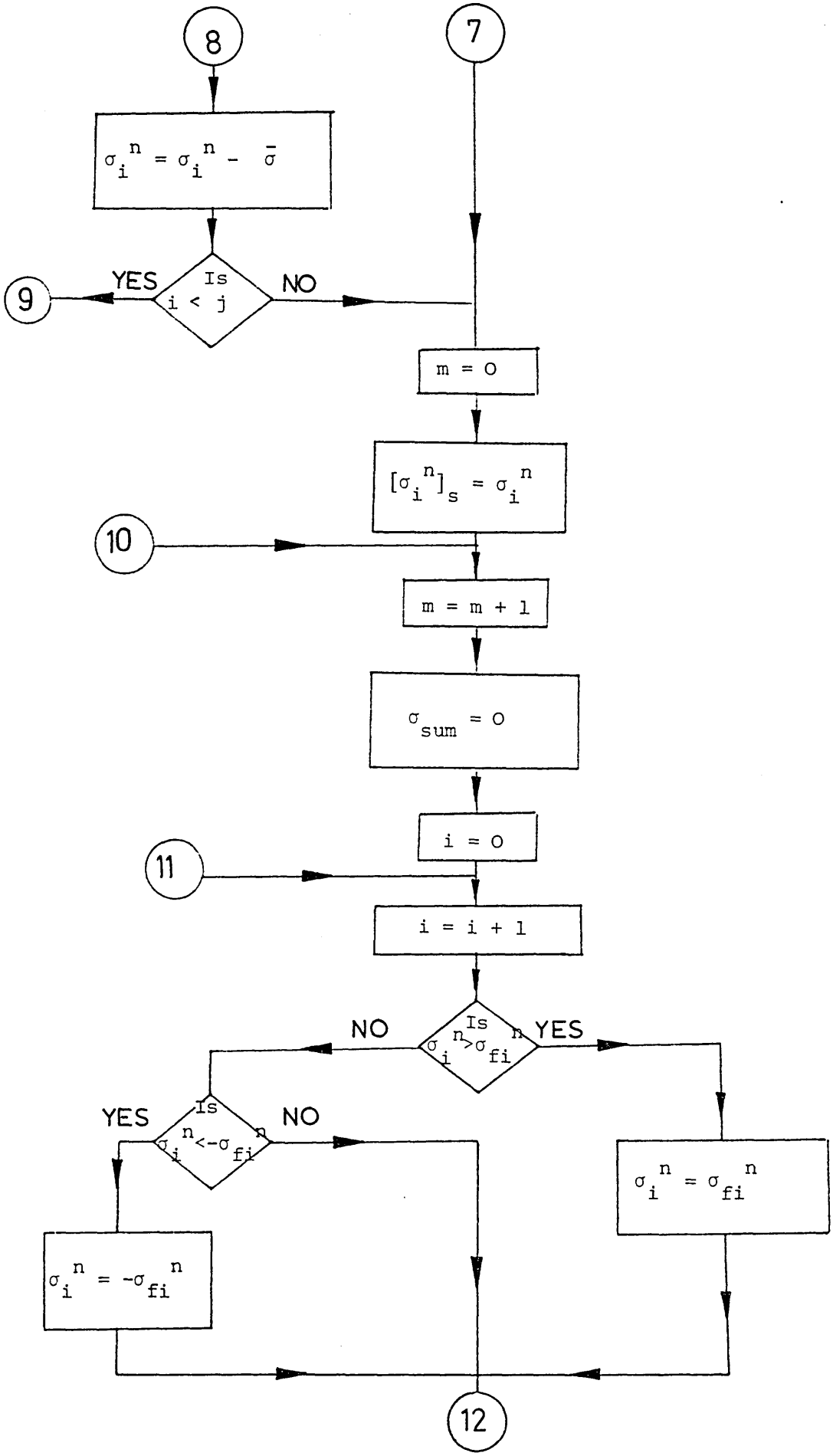
8
7
$\sigma_i^n = \sigma_i^n - \bar{\sigma}$
YES
Is
$i < j$
NO
9
m = O
$[\sigma_i^n]_s = \sigma_i^n$
10
m = m + 1
σ_{sum} = O
i = O
11
i = i + 1
NO
Is
$\sigma_i^n > \sigma_{fi}^n$
YES
YES
Is
$\sigma_i^n < -\sigma_{fi}^n$
NO
$\sigma_i^n = \sigma_{fi}^n$
$\sigma_i^n = -\sigma_{fi}^n$
12

Continue:-

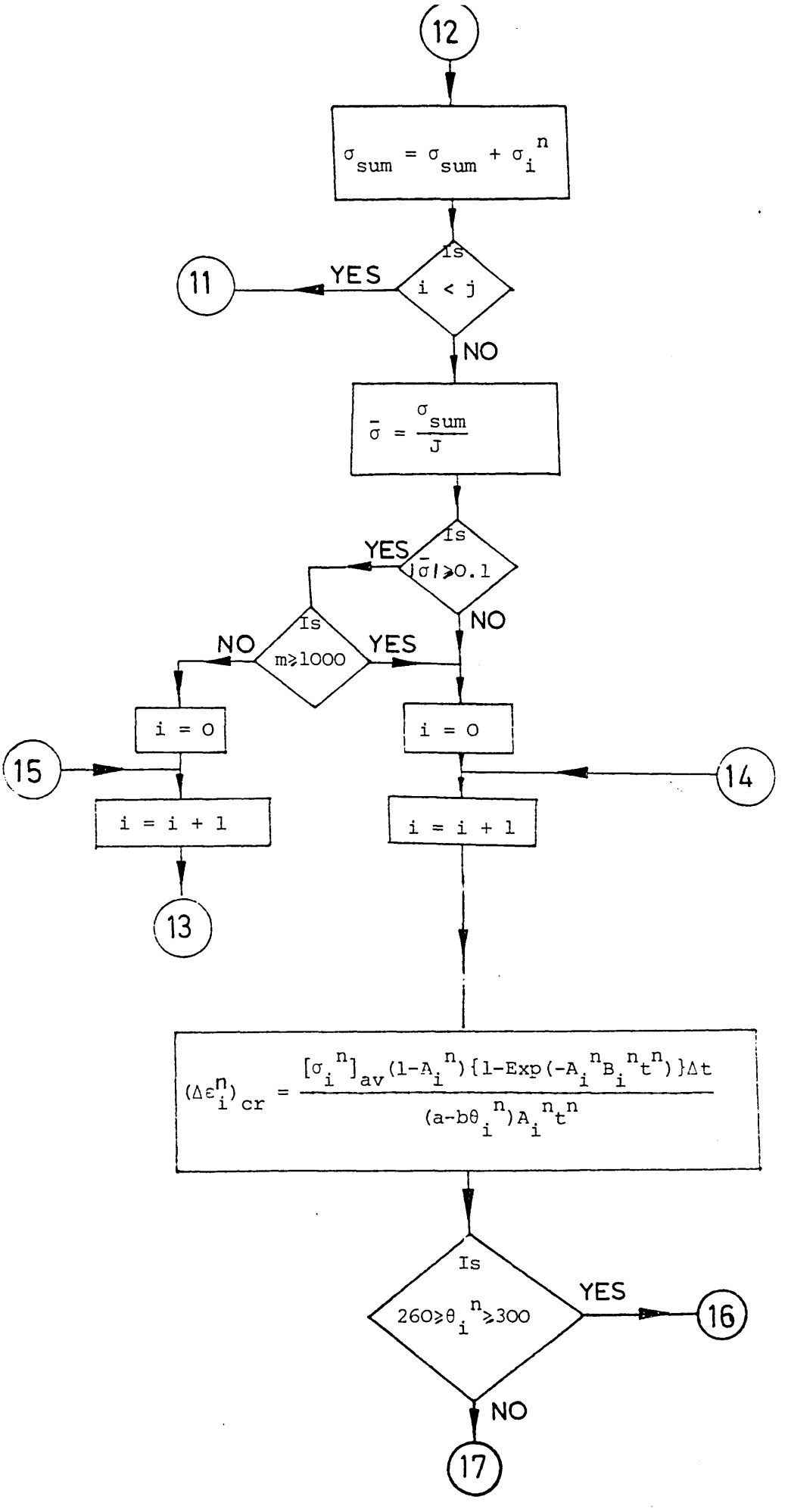
12
$\sigma_{sum} = \sigma_{sum} + \sigma_i^n$
Is
i < j
YES
11
NO
$\bar{\sigma} = \frac{\sigma_{sum}}{J}$
Is
$|\bar{\sigma}| \geq 0.1$
YES
NO
Is
m≥1000
NO
YES
i = 0
i = 0
15
14
i = i + 1
i = i + 1
13
$(\Delta\varepsilon_i^n)_{cr} = \frac{[\sigma_i^n]_{av}(1-A_i^n)\{1-Exp(-A_i^n B_i^n t^n)\}\Delta t}{(a-b\theta_i^n)A_i^n t^n}$
Is
$260 \geq \theta_i^n \geq 300$
YES
16
NO
17

Continue:-

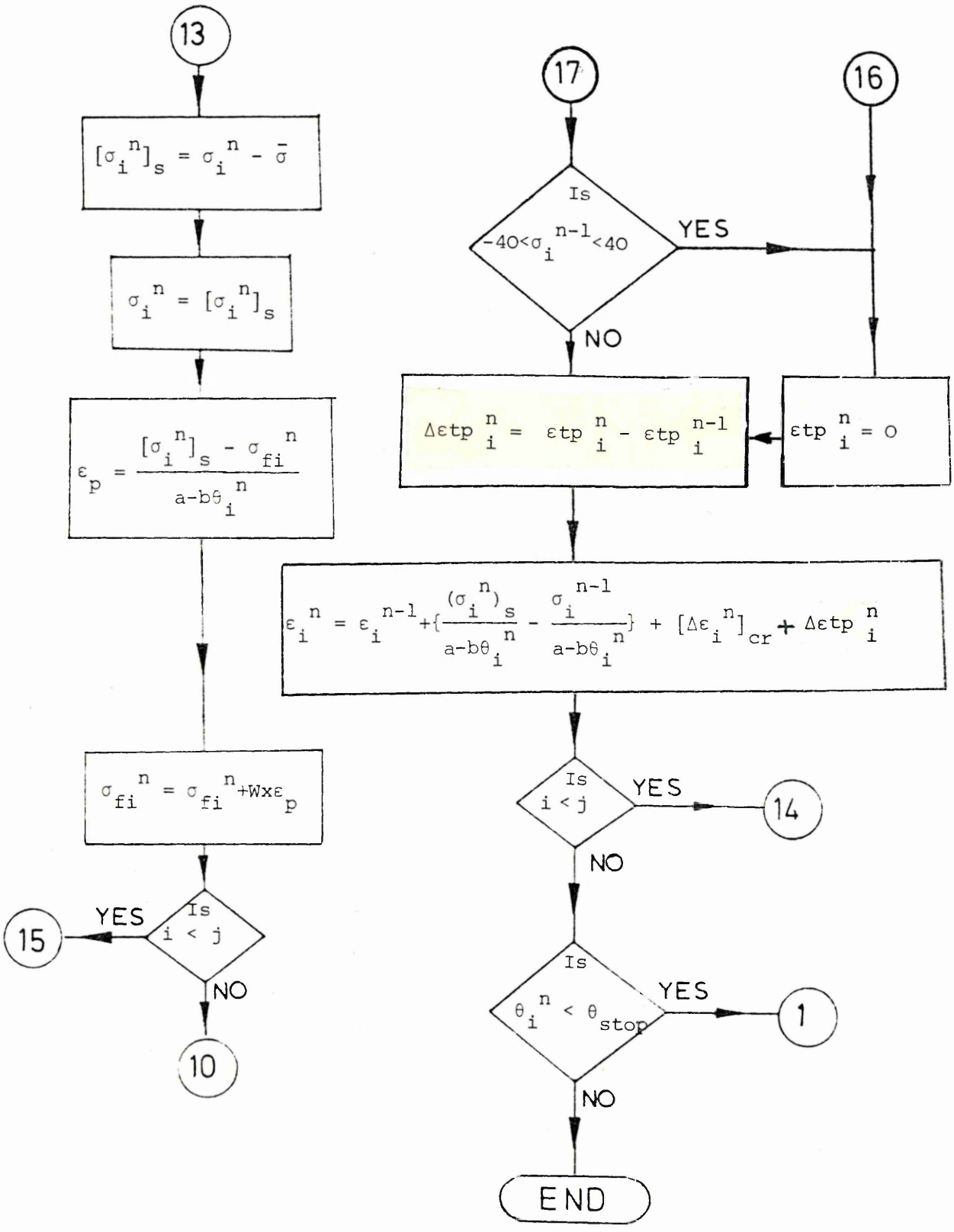
13
$[\sigma_i^n]_s = \sigma_i^n - \bar{\sigma}$
$\sigma_i^n = [\sigma_i^n]_s$
$\varepsilon_p = \frac{[\sigma_i^n]_s - \sigma_{fi}^n}{a-b\theta_i^n}$
$\sigma_{fi}^n = \sigma_{fi}^n + W x \varepsilon_p$
Is $i < j$
YES
15
NO
10
17
Is $-40 < \sigma_i^{n-1} < 40$
YES
NO
16
$\Delta\varepsilon tp_i^n = \varepsilon tp_i^n - \varepsilon tp_i^{n-1}$
$\varepsilon tp_i^n = 0$
$\varepsilon_i^n = \varepsilon_i^{n-1} + \{\frac{(\sigma_i^n)_s}{a-b\theta_i^n} - \frac{\sigma_i^{n-1}}{a-b\theta_i^n}\} + [\Delta\varepsilon_i^n]_{cr} + \Delta\varepsilon tp_i^n$
Is $i < j$
YES
14
NO
Is $\theta_i^n < \theta_{stop}$
YES
1
NO
END

FIGURE 44: Determination of the volume fraction of austenite and martensite present below Ms temperature.

(After Fletcher and Price)[30].

FIGURE 45: Variation of uniaxial flow stress with temperature in 835M30 steel.

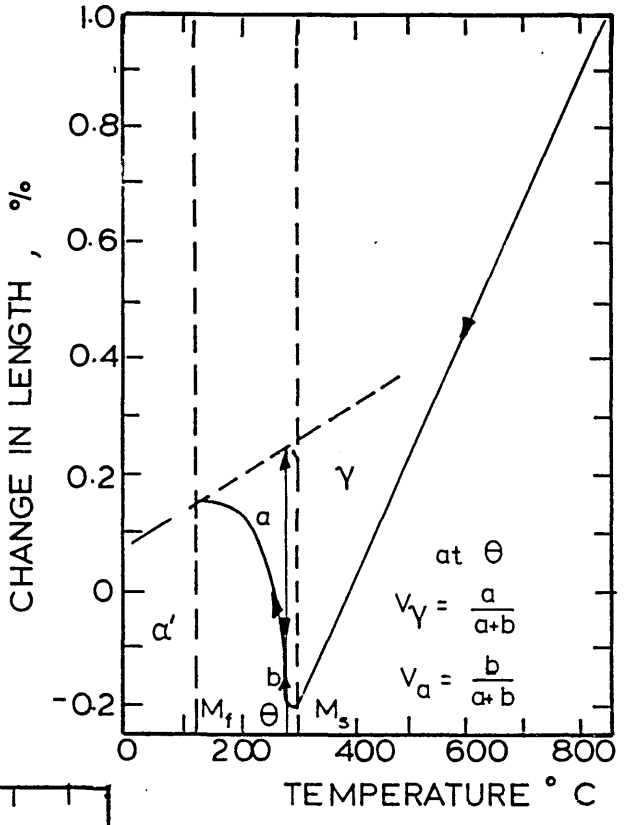
CHANGE IN LENGTH , %
1.0
0.8
0.6
0.4
0.2
0
-0.2
0
200
400
600
800
TEMPERATURE ° C
α'
γ
a
b
M_f
θ
M_s
at θ
$V_\gamma = \frac{a}{a+b}$
$V_a = \frac{b}{a+b}$

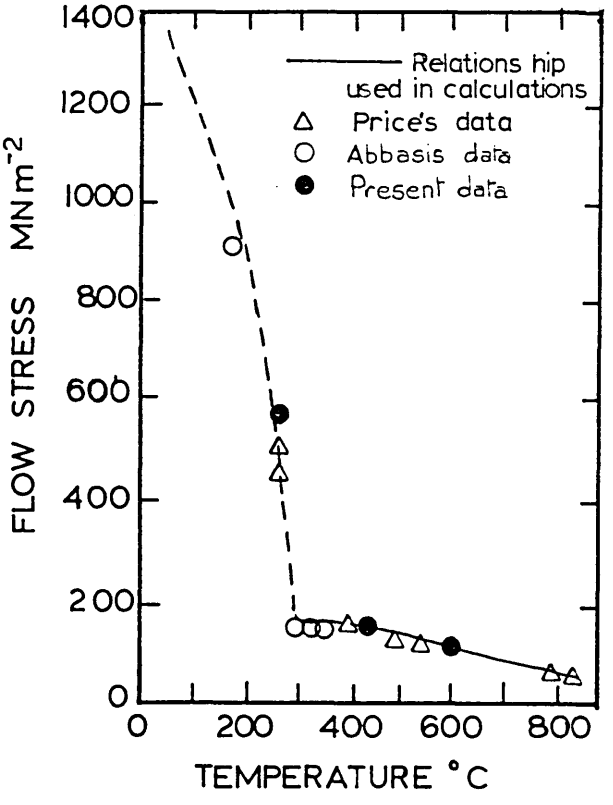
FLOW STRESS MN m^{-2}
1400
1200
1000
800
600
400
200
0
0
200
400
600
800
TEMPERATURE °C
Relations hip used in calculations
Price's data
Abbasis data
Present data

FIGURE 46: Calculated stress and strain at the surface and the centre of a 20 mm plate during water quenching without stress relaxation and transformation plasticity (calculation FP_1).

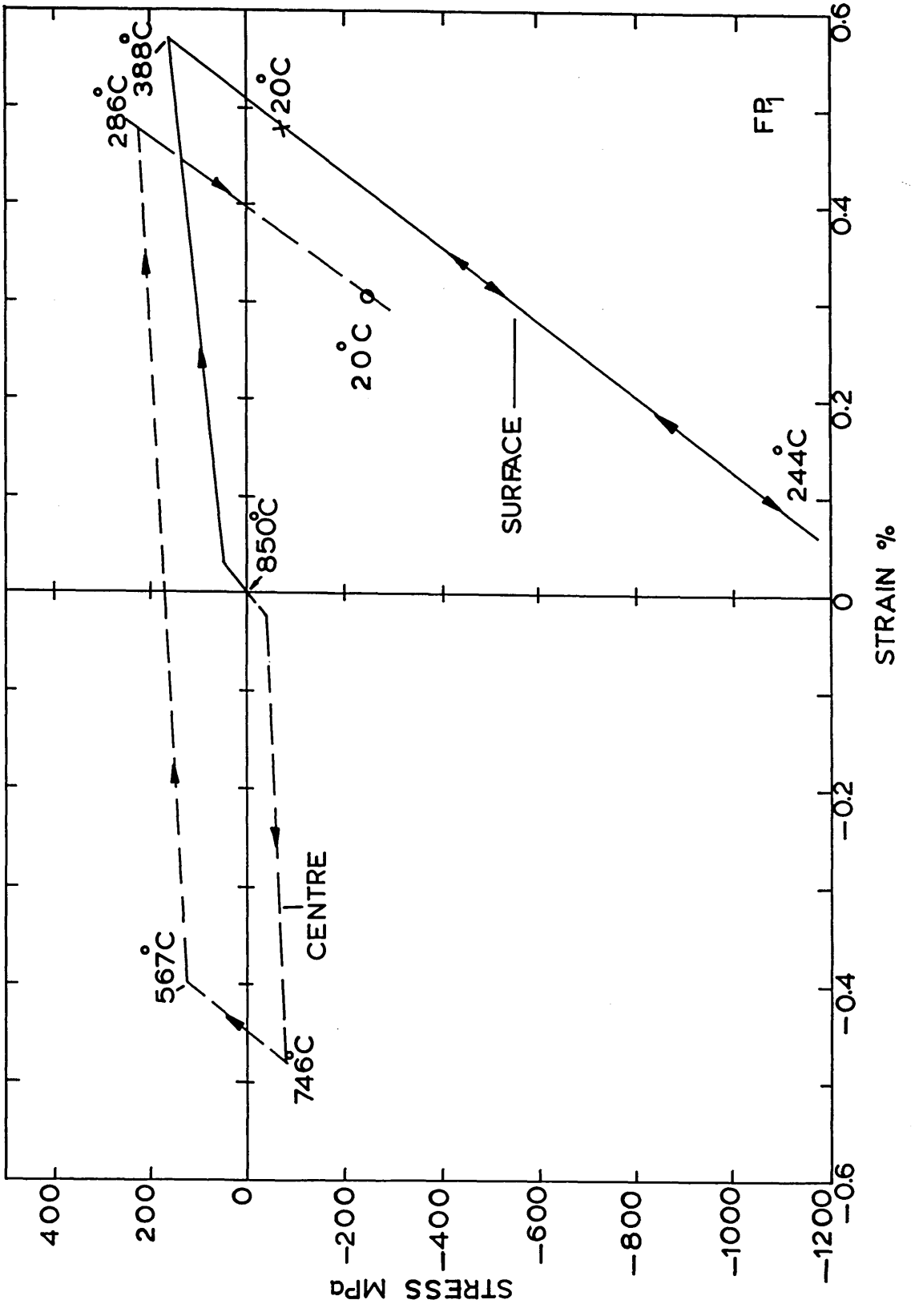
FP1
SURFACE
CENTRE
20°C
20°C
244°C
286°C
388°C
850°C
567°C
746°C
STRESS MPa
STRAIN %
400
200
0
-200
-400
-600
-800
-1000
-1200
0.6
0.4
0.2
0
-0.2
-0.4
-0.6

FIGURE 47: Calculated stress and strain at the surface and the centre of a 20 mm plate during water quenching with stress relaxation represented by method one (calculation FP_2).

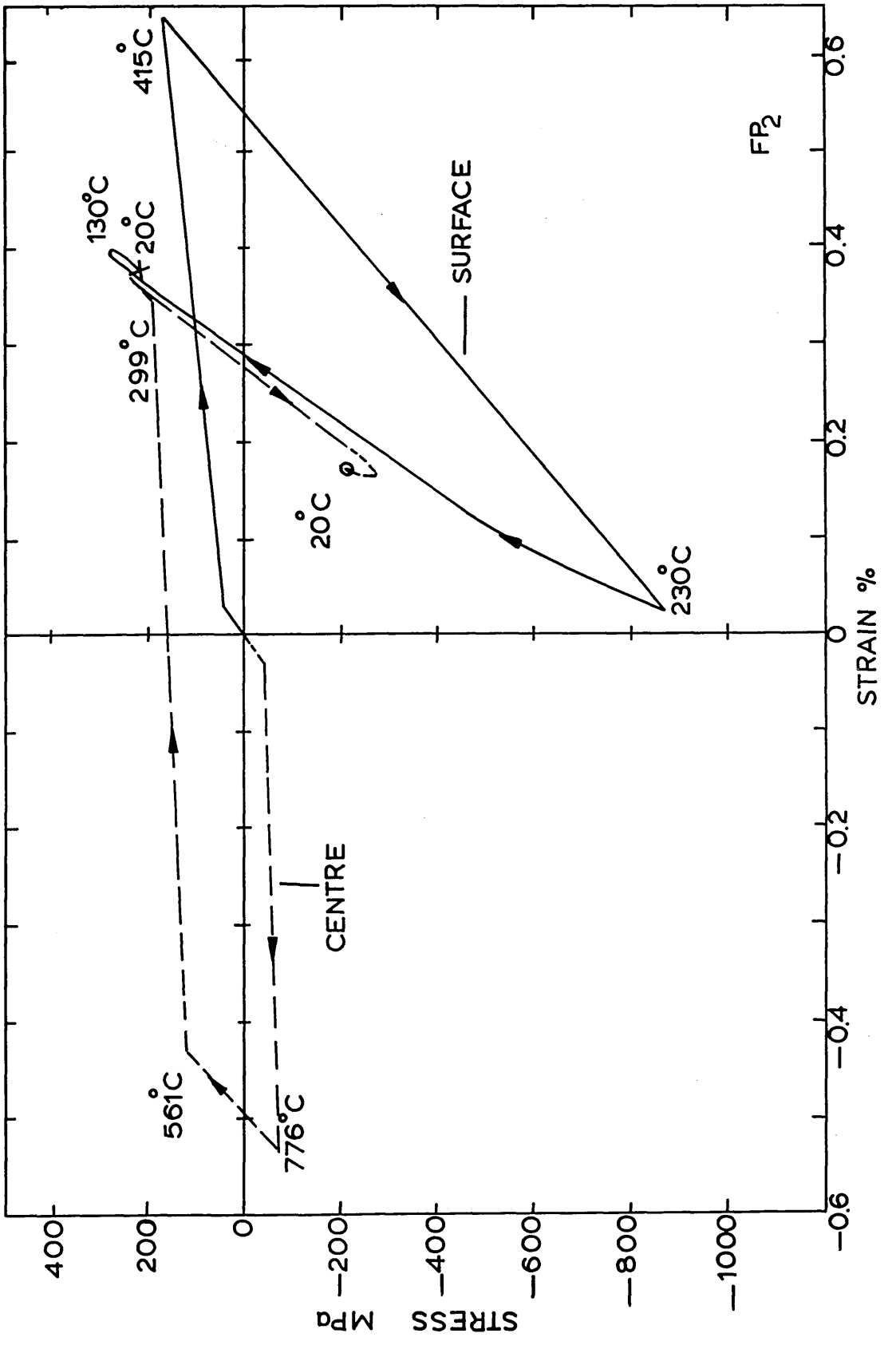
FP2
SURFACE
CENTRE
415°C
130°C
20°C
299°C
20°C
230°C
561°C
776°C
STRESS MPa
STRAIN %
400
200
0
−200
−400
−600
−800
−1000
0.6
0.4
0.2
0
−0.2
−0.4
−0.6

FIGURE 48: Calculated stress and strain at the surface and the centre of a 20 mm plate during water quenching with stress relaxation represented by method two (calculation FP_3).

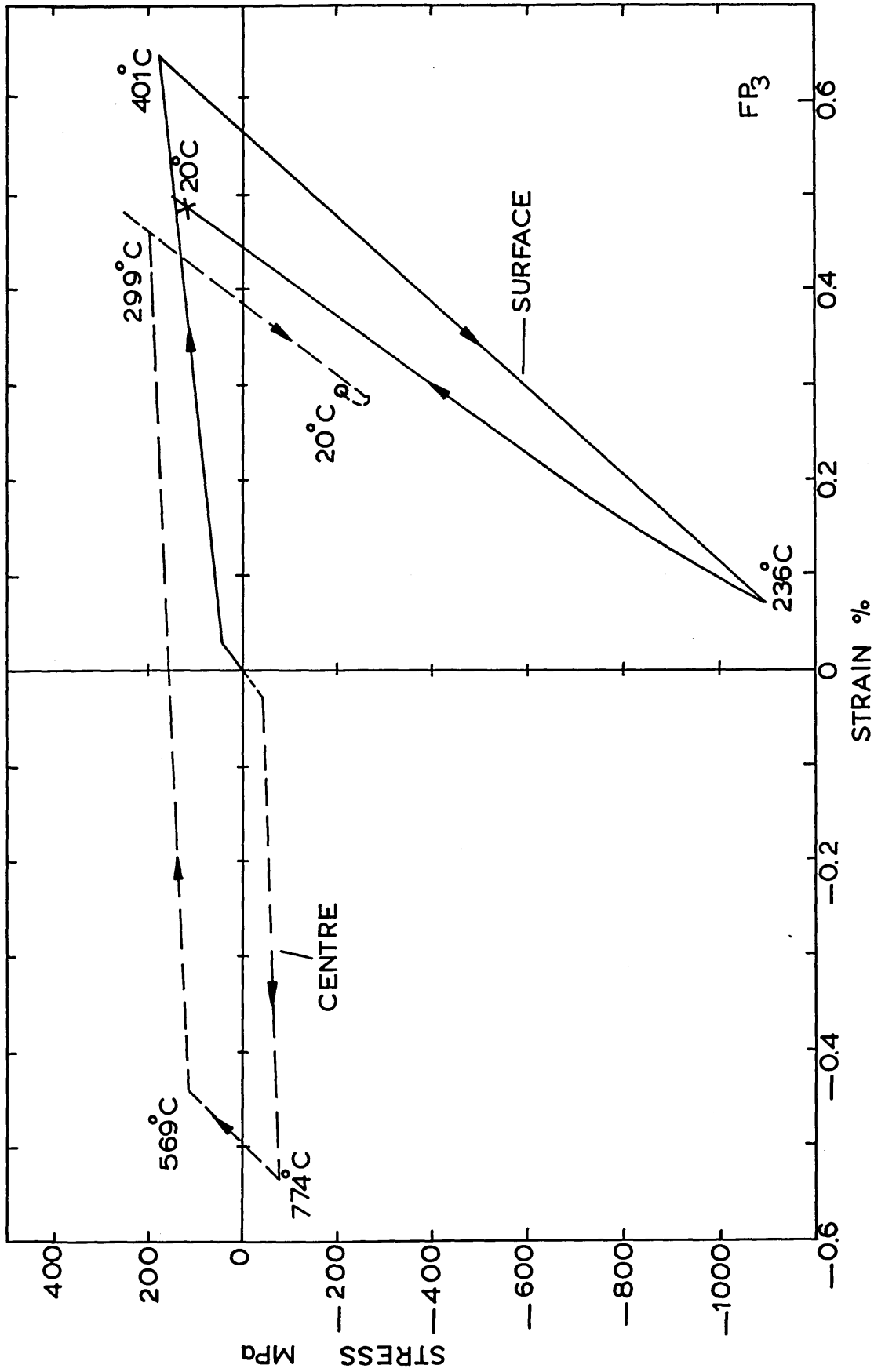
FR3
SURFACE
CENTRE
401°C
20°C
299°C
20°C
236°C
569°C
774°C
STRESS MPa
STRAIN %
400
200
0
−200
−400
−600
−800
−1000
0.6
0.4
0.2
0
−0.2
−0.4
−0.6

FIGURE 49: Calculated stress and strain at the surface and the centre of a 20 mm plate during water quenching with transformation plasticity and stress relaxation represented by method one (calculation FP_4).

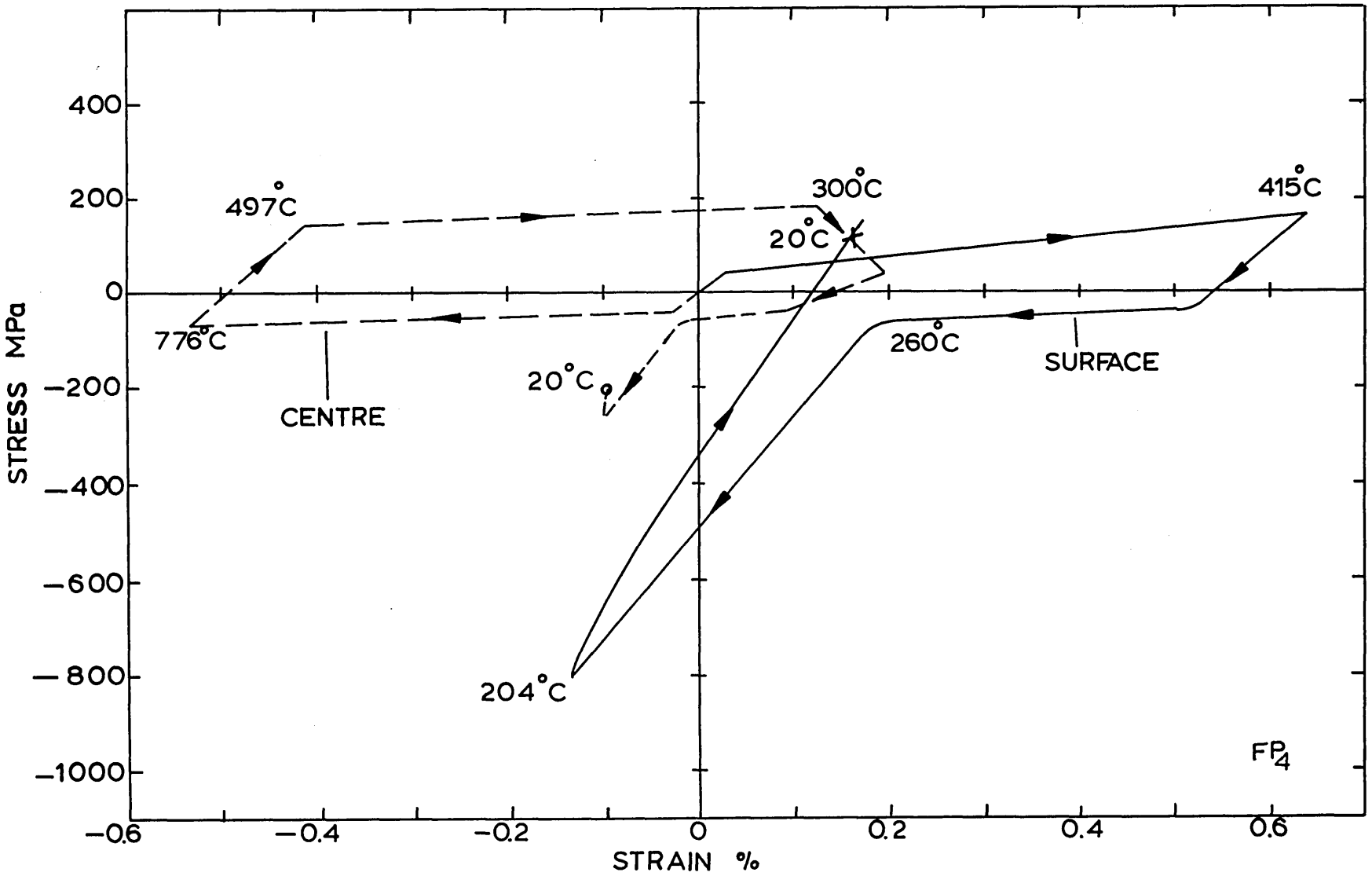
400
200
0
−200
−400
−600
−800
−1000
STRESS MPa
−0.6
−0.4
−0.2
0
0.2
0.4
0.6
STRAIN %
497°C
776°C
CENTRE
20°C
300°C
20°C
204°C
260°C
SURFACE
415°C
FP4

FIGURE 50: Calculated stress and strain at the surface and the centre of a 20 mm plate during water quenching with transformation plasticity and stress relaxation represented by method two (calculation FP_5).

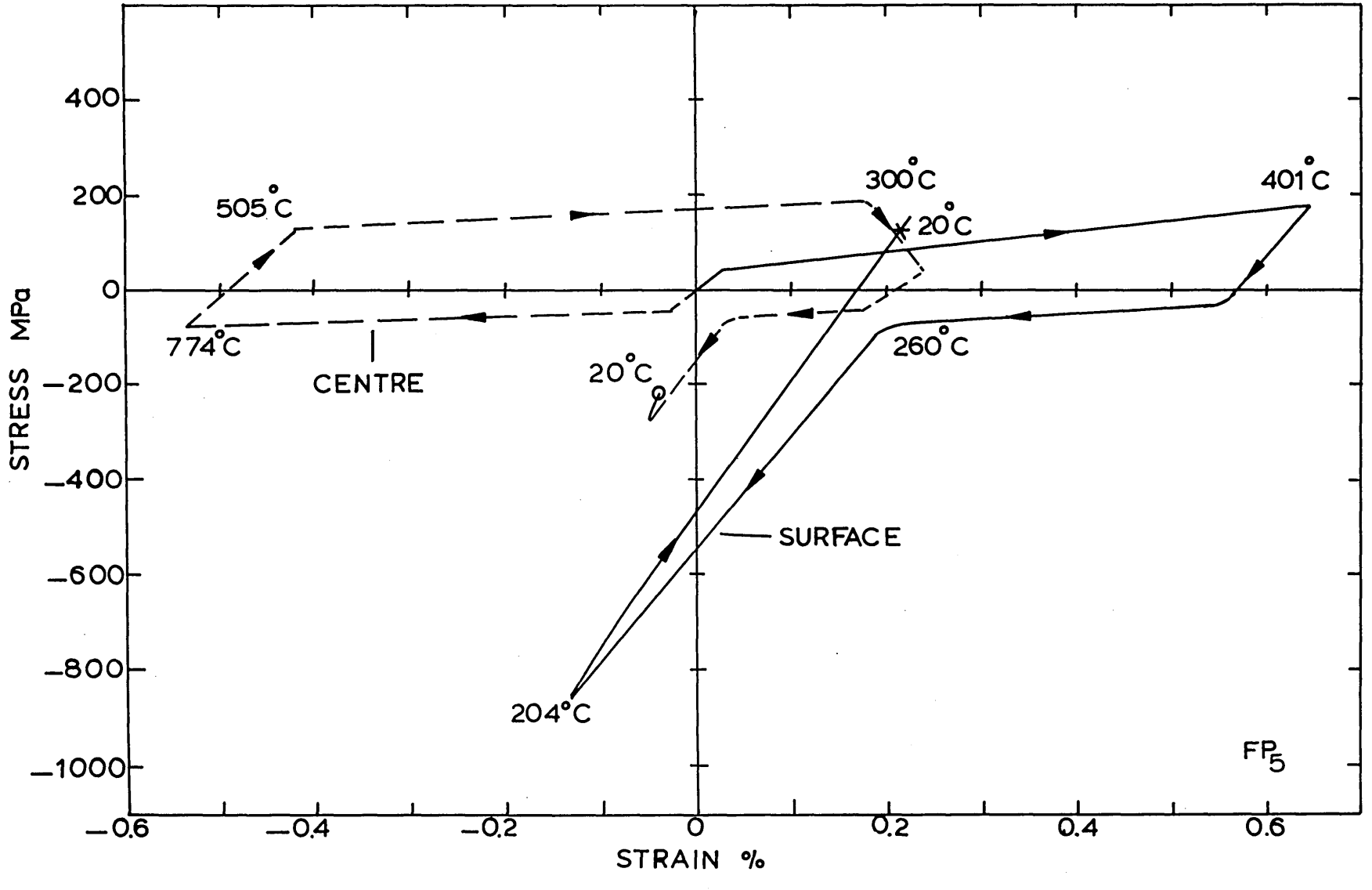
400
200
0
−200
−400
−600
−800
−1000
STRESS MPa
−0.6
−0.4
−0.2
0
0.2
0.4
0.6
STRAIN %
505°C
774°C
CENTRE
300°C
20°C
401°C
20°C
260°C
SURFACE
204°C
FP5

FIGURE 51: Calculated stress and strain at the surface and the centre of a 20 mm plate during water quenching with transformation plasticity, no stress relaxation (calculation FP_6).

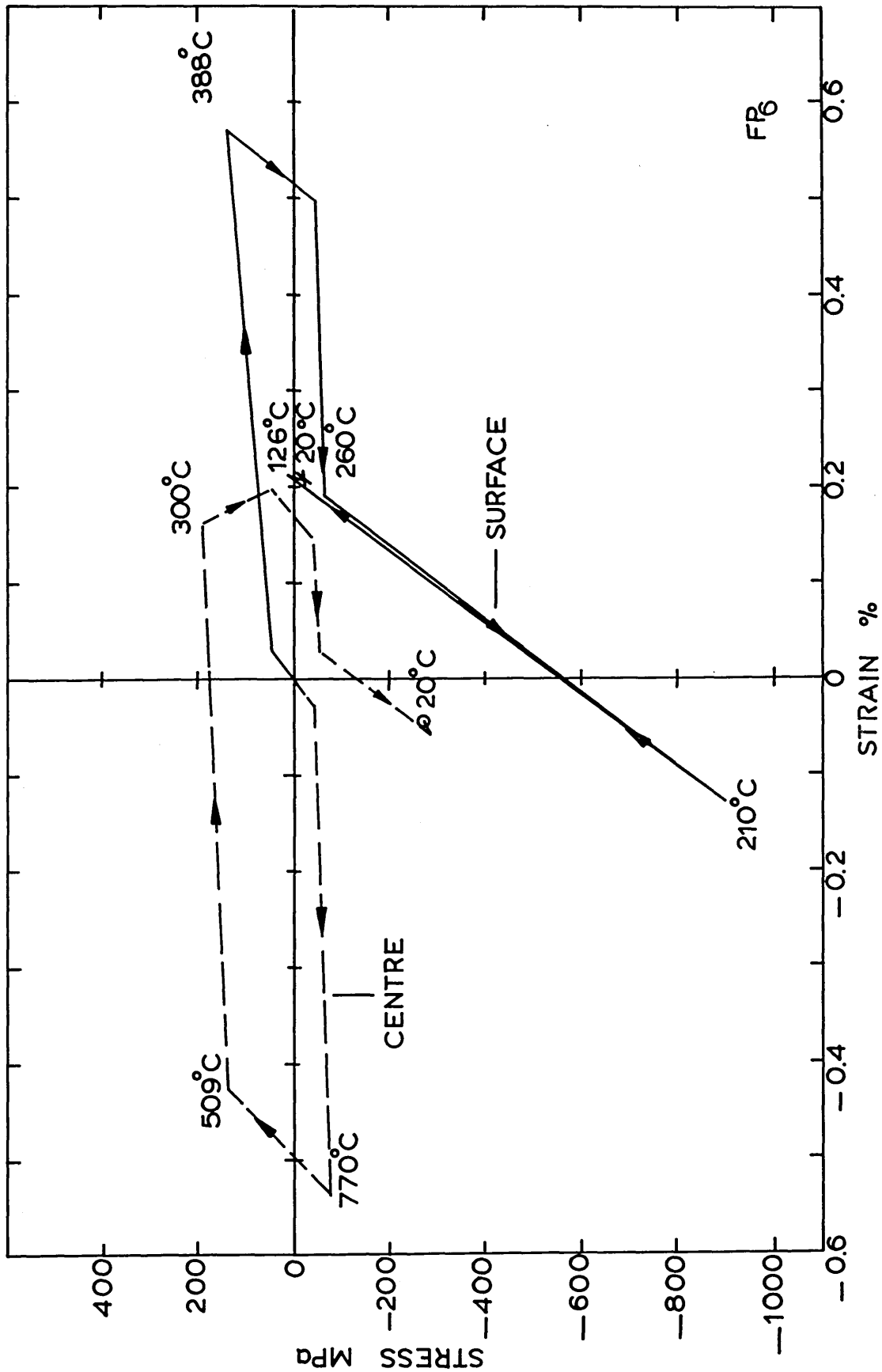
FR6
388°C
300°C
126°C
20°C
260°C
SURFACE
20°C
210°C
509°C
770°C
CENTRE
STRESS MPa
STRAIN %
400
200
0
-200
-400
-600
-800
-1000
0.6
0.4
0.2
0
-0.2
-0.4
-0.6

FIGURE 52: Calculated residual stress distribution in a 20 mm plate after water quenching.

Calculation number:

FP_1 - No stress relaxation.
FP_2 - Stress relaxation method 1.
FP_3 - Stress relaxation method 2.
FP_4 - Stress relaxation method 1 and transformation plasticity.
FP_5 - Stress relaxation method 2 and transformation plasticity.
FP_6 - Transformation plasticity, no stress relaxation.

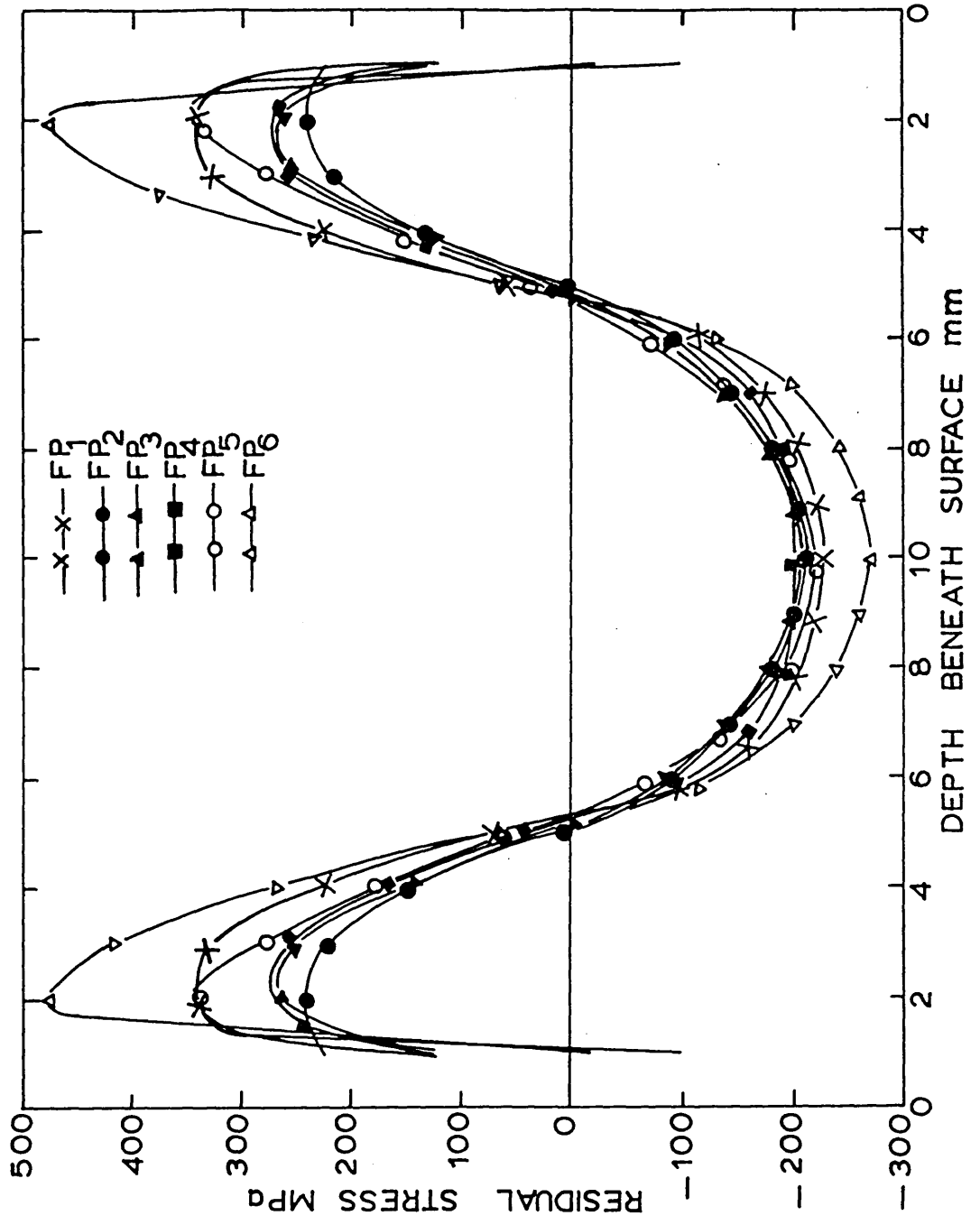
FP1
FP2
FP3
FP4
FP5
FP6
500
400
300
200
100
0
−100
−200
−300
RESIDUAL STRESS MPa
0
2
4
6
8
10
8
6
4
2
0
DEPTH BENEATH SURFACE mm

FIGURE 53: Calculated residual strain distribution in a 20 mm plate after water quenching.

(For Key see figure 52).

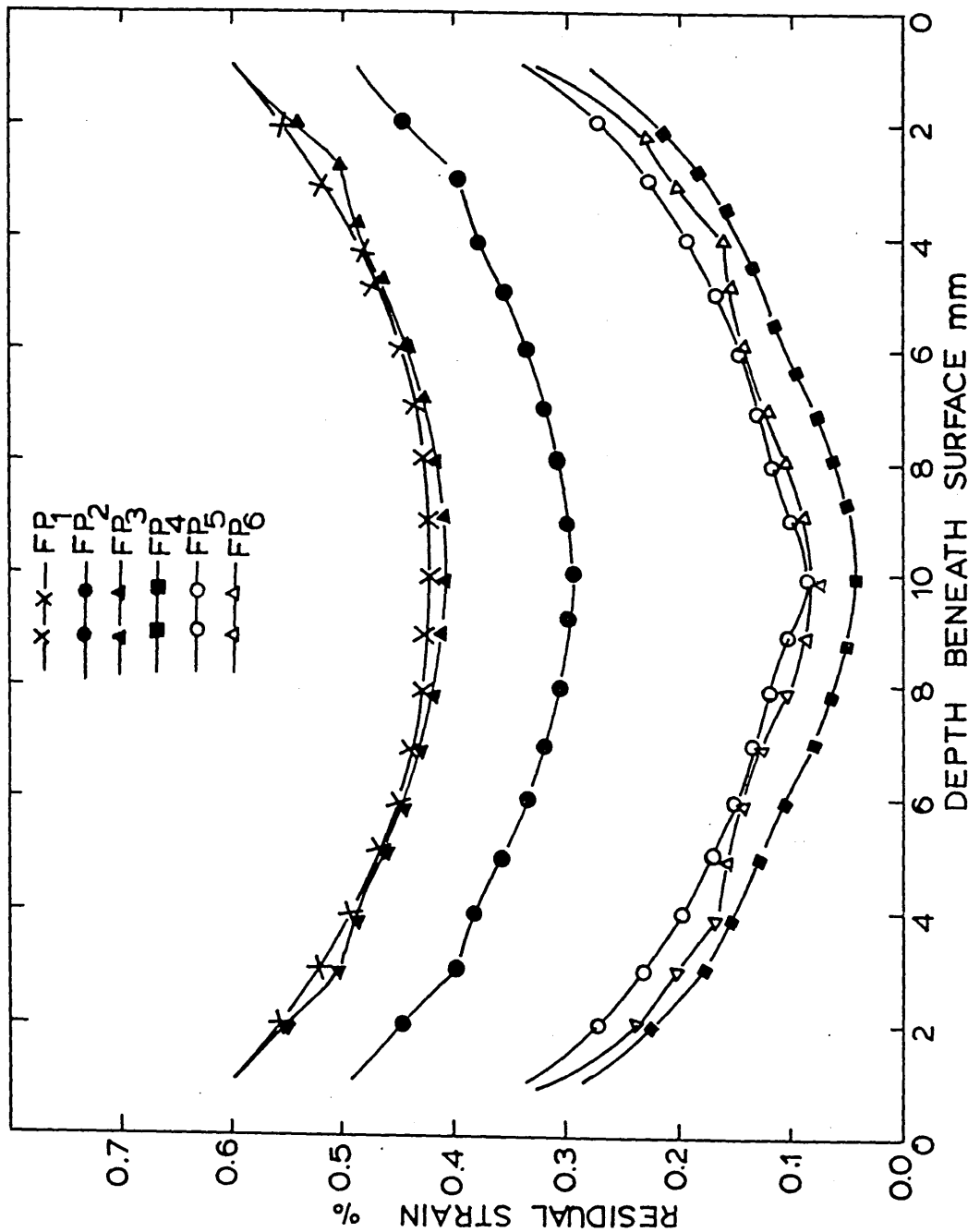
FP1
FP2
FP3
FP4
FP5
FP6
RESIDUAL STRAIN %
0.0
0.1
0.2
0.3
0.4
0.5
0.6
0.7
DEPTH BENEATH SURFACE mm
0
2
4
6
8
10
8
6
4
2
0

FIGURE 54: Calculated stress and strain at the surface and the centre of a 15 mm plate during oil quenching without stress relaxation (calculation FP_7).

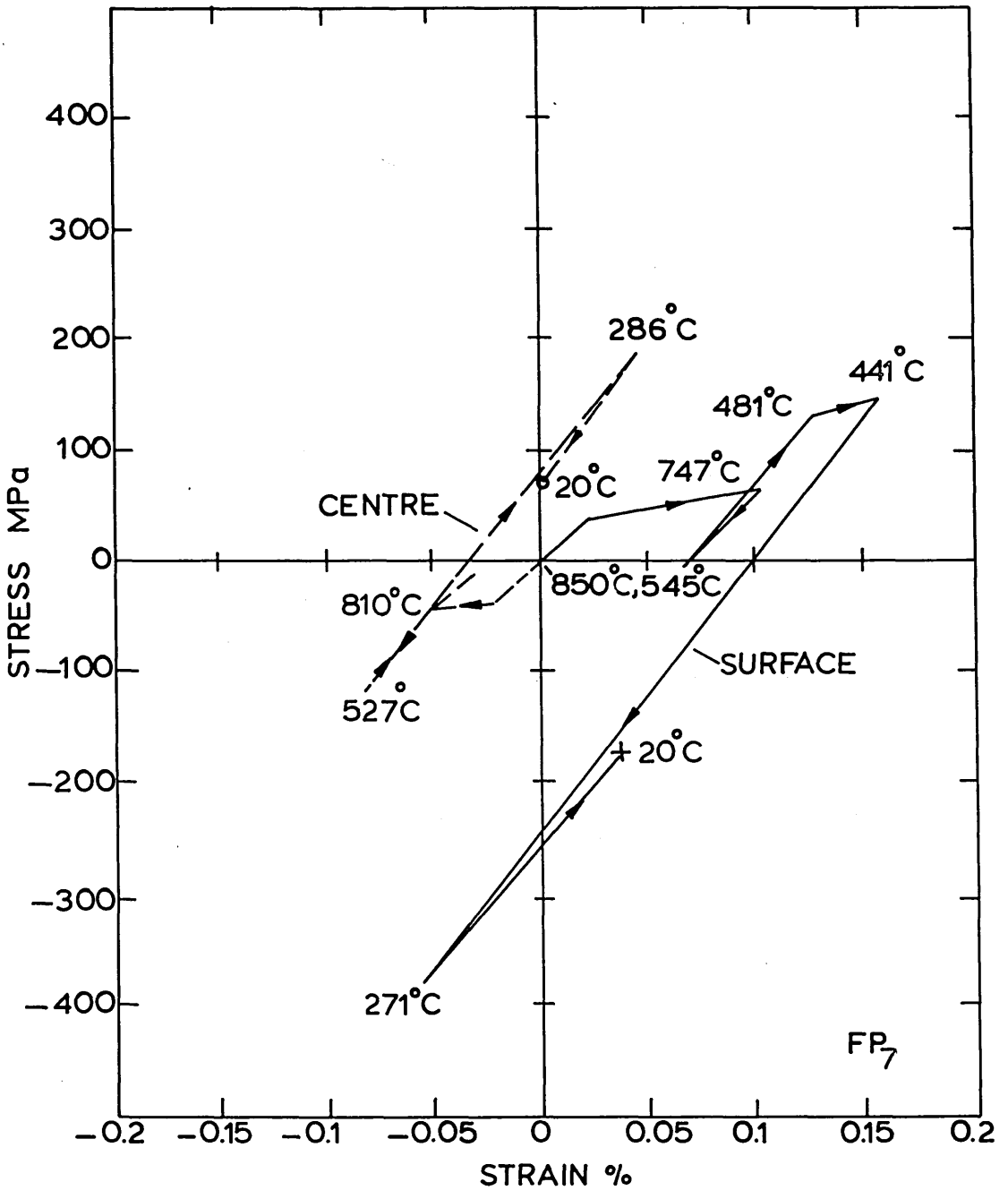
400
300
200
100
0
−100
−200
−300
−400
STRESS MPa
−0.2
−0.15
−0.1
−0.05
0
0.05
0.1
0.15
0.2
STRAIN %
286°C
441°C
481°C
747°C
20°C
CENTRE
850°C,545°C
810°C
527°C
SURFACE
20°C
271°C
FP7

FIGURE 55: Calculated stress and strain at the surface and the centre of a 15 mm plate during oil quenching with stress relaxation represented by method one (calculation FP_8).

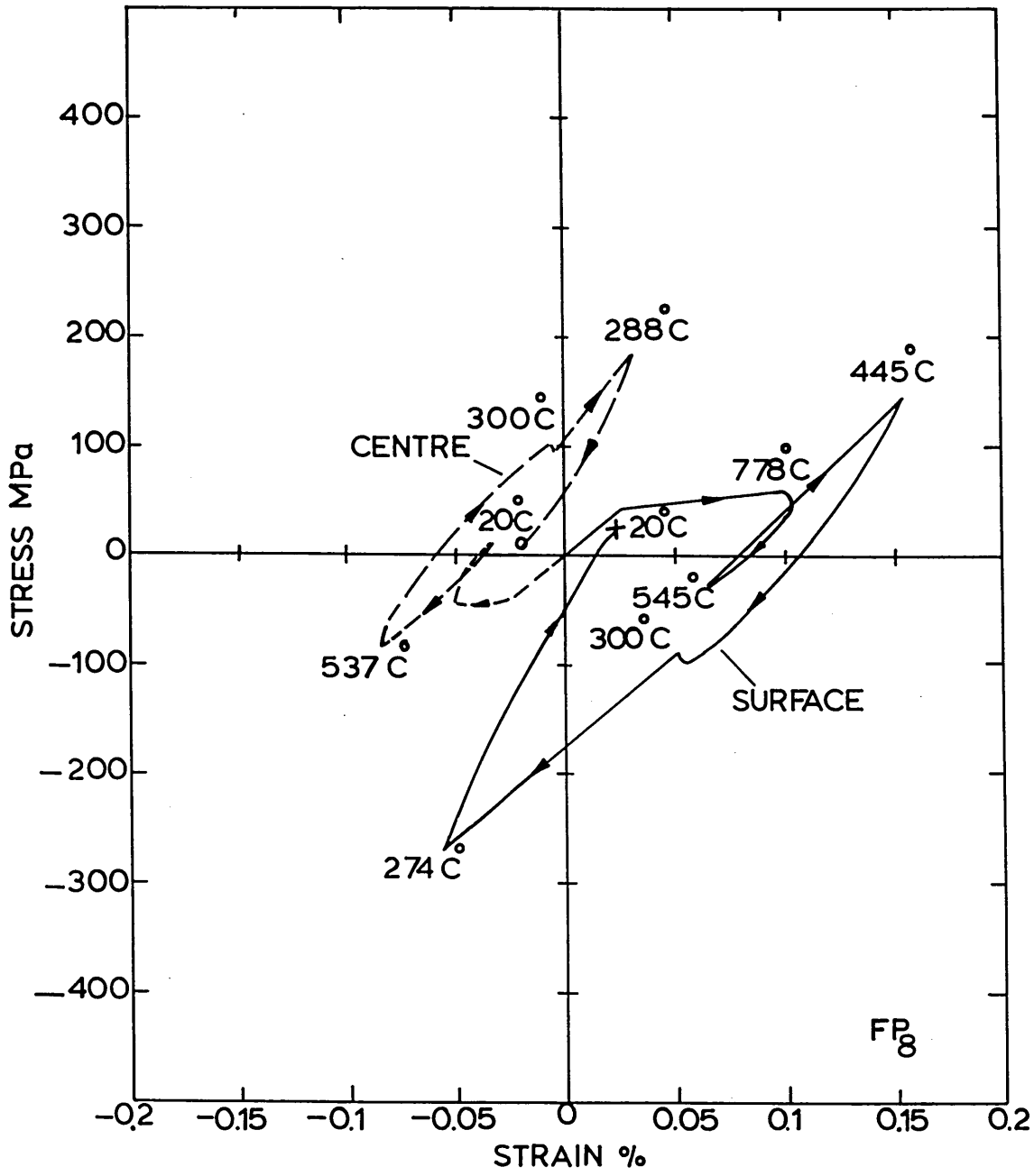
400
300
200
100
0
−100
−200
−300
−400
STRESS MPa
−0.2
−0.15
−0.1
−0.05
0
0.05
0.1
0.15
0.2
STRAIN %
288°C
445°C
300°C
CENTRE
778°C
20°C
+20°C
545°C
300°C
537°C
SURFACE
274°C
FP8

FIGURE 56: Calculated stress and strain at the surface and the centre of a 15 mm plate during oil quenching with stress relaxation represented by method two (calculation FP_9).

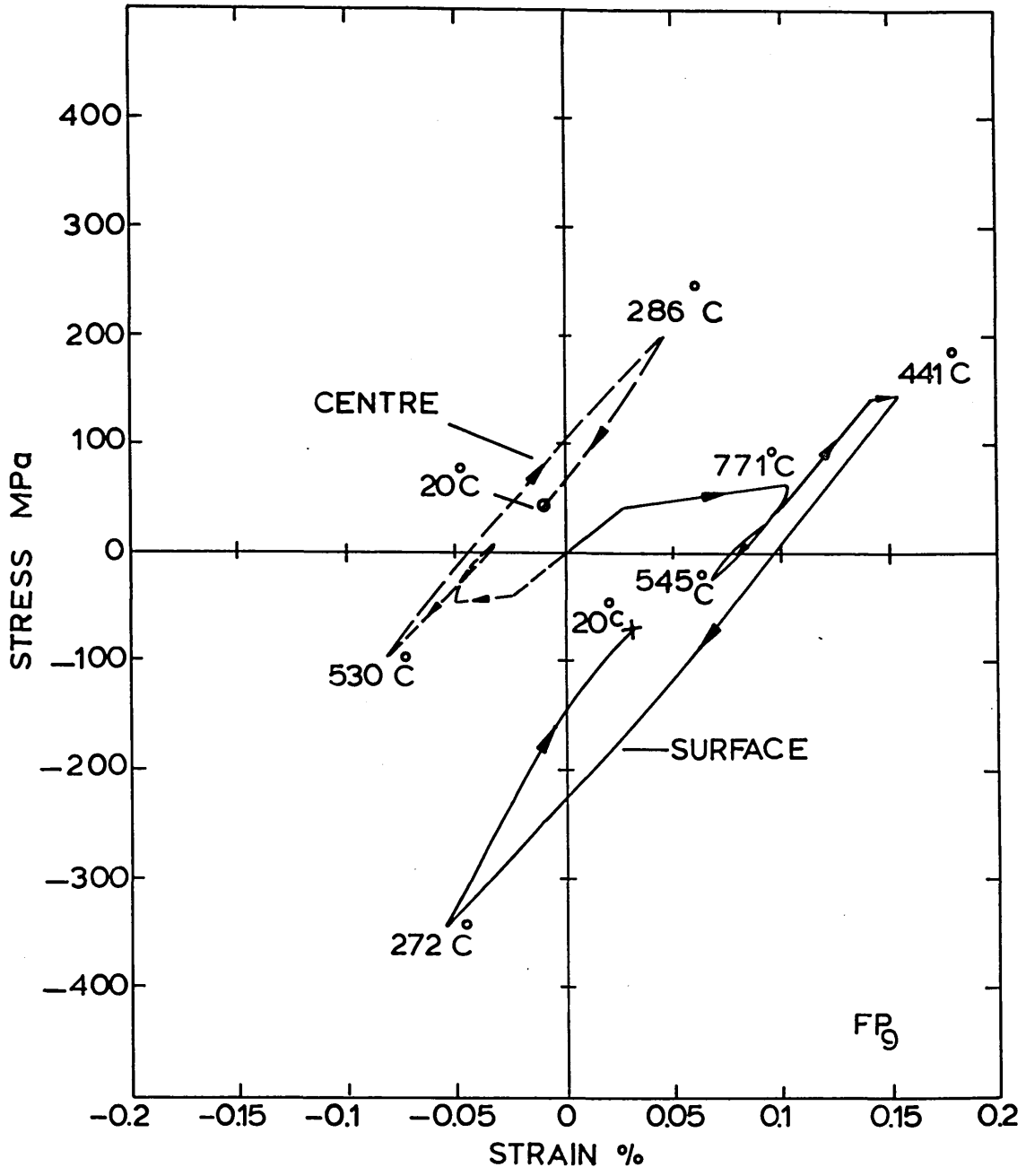
400
300
200
100
0
−100
−200
−300
−400
STRESS MPa
−0.2
−0.15
−0.1
−0.05
0
0.05
0.1
0.15
0.2
STRAIN %
286°C
441°C
CENTRE
20°C
771°C
545°C
20°C
530°C
SURFACE
272°C
FP9

FIGURE 57: Calculated stress and strain at the surface and the centre of a 15 mm plate during oil quenching with transformation plasticity and stress relaxation represented by method one (calculation FP_{10}).

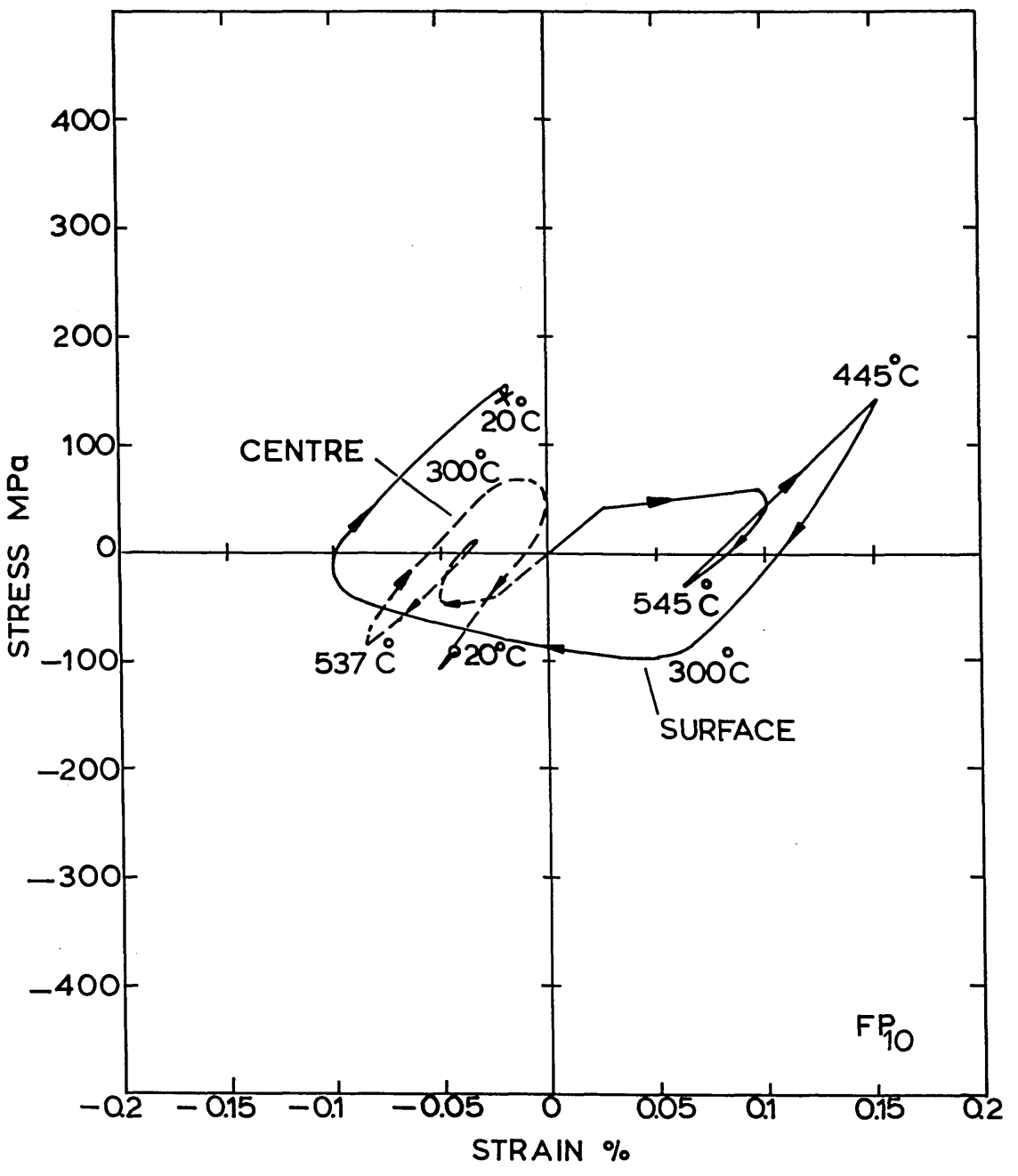
400
300
200
100
0
−100
−200
−300
−400
STRESS MPa
−0.2
−0.15
−0.1
−0.05
0
0.05
0.1
0.15
0.2
STRAIN %
CENTRE
20°C
300°C
537°C
20°C
445°C
545°C
300°C
SURFACE
FP10

FIGURE 58: Calculated stress and strain at the surface and the centre of a 15 mm plate during oil quenching with transformation plasticity and stress relaxation represented by method two (calculation FP_{11}).

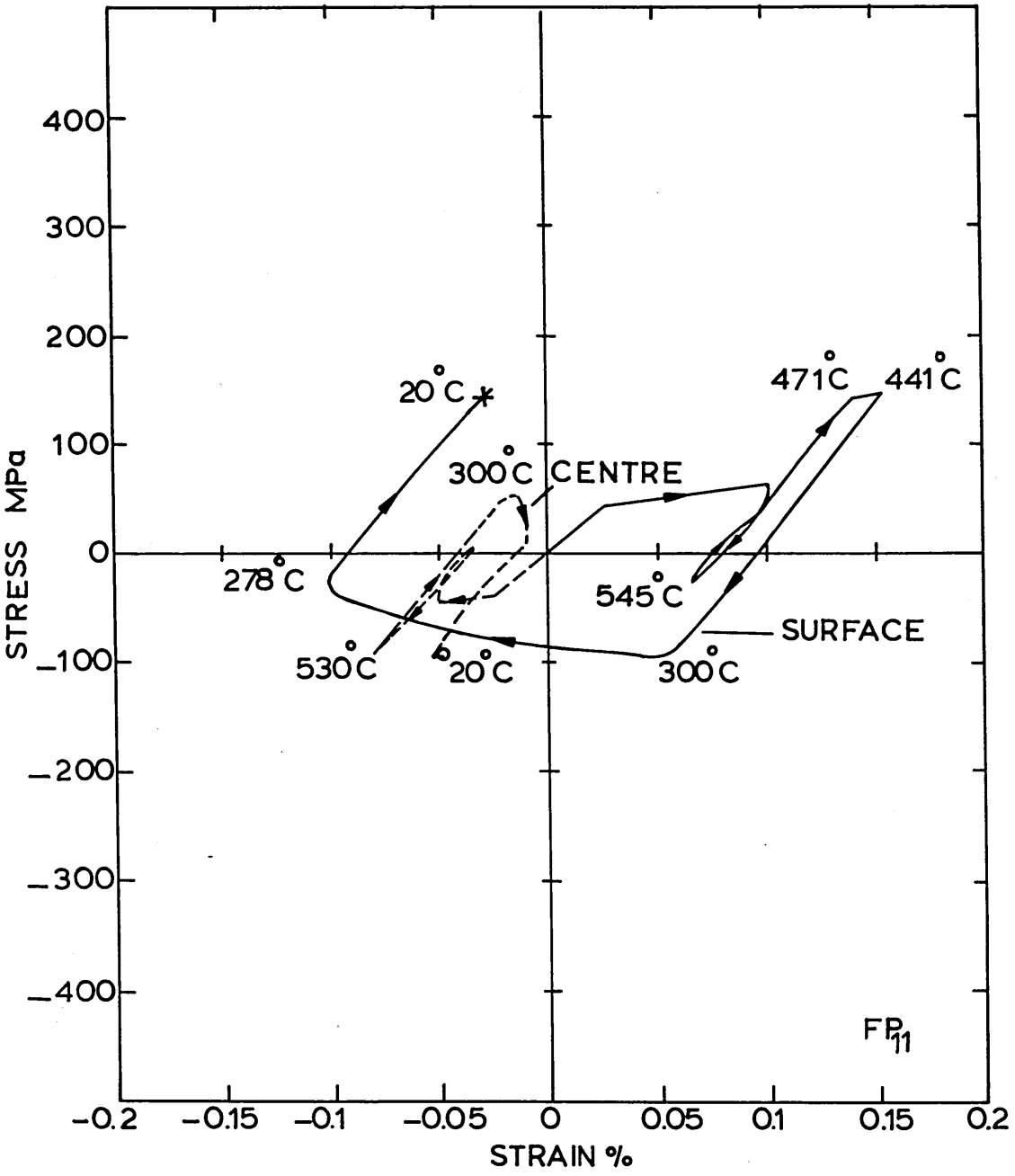
400
300
200
100
0
−100
−200
−300
−400
STRESS MPa
−0.2
−0.15
−0.1
−0.05
0
0.05
0.1
0.15
0.2
STRAIN %
20°C
300°C CENTRE
278°C
530°C
20°C
545°C
471°C
441°C
SURFACE
300°C
FP11

FIGURE 59: Calculated stress and strain at the surface and the centre of a 15 mm plate during oil quenching with transformation plasticity, no stress relaxation (calculation FP_{12}).

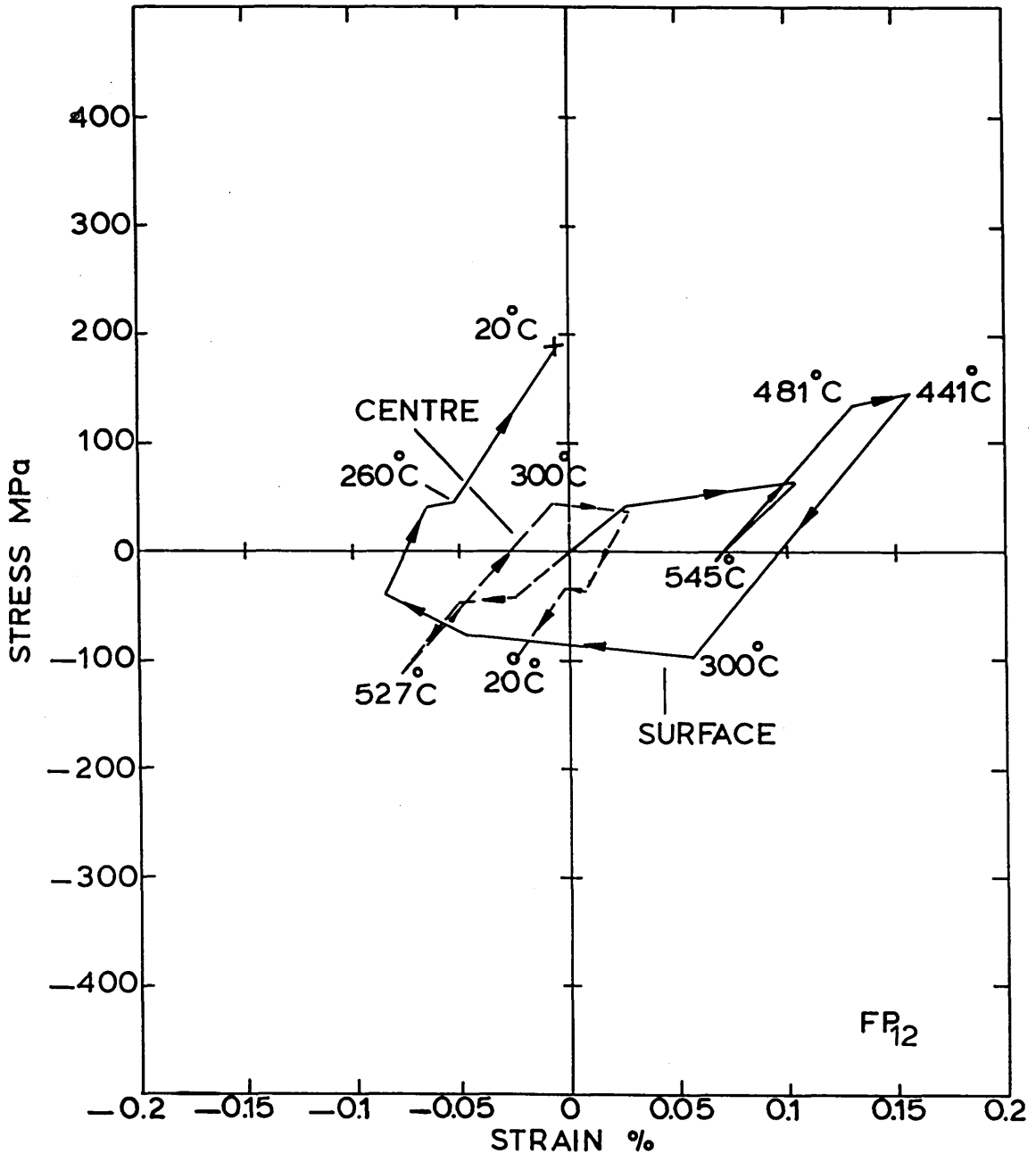
400
300
200
100
0
−100
−200
−300
−400
STRESS MPa
−0.2
−0.15
−0.1
−0.05
0
0.05
0.1
0.15
0.2
STRAIN %
20°C
CENTRE
260°C
300°C
481°C
441°C
545°C
527°C
20°C
300°C
SURFACE
FP12

FIGURE 60: Calculated residual stress distribution in a 15 mm plate after oil quenching.

Calculation number:-

FP_7 - No stress relaxation.
FP_8 - Stress relaxation method 1.
FP_9 - Stress relaxation method 2.
FP_{10} - Stress relaxation method 1 and transformation plasticity.
FP_{11} - Stress relaxation method 2 and transformation plasticity.
FP_{12} - Transformation plasticity, no stress relaxation.

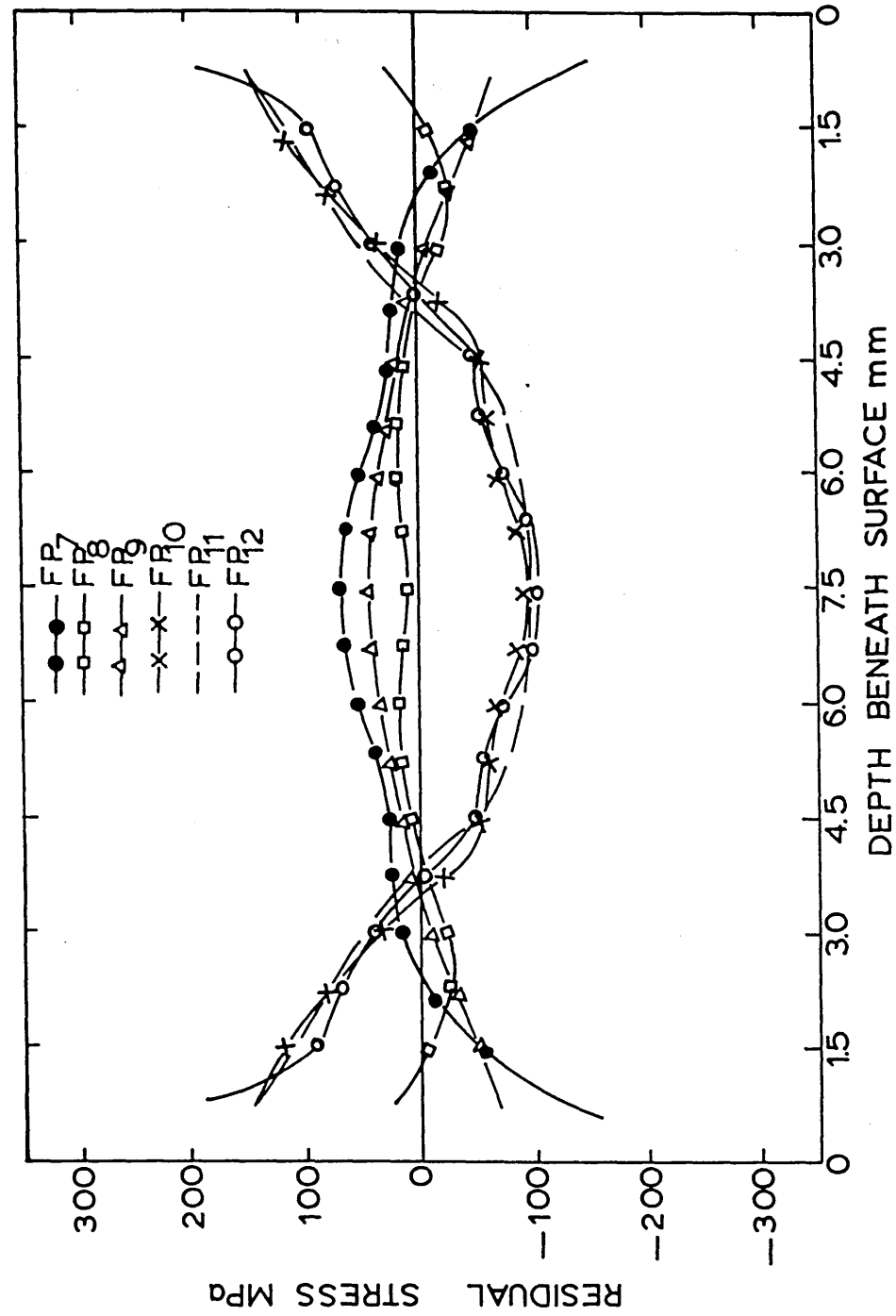
FR7
FR8
FR9
FR10
FR11
FR12
300
200
100
0
−100
−200
−300
RESIDUAL STRESS MPa
0
1.5
3.0
4.5
6.0
7.5
6.0
4.5
3.0
1.5
0
DEPTH BENEATH SURFACE mm

FIGURE 61: Calculated residual strain distribution in a 15 mm plate after oil quenching.

(For Key see figure 60).

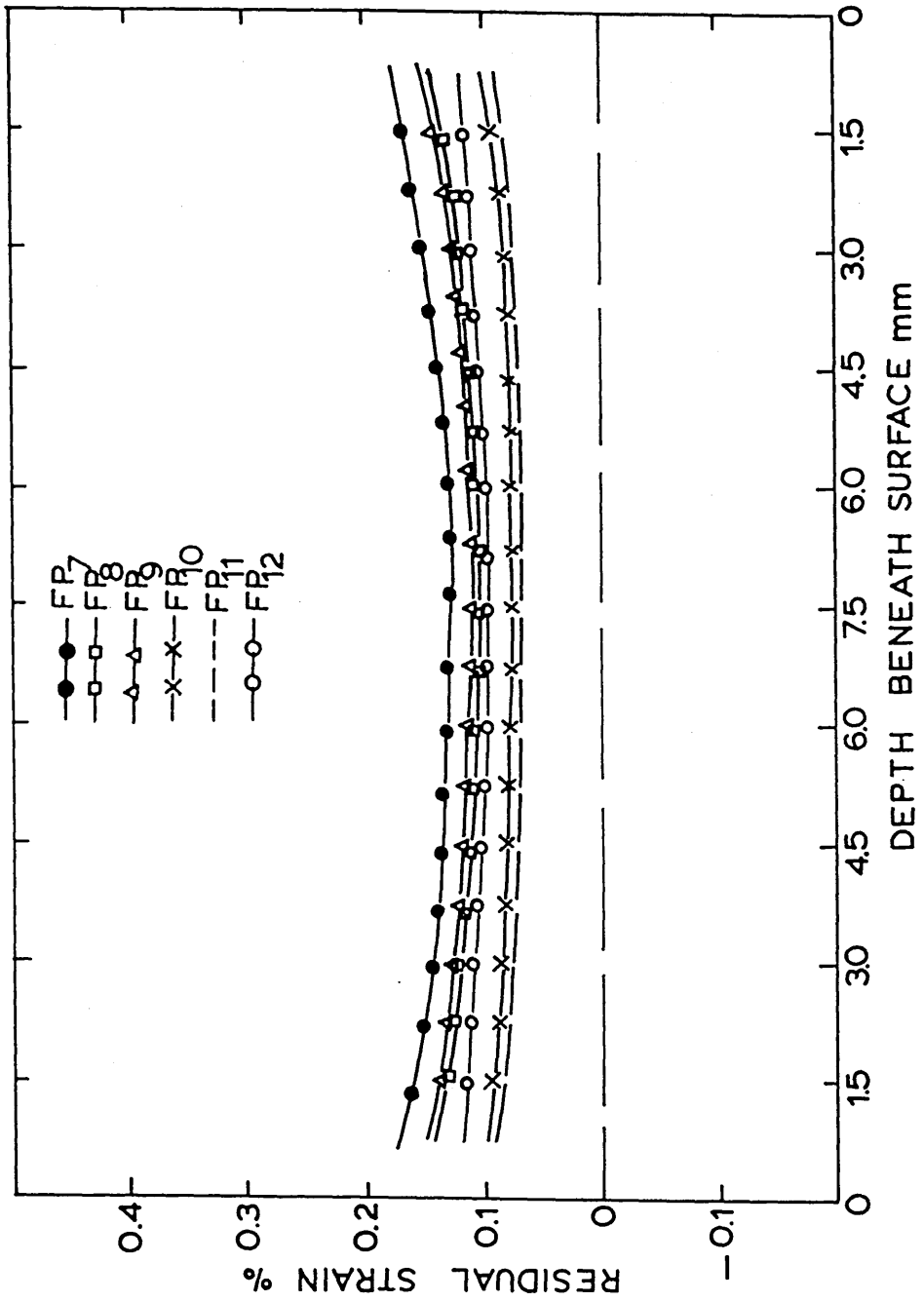
FP7
FP8
FP9
FP10
FP11
FP12
RESIDUAL STRAIN %
0.4
0.3
0.2
0.1
0
−0.1
0
1.5
3.0
4.5
6.0
7.5
6.0
4.5
3.0
1.5
0
DEPTH BENEATH SURFACE mm

FIGURE 62: Calculated stress and strain at the surface and the centre of a 20 mm plate during polymer quenching without stress relaxation (calculation FP_{13}).

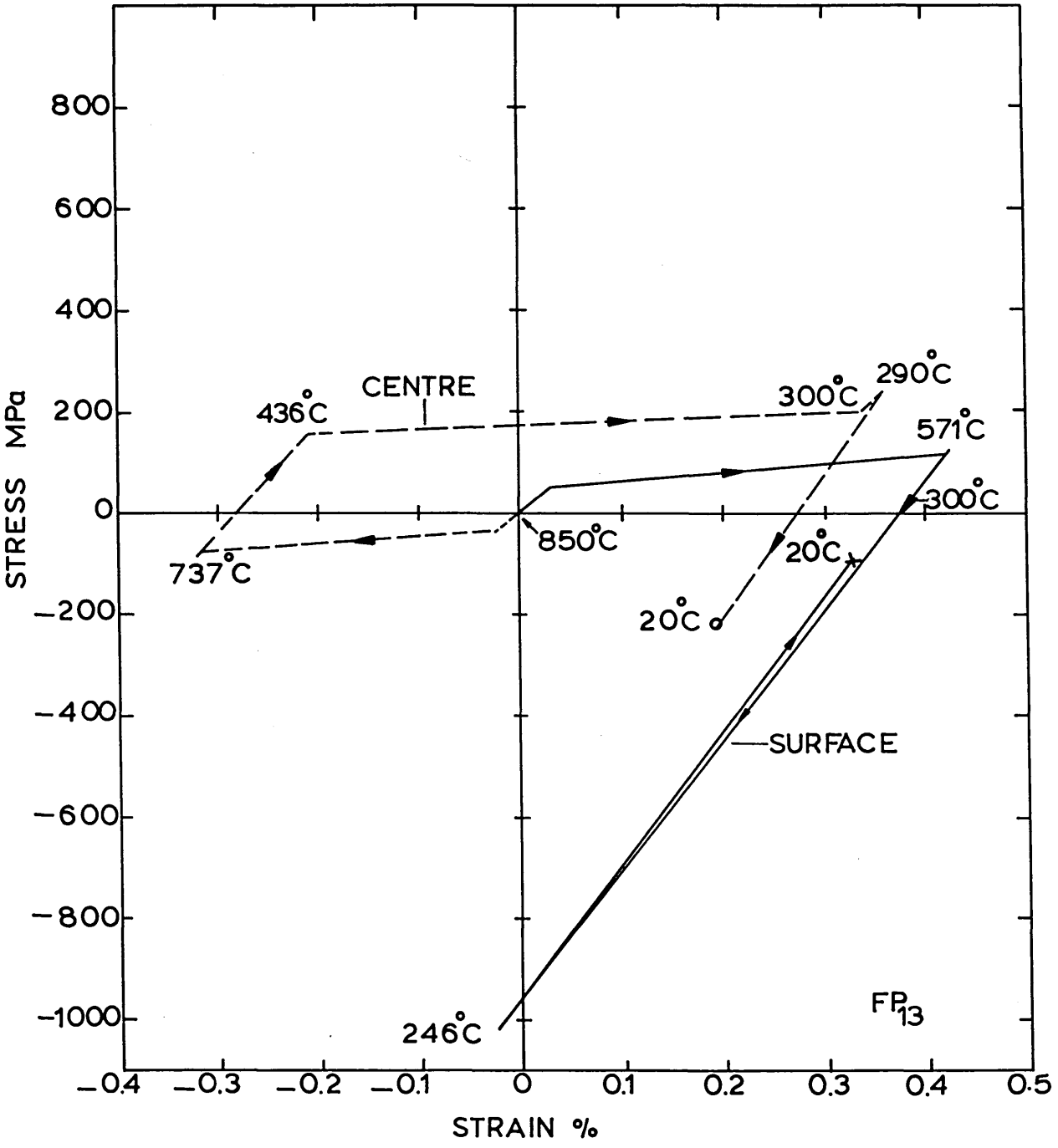
800
600
400
200
0
−200
−400
−600
−800
−1000
STRESS MPa
−0.4
−0.3
−0.2
−0.1
0
0.1
0.2
0.3
0.4
0.5
STRAIN %
CENTRE
436°C
737°C
850°C
300°C
290°C
571°C
300°C
20°C
20°C
SURFACE
246°C
FP13

FIGURE 63: Calculated stress and strain at the surface and the centre of a 20 mm plate during polymer quenching with stress relaxation represented by method one. (calculation FP_{14}).

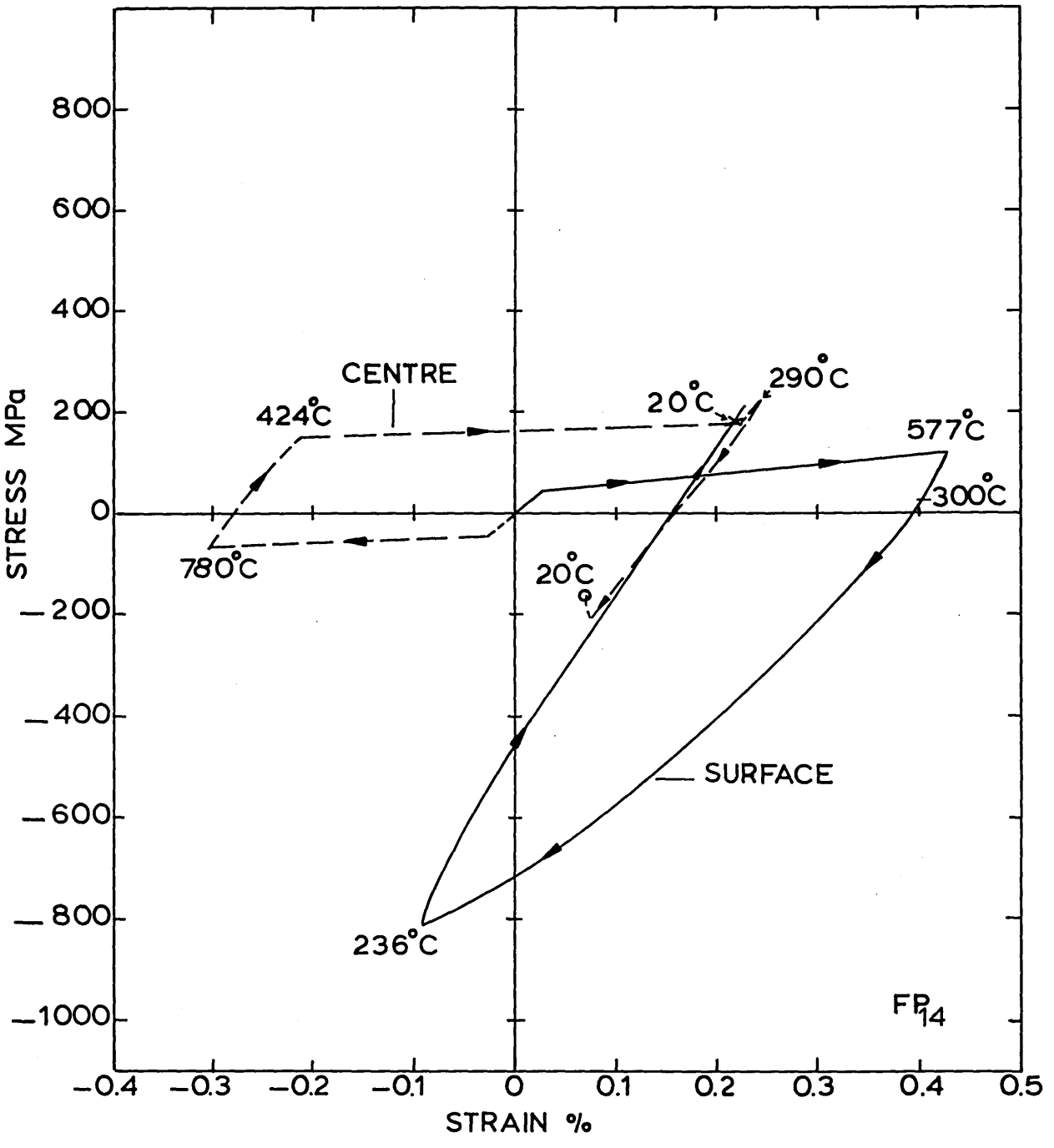
800
600
400
200
0
−200
−400
−600
−800
−1000
STRESS MPa
−0.4
−0.3
−0.2
−0.1
0
0.1
0.2
0.3
0.4
0.5
STRAIN %
CENTRE
424°C
780°C
20°C
290°C
577°C
300°C
20°C
SURFACE
236°C
FP14

FIGURE 64: Calculated stress and strain at the surface and the centre of a 20 mm plate during polymer quenching with stress relaxation represented by method two (calculation FP_{15}).

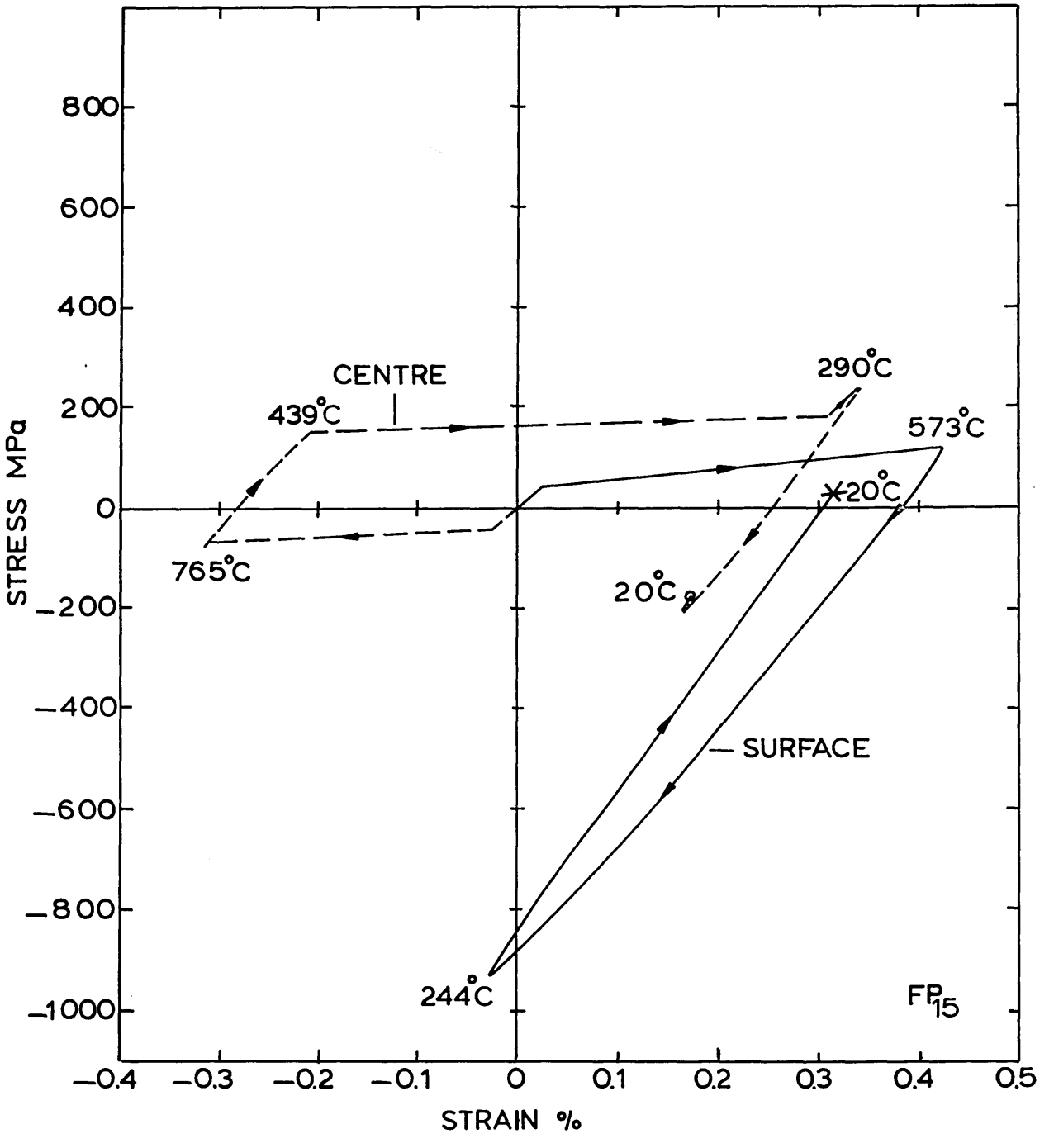
800
600
400
200
0
−200
−400
−600
−800
−1000
STRESS MPa
−0.4
−0.3
−0.2
−0.1
0
0.1
0.2
0.3
0.4
0.5
STRAIN %
CENTRE
439°C
765°C
290°C
573°C
20°C
20°C
SURFACE
244°C
FP15

FIGURE 65: Calculated stress and strain at the surface and the centre of a 20 mm plate during polymer quenching with transformation plasticity and stress relaxation represented by method one (calculation FP_{16}).

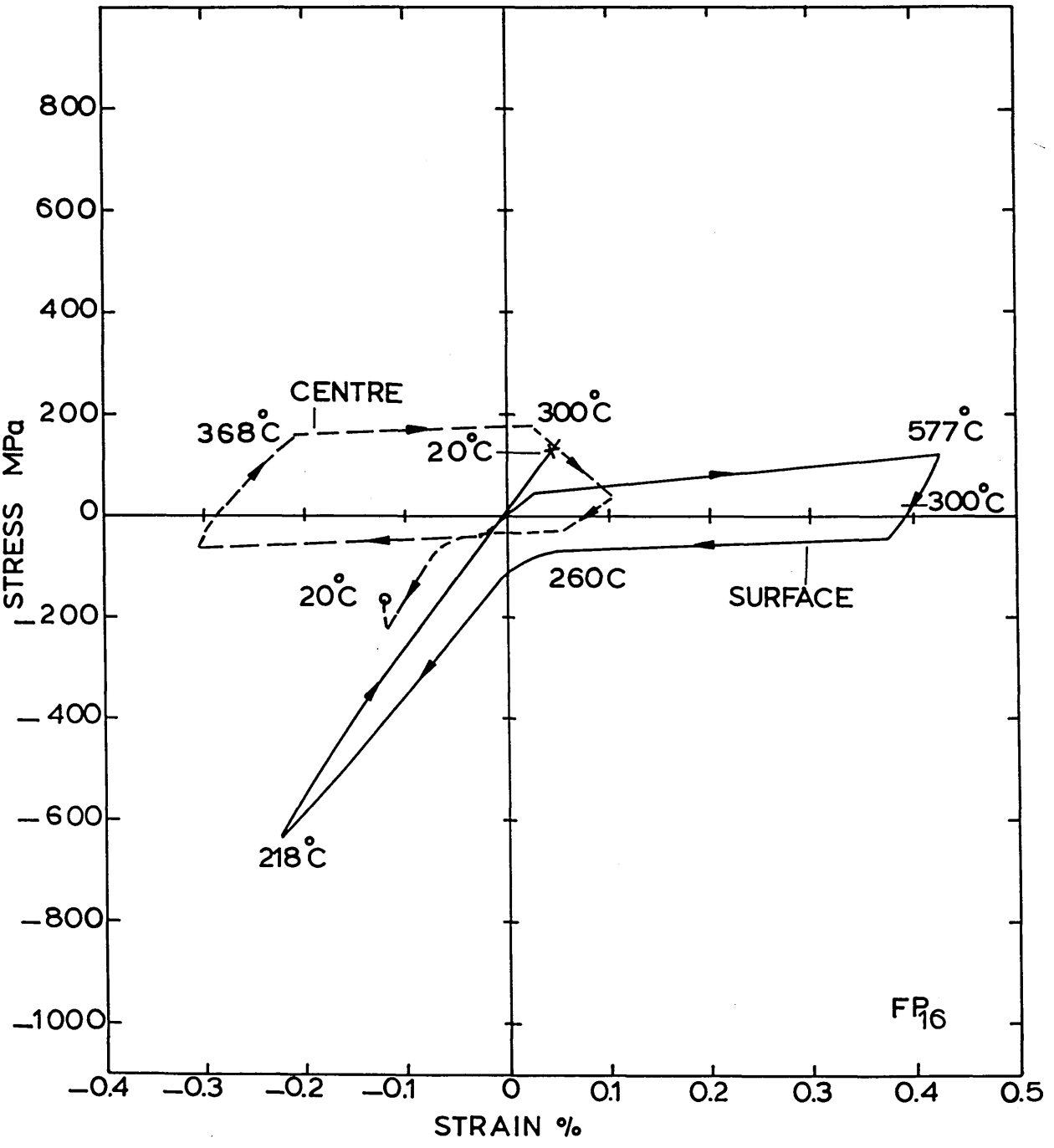
800
600
400
200
0
-200
-400
-600
-800
-1000
STRESS MPa
CENTRE
368°C
300°C
20°C
577°C
300°C
20°C
260C
SURFACE
218°C
FP16
-0.4
-0.3
-0.2
-0.1
0
0.1
0.2
0.3
0.4
0.5
STRAIN %

FIGURE 66: Calculated stress and strain at the surface and the centre of a 20 mm plate during polymer quenching with transformation plasticity and stress relaxation represented by method two (calculation FP_{17}).

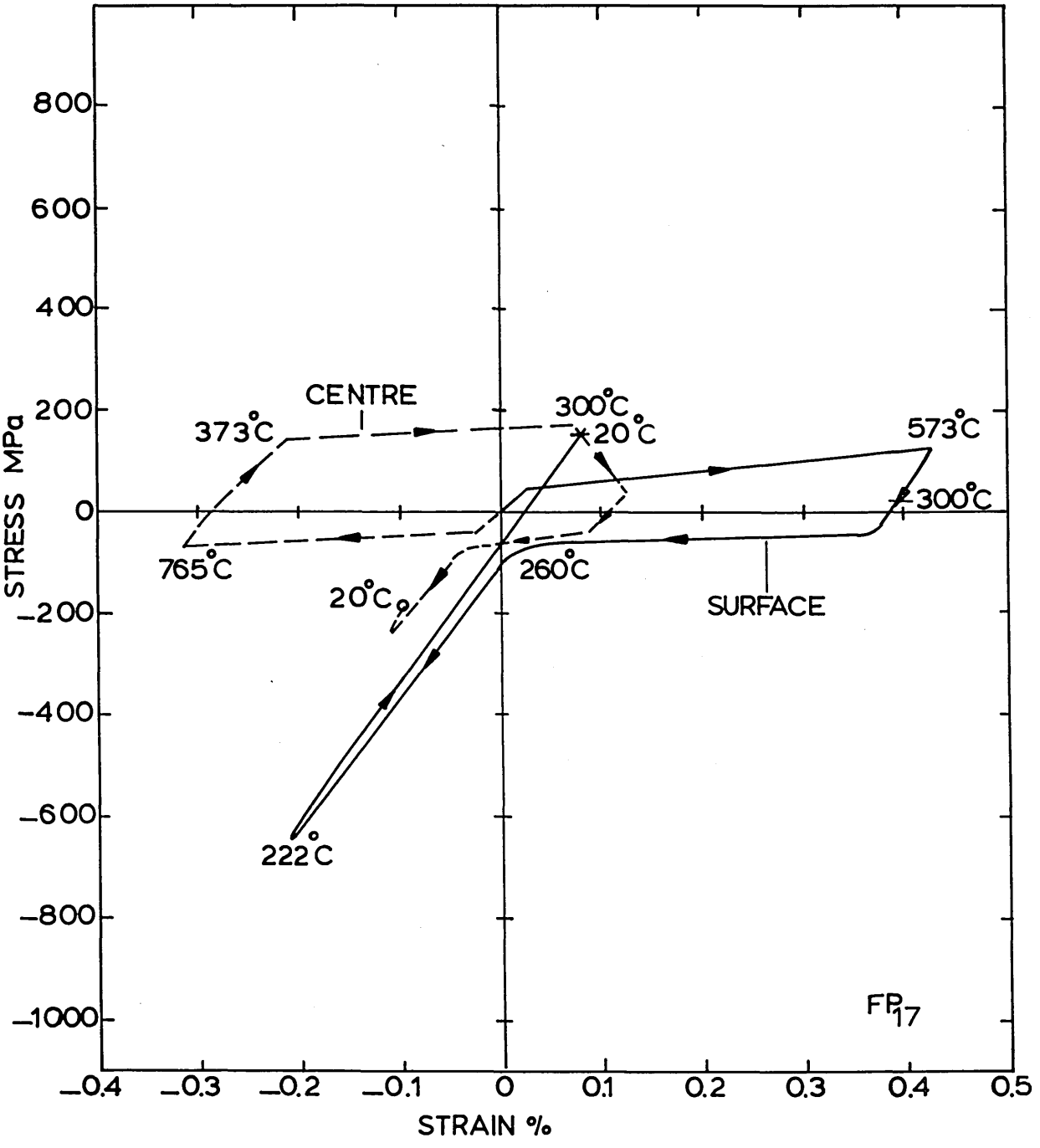
800
600
400
200
0
-200
-400
-600
-800
-1000
STRESS MPa
-0.4
-0.3
-0.2
-0.1
0
0.1
0.2
0.3
0.4
0.5
STRAIN %
CENTRE
373°C
765°C
20°C
300°C
20°C
573°C
300°C
260°C
SURFACE
222°C
FP17

FIGURE 67: Calculated stress and strain at the surface and the centre of a 20 mm plate during polymer quenching with transformation plasticity, no stress relaxation (calculation FP_{18}).

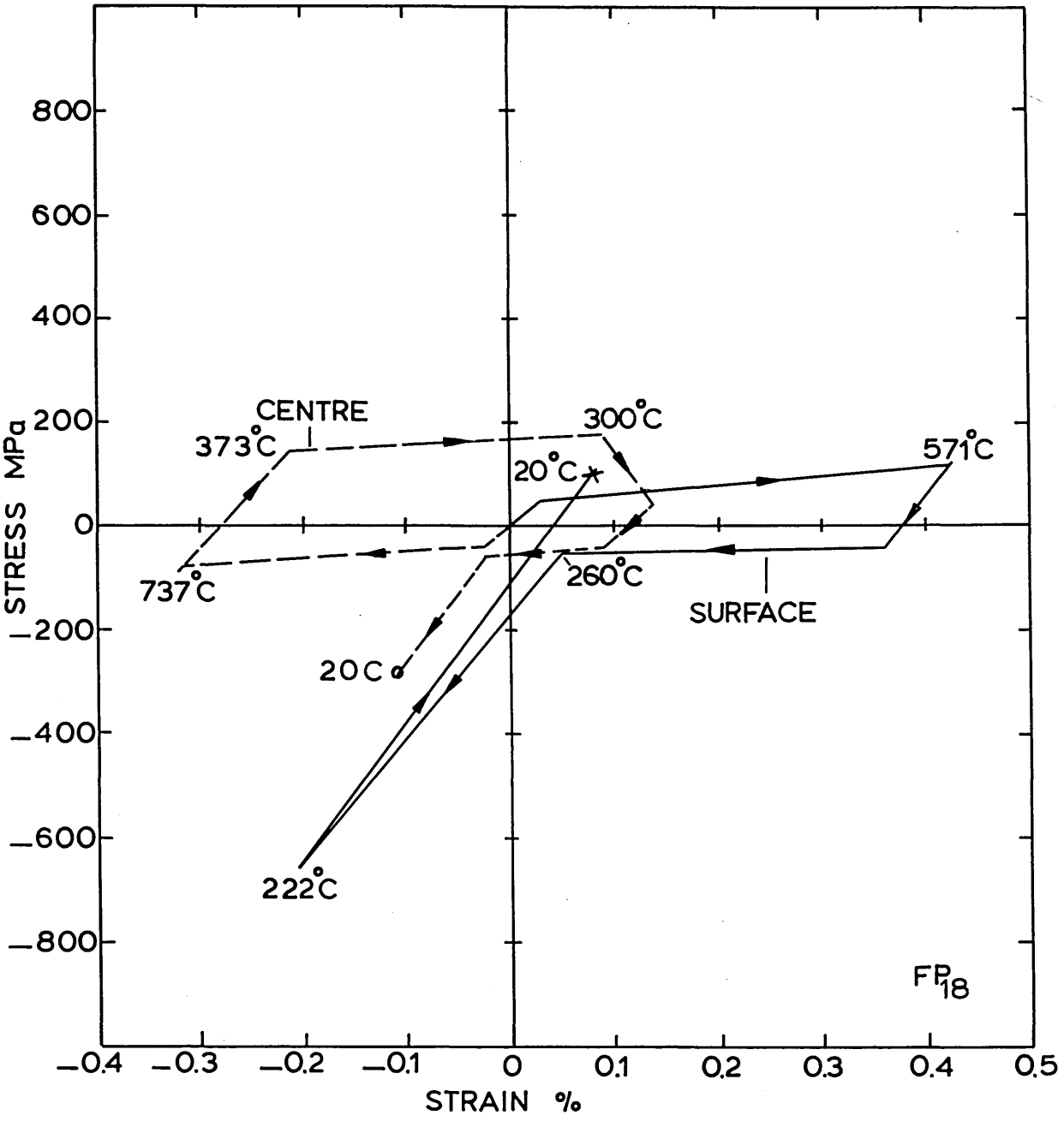
800
600
400
200
0
−200
−400
−600
−800
STRESS MPa
CENTRE
373°C
300°C
20°C
571°C
737°C
260°C
SURFACE
20C
222°C
FP18
−0.4
−0.3
−0.2
−0.1
0
0.1
0.2
0.3
0.4
0.5
STRAIN %

FIGURE 68: Calculated residual stress distribution in a 20 mm plate after polymer quenching.

Calculation number:-

FP_{13} - No stress relaxation.
FP_{14} - Stress relaxation method 1.
FP_{15} - Stress relaxation method 2.
FP_{16} - Stress relaxation method 1 and transformation plasticity.
FP_{17} - Stress relaxation method 2 and transformation plasticity.
FP_{18} - Transformation plasticity, no stress relaxation.

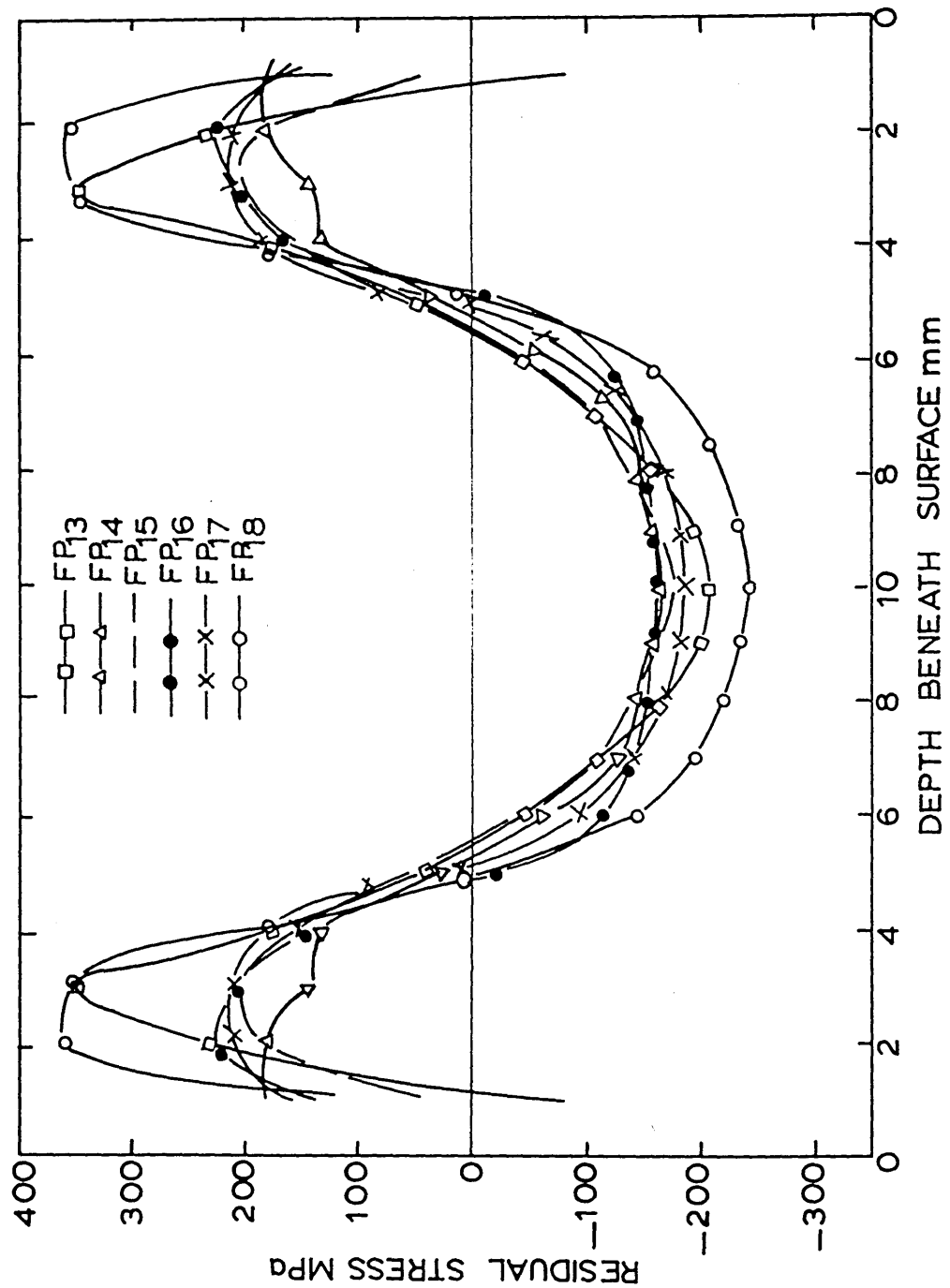
FP13
FP14
FP15
FP16
FP17
FP18
RESIDUAL STRESS MPa
400
300
200
100
0
-100
-200
-300
DEPTH BENEATH SURFACE mm
0
2
4
6
8
10
8
6
4
2
0

FIGURE 69: Calculated residual strain distribution in a 20 mm plate after polymer quenching.

(For Key see figure 68).

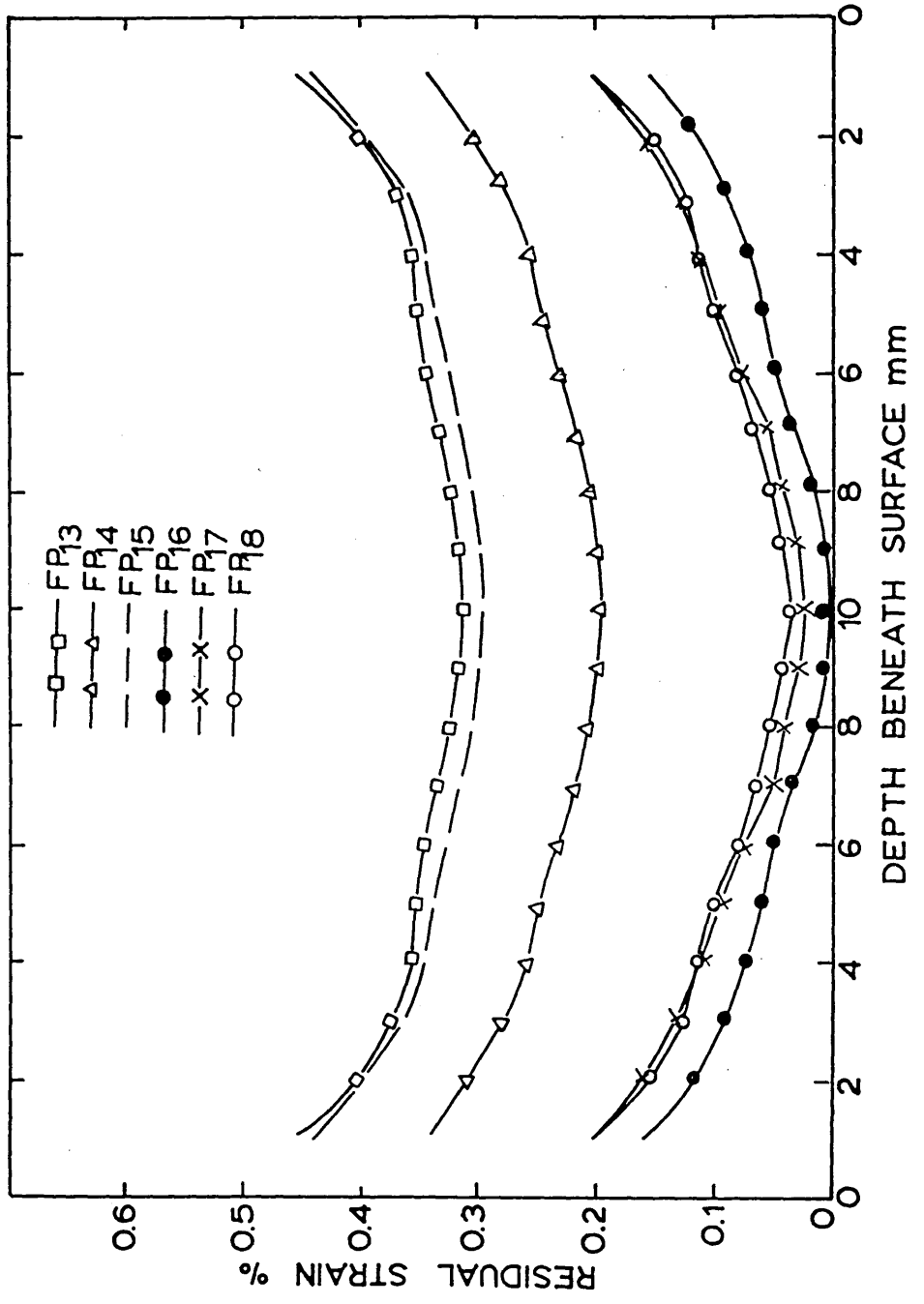
FP13
FP14
FP15
FP16
FP17
FP18
RESIDUAL STRAIN %
0.6
0.5
0.4
0.3
0.2
0.1
0
DEPTH BENEATH SURFACE mm
0
2
4
6
8
10
8
6
4
2
0

FIGURE 70: Calculated stress and strain at the surface and the centre of a 15 mm plate during martempering (followed by air cooling) without stress relaxation (calculation FP_{19}).

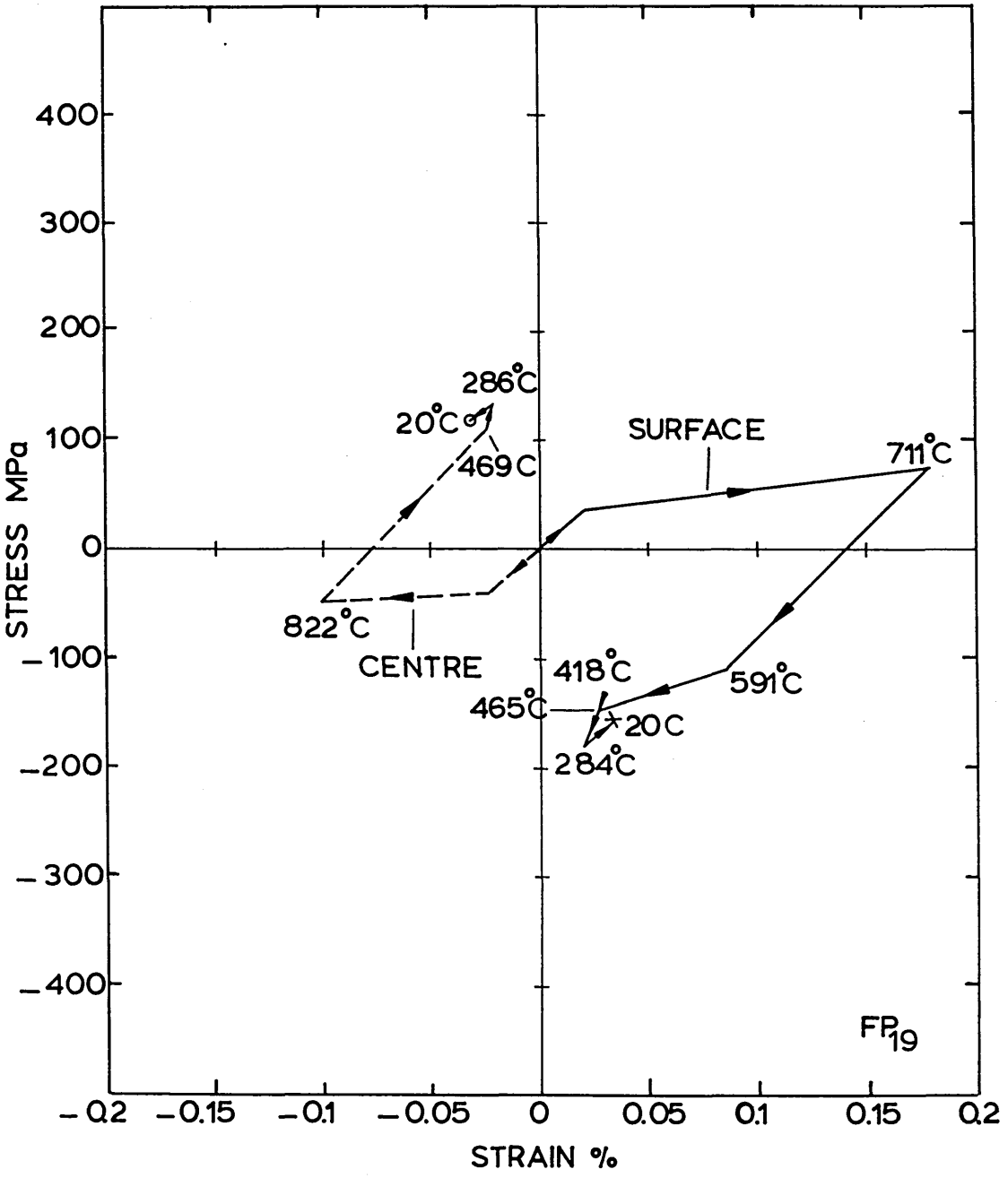
400
300
200
100
0
−100
−200
−300
−400
STRESS MPa
286°C
20°C
469C
SURFACE
711°C
822°C
CENTRE
418°C
591°C
465°C
20C
284°C
FP19
−0.2
−0.15
−0.1
−0.05
0
0.05
0.1
0.15
0.2
STRAIN %

FIGURE 71: Calculated stress and strain at the surface and the centre of a 15 mm plate during martempering (followed by air cooling) with stress relaxation represented by method one (calculation FP_{20}).

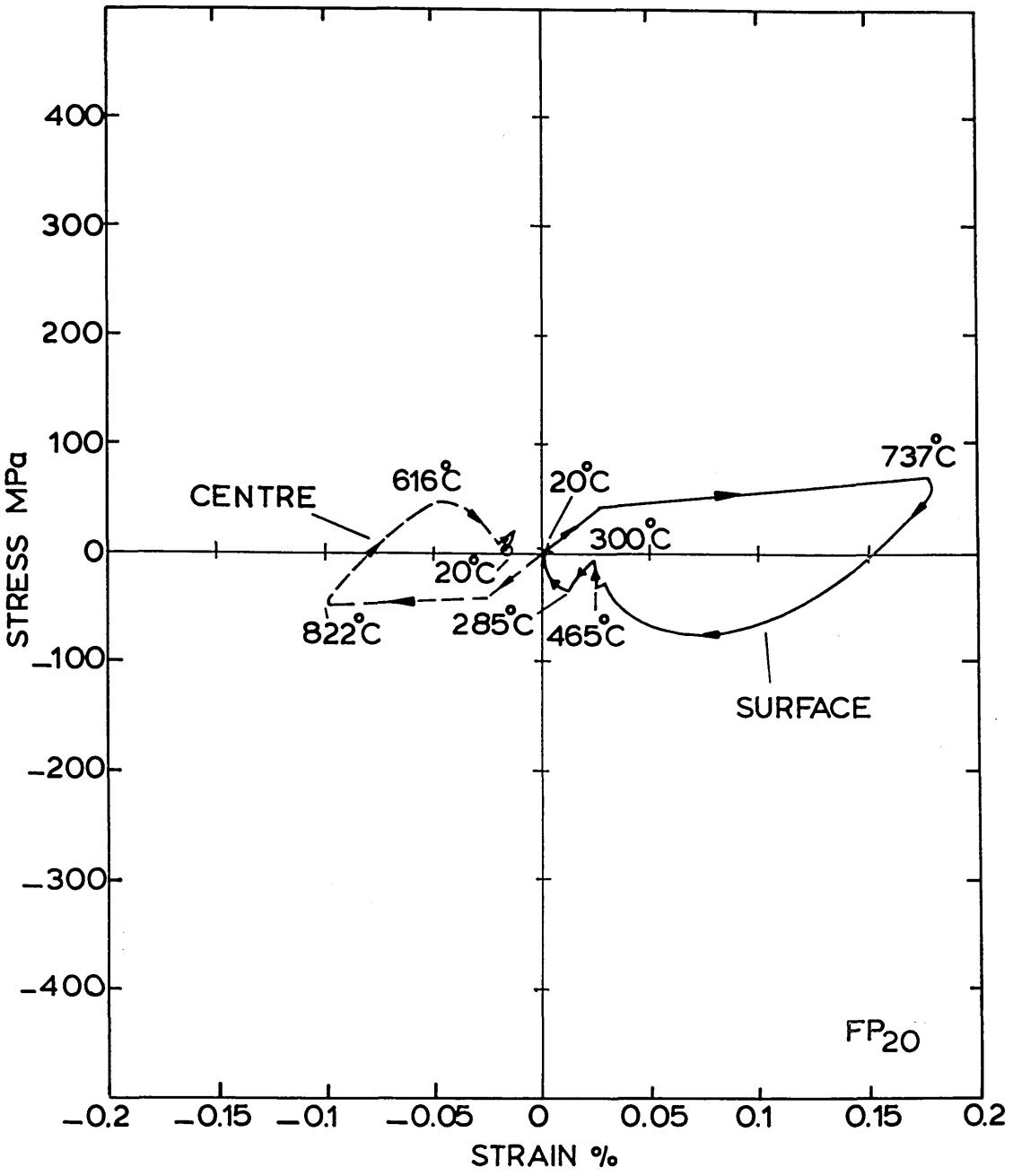
400
300
200
100
0
−100
−200
−300
−400
STRESS MPa
−0.2
−0.15
−0.1
−0.05
0
0.05
0.1
0.15
0.2
STRAIN %
CENTRE
616°C
20°C
737°C
300°C
20°C
822°C
285°C
465°C
SURFACE
FP20

FIGURE 72: Calculated stress and strain at the surface and the centre of a 15 mm plate during martempering (followed by air cooling) with stress relaxation represented by method two (calculation FP_{21}).

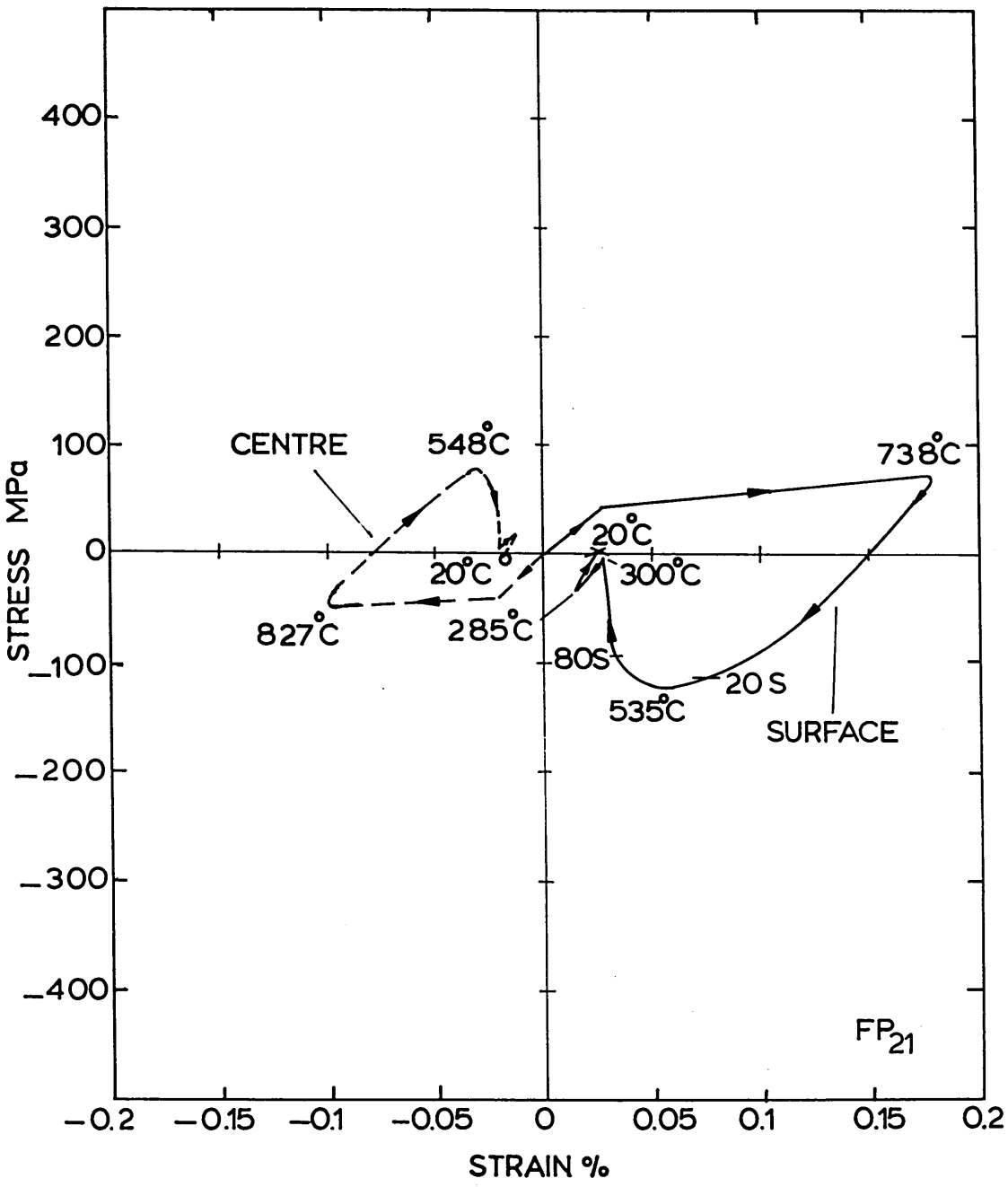
400
300
200
100
0
−100
−200
−300
−400
STRESS MPa
CENTRE
548°C
738°C
20°C
20°C
300°C
827°C
285°C
80S
20 S
535°C
SURFACE
FP21
−0.2
−0.15
−0.1
−0.05
0
0.05
0.1
0.15
0.2
STRAIN %

FIGURE 73: Calculated residual stress distribution in a 15 mm plate after martempering (followed by air cooling).

Calculation number:

FP_{19} - No stress relaxation.
FP_{20} - Stress relaxation method 1.
FP_{21} - Stress relaxation method 2.

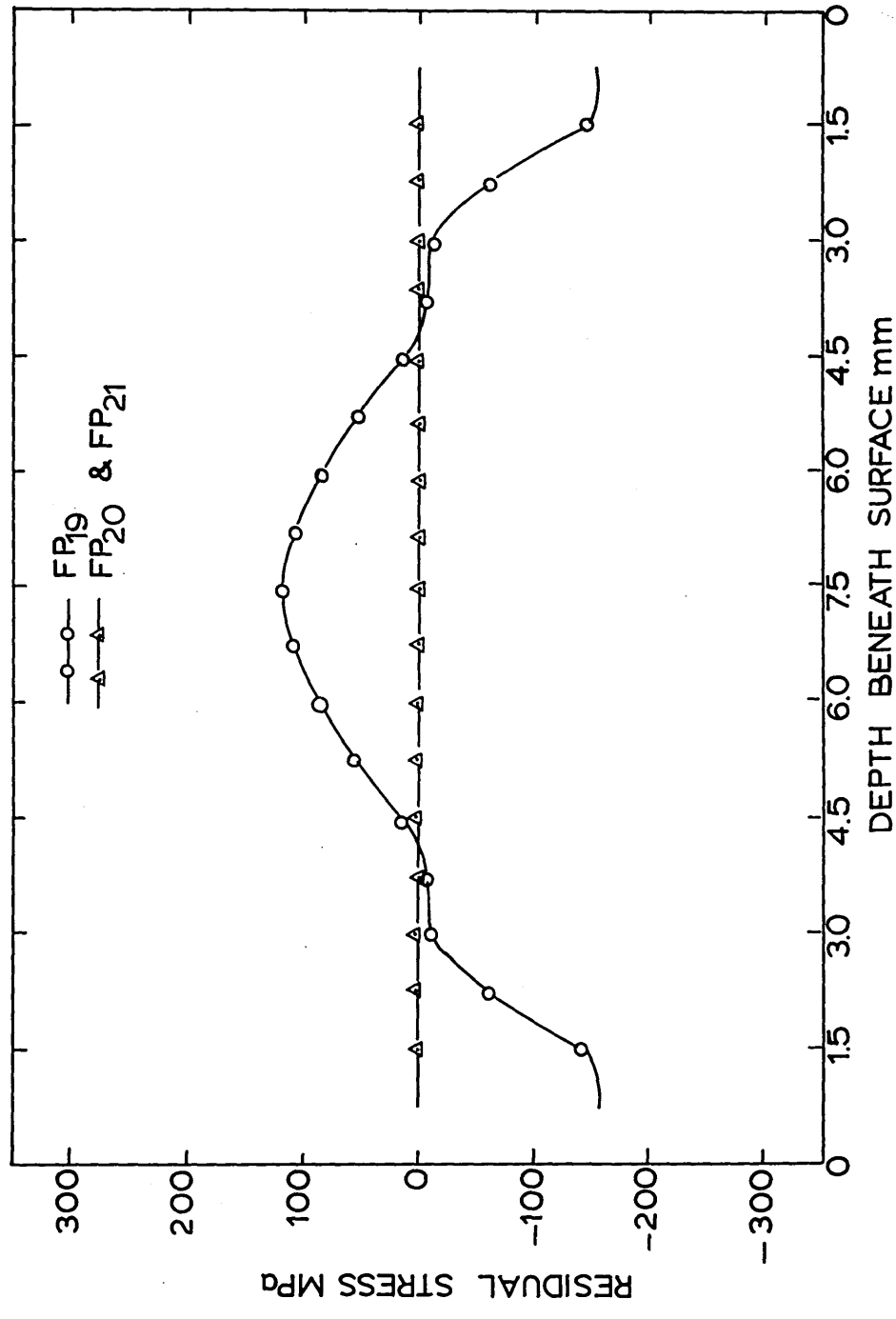
FP19
FP20 & FP21
RESIDUAL STRESS MPa
300
200
100
0
-100
-200
-300
0
1.5
3.0
4.5
6.0
7.5
6.0
4.5
3.0
1.5
0
DEPTH BENEATH SURFACE mm

FIGURE 74: Calculated residual strain distribution in a 15 mm plate after martempering (followed by air cooling).

(For Key see figure 73).

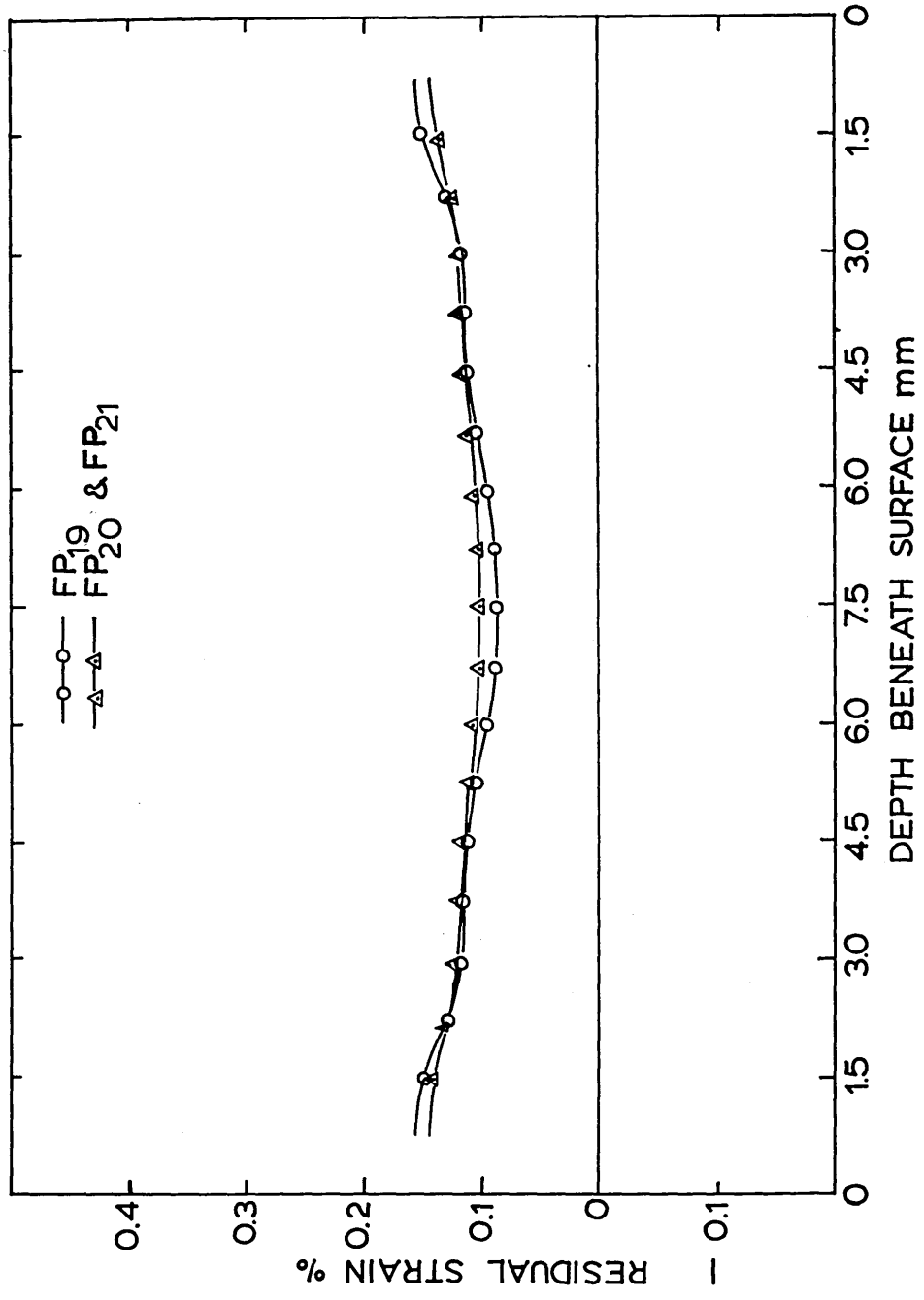
FP19
FP20 & FP21
RESIDUAL STRAIN %
0.4
0.3
0.2
0.1
0
0.1
0
1.5
3.0
4.5
6.0
7.5
6.0
4.5
3.0
1.5
0
DEPTH BENEATH SURFACE mm

FIGURE 75: Calculated stress and strain at the surface and the centre of a 15 mm plate during martempering (followed by oil quenching) without stress relaxation (calculation FP_{22}).

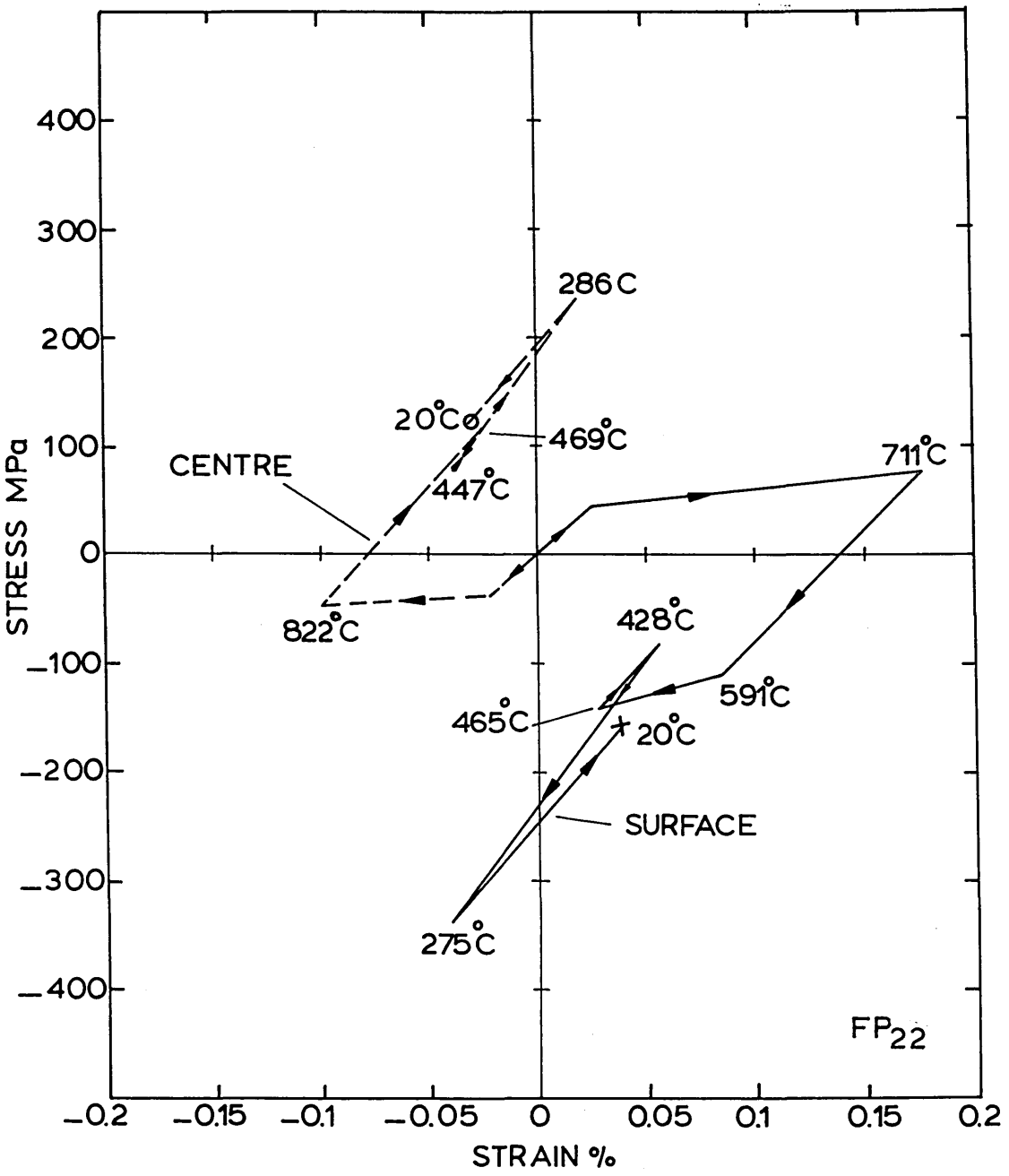
400
300
200
100
0
−100
−200
−300
−400
STRESS MPa
−0.2
−0.15
−0.1
−0.05
0
0.05
0.1
0.15
0.2
STRAIN %
286C
20°C
469°C
CENTRE
447°C
711°C
822°C
428°C
591°C
465°C
20°C
SURFACE
275°C
FP22

FIGURE 76: Calculated stress and strain at the surface and the centre of a 15 mm plate during martempering (followed by oil quenching) with stress relaxation represented by method one (calculation FP_{23}).

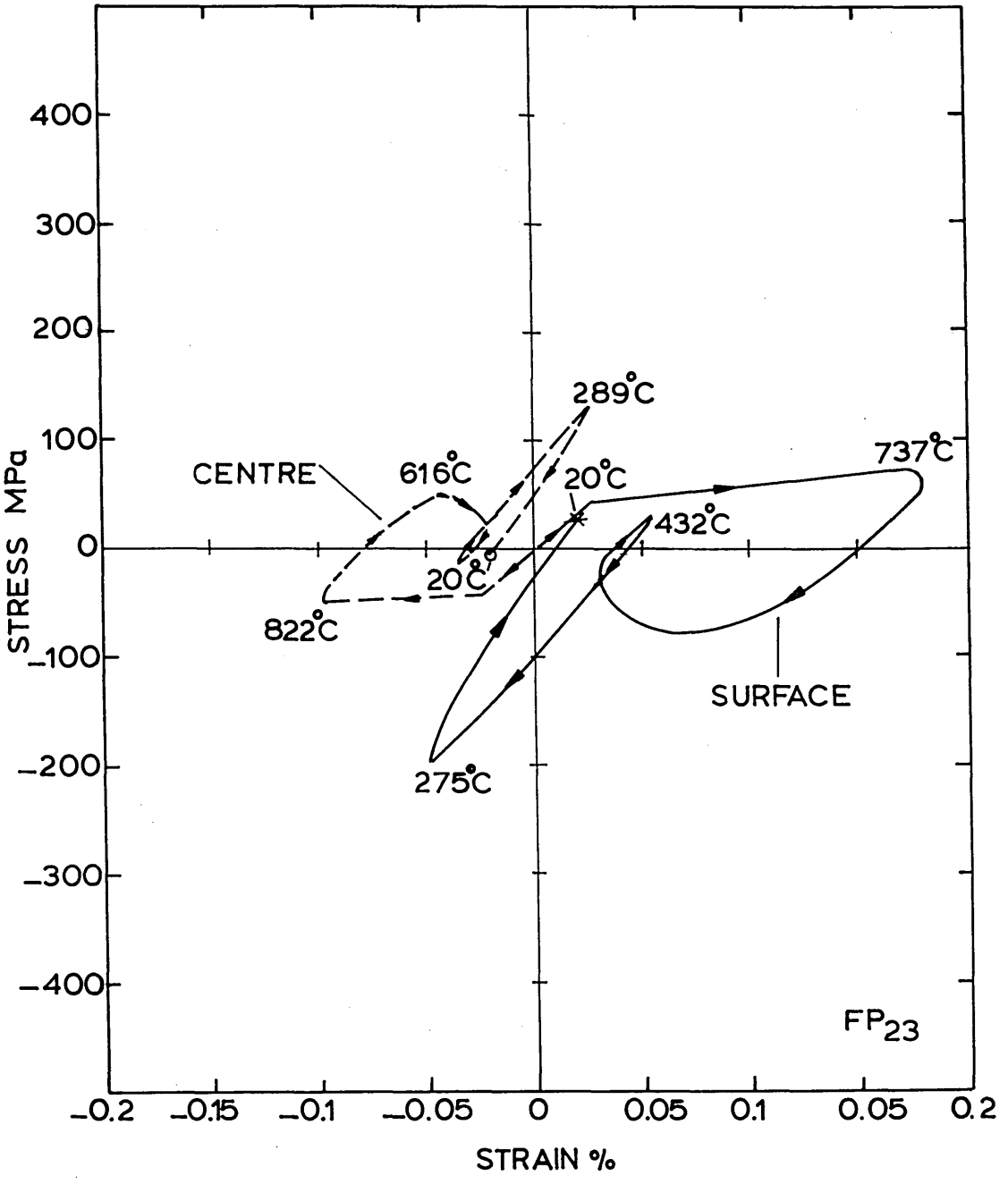
400
300
200
100
0
−100
−200
−300
−400
STRESS MPa
−0.2
−0.15
−0.1
−0.05
0
0.05
0.1
0.05
0.2
STRAIN %
289°C
CENTRE
616°C
20°C
737°C
432°C
20°C
822°C
275°C
SURFACE
FP23

FIGURE 77: Calculated stress and strain at the surface and the centre of a 15 mm plate during martempering (followed by oil quenching) with stress relaxation represented by method two (calculation FP_{24}).

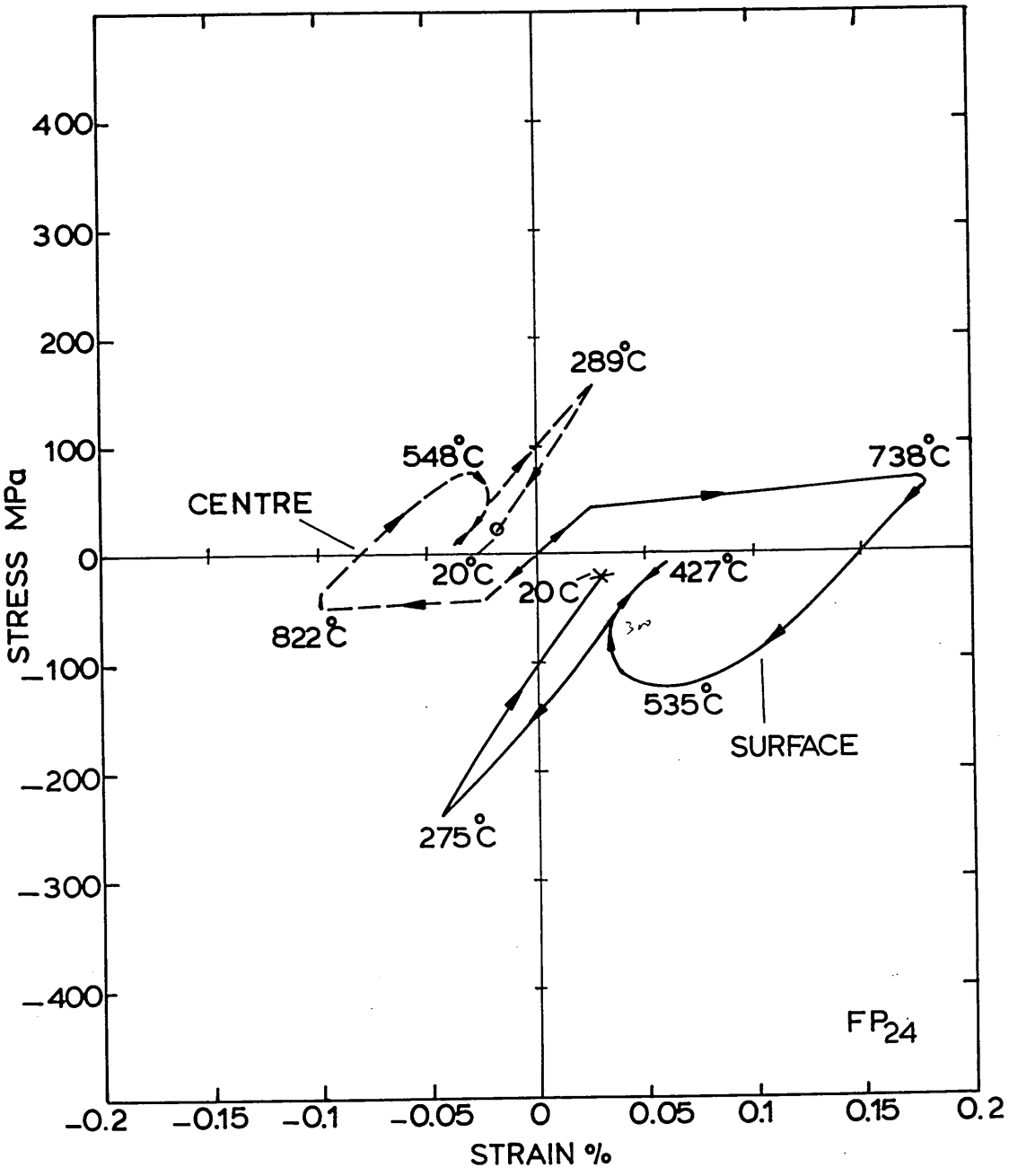
400
300
200
100
0
−100
−200
−300
−400
STRESS MPa
−0.2
−0.15
−0.1
−0.05
0
0.05
0.1
0.15
0.2
STRAIN %
289°C
548°C
738°C
CENTRE
20°C
20°C
427°C
822°C
535°C
SURFACE
275°C
FP24

FIGURE 78: Calculated stress and strain at the surface and the centre of a 15 mm plate during martempering (followed by oil quenching) with transformation plasticity and stress relaxation represented by method one (calculation FP_{25}).

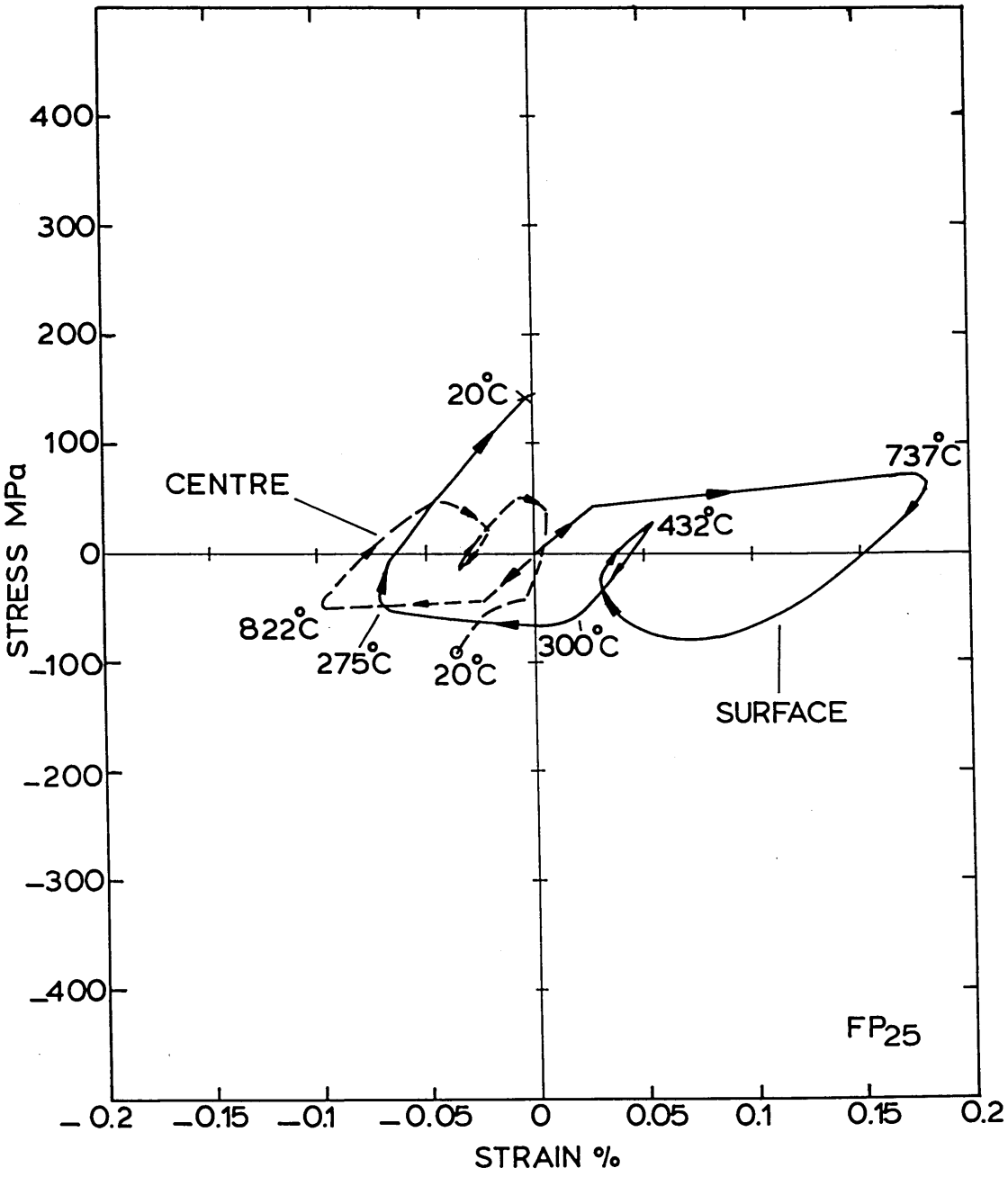
400
300
200
100
0
-100
-200
-300
-400
STRESS MPa
20°C
737°C
CENTRE
432°C
822°C
275°C
20°C
300°C
SURFACE
FP25
-0.2
-0.15
-0.1
-0.05
0
0.05
0.1
0.15
0.2
STRAIN %

FIGURE 79: Calculated stress and strain at the surface and the centre of a 15 mm plate during martempering (followed by oil quenching) with transformation plasticity and stress relaxation represented by method two (calculation FP_{26}).

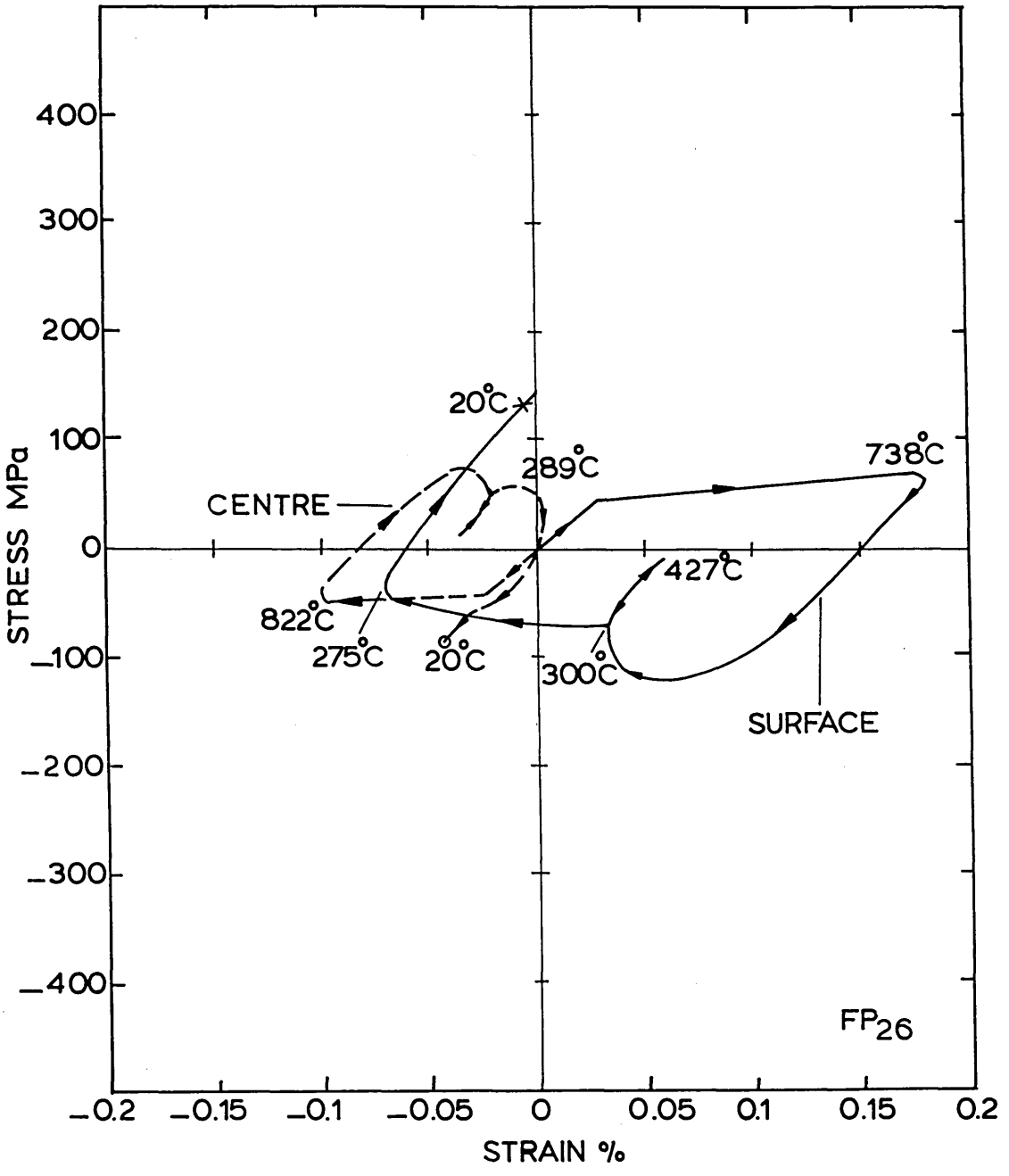
400
300
200
100
0
−100
−200
−300
−400
STRESS MPa
−0.2
−0.15
−0.1
−0.05
0
0.05
0.1
0.15
0.2
STRAIN %
20°C
289°C
738°C
CENTRE
427°C
822°C
275°C
20°C
300°C
SURFACE
FP26

FIGURE 80: Calculated residual stress distribution in a 15 mm plate after martempering (followed by oil quenching).

Calculation number:

FP_{22} - No stress relaxation.
FP_{23} - Stress relaxation method 1.
FP_{24} - Stress relaxation method 2.
FP_{25} - Stress relaxation method 1 and transformation plasticity.
FP_{26} - Stress relaxation method 2 and transformation plasticity.

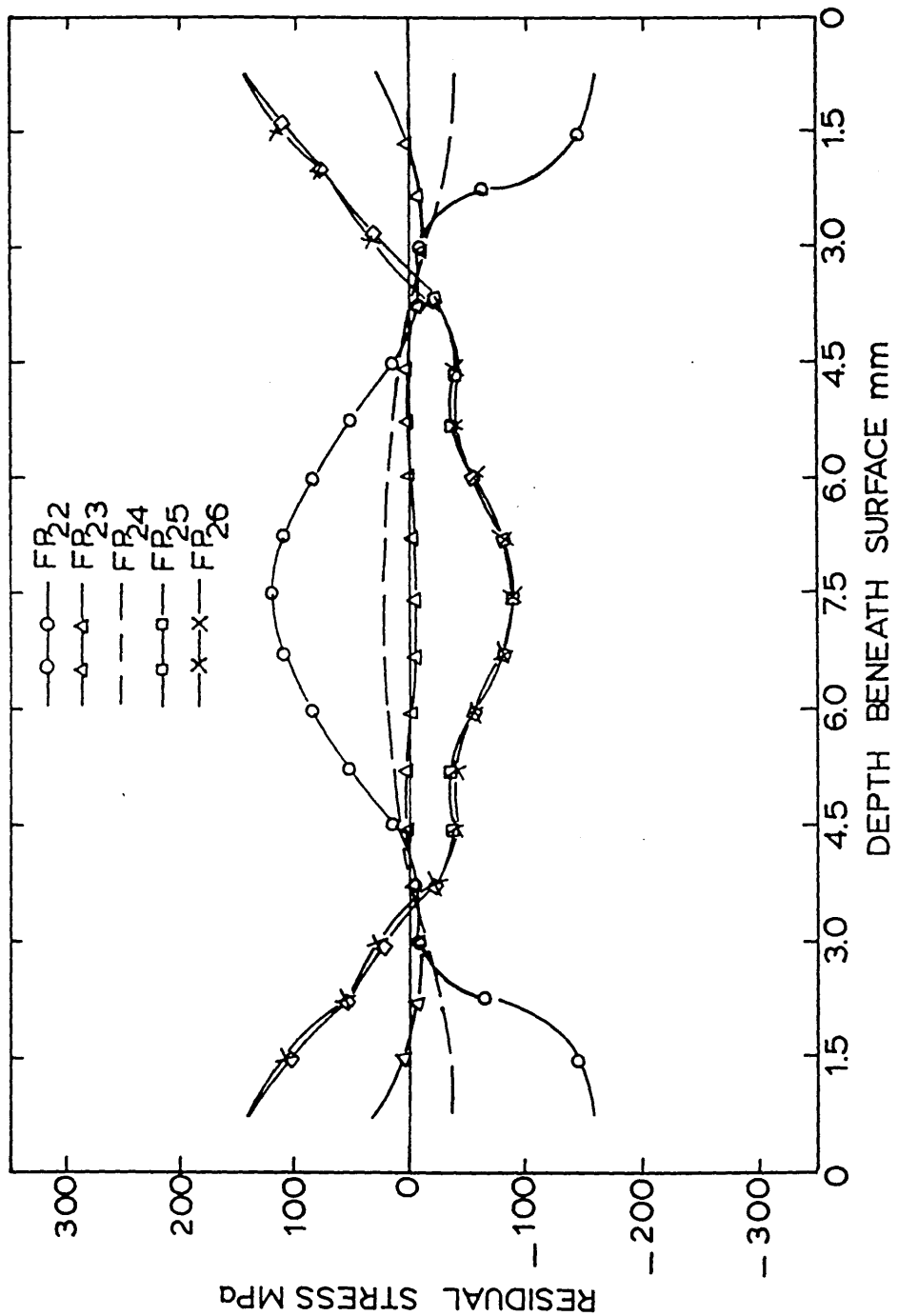
FP22
FP23
FP24
FP25
FP26
300
200
100
0
-100
-200
-300
RESIDUAL STRESS MPa
0
1.5
3.0
4.5
6.0
7.5
6.0
4.5
3.0
1.5
0
DEPTH BENEATH SURFACE mm

FIGURE 81: Calculated residual strain distribution in a 15 mm plate after martempering (followed by oil quenching).

(For Key see figure 80).

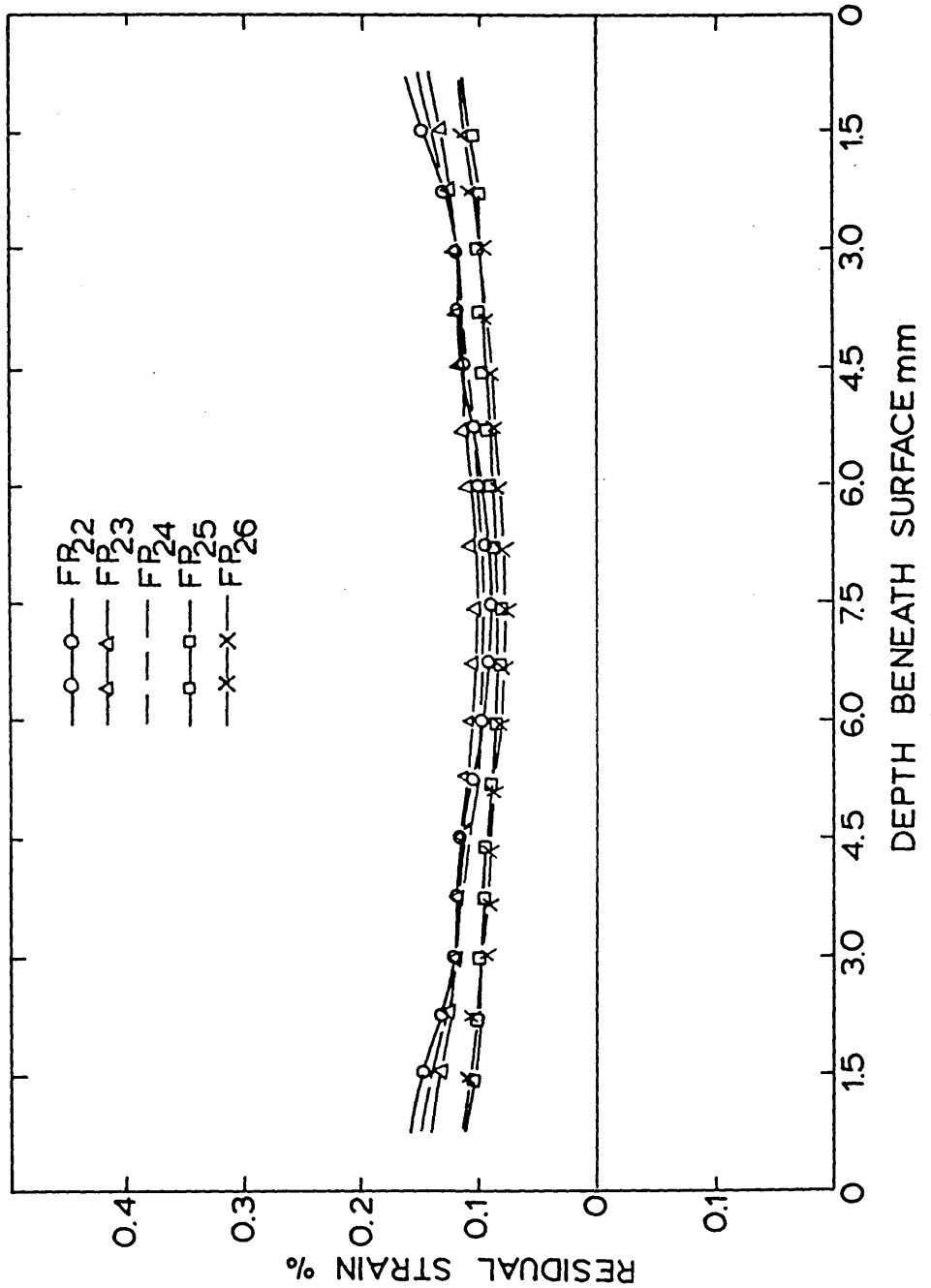
FR22
FR23
FR24
FR25
FR26
0.4
0.3
0.2
0.1
0
0.1
RESIDUAL STRAIN %
0
1.5
3.0
4.5
6.0
7.5
6.0
4.5
3.0
1.5
0
DEPTH BENEATH SURFACE mm

FIGURE 82: Variations in the calculated relationships between stress & strain at the surface, with the change in plate thickness during water quenching (calculation FP_{27}).

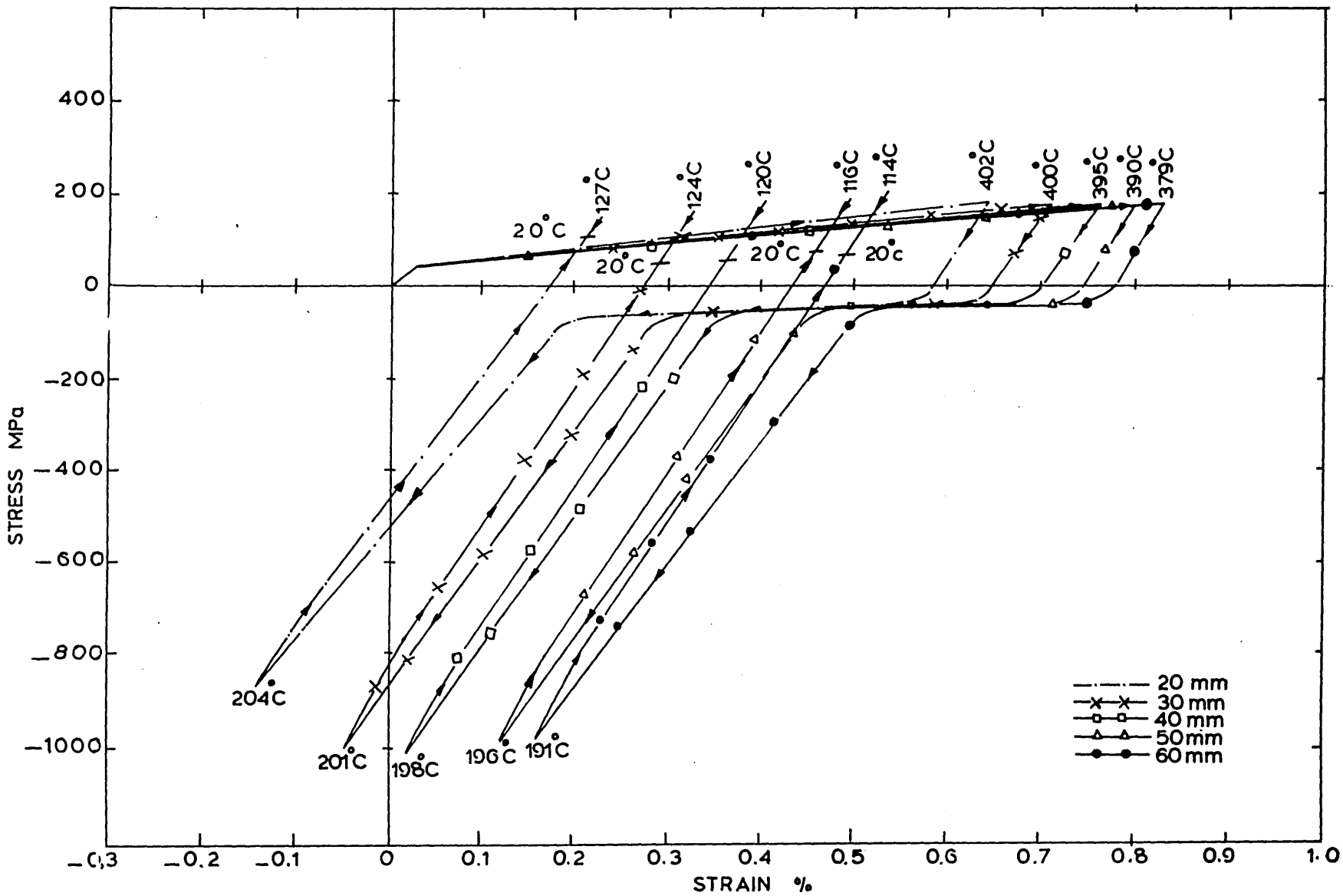
400
200
0
−200
−400
−600
−800
−1000
STRESS MPa
−0.3
−0.2
−0.1
0
0.1
0.2
0.3
0.4
0.5
0.6
0.7
0.8
0.9
1.0
STRAIN %
20°C
127°C
20°C
124°C
20°C
120°C
20°C
116°C
20°c
114°C
402°C
400°C
395°C
390°C
379°C
204°C
201°C
198°C
196°C
191°C
20 mm
30 mm
40 mm
50 mm
60 mm

FIGURE 83: Variations in the calculated relationships between stress and strain at the centre, with the change in plate thickness during water quenching (calculation FP_{27}).

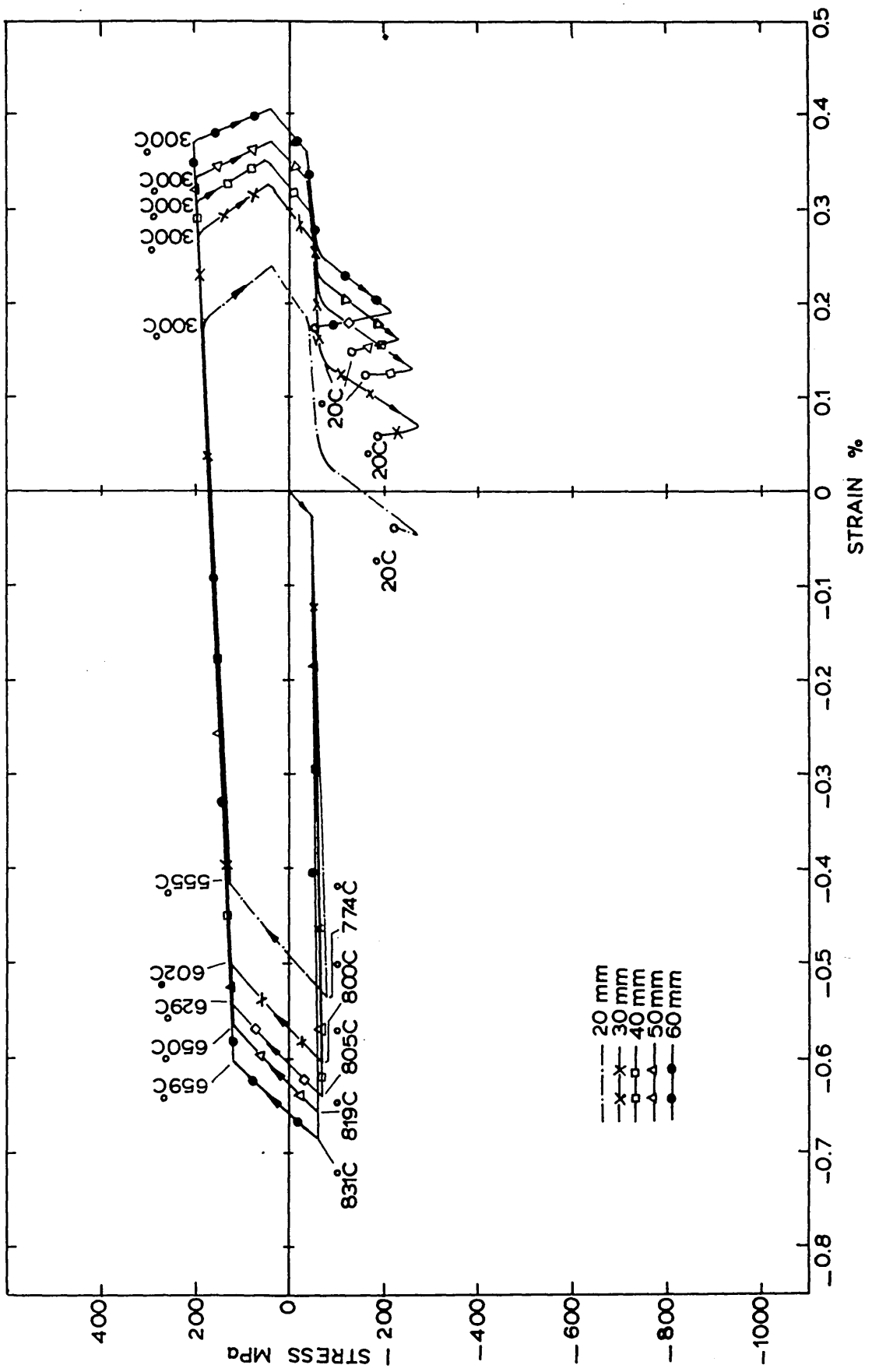
STRESS MPa
STRAIN %
400
200
0
-200
-400
-600
-800
-1000
0.5
0.4
0.3
0.2
0.1
0
-0.1
-0.2
-0.3
-0.4
-0.5
-0.6
-0.7
-0.8
300°C
300°C
300°C
300°C
300°C
20°C
20°C
20°C
555°C
602°C
629°C
650°C
659°C
774°C
800°C
805°C
819°C
831°C
20 mm
30 mm
40 mm
50 mm
60 mm

FIGURE 84: The effect of plate thickness on the calculated residual stress distribution at the end of a water quench.

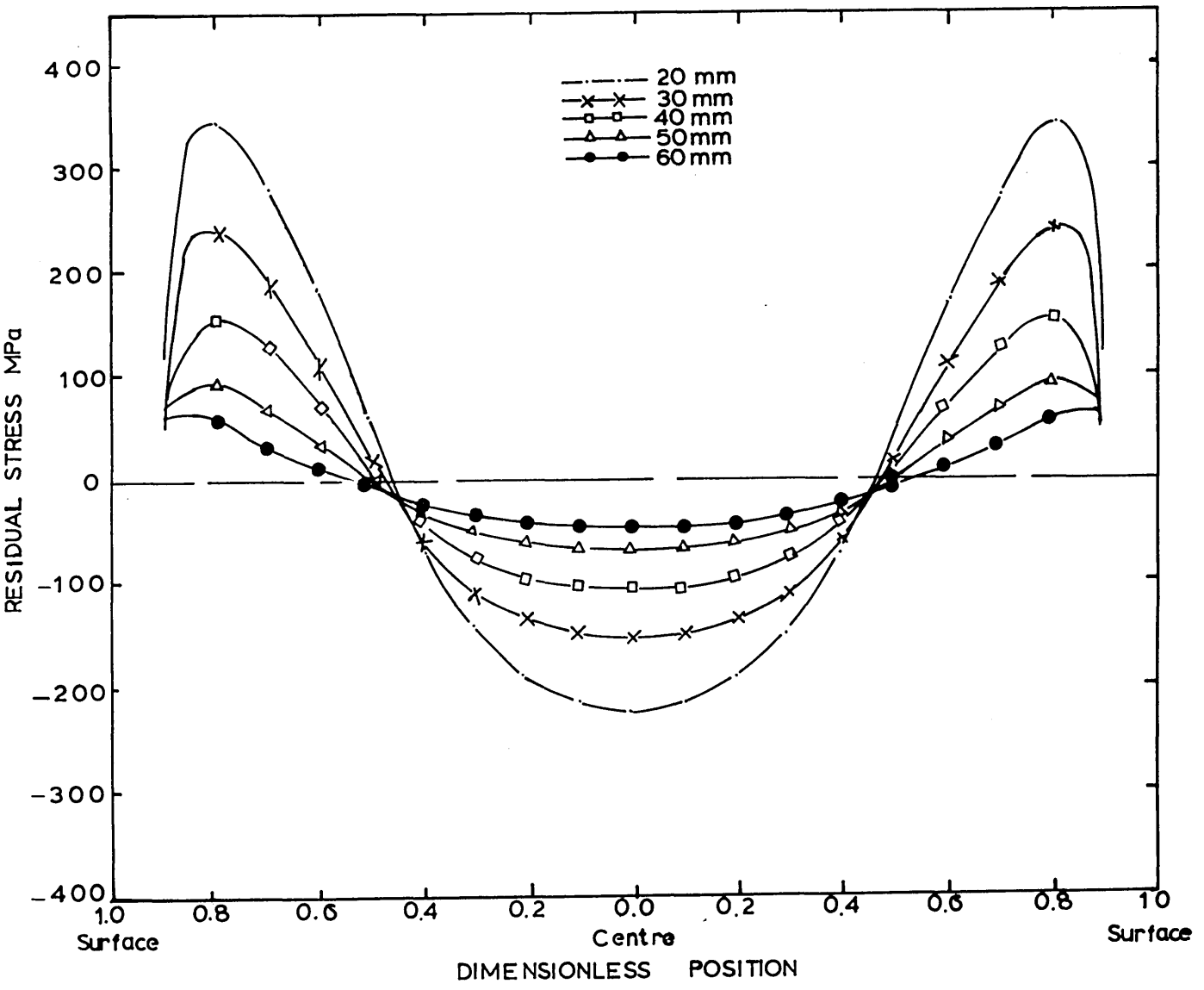
20 mm
30 mm
40 mm
50mm
60 mm
400
300
200
100
0
-100
-200
-300
-400
RESIDUAL STRESS MPa
1.0
0.8
0.6
0.4
0.2
0.0
0.2
0.4
0.6
0.8
1.0
Surface
Centre
Surface
DIMENSIONLESS POSITION

FIGURE 85: The effect of plate thickness on the calculated residual strain distribution at the end of a water quench.

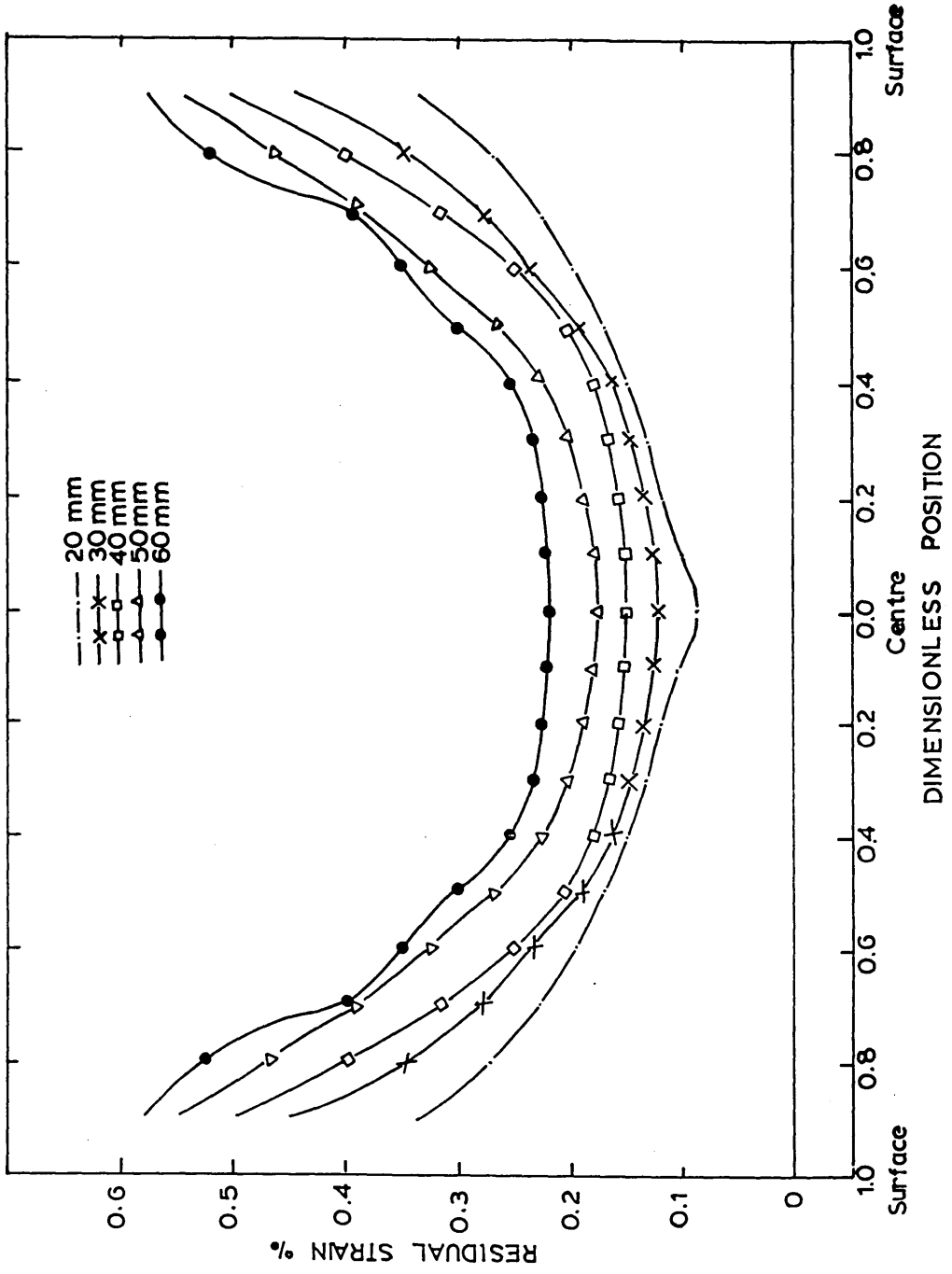
RESIDUAL STRAIN %
0.6
0.5
0.4
0.3
0.2
0.1
0
20 mm
30 mm
40 mm
50 mm
60 mm
1.0 Surface
0.8
0.6
0.4
0.2
0.0 Centre
0.2
0.4
0.6
0.8
1.0 Surface
DIMENSIONLESS POSITION

FIGURE 86: Variations in the calculated relationships between stress and strain at the surface, with the change in plate thickness during oil quenching (calculation FP_{27}).

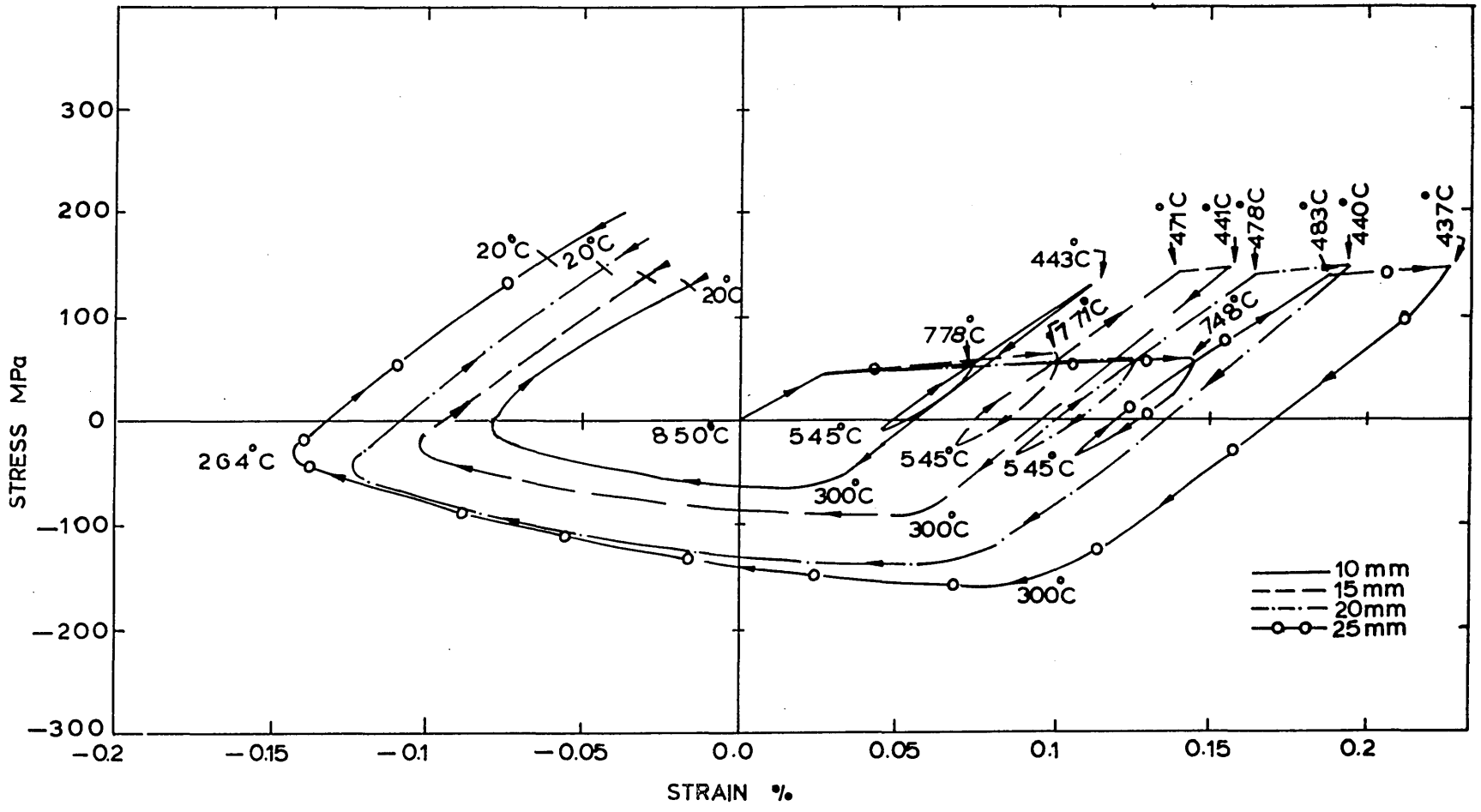
300
200
100
0
−100
−200
−300
STRESS MPa
−0.2
−0.15
−0.1
−0.05
0.0
0.05
0.1
0.15
0.2
STRAIN %
20°C
20°C
20°C
264°C
850°C
778°C
443°C
771°C
545°C
545°C
545°C
300°C
300°C
300°C
471°C
441°C
478°C
483°C
440°C
437°C
748°C
10 mm
15 mm
20mm
25mm

FIGURE 87: The effect of plate thickness on the calculated residual stress distribution at the end of an oil quench.

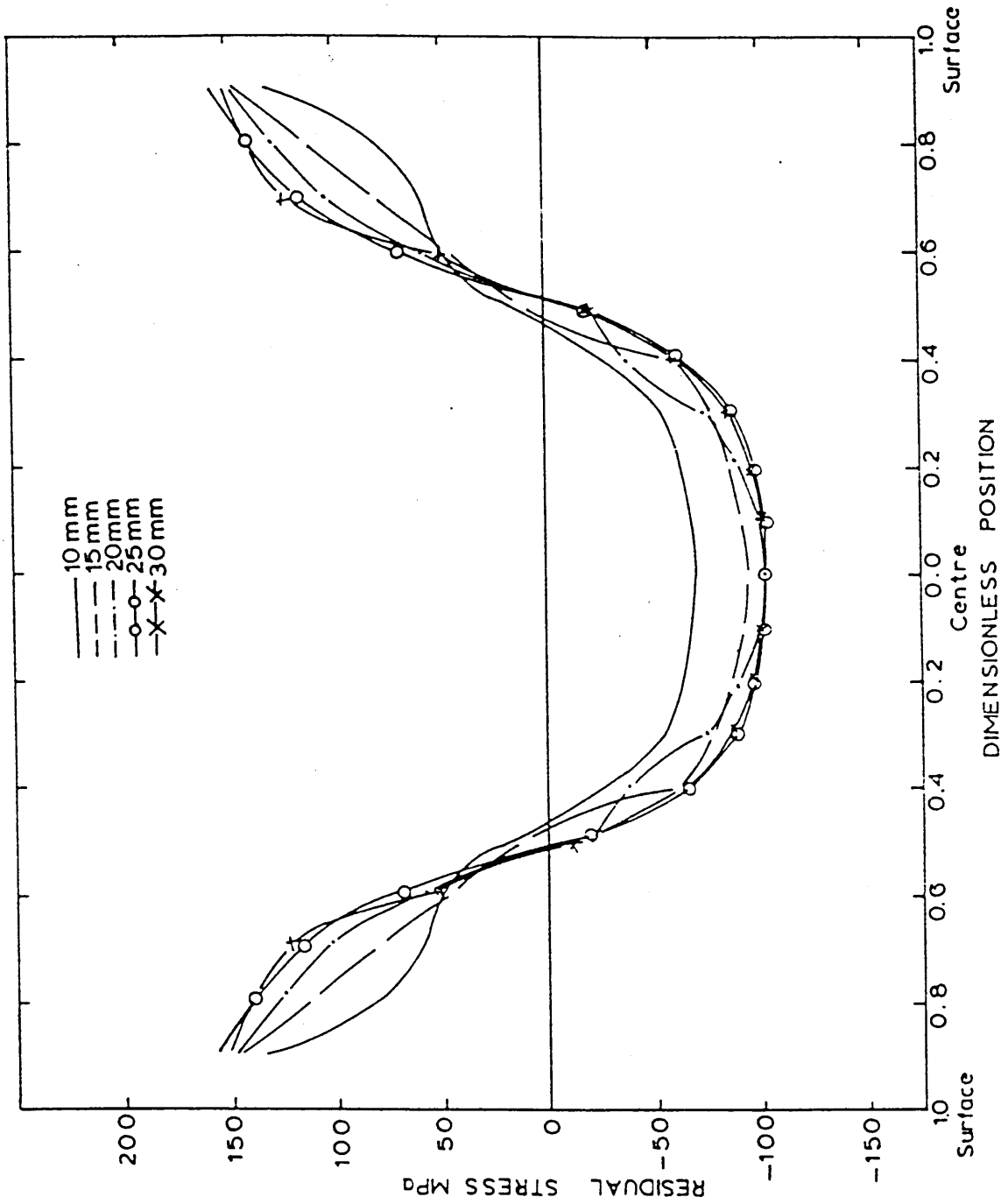
10 mm
15 mm
20 mm
25 mm
30 mm
RESIDUAL STRESS MPa
200
150
100
50
0
-50
-100
-150
1.0
Surface
0.8
0.6
0.4
0.2
0.0
Centre
0.2
0.4
0.6
0.8
1.0
Surface
DIMENSIONLESS POSITION

FIGURE 88: The effect of plate thickness on the calculated residual strain distribution at the end of an oil quench.

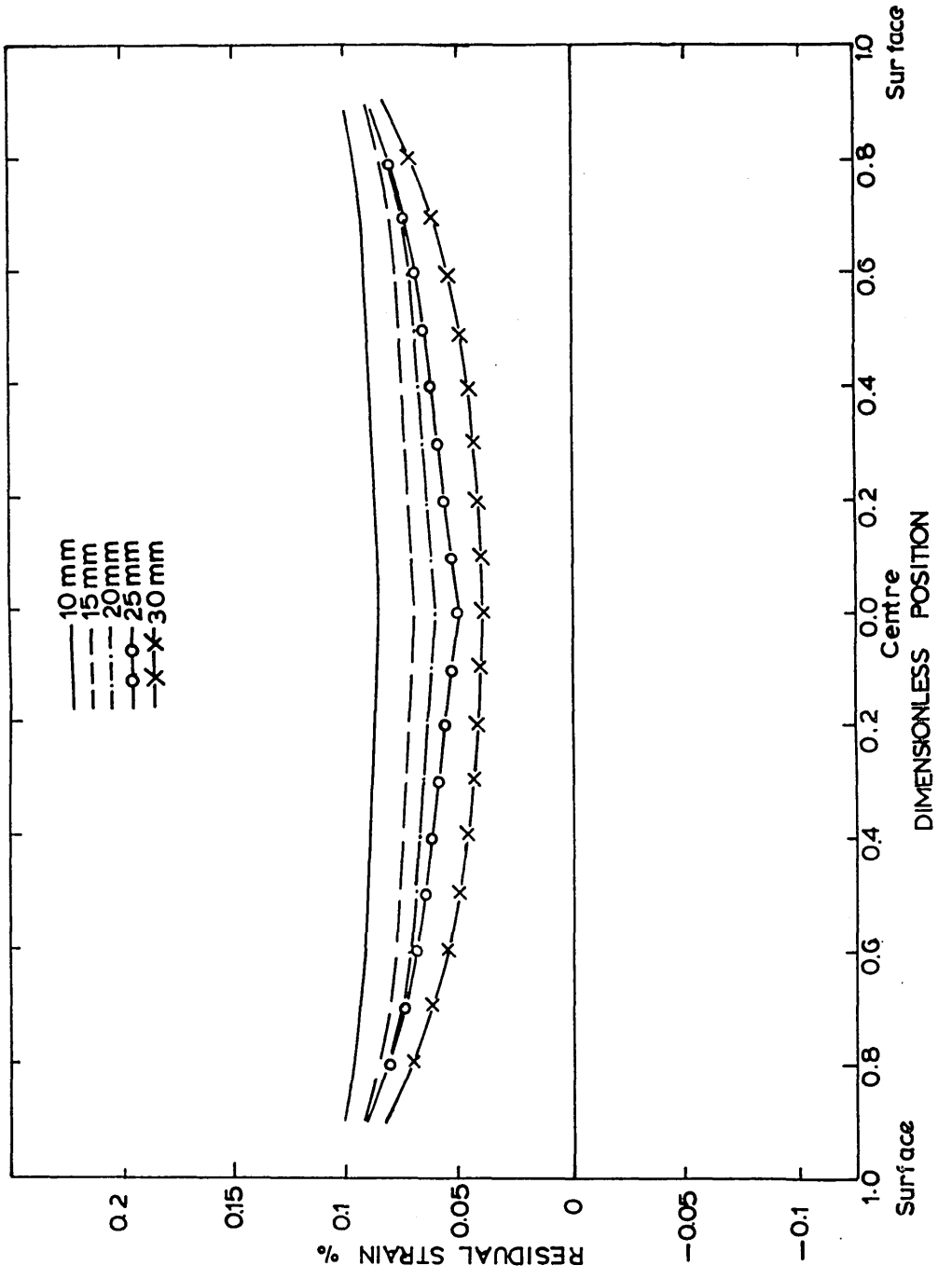
10 mm
15 mm
20 mm
25 mm
30 mm
RESIDUAL STRAIN %
0.2
0.15
0.1
0.05
0
−0.05
−0.1
Surface
1.0
0.8
0.6
0.4
0.2
0.0
Centre
0.2
0.4
0.6
0.8
1.0
Surface
DIMENSIONLESS POSITION

FIGURE 89: The effect of Ms temperature on the generation of stress and strain at the surface of a water quenched plate (calculation FP_{28}).

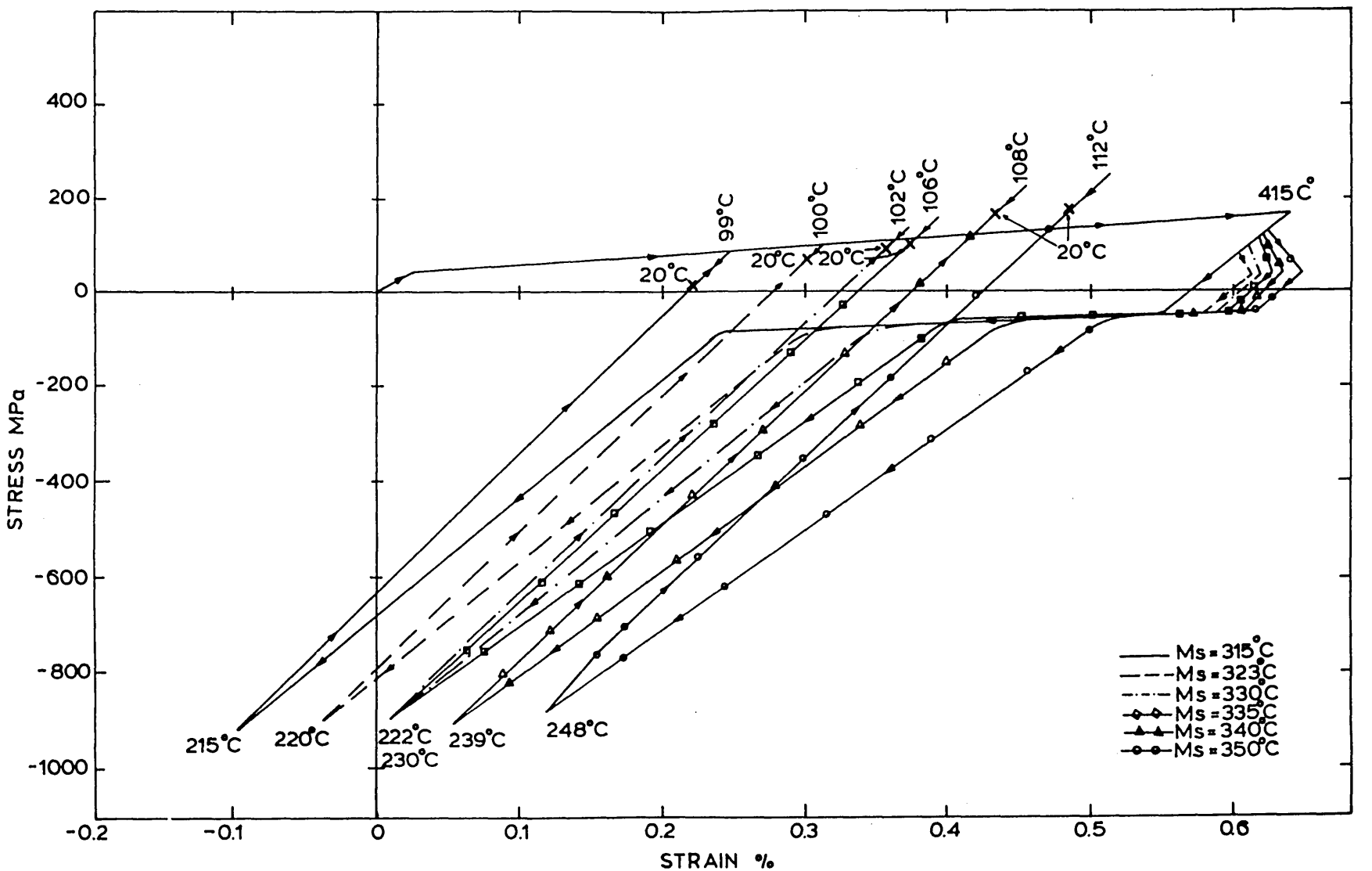
400
200
0
-200
-400
-600
-800
-1000
STRESS MPa
-0.2
-0.1
0
0.1
0.2
0.3
0.4
0.5
0.6
STRAIN %
99°C
100°C
102°C
106°C
108°C
112°C
415°C
20°C
20°C
20°C
20°C
215°C
220°C
222°C
230°C
239°C
248°C
Ms = 315°C
Ms = 323°C
Ms = 330°C
Ms = 335°C
Ms = 340°C
Ms = 350°C

FIGURE 90: The effect of Ms temperature on the generation of stress and strain at the centre of a water quenched plate (calculation FP_{28}).

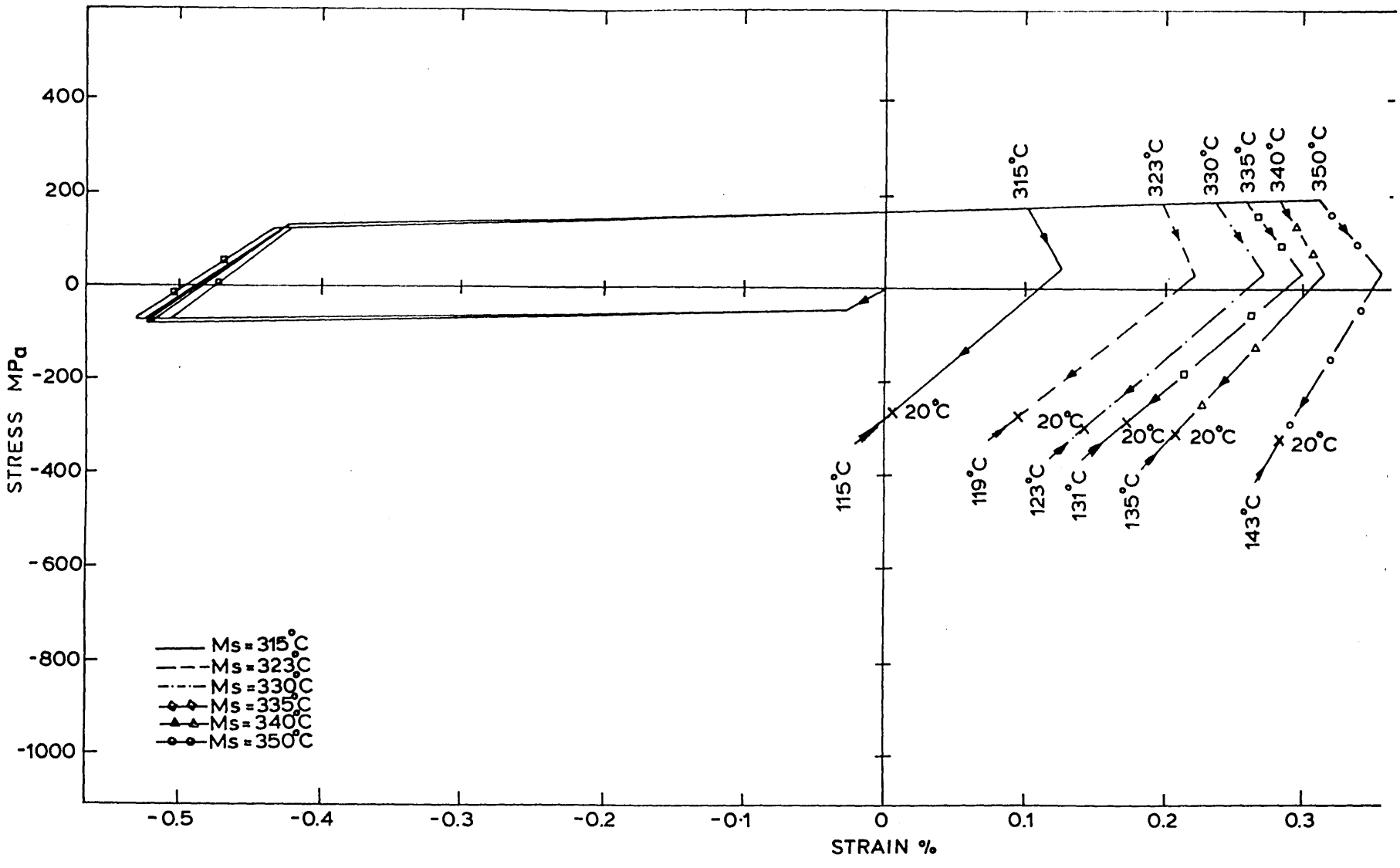
400
200
0
-200
-400
-600
-800
-1000
STRESS MPa
-0.5
-0.4
-0.3
-0.2
-0.1
0
0.1
0.2
0.3
STRAIN %
Ms = 315°C
Ms = 323°C
Ms = 330°C
Ms = 335°C
Ms = 340°C
Ms = 350°C
315°C
323°C
330°C
335°C
340°C
350°C
115°C
119°C
123°C
131°C
135°C
143°C
20°C

FIGURE 91: The effect of Ms temperature on the residual stress distribution at the end of a water quench.

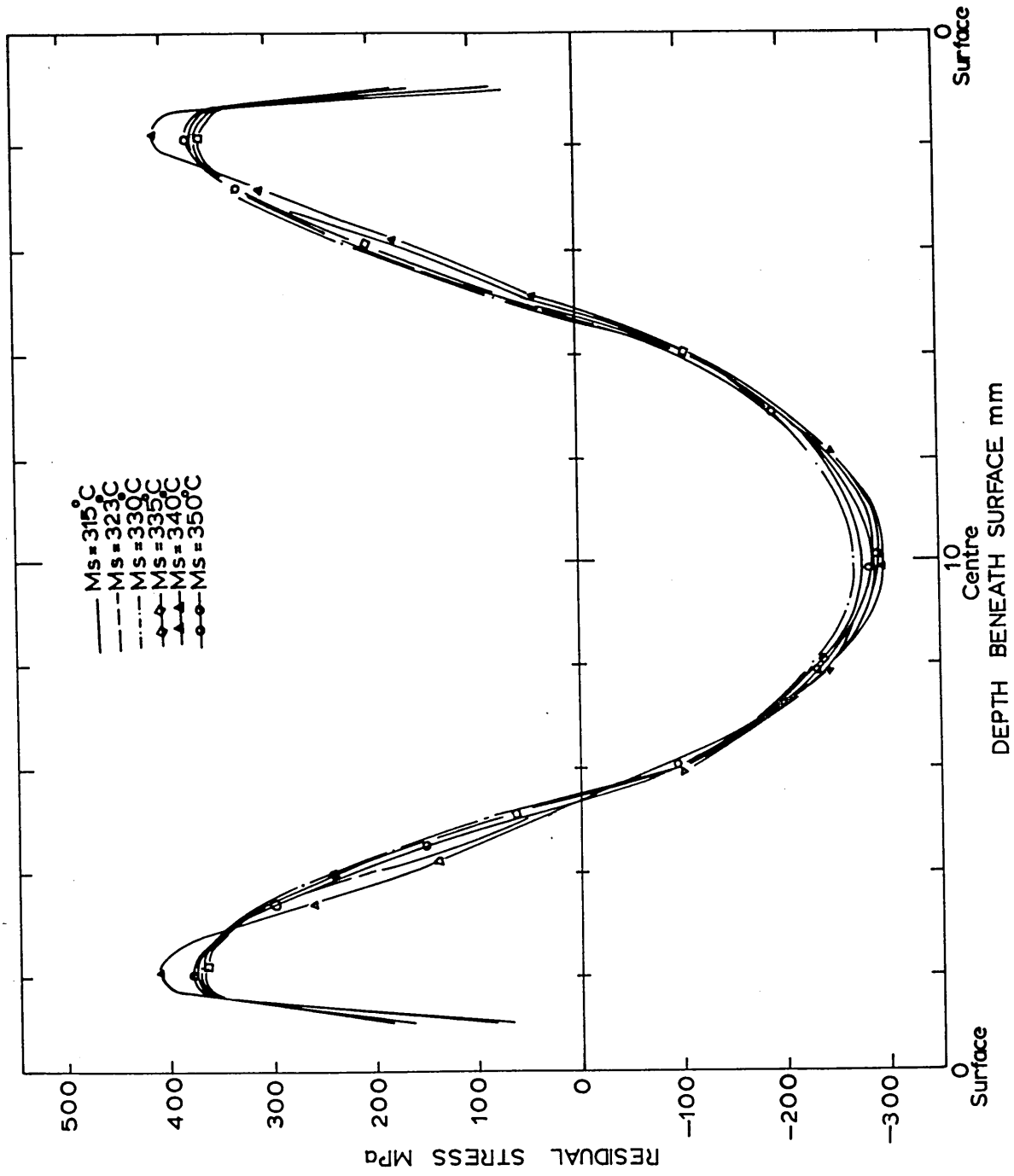
Ms=315°C
Ms=323°C
Ms=330°C
Ms=335°C
Ms=340°C
Ms=350°C
RESIDUAL STRESS MPa
500
400
300
200
100
0
−100
−200
−300
0
Surface
10
Centre
0
Surface
DEPTH BENEATH SURFACE mm

FIGURE 92: The effect of Ms temperature on the residual strain distribution at the end of a water quench.

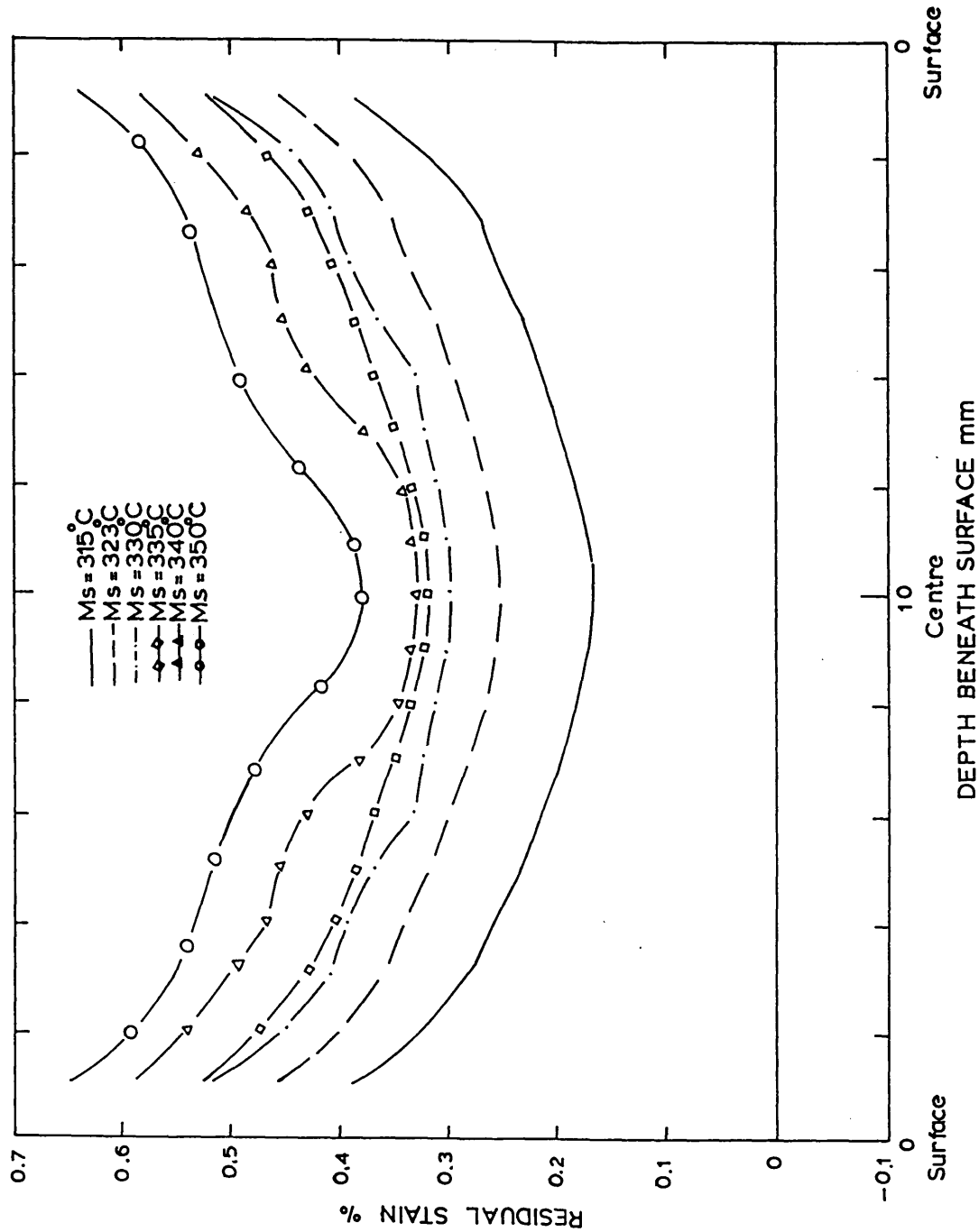
Ms = 315°C
Ms = 323°C
Ms = 330°C
Ms = 335°C
Ms = 340°C
Ms = 350°C
RESIDUAL STAIN %
0.7
0.6
0.5
0.4
0.3
0.2
0.1
0
-0.1
0
Surface
0
Surface
10
Centre
DEPTH BENEATH SURFACE mm

FIGURE 93: The effect of Ms temperature on the residual stress distribution at the end of an oil quench.

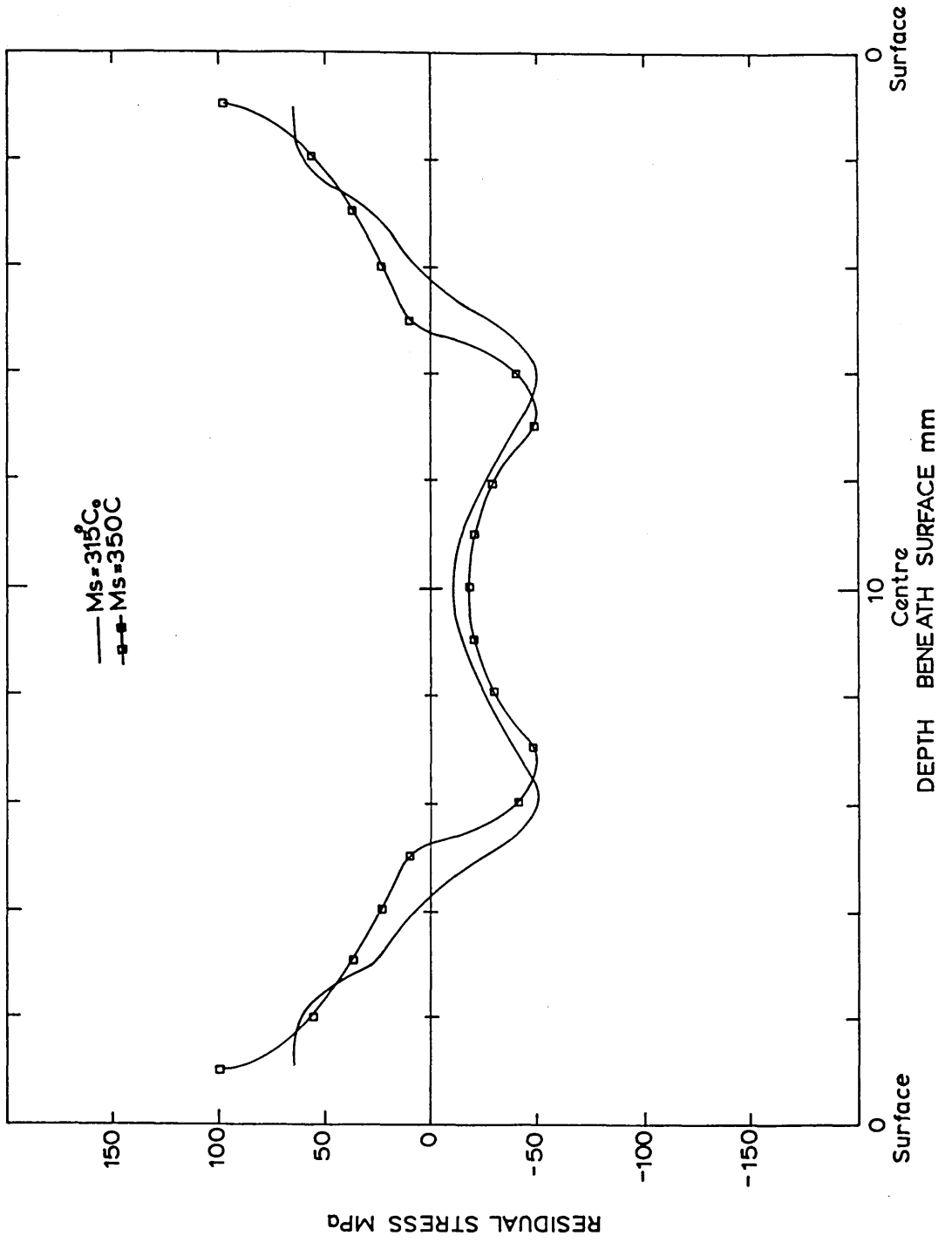
Ms=315°C
Ms=350C
150
100
50
0
-50
-100
-150
RESIDUAL STRESS MPa
0
Surface
10
Centre
0
Surface
DEPTH BENEATH SURFACE mm

FIGURE 94: The effect of Ms temperature on the residual strain distribution at the end of an oil quench.

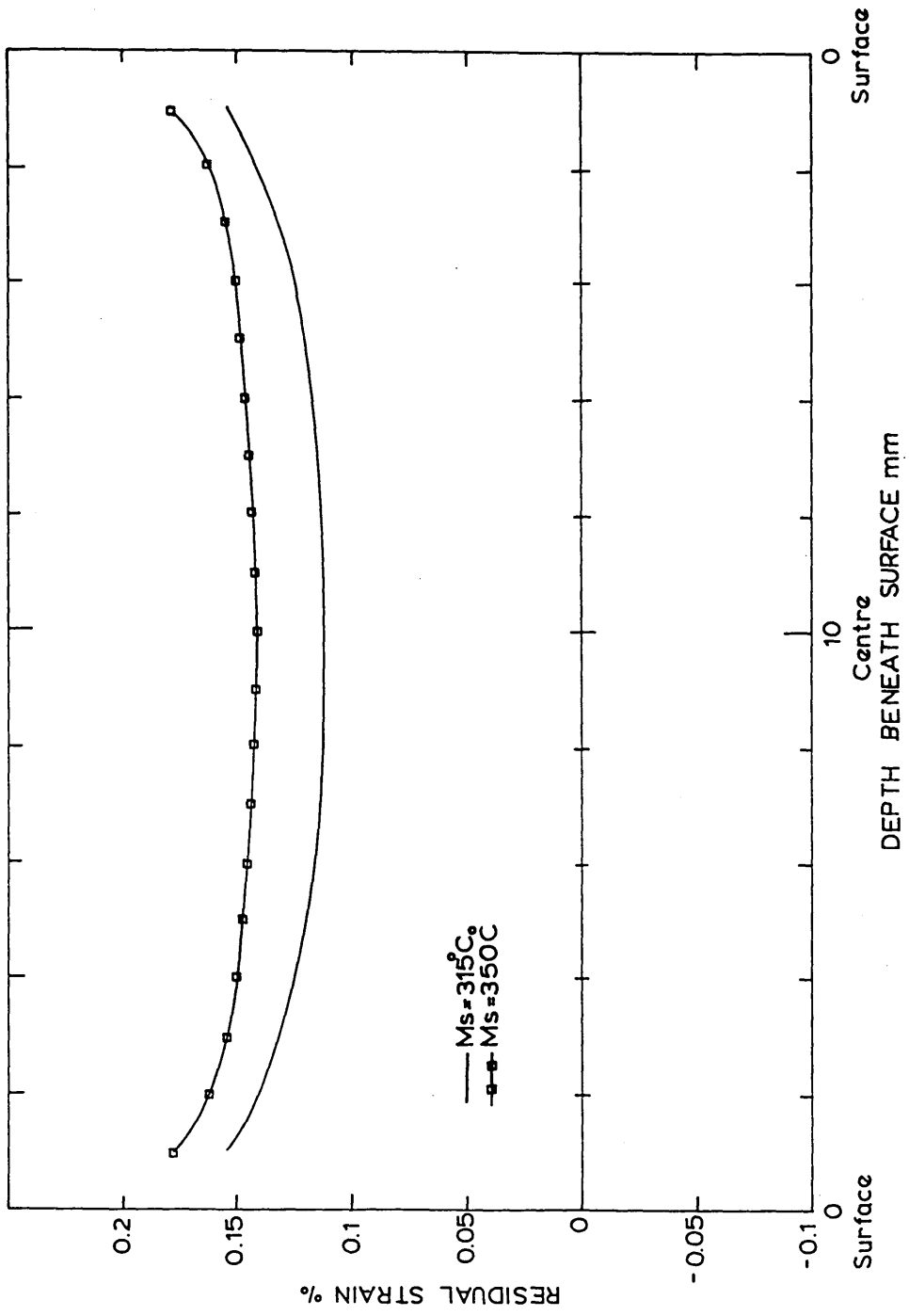
RESIDUAL STRAIN %
0.2
0.15
0.1
0.05
0
-0.05
-0.1
Ms=315°C
Ms=350C
0
Surface
10
Centre
0
Surface
DEPTH BENEATH SURFACE mm

FIGURE 95: 835M30 Steel specimen used for the experimental determination of residual stress and strain.

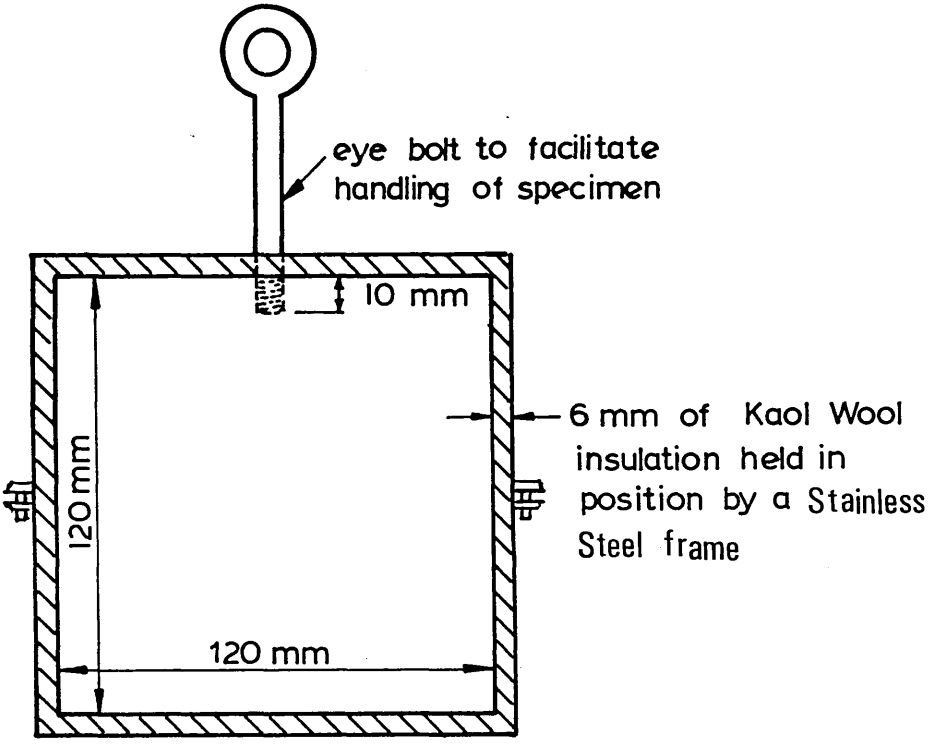

Material - 835M30 steel, all surfaces plated with 0·05 mm of nickel.

FIGURE 96: Quenching tank, fixture and stirrers used during the experimental quenching.

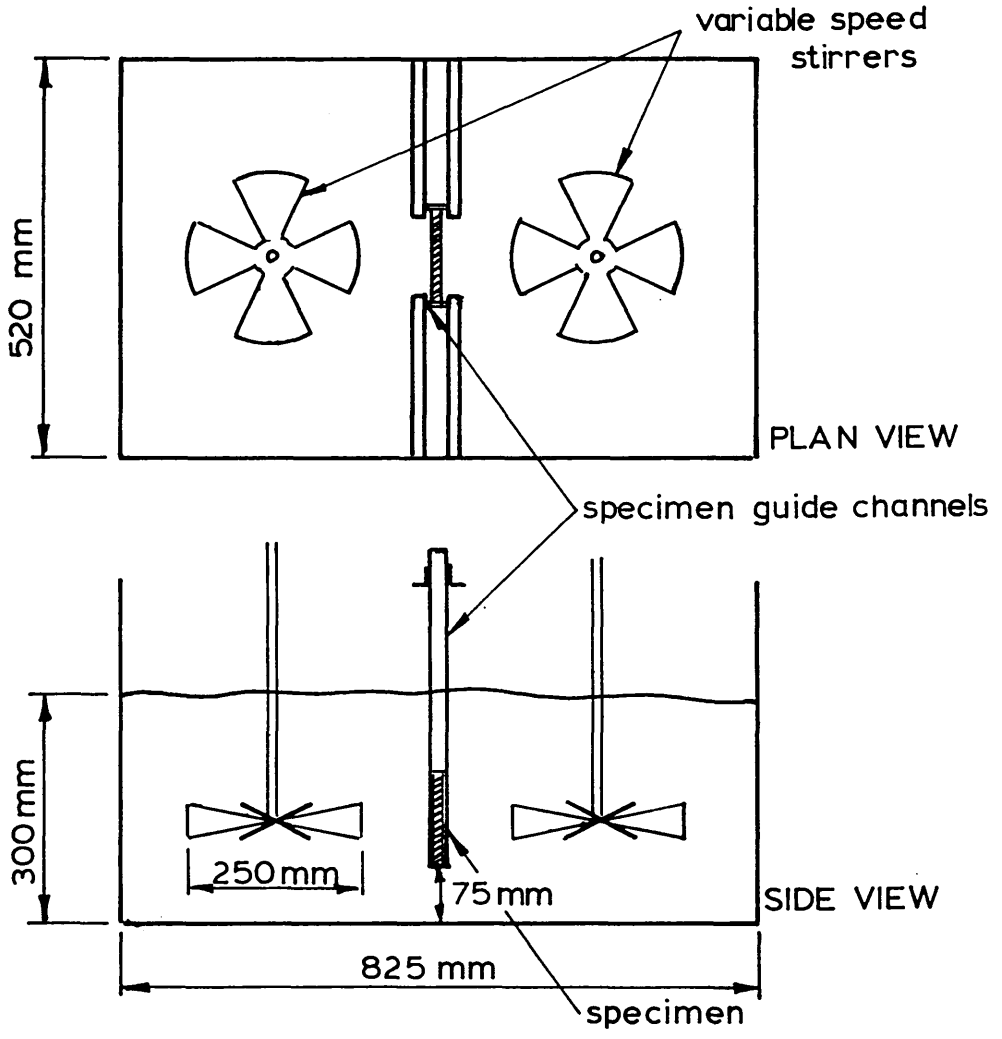
variable speed
stirrers
520 mm
PLAN VIEW
specimen guide channels
300mm
250mm
75mm
SIDE VIEW
825 mm
specimen

FIGURE 97: The plate specimens showing the location of the measurements used to determine the distortion between the edges of the plate.

a. 20 mm plate
b. 15 mm plate

a.

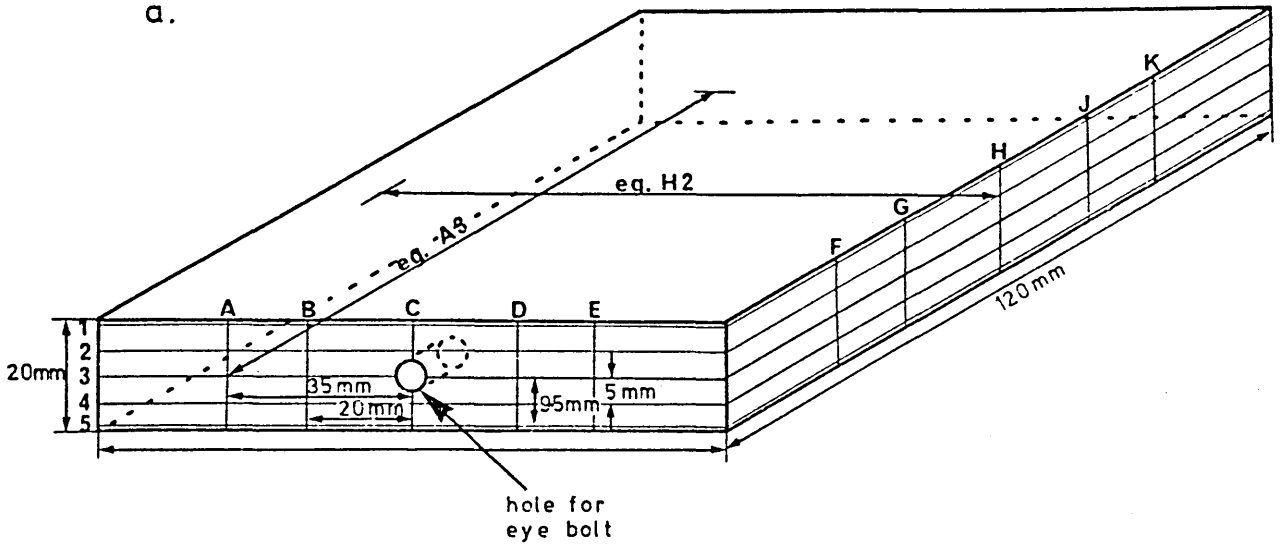
eg. H2
eg. A3
A
B
C
D
E
F
G
H
J
K
1
2
3
4
5
20mm
35 mm
20mm
95mm
5 mm
120 mm
hole for
eye bolt

b.

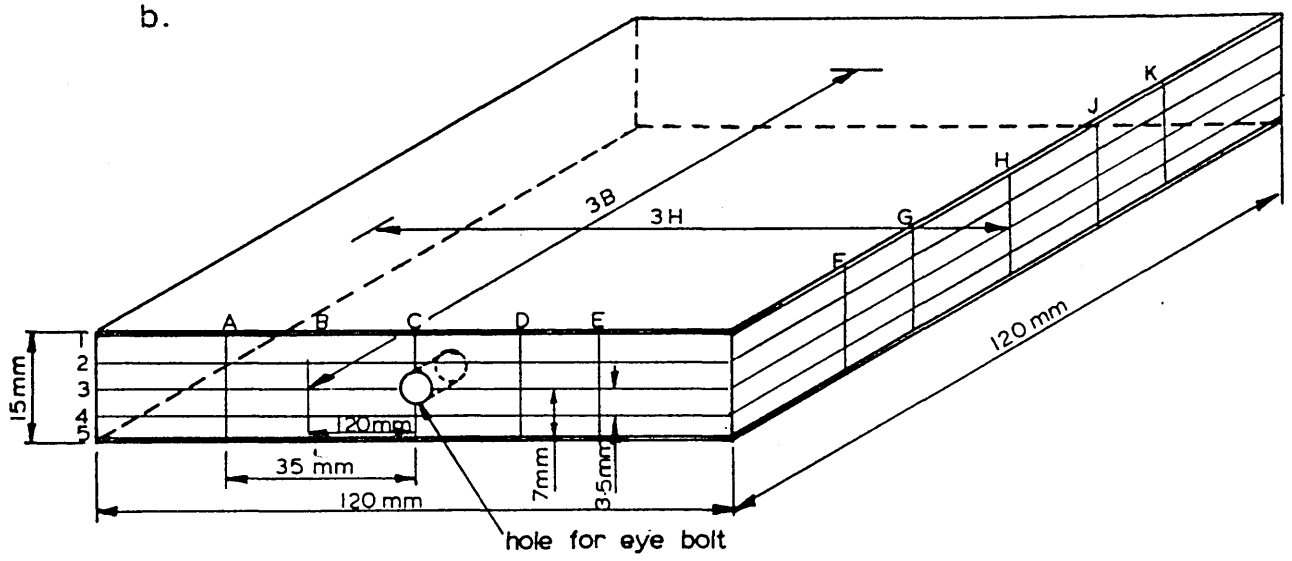
3B
3H
A
B
C
D
E
F
G
H
J
K
1
2
3
4
5
15mm
120mm
35 mm
120 mm
7mm
3.5mm
120 mm
hole for eye bolt

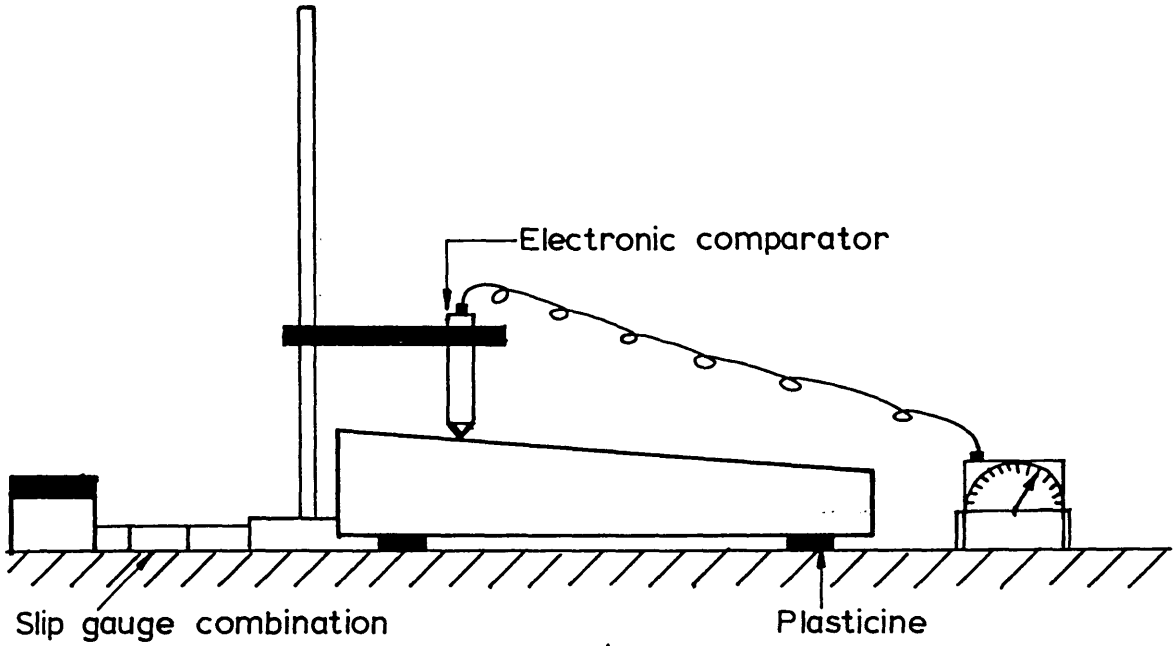
Electronic comparator
Slip gauge combination
Plasticine

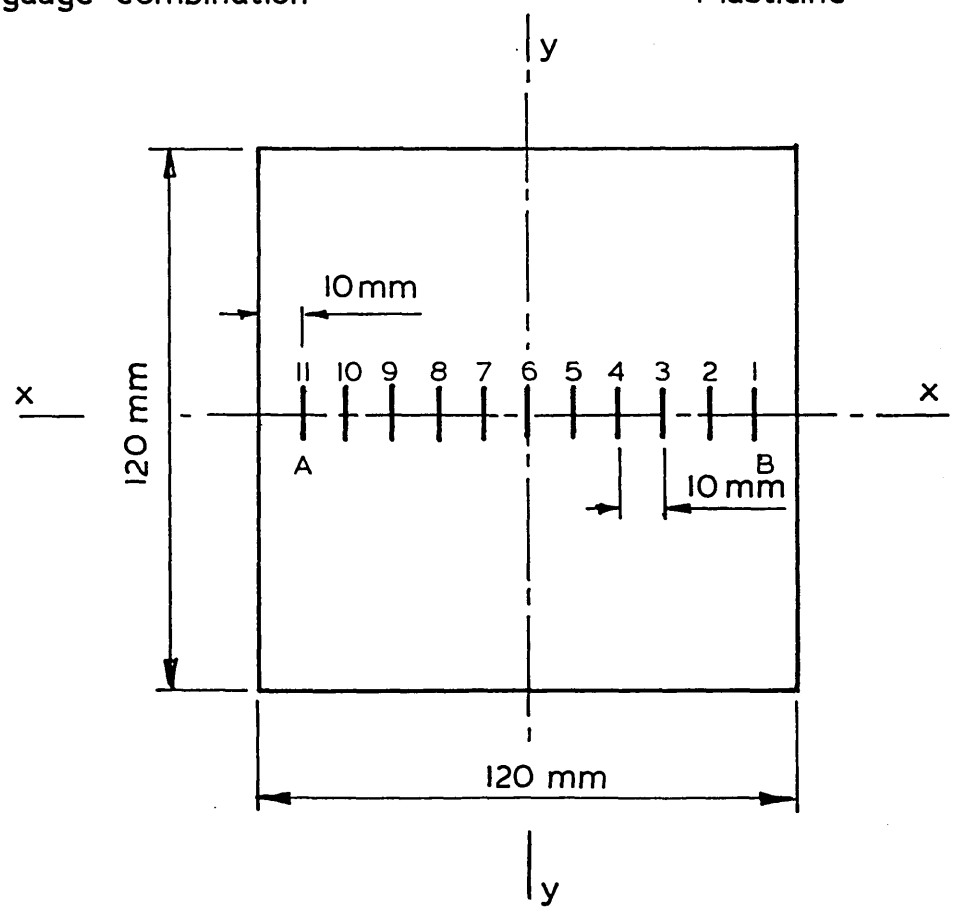
y
x
x
10 mm
11 10 9 8 7 6 5 4 3 2 1
A
B
10 mm
120 mm
120 mm
y

FIGURE 99: Positions at which the comparator readings are taken to determine the through thickness of the plate.

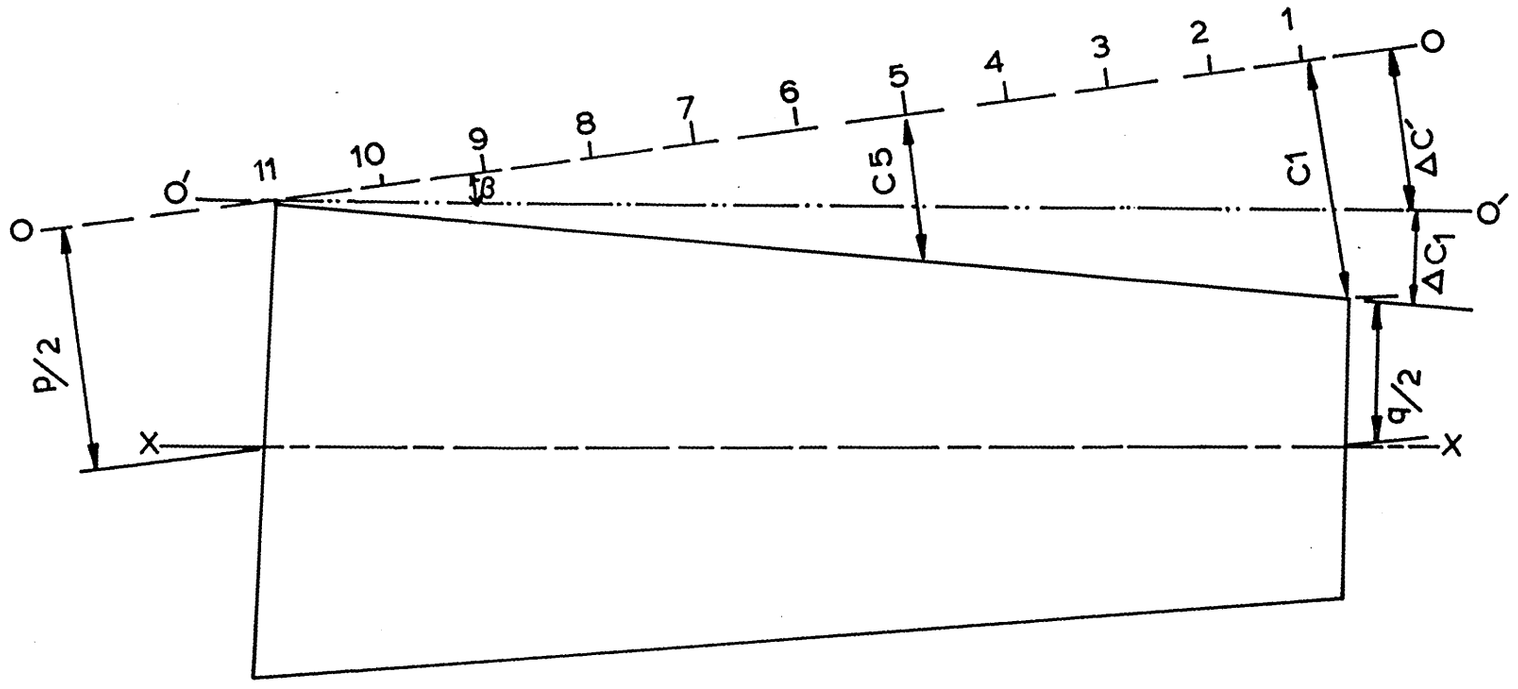

i. $\Delta C' = C1 - (\frac{p-q}{2})$

ii. $\Delta C1 = C1 - \Delta C'$

iii. $\frac{1}{2} T_1 = \frac{p}{2} - \Delta C1$

FIGURE 100: Plan view of underside of the plate showing strain gauge installation prior to surface grinding of the opposite surface of the plate for the residual stress determination.

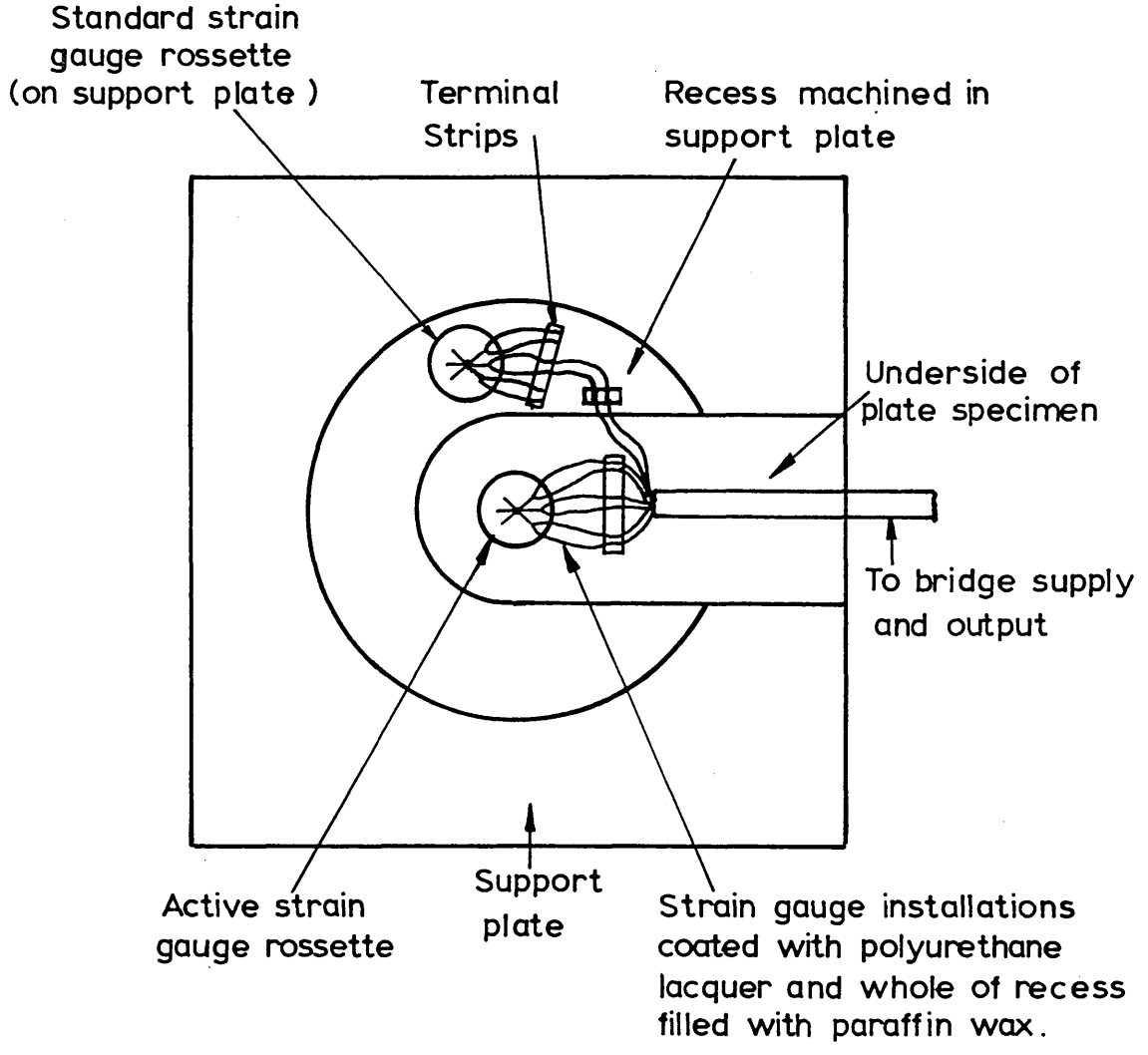
Standard strain gauge rossette (on support plate)
Terminal Strips
Recess machined in support plate
Underside of plate specimen
To bridge supply and output
Active strain gauge rossette
Support plate
Strain gauge installations coated with polyurethane lacquer and whole of recess filled with paraffin wax.

VOLT METER
AMPLIFIER AND BALANCE UNIT
Strain rosette on the specimen plate
Strain rosette on the support plate
o/p
Wheatstone bridge
+
-
o/p
1
2
3
4
5
6
6 V.DC
POWER SUPPLY
240 V.AC

FIGURE 102: Experimentally determined residual strain distribution in a 20 mm plate after water quenching. (After Price)[18].

—O— Measured between the edges of plate.

— — — Obtained from the change in thickness of plate.

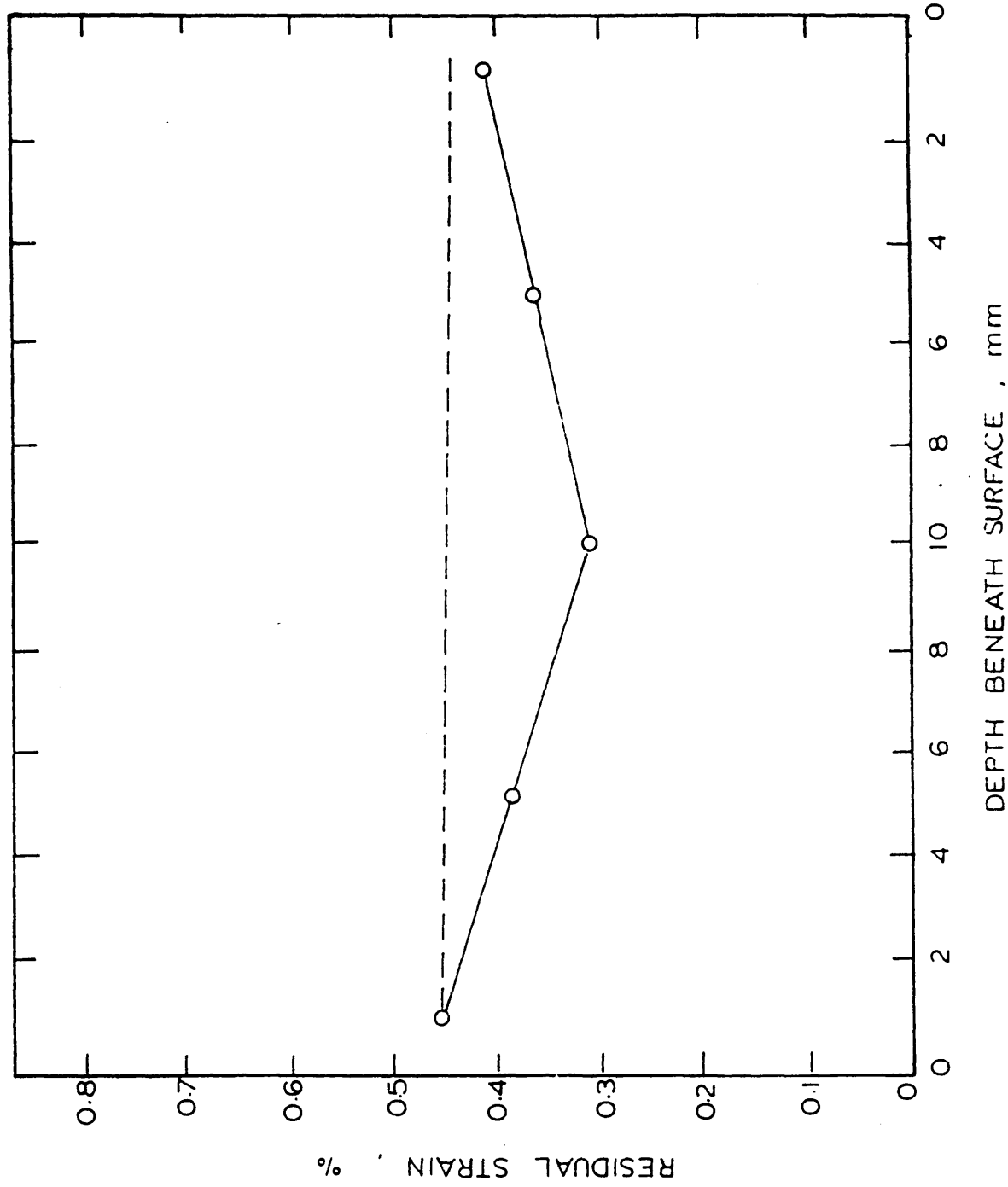
RESIDUAL STRAIN , %
0.8
0.7
0.6
0.5
0.4
0.3
0.2
0.1
0
0
2
4
6
8
10
8
6
4
2
0
DEPTH BENEATH SURFACE , mm

FIGURE 103: Experimentally determined residual stress distribution in a 20 mm plate after water quenching.

(After Price)[18].

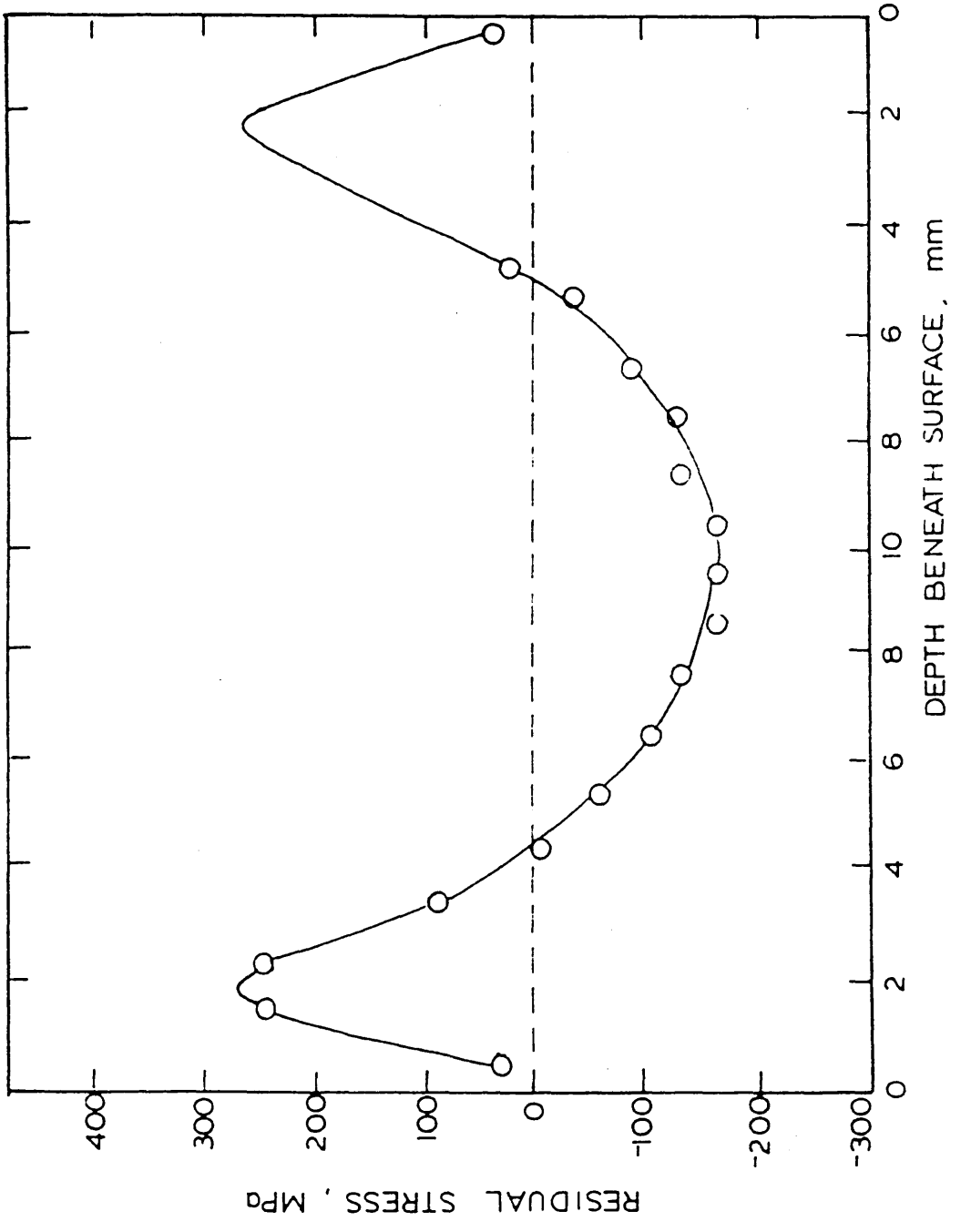
RESIDUAL STRESS, MPa
400
300
200
100
0
-100
-200
-300
0
2
4
6
8
10
8
6
4
2
0
DEPTH BENEATH SURFACE, mm

FIGURE 104: Experimentally determined residual strain distribution in a 15 mm plate after oil quenching.

(After Abbasi)[41].

—o— Measured between the edges of plate.

— — — Obtained from the change in thickness of plate.

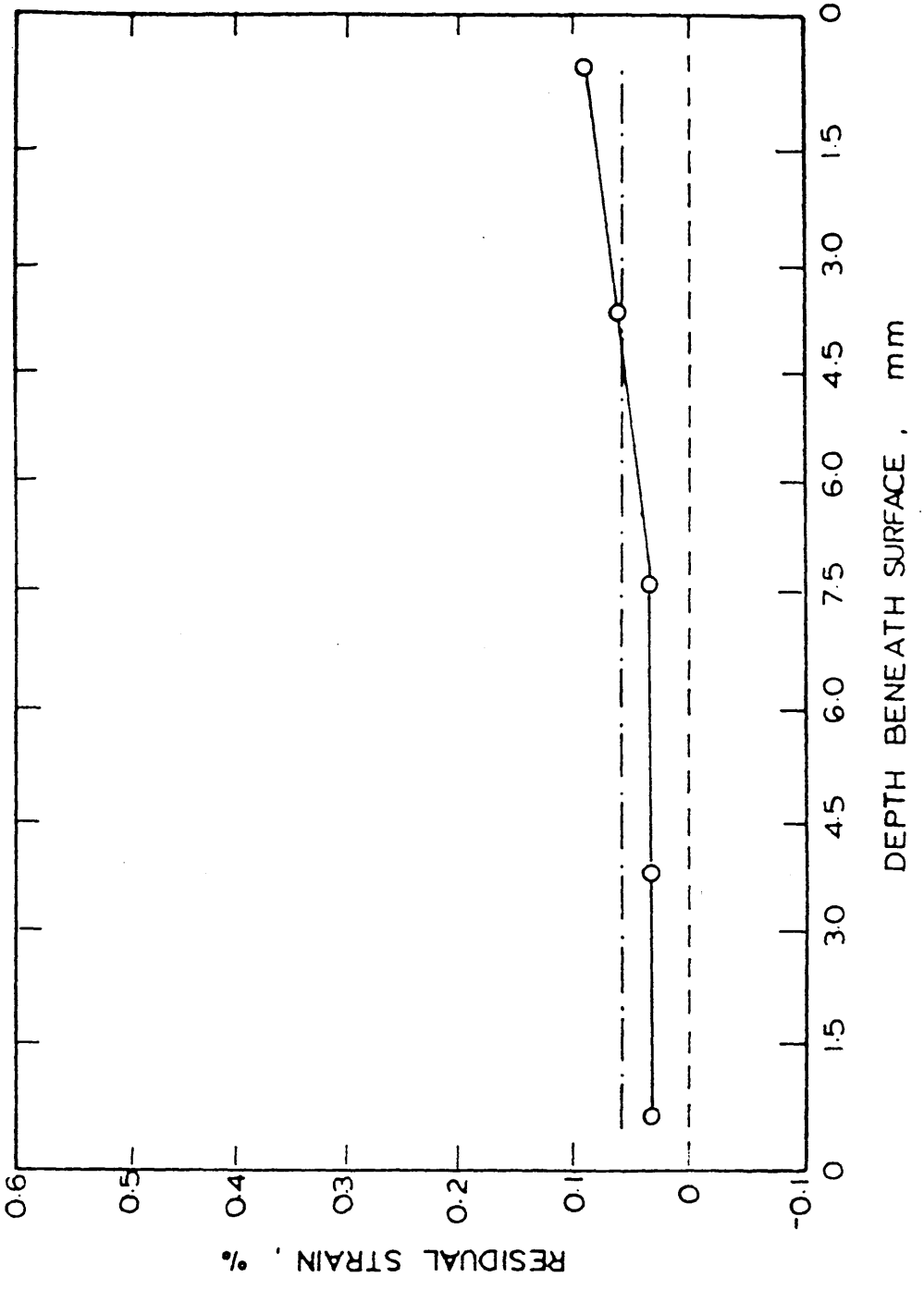
RESIDUAL STRAIN , %
0.6
0.5
0.4
0.3
0.2
0.1
0
-0.1
DEPTH BENEATH SURFACE , mm
0
1.5
3.0
4.5
6.0
7.5
6.0
4.5
3.0
1.5
0

FIGURE 105: Experimentally determined residual stress distribution in a 15 mm plate after oil quenching. (After Abbasi)[41].

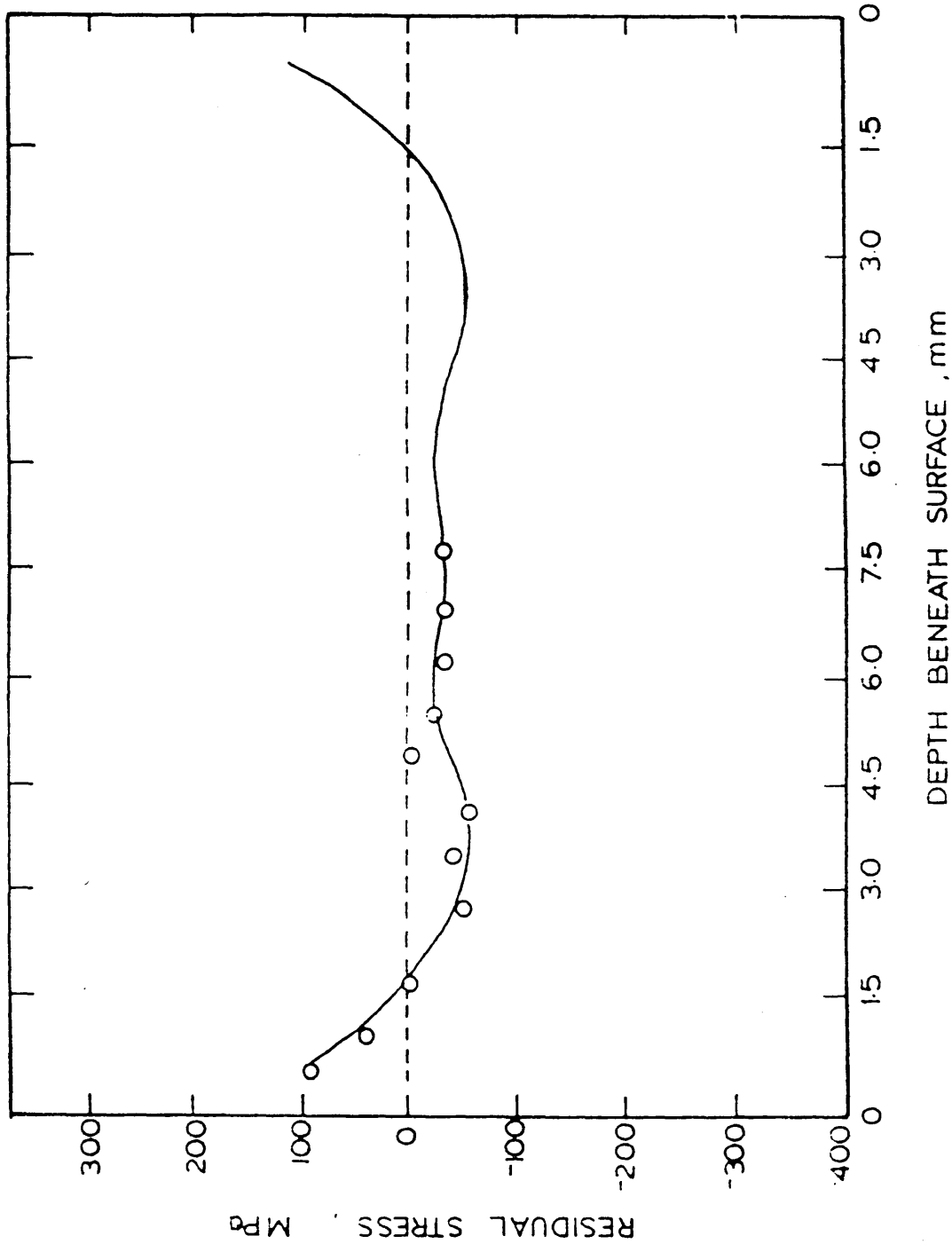
RESIDUAL STRESS , MPa
300
200
100
0
-100
-200
-300
-400
0
1.5
3.0
4.5
6.0
7.5
6.0
4.5
3.0
1.5
0
DEPTH BENEATH SURFACE , mm

FIGURE 106: Experimentally determined residual strain distribution in a 15 mm plate after martempering (followed by oil quenching).

—O— Measured between the edges of plate.

— — — Obtained from the change in thickness of plate.

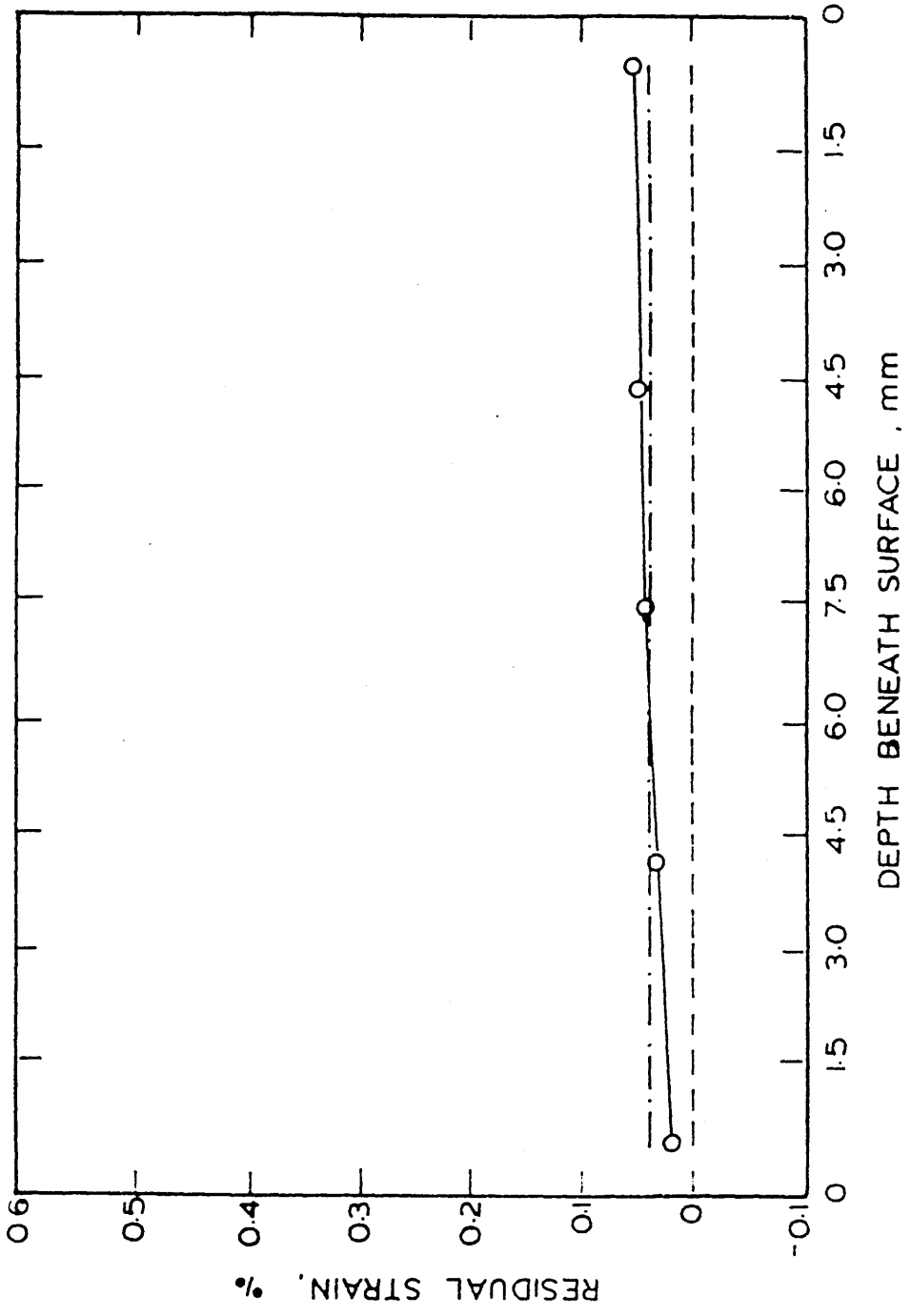
RESIDUAL STRAIN, %
0.6
0.5
0.4
0.3
0.2
0.1
0
-0.1
DEPTH BENEATH SURFACE, mm
0
1.5
3.0
4.5
6.0
7.5
6.0
4.5
3.0
1.5
0

FIGURE 107: Experimentally determined residual stress distribution in a 15 mm plate after martempering (followed by oil quenching).

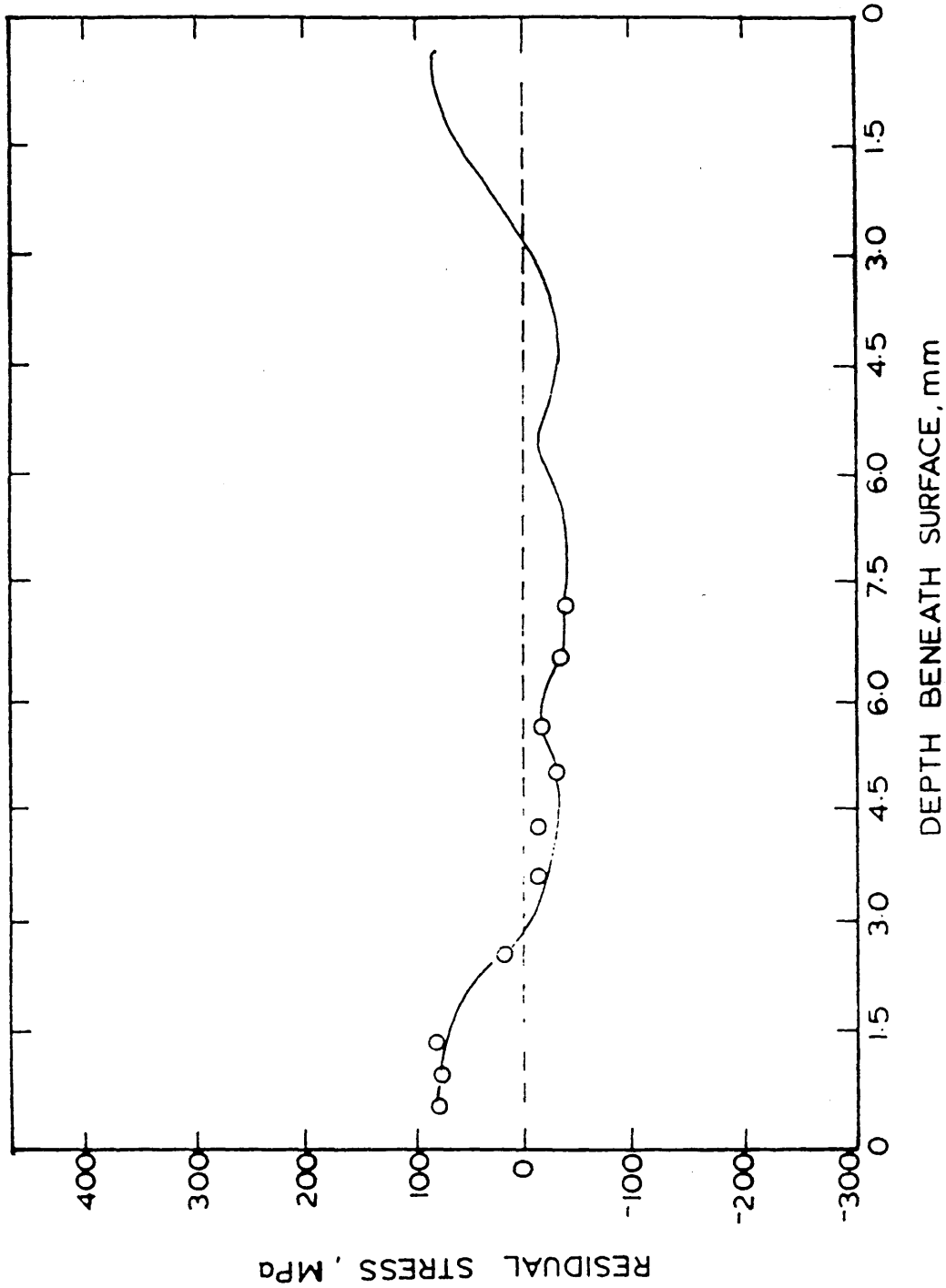
RESIDUAL STRESS, MPa
400
300
200
100
0
-100
-200
-300
0
1.5
3.0
4.5
6.0
7.5
6.0
4.5
3.0
1.5
0
DEPTH BENEATH SURFACE, mm

FIGURE 108: Experimentally determined residual strain distribution in a 20 mm plate after Polymer quenching.

—O— Measured between the edges of plate.

— — — Obtained from the change in thickness of plate.

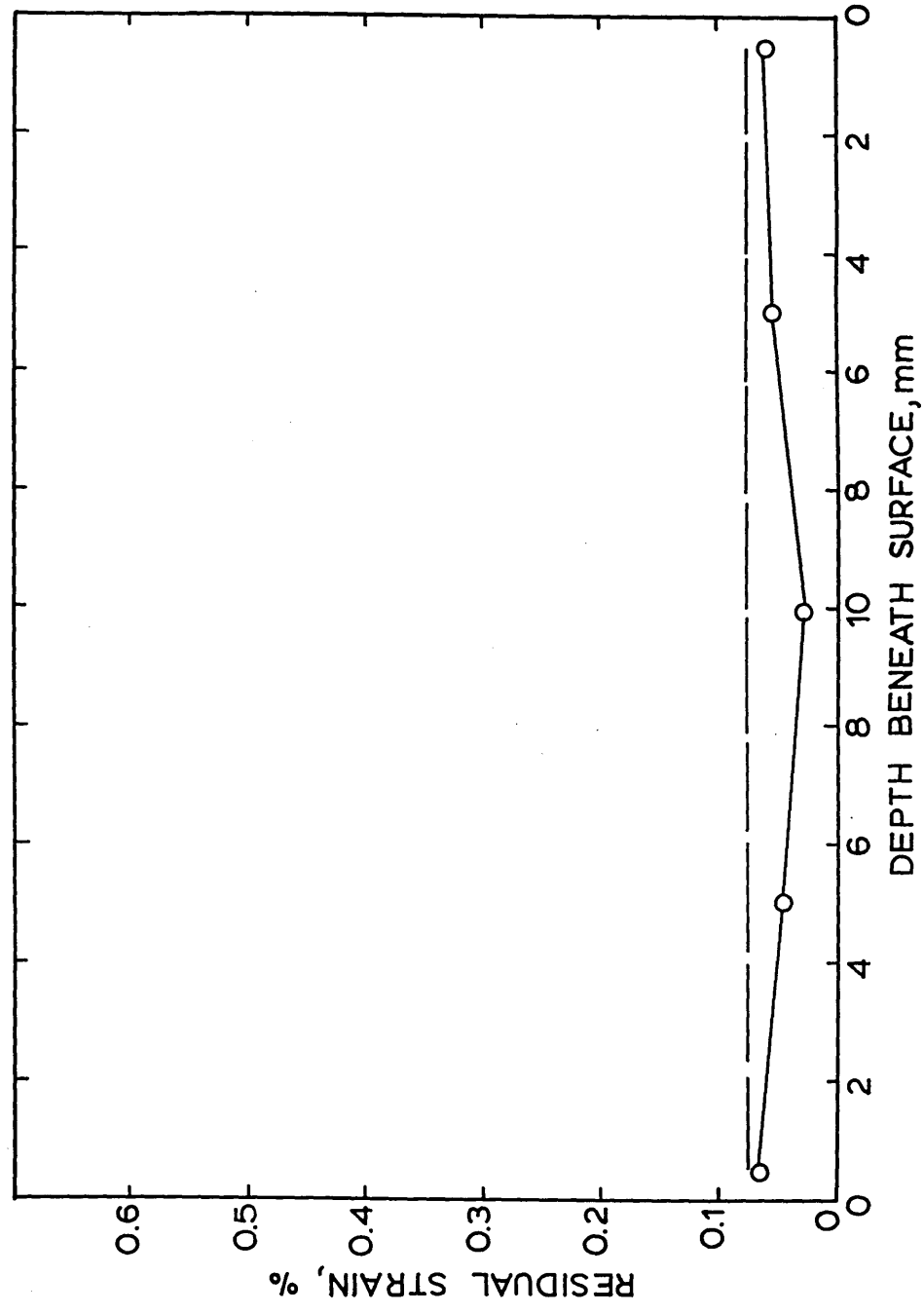
RESIDUAL STRAIN, %
0.6
0.5
0.4
0.3
0.2
0.1
0
0
2
4
6
8
10
8
6
4
2
0
DEPTH BENEATH SURFACE, mm

FIGURE 109: Experimentally determined residual stress distribution in a 20 mm plate after Polymer quenching.

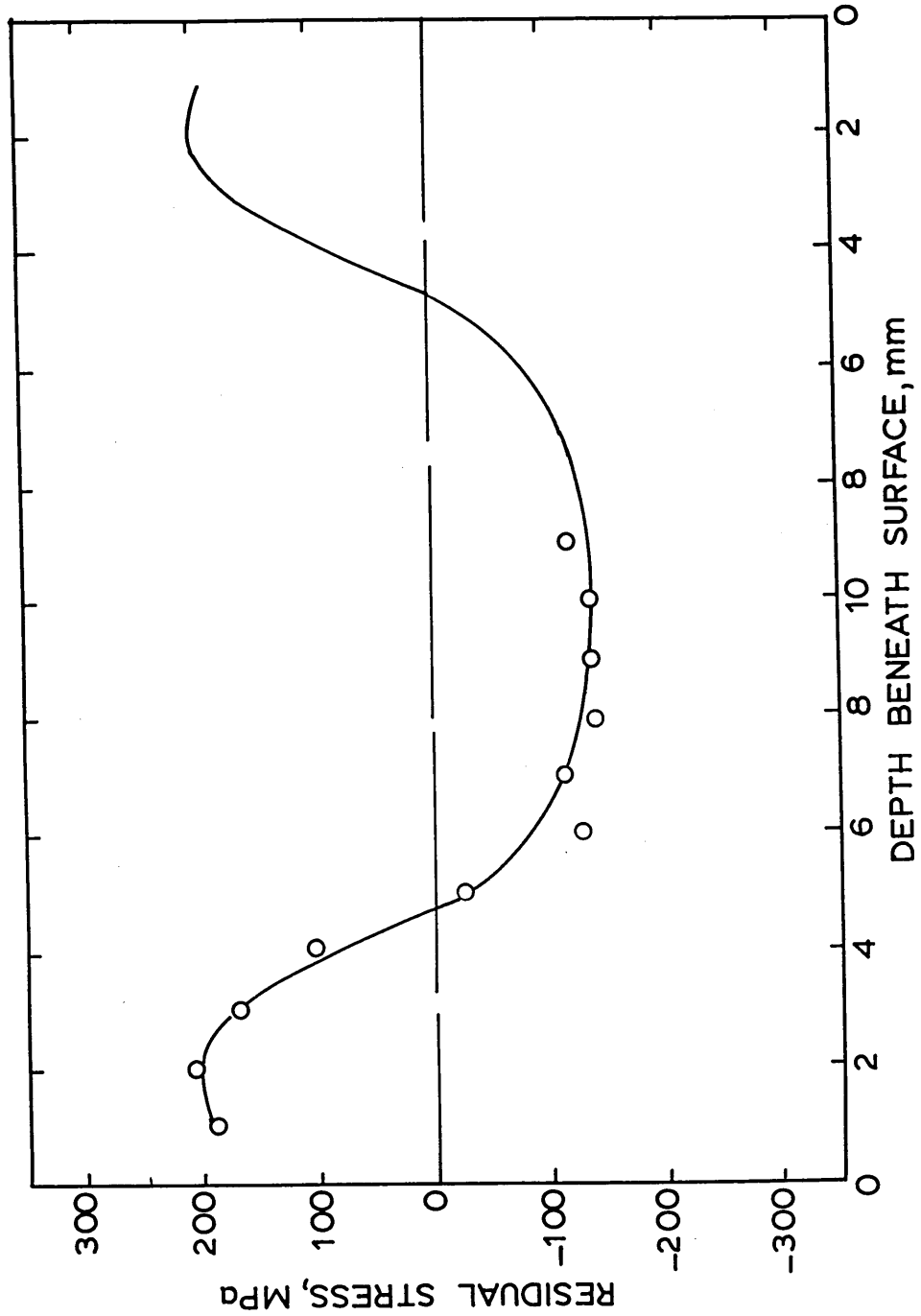
RESIDUAL STRESS, MPa
300
200
100
0
-100
-200
-300
0
2
4
6
8
10
DEPTH BENEATH SURFACE, mm
0
2
4
6
8

FIGURE 111: Experimentally determined residual stress distribution in a 15 mm plate after martempering (followed by air cooling).

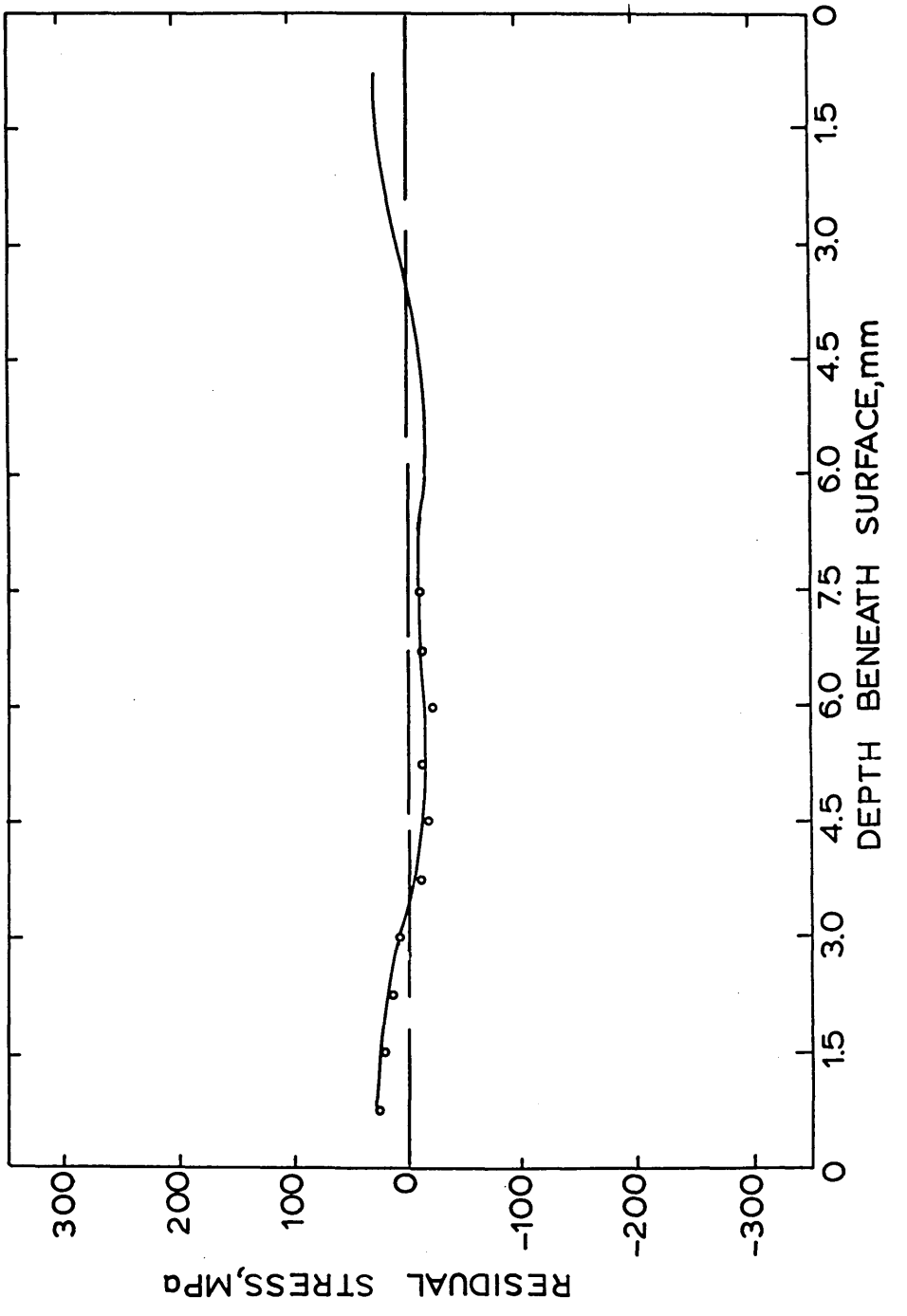
RESIDUAL STRESS,MPa
300
200
100
0
-100
-200
-300
0
1.5
3.0
4.5
6.0
7.5
6.0
4.5
3.0
1.5
0
DEPTH BENEATH SURFACE,mm

FIGURE 112: Schematic representation of characteristic stages in the relationship between stress and strain at the surface and the centre of a plate during quenching.

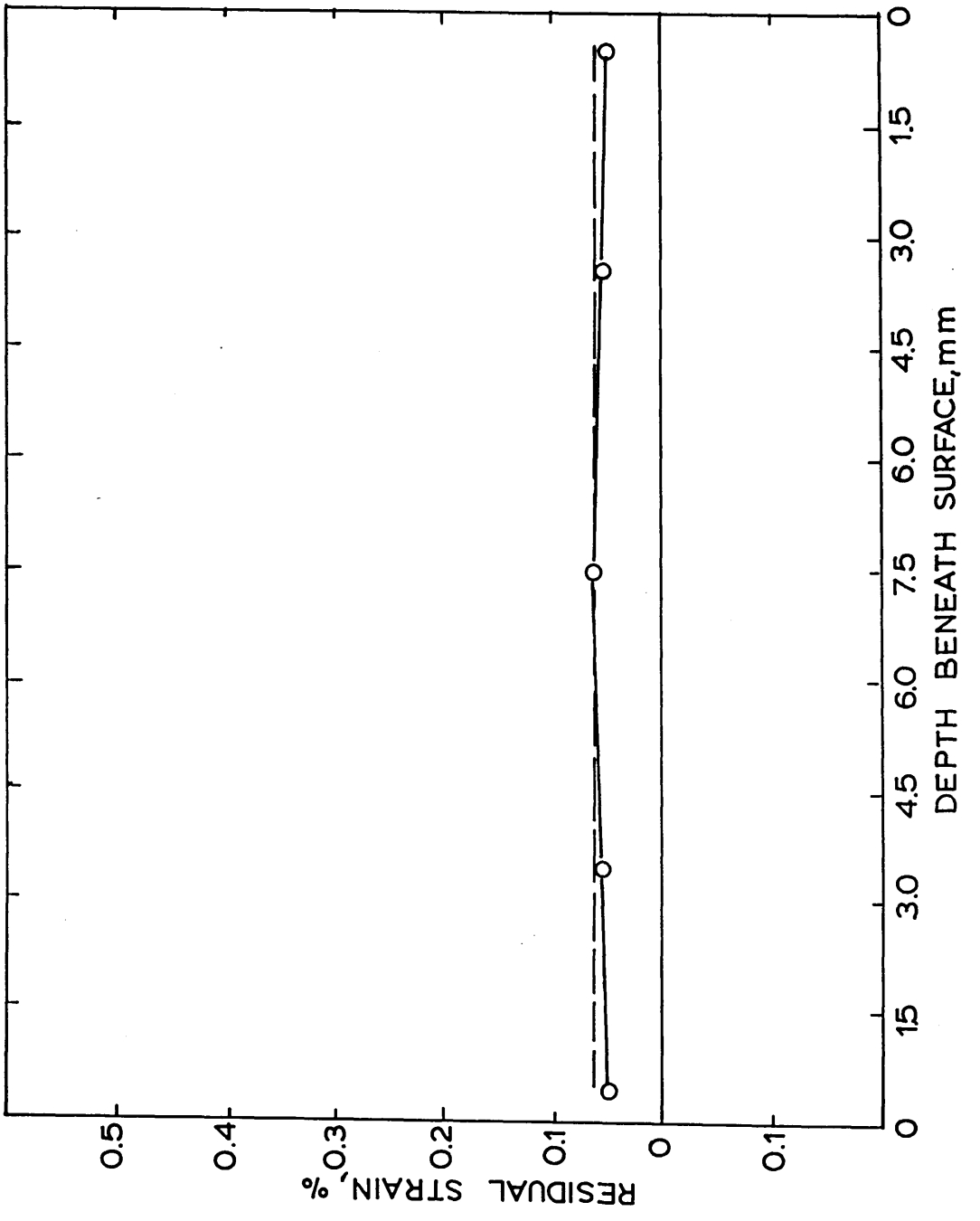
RESIDUAL STRAIN, %
0.5
0.4
0.3
0.2
0.1
0
0.1
0
15
3.0
4.5
6.0
7.5
6.0
4.5
3.0
1.5
0
DEPTH BENEATH SURFACE, mm

FIGURE 110: Experimentally determined residual strain distribution in a 15 mm plate after martempering (followed by air cooling).

—O— Measured between the edges of plate.

— — — Obtained from change in thickness of plate.

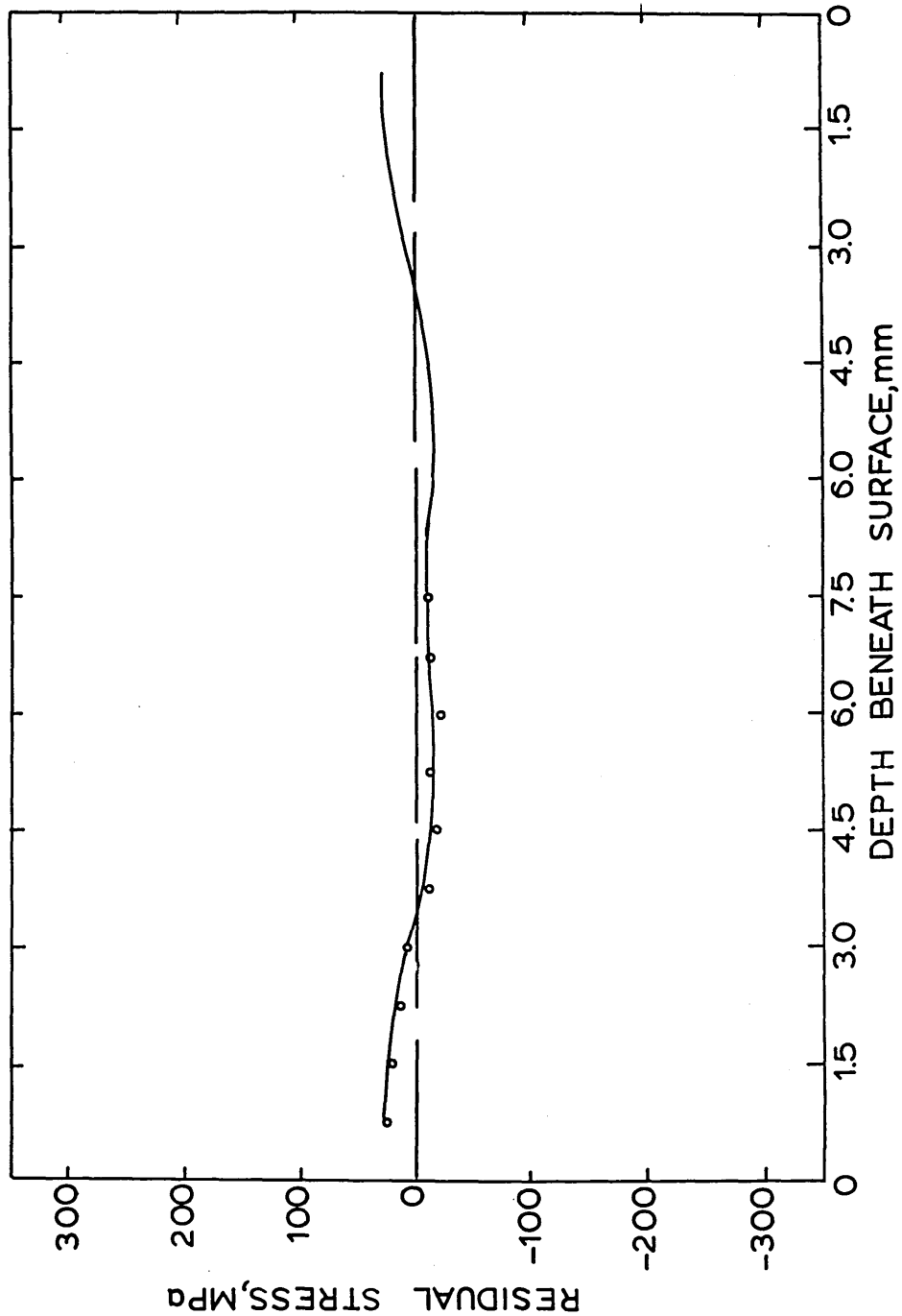
RESIDUAL STRESS,MPa
300
200
100
0
-100
-200
-300
0
1.5
3.0
4.5
6.0
7.5
6.0
4.5
3.0
1.5
0
DEPTH BENEATH SURFACE,mm

FIGURE 111: Experimentally determined residual stress distribution in a 15 mm plate after martempering (followed by air cooling).

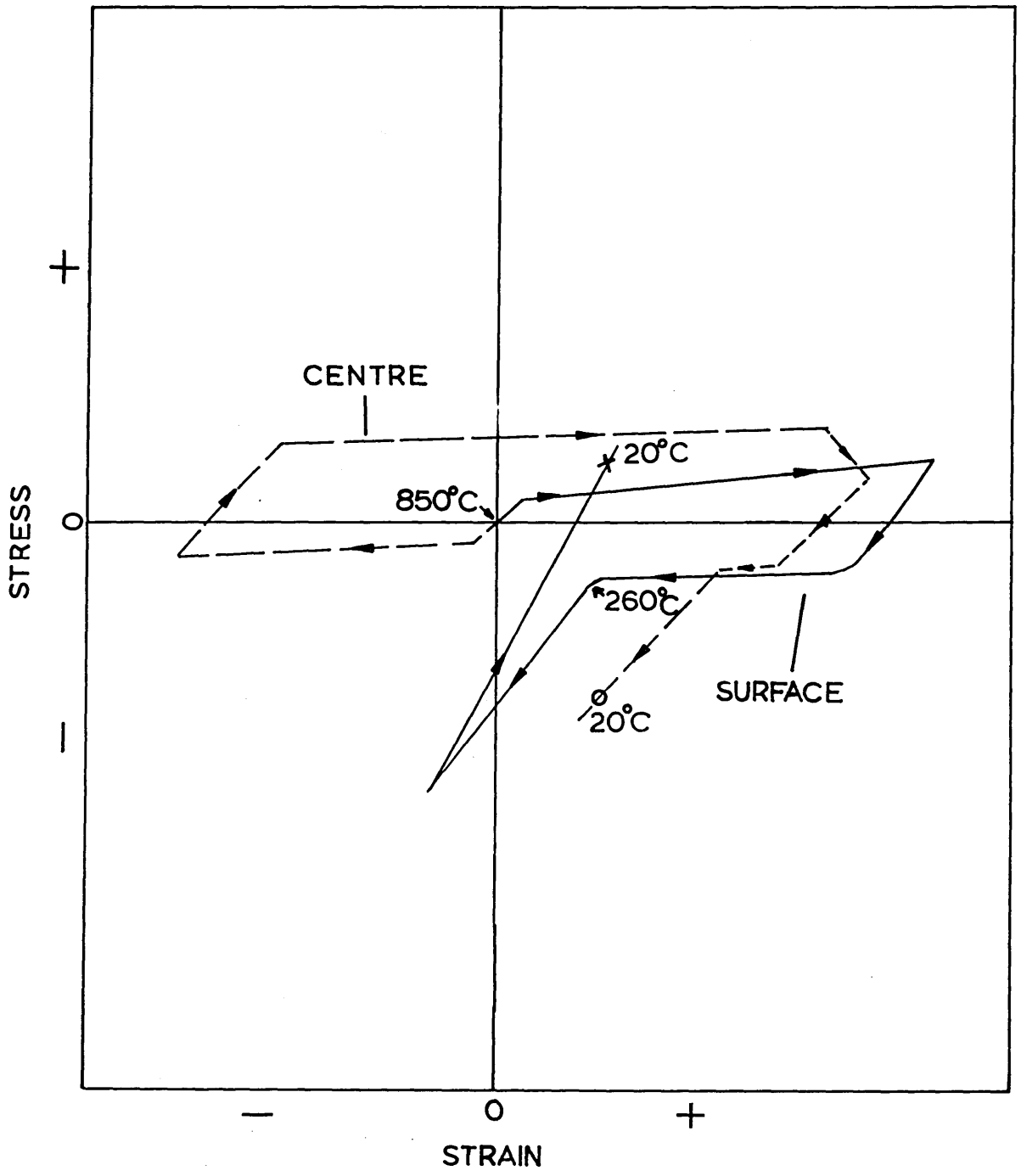
+
CENTRE
20°C
850°C
STRESS
0
260°C
SURFACE
20°C
−
0
+
STRAIN

FIGURE 113: Calculated stress and strain at the surface and the centre of a 15 mm plate during oil quenching (viscous flow as represented by method 1).

(After Abbasi[41]).

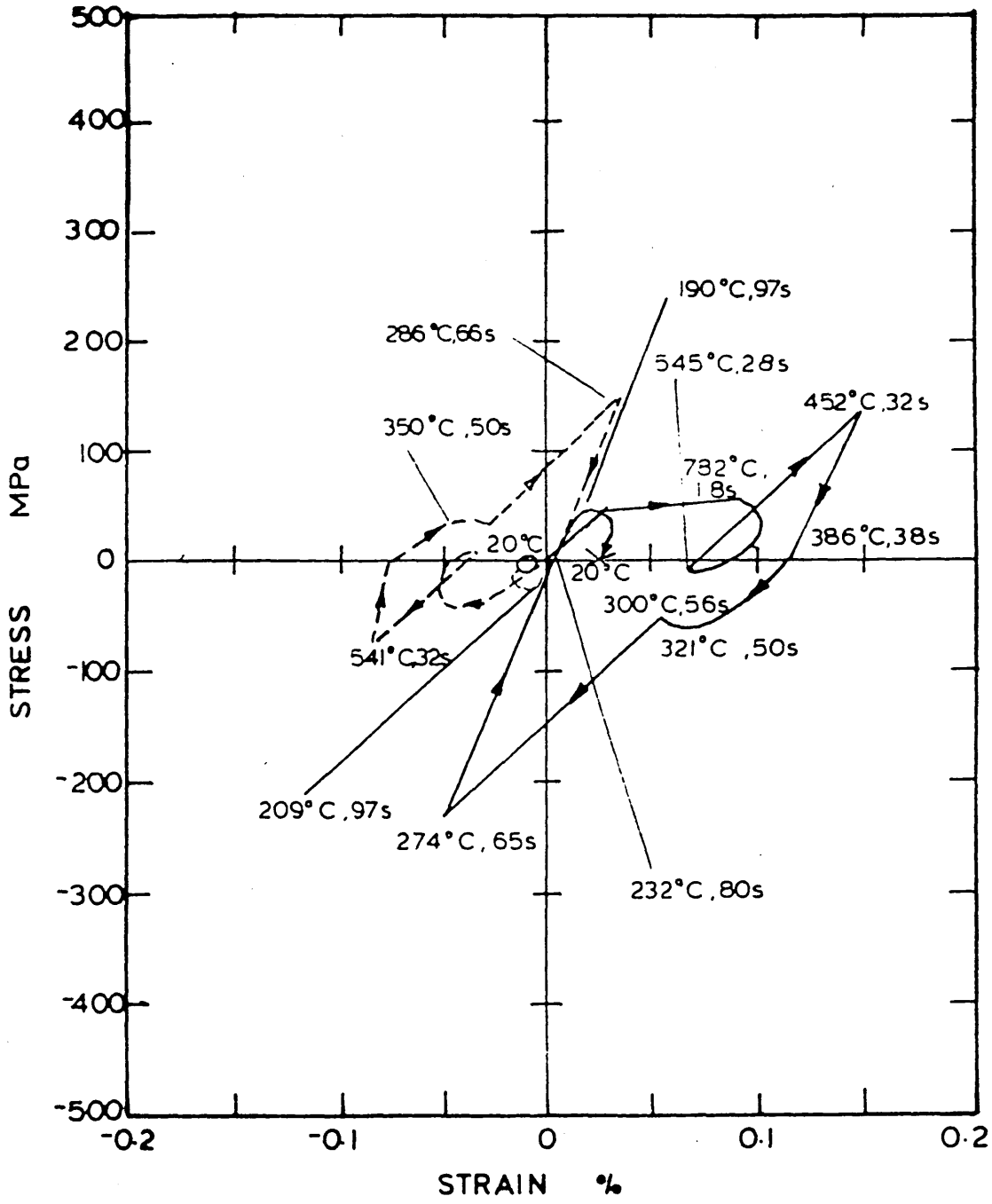
500
400
300
200
100
0
-100
-200
-300
-400
-500
-0·2
-0·1
0
0·1
0·2
STRESS MPa
STRAIN %
190°C,97s
286°C,66s
545°C,28s
452°C,32s
350°C,50s
782°C,
18s
20°C
386°C,38s
20°C
300°C,56s
541°C,32s
321°C,50s
209°C,97s
274°C,65s
232°C,80s

FIGURE 114: Calculated stress and strain at the surface and the centre of a 20 mm plate during water quenching (viscous flow as represented by method one).

(After Abbasi)[41].

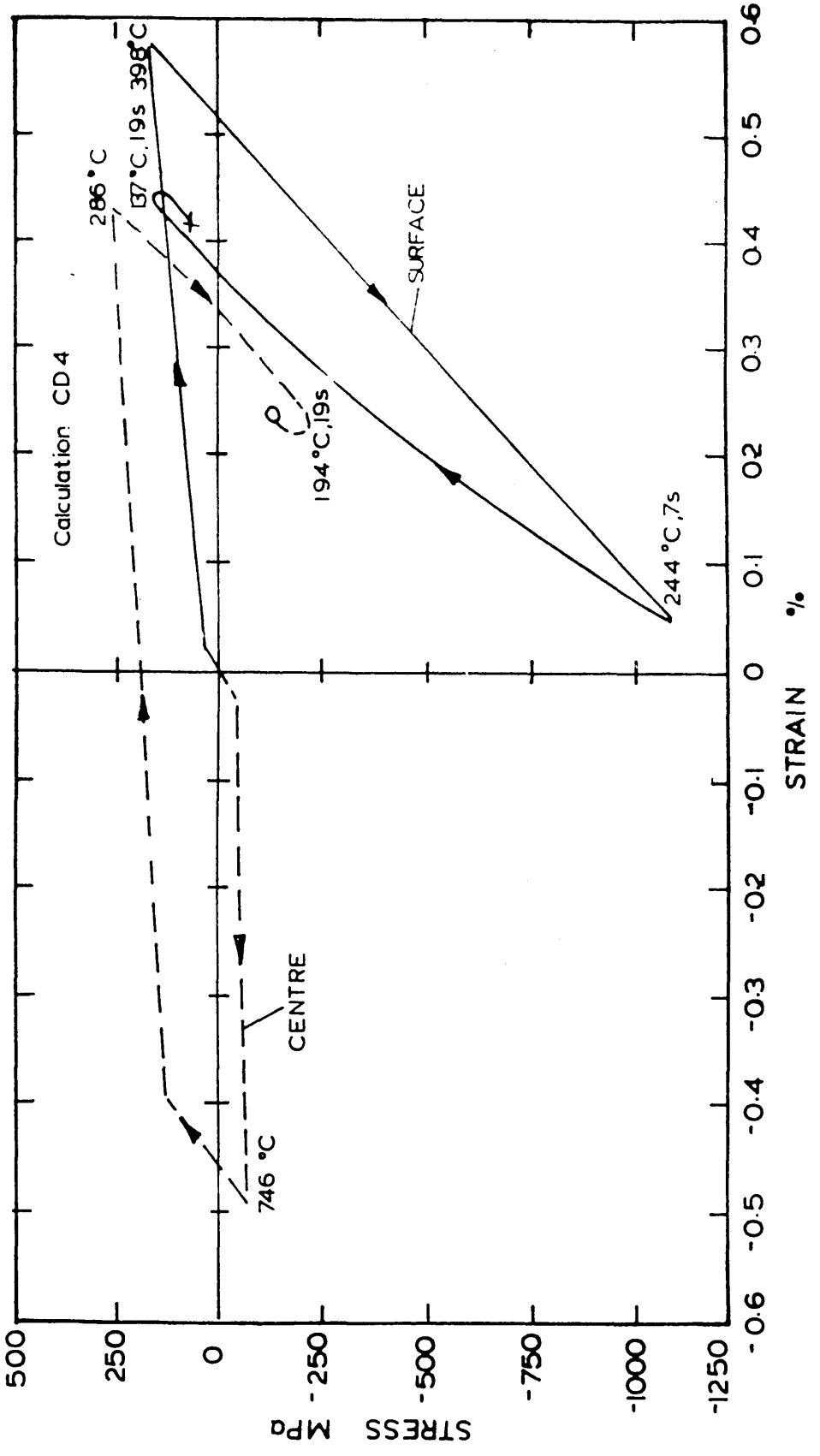
Calculation CD 4
286 °C
137 °C, 19s 398 °C
194 °C, 19s
244 °C, 7s
SURFACE
CENTRE
746 °C
STRESS MPa
STRAIN %
500
250
0
-250
-500
-750
-1000
-1250
0.6
0.5
0.4
0.3
0.2
0.1
0
-0.1
-0.2
-0.3
-0.4
-0.5
-0.6

FIGURE 115: Comparison of experimental and calculated residual stress distribution in a 20 mm plate after water quenching.

Calculation number:-

FP_1 - No stress relaxation.
FP_2^1 - Stress relaxation method 1.
FP_3^2 - Stress relaxation method 2.
FP_4^3 - Stress relaxation method 1 and transformation plasticity.
FP_5 - Stress relaxation method 2 and transformation plasticity.
FP_6 - Transformation plasticity, no stress relaxation.

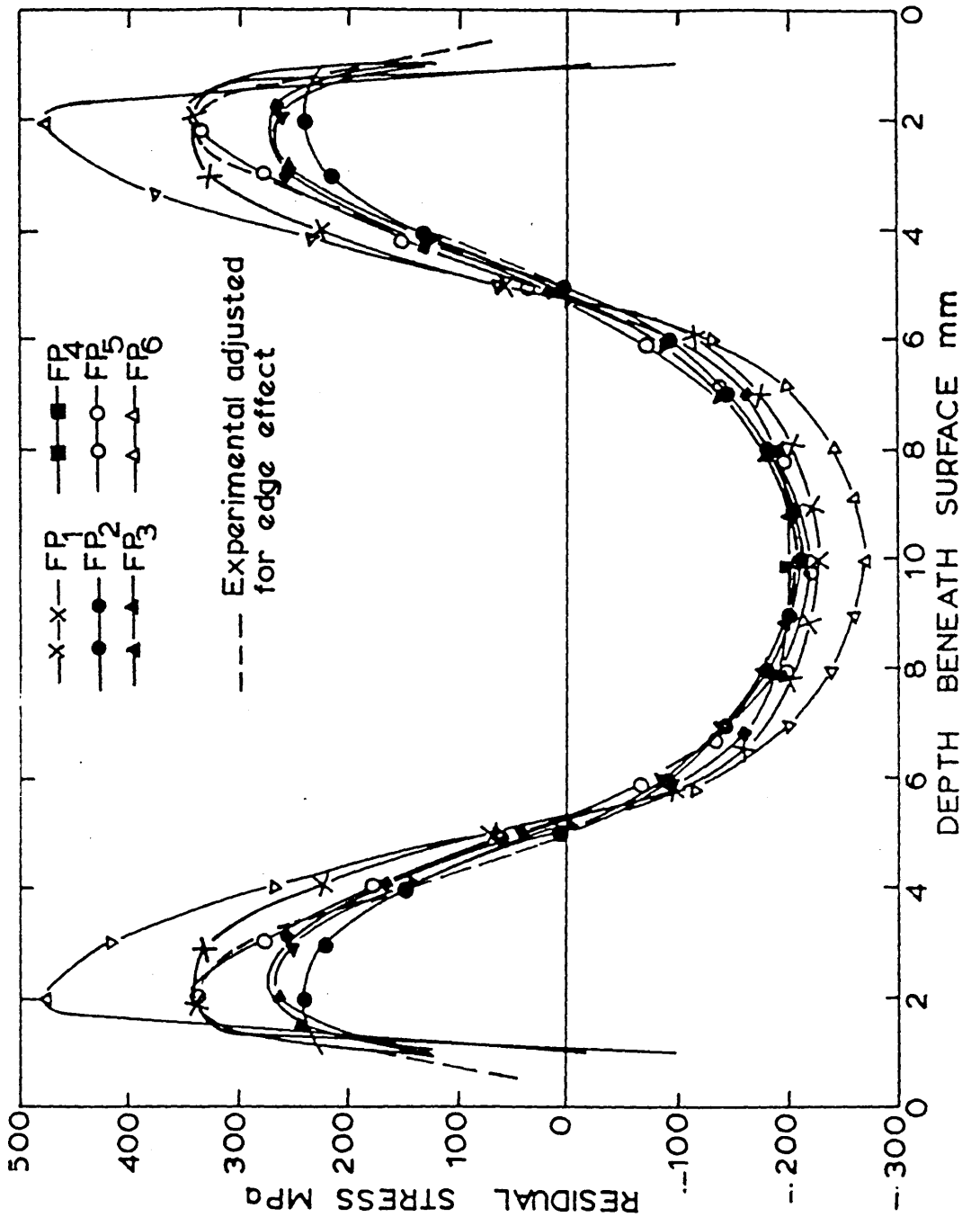
RESIDUAL STRESS MPa
500
400
300
200
100
0
-100
-200
-300
DEPTH BENEATH SURFACE mm
0
2
4
6
8
10
FP1
FP2
FP3
FP4
FP5
FP6
Experimental adjusted for edge effect

FIGURE 116: Comparison of experimental and calculated (viscous flow method two + transformation plasticity) residual stress distribution in a 20 mm plate after water quenching.

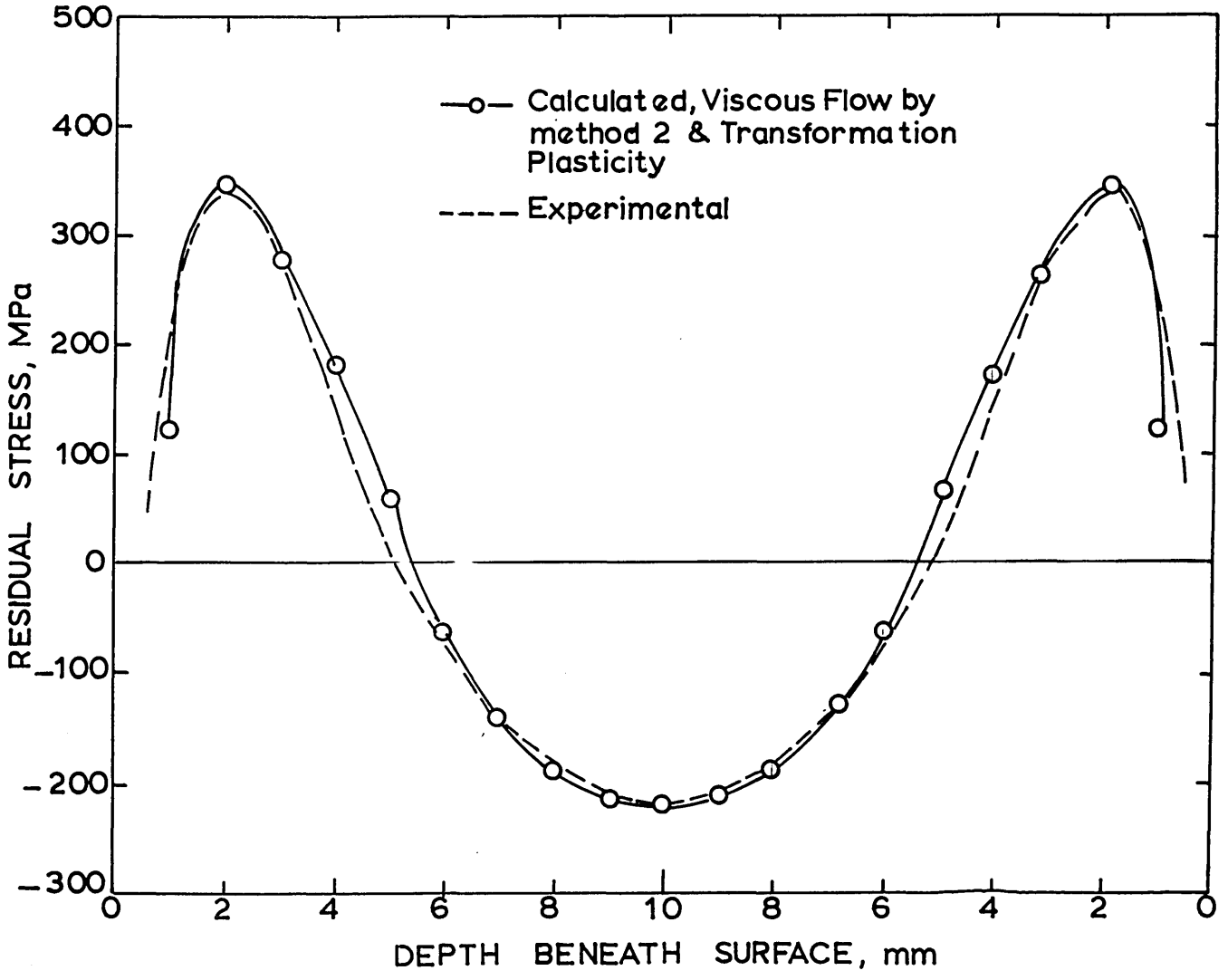
Calculated, Viscous Flow by method 2 & Transformation Plasticity
Experimental
RESIDUAL STRESS, MPa
500
400
300
200
100
0
-100
-200
-300
0
2
4
6
8
10
8
6
4
2
0
DEPTH BENEATH SURFACE, mm

FIGURE 117: Comparison of experimental and calculated residual strain distribution in a 20 mm plate after water quenching.

(For Key see figure 115).

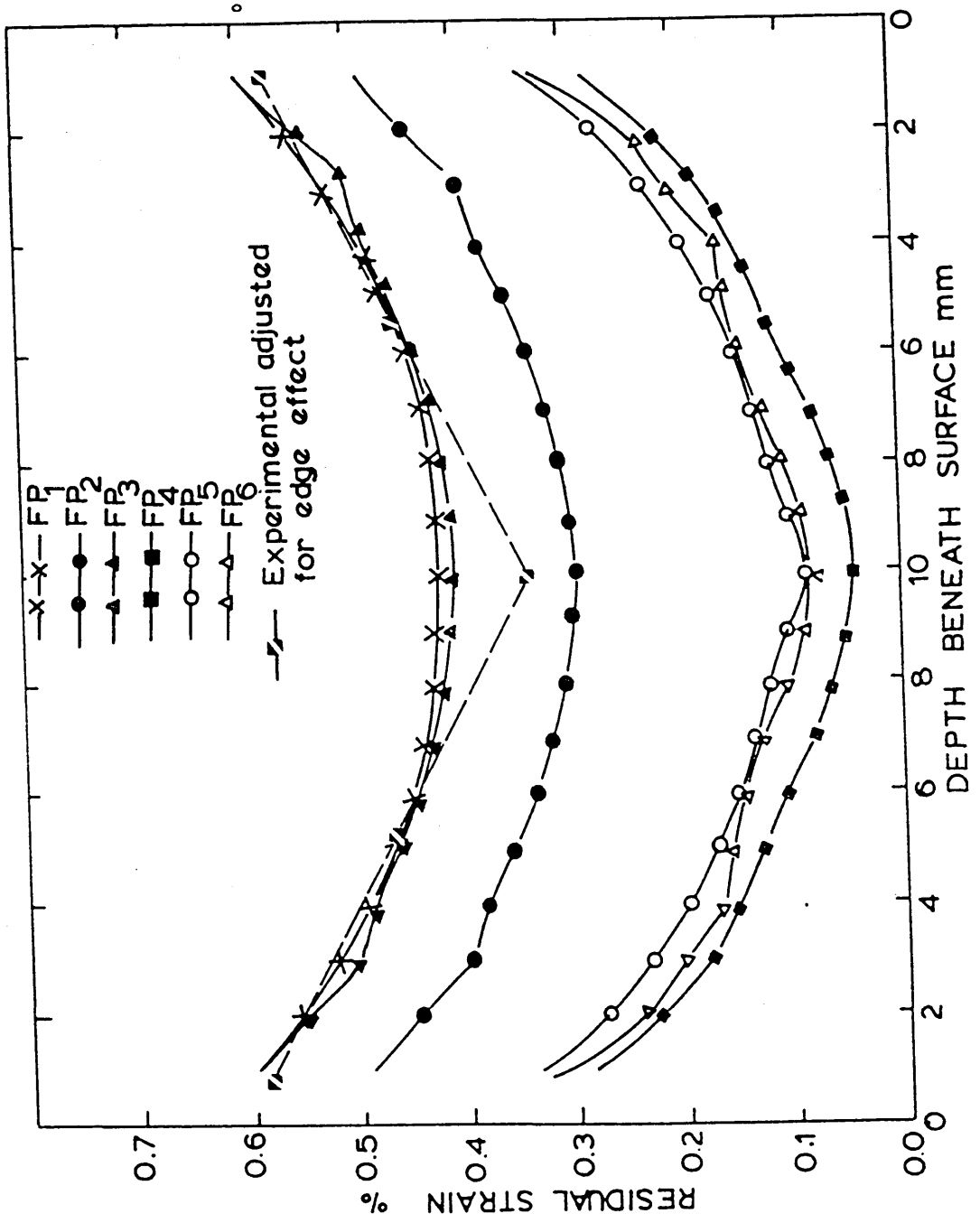
RESIDUAL STRAIN %
DEPTH BENEATH SURFACE mm
FP1
FP2
FP3
FP4
FP5
FP6
Experimental adjusted for edge effect

FIGURE 118: Comparison of experimental and calculated residual stress distribution in a 15 mm plate after oil quenching.

(For Key see figure 119).

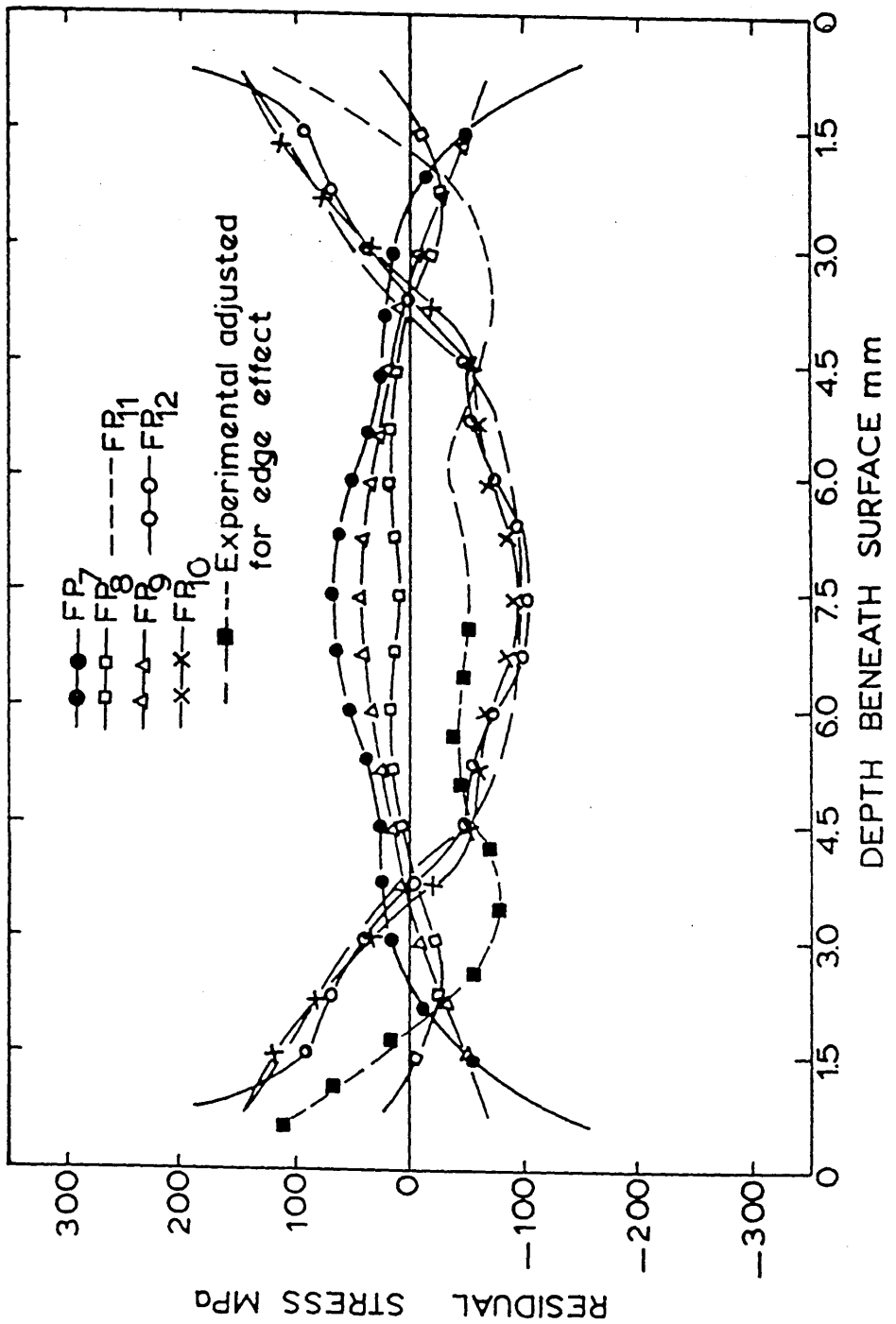
FP7
FP8
FP9
FP10
FP11
FP12
Experimental adjusted for edge effect
RESIDUAL STRESS MPa
300
200
100
0
−100
−200
−300
DEPTH BENEATH SURFACE mm
0
1.5
3.0
4.5
6.0
7.5
6.0
4.5
3.0
1.5
0

FIGURE 119: Comparison of experimental and calculated residual strain distribution in a 15 mm plate after oil quenching.

Calculation number:

FP_7 - No stress relaxation.
FP_8 - Stress relaxation method 1.
FP_9 - Stress relaxation method 2.
FP_{10} - Stress relaxation method 1 and transformation plasticity.
FP_{11} - Stress relaxation method 2 and transformation plasticity.
FP_{12} - Transformation plasticity, no stress relaxation.

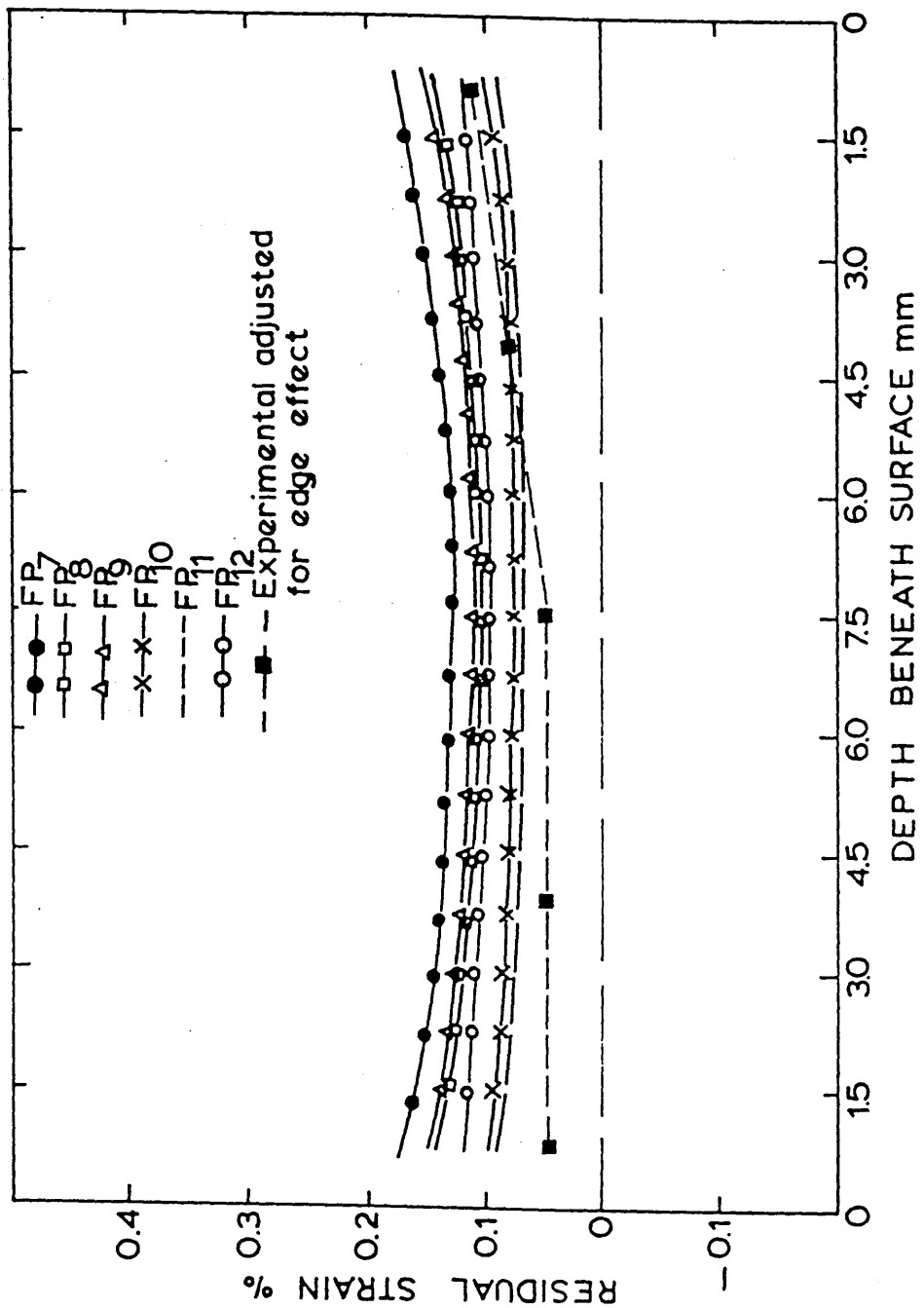
RESIDUAL STRAIN %
0.4
0.3
0.2
0.1
0
−0.1
DEPTH BENEATH SURFACE mm
0
1.5
3.0
4.5
6.0
7.5
6.0
4.5
3.0
1.5
0
FR7
FR8
FR9
FR10
FR11
FR12
Experimental adjusted for edge effect

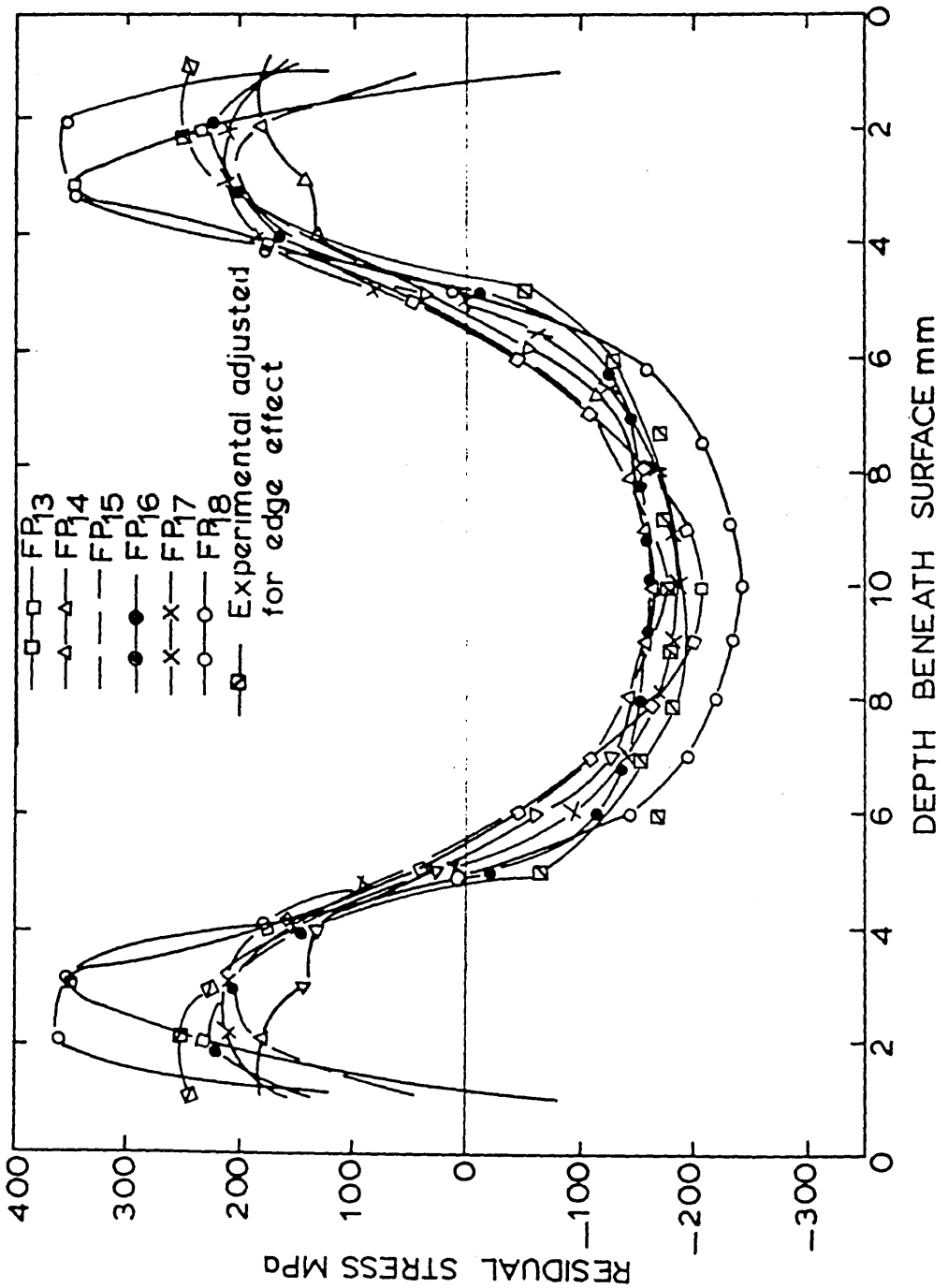
FP13
FP14
FP15
FP16
FP17
FP18
Experimental adjusted for edge effect
RESIDUAL STRESS MPa
400
300
200
100
0
−100
−200
−300
DEPTH BENEATH SURFACE mm
0
2
4
6
8
10
0
2
4
6
8

FIGURE 120: Comparison of experimental and calculated residual stress distribution in a 20 mm plate after polymer (Aquaquench 1250) quenching.

Calculation number:

FP_{13} - No stress relaxation.
FP_{14} - Stress relaxation method 1.
FP_{15} - Stress relaxation method 2.
FP_{16} - Stress relaxation method 1 and transformation plasticity.
FP_{17} - Stress relaxation method 2 and transformation plasticity.
FP_{18} - Transformation plasticity, no stress relaxation.

FIGURE 121: Comparison of experimental and calculated (viscous flow + transformation plasticity) residual stress distribution in a 20 mm plate after polymer (Aquaquench 1250) quenching.

Calculation number:

FP_{16} - Stress relaxation method 1 and transformation plasticity.

FP_{17} - Stress relaxation method 2 and transformation plasticity.

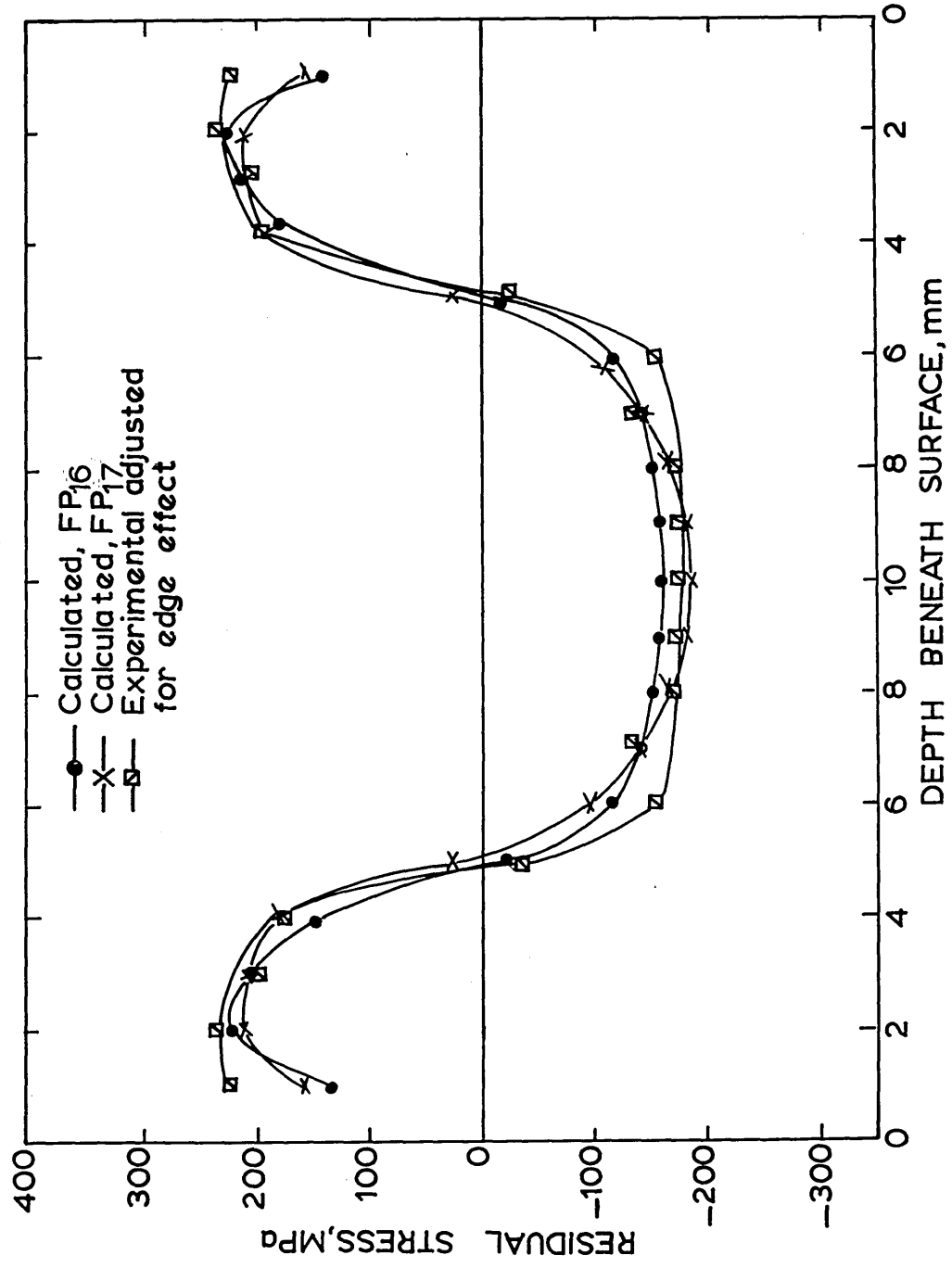
Calculated, FP16
Calculated, FP17
Experimental adjusted for edge effect
RESIDUAL STRESS, MPa
400
300
200
100
0
-100
-200
-300
0
2
4
6
8
10
DEPTH BENEATH SURFACE, mm

FIGURE 122: Comparison of experimental and calculated residual strain distribution in a 20 mm plate after polymer (Aquaquench 1250) quenching.

(For Key see figure 120).

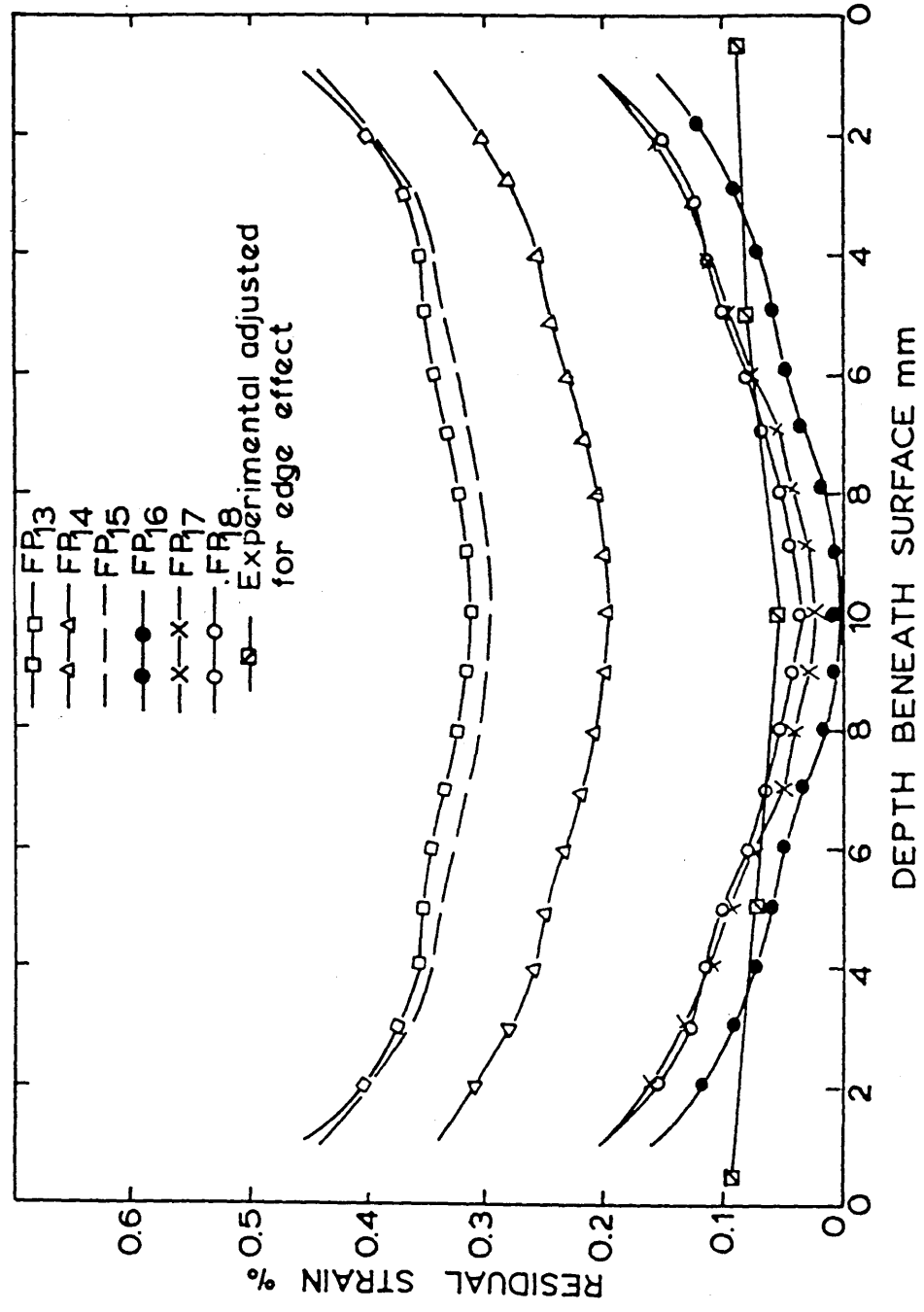
RESIDUAL STRAIN %
0.6
0.5
0.4
0.3
0.2
0.1
0
DEPTH BENEATH SURFACE mm
0
2
4
6
8
10
FP13
FP14
FP15
FP16
FP17
FP18
Experimental adjusted for edge effect

FIGURE 123: Comparison of experimental and calculated residual stress distribution in a 15 mm plate after martempering (followed by air cooling).

Calculation number:

FP_{19} - No stress relaxation.

FP_{20} - Stress relaxation method 1.

FP_{21} - Stress relaxation method 2.

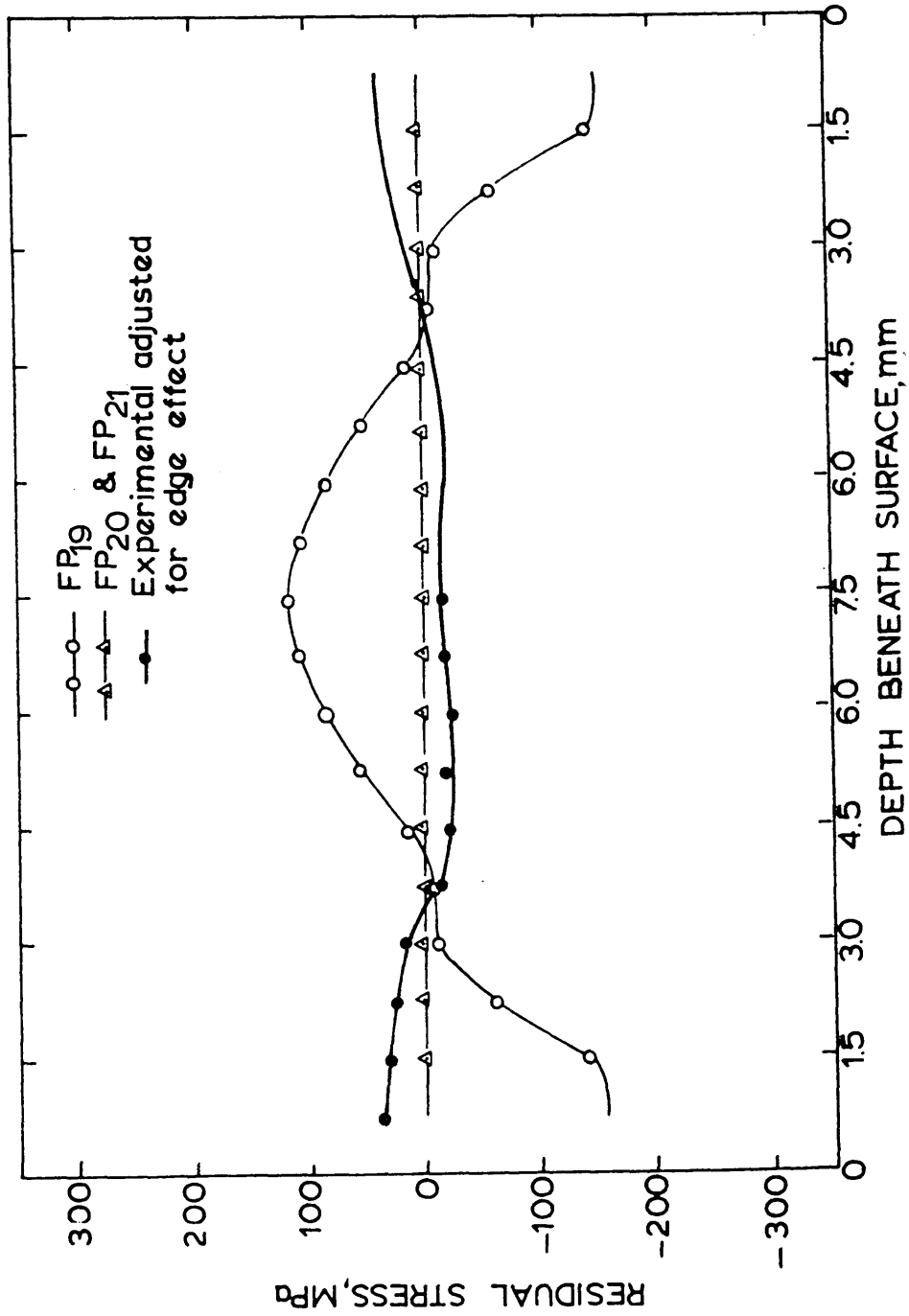
RESIDUAL STRESS, MPa
300
200
100
0
-100
-200
-300
DEPTH BENEATH SURFACE, mm
0
1.5
3.0
4.5
6.0
7.5
6.0
4.5
3.0
1.5
0
FP19
FP20 & FP21
Experimental adjusted for edge effect

FIGURE 124: Comparison of experimental and calculated residual strain distribution in a 15 mm plate after martempering (followed by air cooling).

(For Key see figure 123).

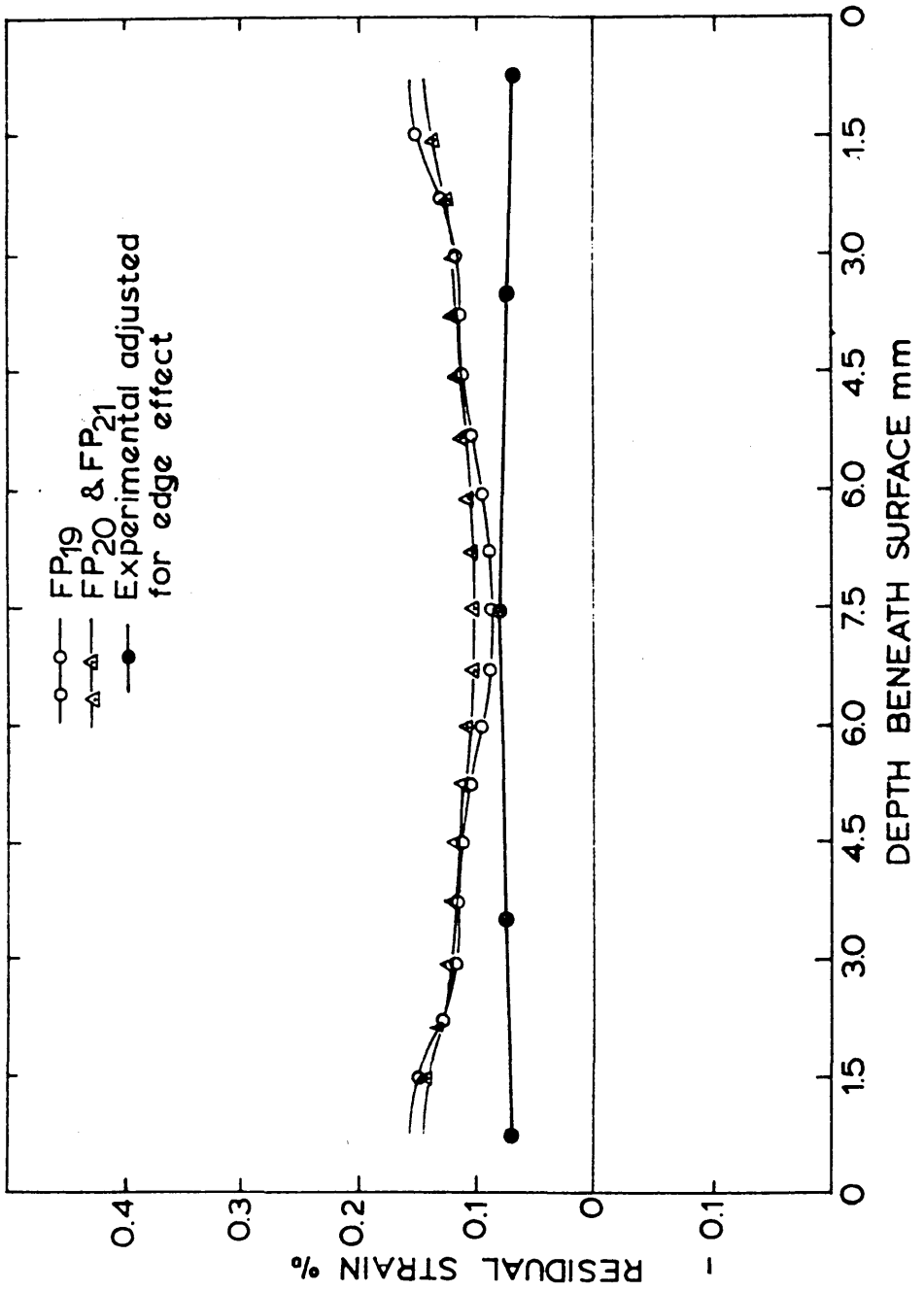
FP19
FP20 & FP21
Experimental adjusted for edge effect
RESIDUAL STRAIN %
0.4
0.3
0.2
0.1
0
- 0.1
0
1.5
3.0
4.5
6.0
7.5
6.0
4.5
3.0
1.5
0
DEPTH BENEATH SURFACE mm

FIGURE 125: Comparison of experimental and calculated residual stress distribution in a 15 mm plate after martempering (followed by oil cooling).

Calculation number:-

FP_{22} - No stress relaxation.
FP_{23} - Stress relaxation method 1.
FP_{24} - Stress relaxation method 2.
FP_{25} - Stress relaxation method 1 and transformation plasticity.
FP_{26} - Stress relaxation method 2 and transformation plasticity.

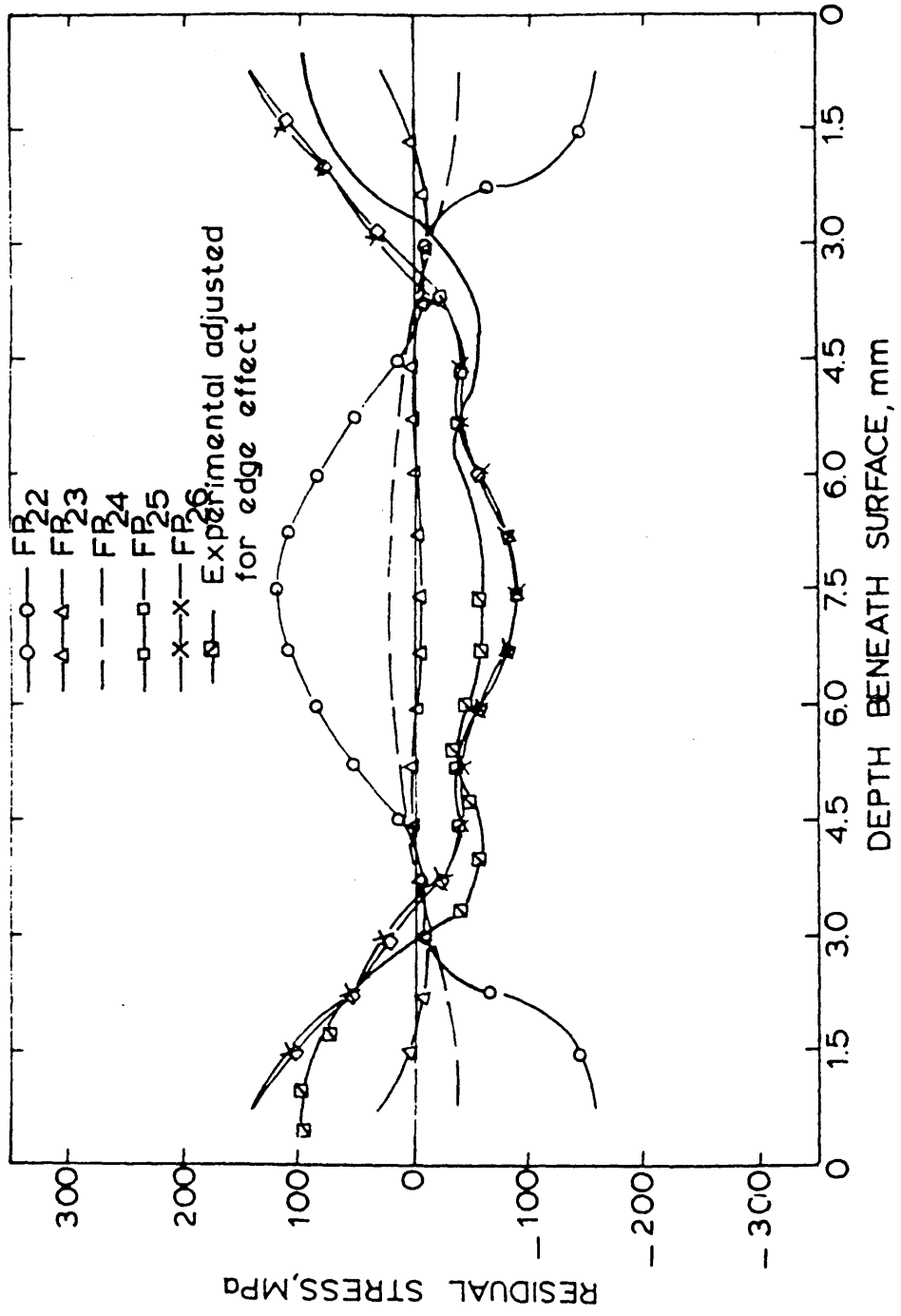
FB22
FB23
FB24
FB25
FB26
Experimental adjusted for edge effect
RESIDUAL STRESS, MPa
300
200
100
0
-100
-200
-300
DEPTH BENEATH SURFACE, mm
0
1.5
3.0
4.5
6.0
7.5
6.0
4.5
3.0
1.5
0

FIGURE 126: Comparison of experimental and calculated residual strain distribution in a 15 mm plate after martempering (followed by oil cooling).

(For Key see figure 125).

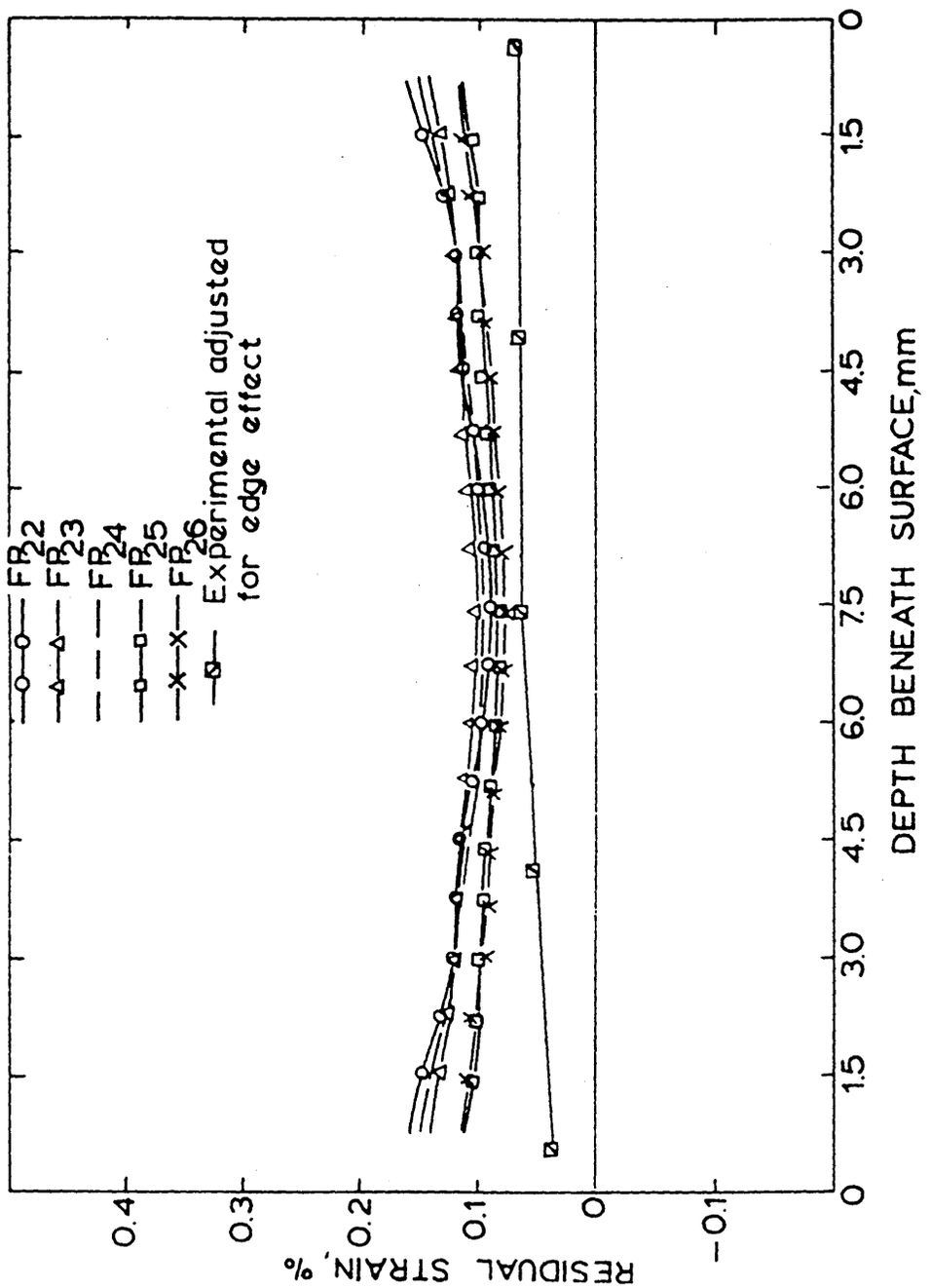
FB22
FB23
FB24
FB25
FB26
Experimental adjusted for edge effect
RESIDUAL STRAIN, %
0.4
0.3
0.2
0.1
0
−0.1
DEPTH BENEATH SURFACE, mm
0
1.5
3.0
4.5
6.0
7.5
6.0
4.5
3.0
1.5
0

FIGURE 127: Experimental and calculated residual strain distribution in the water quenched plate specimen, showing the effect of specimen thickness.

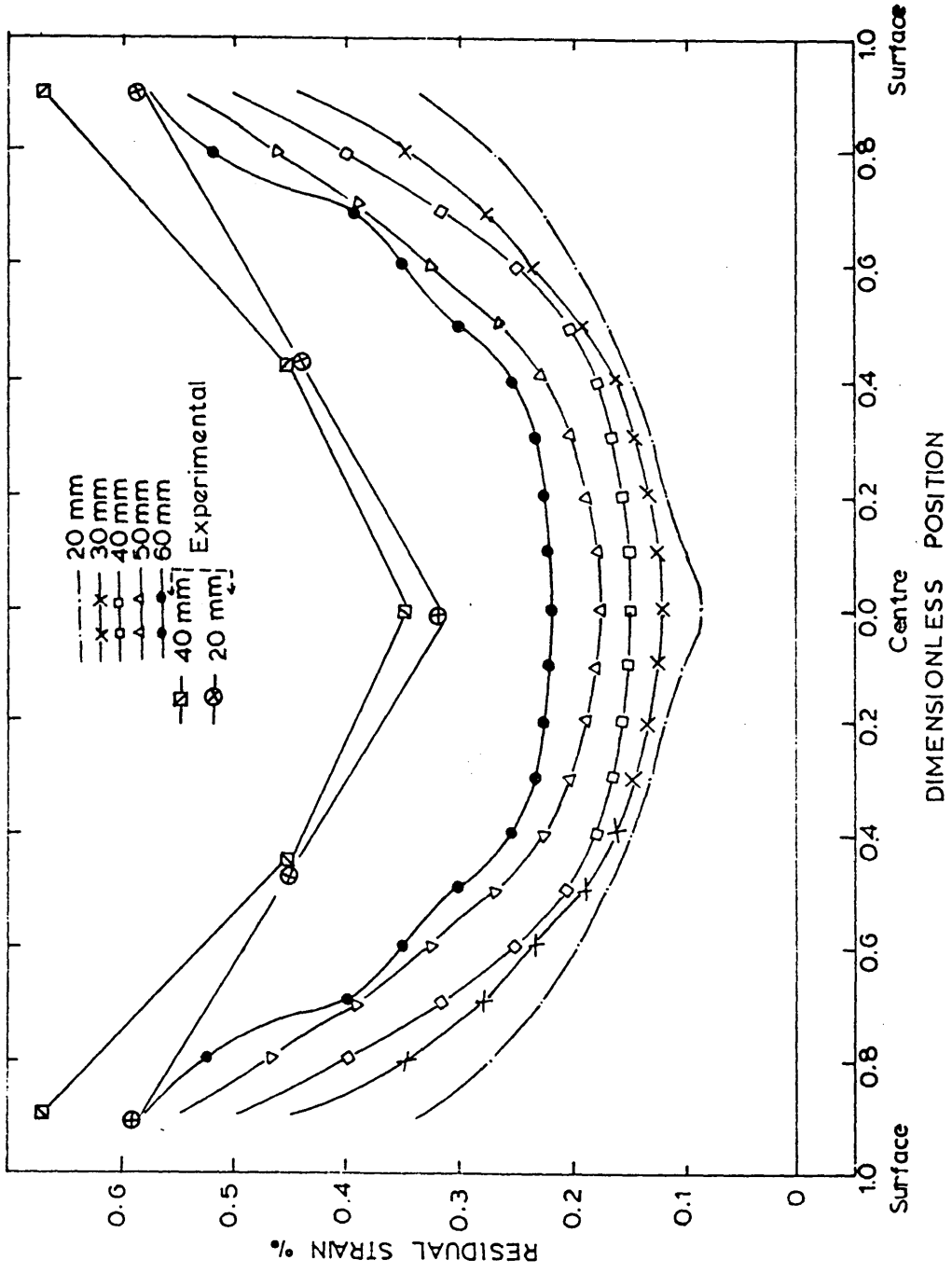
RESIDUAL STRAIN %
0.6
0.5
0.4
0.3
0.2
0.1
0
1.0
0.8
0.6
0.4
0.2
0.0
0.2
0.4
0.6
0.8
1.0
Surface
Centre
Surface
DIMENSIONLESS POSITION
20 mm
30 mm
40 mm
50 mm
60 mm
Experimental
40 mm
20 mm

FIGURE 128: Effect of the transformation temperature range on the transformation strain.

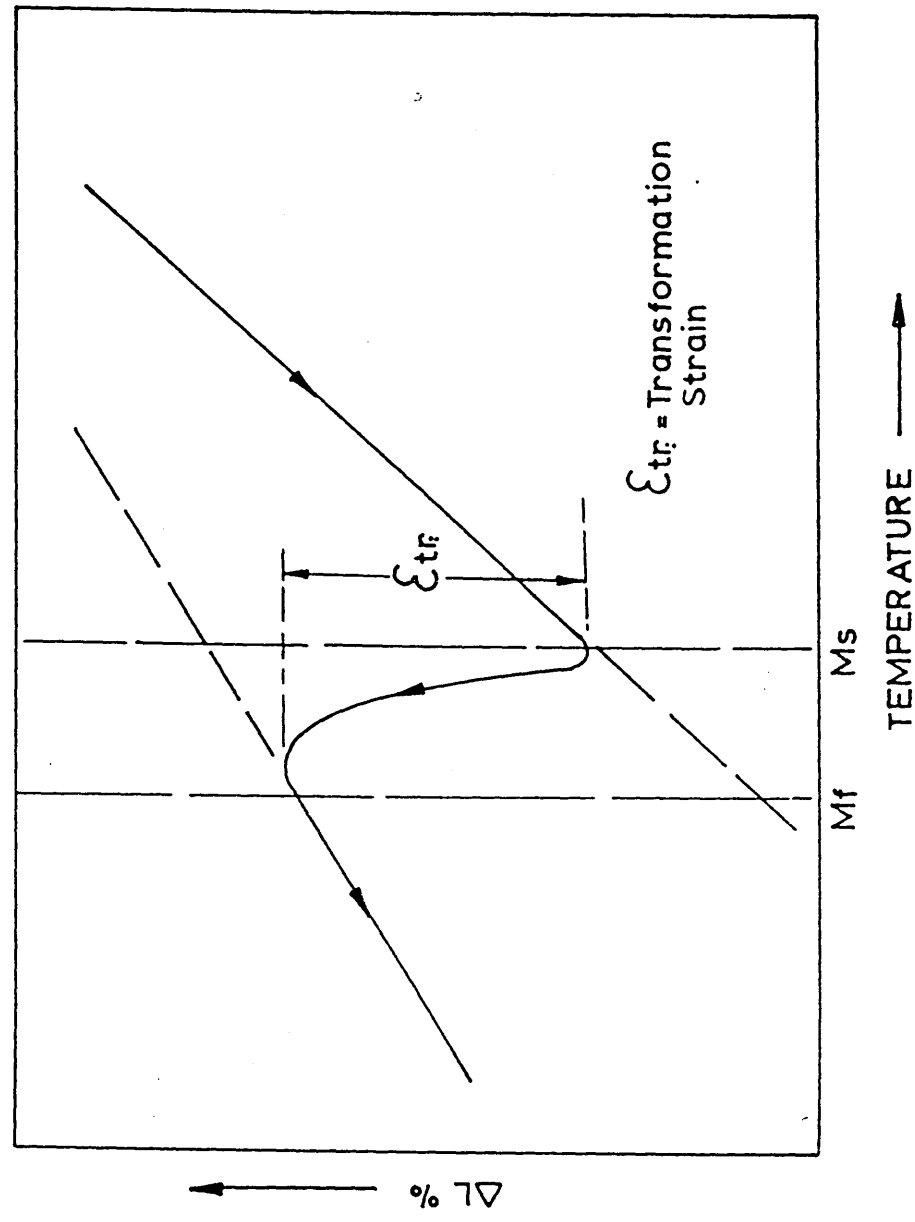
ε_{tr} = Transformation Strain
ε_{tr}
Ms
Mf
TEMPERATURE
% ΔL

FIGURE 129: Comparison of experimental and calculated residual strain distributions after water quench. The influence of Ms temperature is shown to be the reason for discrepancies between calculated and experimental residual strains after water quench.

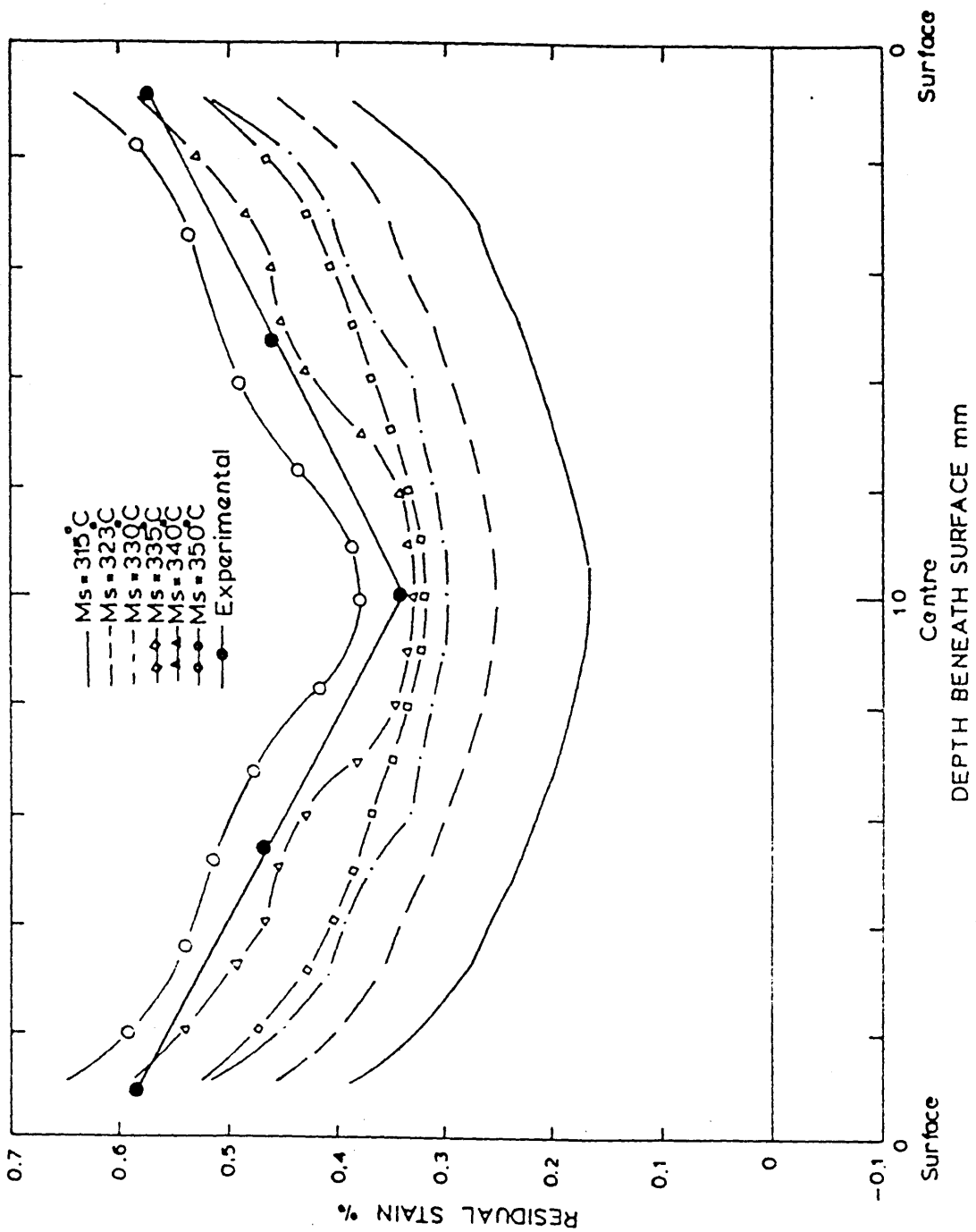
Ms = 315°C
Ms = 323°C
Ms = 330°C
Ms = 335°C
Ms = 340°C
Ms = 350°C
Experimental
RESIDUAL STAIN %
0.7
0.6
0.5
0.4
0.3
0.2
0.1
0
-0.1
Surface
Surface
0
10
Centre
DEPTH BENEATH SURFACE mm

PLATE 1: High temperature stress relaxation equipment.

PLATE 2: Showing oxidation protective capacity of the Barketekt.

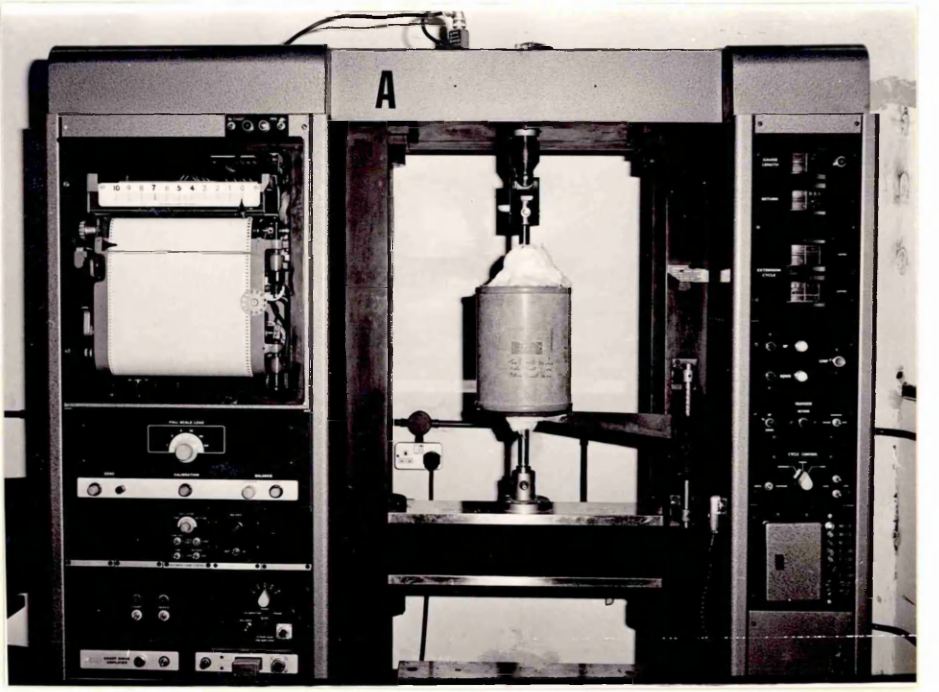
A

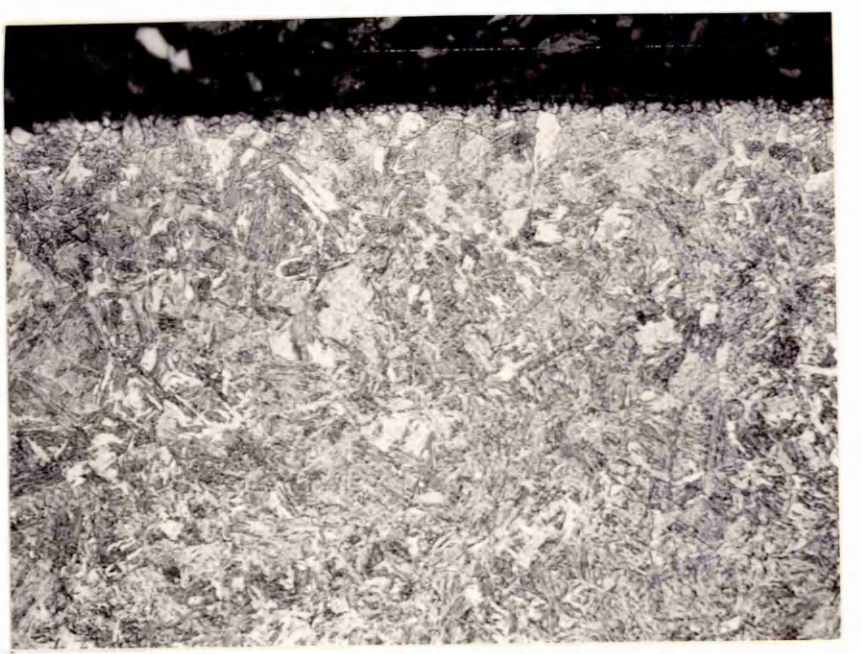

PLATE 3: Equipment used for the determination of distortion between the edges of the plate.

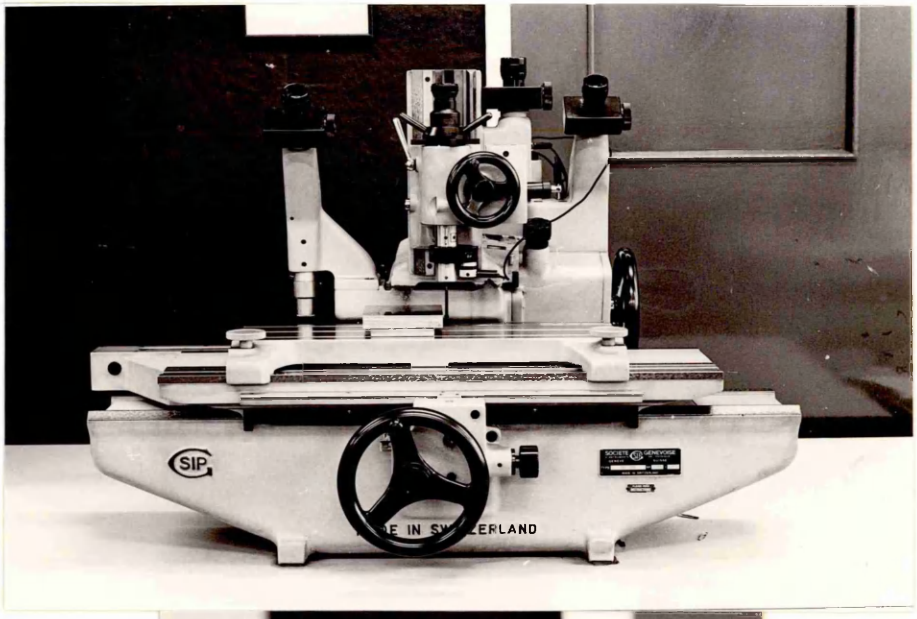
SIP

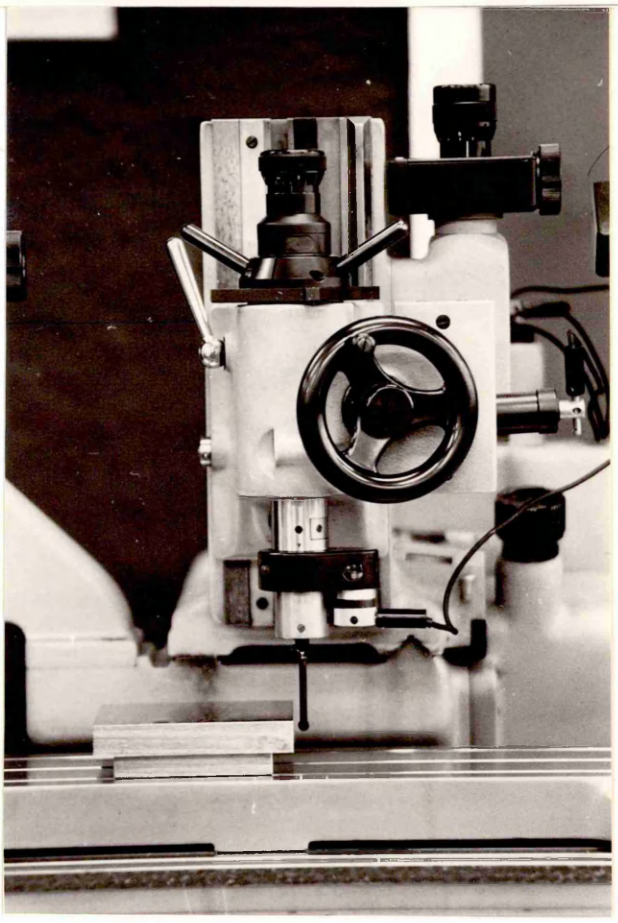

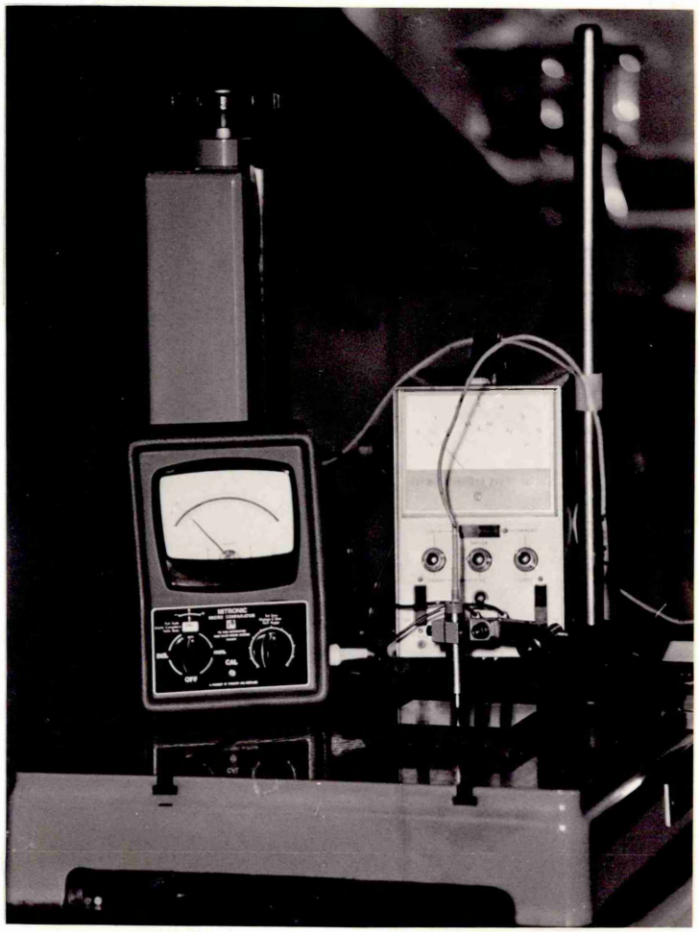

APPENDIX I

Stress relaxation and creep equations for Standard Linear Solid mechanical model under uniaxial conditions for stress

From section 3.2.2,

$$\dot{\varepsilon}xx + \phi\varepsilon xx = \frac{\dot{\sigma}xx}{2G(1+\nu)} + \frac{\sigma xx}{2\eta(1+\nu)} \qquad \ldots\ldots 3.2.11$$

STRESS RELAXATION

Stress relaxation test is conducted at constant strain.

$$\therefore \quad \dot{\varepsilon}xx = 0$$

$$\text{And} \quad \varepsilon xx = \varepsilon^{o}xx$$

By substituting these values in equation 3.2.11, we get,

$$\phi\varepsilon^{o}xx = \frac{\dot{\sigma}xx}{2G(1+\nu)} + \frac{\sigma xx}{2\eta(1+\nu)}$$

or,

$$\phi\varepsilon^{o}xx = \frac{d\sigma xx/dt}{2G(1+\nu)} + \frac{\sigma xx}{2\eta(1+\nu)}$$

$$2G\,\phi(1+\nu)\varepsilon^{o}xx = \frac{d\sigma xx}{dt} + \frac{\sigma xx}{\eta/G}$$

$$2G\,\phi(1+\nu)\varepsilon^{o}xx - \frac{G}{\eta}\sigma xx = \frac{d\sigma xx}{dt}$$

$$dt = \frac{d\sigma xx}{[2G\,\phi(1+\nu)\varepsilon^{o}xx - \frac{G}{\eta}\sigma xx]} \qquad \ldots\ldots \text{I}$$

By integrating equation (I), we get,

$$t + \text{CONSTANT} = Ln\,[2G\phi(1+\nu)\varepsilon^{o}xx - \frac{G}{\eta}\sigma xx\,]\;x\;-\;(\frac{G}{\eta})^{-1} \qquad \ldots\ldots \text{II}$$

At start, $t = 0$, $\sigma xx = \sigma^{o}xx$

Therefore equation II becomes,

$$\text{CONSTANT} = -\frac{\eta}{G} Ln[2G\phi(1+\nu)\varepsilon^{o}xx - \frac{G}{\eta}\sigma^{o}xx]$$

By putting this value in equation II, we get,

$$t - \frac{\eta}{G} Ln[2G\phi(1+\nu)\varepsilon^{o}xx - \frac{G}{\eta}\sigma^{o}xx] = -\frac{\eta}{G} Ln[2\phi G(1+\nu)\ \varepsilon^{o}xx - \frac{G}{\eta}\sigma xx]$$

or

$$\frac{\eta}{G} Ln\ [2G\phi(1+\nu)\varepsilon^{o}xx - \frac{G}{\eta}\sigma xx] - \frac{\eta}{G} Ln[2G\phi(1+\nu)\varepsilon^{o}xx - \frac{G}{\eta}\sigma^{o}xx] = -t$$

$$\therefore \qquad -\frac{tG}{\eta} = Ln\ \frac{2G\phi(1+\nu)\varepsilon^{o}xx - \frac{G}{\eta}\sigma xx}{2G\phi(1+\nu)\varepsilon^{o}xx - \frac{G}{\eta}\sigma^{o}xx} \qquad \ldots\ldots \text{III}$$

By taking anti-log: of equation III, we get,

$$Exp(-\frac{Gt}{\eta}) = \frac{2G\phi(1+\nu)\varepsilon^{o}xx - G/\eta\sigma xx}{2G\phi(1+\nu)\varepsilon^{o}xx - G/\eta\sigma^{o}xx} \qquad \ldots\ldots \text{IV}$$

Modulus of elasticity $E = \frac{\sigma}{\varepsilon}$ $\qquad \therefore \quad \varepsilon^{o}xx = \frac{\sigma^{o}xx}{E}$

By putting this value in equation IV,

$$Exp\ (-\frac{Gt}{\eta}) = \frac{2\phi(1+\nu)\ \frac{\sigma^{o}xx}{E} - \frac{\sigma xx}{\eta}}{2\phi(1+\nu)\ \frac{\sigma^{o}xx}{E} - \frac{\sigma^{o}xx}{\eta}} \qquad \ldots\ldots \text{V}$$

Equation V can further be rearranged as:

$$\frac{2\phi\eta(1+\nu)}{E} - \frac{\sigma xx}{\sigma^{o}xx} = [\frac{2\phi\eta(1+\nu)}{E} - 1]\ \ Exp(-\frac{Gt}{\eta}) \qquad \ldots\ldots \text{VI}$$

If $\frac{2\phi\eta(1+\nu)}{E} = A$, and $\frac{G}{\eta} = B$

Equation VI can be written as:

$$A - \frac{\sigma xx}{\sigma^{o}xx} = (A-1)\ \text{Exp}\ (-Bt)$$

$$- \frac{\sigma xx}{\sigma^{o}xx} = (A-1)\ \text{Exp}\ (-Bt) - A$$

or

$$\frac{\sigma xx}{\sigma^{o}xx} = (1-A)\ \text{Exp}\ (-Bt) + A$$

If $\sigma^{o}xx$ = Initial stress = σ^{o}

And σxx = Stress at time t = σt

$$\therefore \quad \frac{\sigma t}{\sigma o} = (1-A)\ \text{Exp}\ (-Bt) + A \qquad \ldots\ldots \text{VII}$$

CREEP

Creep is observed at constant stress therefore,

$$\dot{\sigma}xx = 0 \text{ and } \sigma xx = \sigma^{o}xx$$

By putting these values in equation 3.2.11, this equation will be reduced to:

$$\dot{\varepsilon}xx + \phi\varepsilon xx = \frac{\sigma^{o}xx}{2\eta(1+\nu)} \qquad \ldots\ldots \text{VIII}$$

Equation VIII can be rearranged as:

$$\frac{d\varepsilon xx}{dt} = \frac{\sigma^{o}xx}{2\eta(1+\nu)} - \phi\ \varepsilon xx$$

or,

$$dt = \frac{d\varepsilon xx}{[\sigma^{o}xx/2\eta(1+\nu)]-\phi\varepsilon xx}$$

By integrating this equation, we get,

$$t + \text{CONSTANT} = -\frac{1}{\phi} Ln \left[\frac{\sigma^{o}xx}{2\eta(1+\nu)} - \phi\ \varepsilon xx\right] \qquad \ldots\ldots \text{IX}$$

At start, $t = 0$, $\varepsilon xx = \varepsilon^{o}xx = \frac{\sigma^{o}xx}{E}$

Hence, equation IX will give,

$$\text{CONSTANT} = -\frac{1}{\phi} Ln \left[\frac{\sigma^{o}xx}{2\eta(1+\nu)} - \phi\ \frac{\sigma^{o}xx}{E}\right]$$

By putting this value in equation IX, we get,

$$t - \frac{1}{\phi} Ln \left[\frac{\sigma^{o}xx}{2\eta(1+\nu)} - \phi\ \frac{\sigma^{o}xx}{E}\right] = -\frac{1}{\phi} Ln \left[\frac{\sigma^{o}xx}{2\eta(1+\nu)} - \phi\varepsilon xx\right]$$

or,

$$-t\phi = Ln \frac{\left[\frac{\sigma^{o}xx}{2\eta(1+\nu)} - \phi\ \varepsilon xx\right]}{\left[\frac{\sigma^{o}xx}{2\eta(1+\nu)} - \phi\ \frac{\sigma^{o}xx}{E}\right]}$$

By taking anti-log: of this equation we get,

$$Exp(-t\phi) = \frac{\frac{\sigma^{o}xx}{2\eta(1+\nu)} - \phi\ \varepsilon xx}{\frac{\sigma^{o}xx}{2\eta(1+\nu)} - \phi\ \frac{\sigma^{o}xx}{E}}$$

or,

$$Exp(-t\phi) = \frac{\sigma^{o}xx/2\eta\phi(1+\nu) - \varepsilon xx}{\sigma^{o}xx/2\eta\phi(1+\nu) - \sigma^{o}xx/E} \qquad \ldots\ldots \text{X}$$

As, $A = \frac{2\phi\eta(1+\nu)}{E}$

$$2\phi\eta(1+\nu) = AE$$

By putting this value in equation X, we get,

$$\text{Exp}(-t\phi) = \frac{\sigma^{o}xx/AE - \varepsilon xx}{\sigma^{o}xx/AE - \sigma^{o}xx/E} \qquad \ldots\ldots \text{XI}$$

Equation XI can be further solved and rearranged as:

$$\varepsilon xx = \frac{\sigma^{o}xx}{E}\left\{\frac{1}{A} - \frac{\text{Exp}(-t\phi)}{A} + \text{Exp}(-t\phi)\right\} \qquad \ldots\ldots \text{XII}$$

Equation XII gives total strain, if elastic strain introduced at time, t = O is deducted from this equation, the net result will be creep strain.

Thus,

$$\varepsilon xx(\text{creep}) = \frac{\sigma^{o}xx}{E}\left\{\frac{1}{A} - \frac{\text{Exp}(-t\phi)}{A} + \text{Exp}(-t\phi)\right\} - \frac{\sigma^{o}xx}{E}$$

This equation can be further solved as:

$$\varepsilon xx(\text{creep}) = \frac{\sigma^{o}xx}{E}\left(\frac{1}{A} - 1\right)[1 - \text{Exp}(-t\phi)]$$

or,

$$\varepsilon(\text{creep}) = \frac{\sigma^{o}}{E}\left(\frac{1}{A} - 1\right)[1 - \text{Exp}(-t\phi)] \qquad \ldots\ldots \text{XIII}$$

Equation VIII and XIII are obtained under uniaxial stress conditions. These equations can be redetermined for plane-stress conditions as:

$$\dot{e}IJ + \phi eIJ + \frac{\dot{S}IJ}{2G} + \frac{SIJ}{2\eta} \qquad \ldots\ldots 3.2.1$$

Deviatric stress and strain tensors are given as:

$$SIJ = \sigma IJ - \delta IJ\sigma m$$

$$\dot{S}IJ = \sigma IJ - \delta IJ\dot{\sigma}m$$

$$eIJ = \varepsilon IJ - \delta IJ\varepsilon m$$

$$\dot{e}IJ = \dot{\varepsilon}IJ - \delta IJ\dot{\varepsilon}m$$

Thus by substituting these values in equation 3.2.1

$$(\dot{\varepsilon}IJ - \delta IJ\dot{\varepsilon}m) + \phi(\varepsilon IJ - \delta IJ\varepsilon m) = \frac{1}{2G}(\dot{\sigma}IJ - \delta IJ\dot{\sigma}m) + \frac{1}{2\eta}(\sigma IJ - \delta IJ\sigma m)$$

..... XIV

For plane-stress condition,

$$\varepsilon IJ = \varepsilon xx = \varepsilon yy , \quad \varepsilon zz = -\nu(\varepsilon xx + \varepsilon yy)$$

$$\sigma IJ = \sigma xx = \sigma yy , \quad \sigma zz = O$$

$$\varepsilon m = \frac{2}{3}(1-\nu)\varepsilon xx$$

$$\sigma m = \frac{2}{3}\sigma xx$$

Substituting these values in equation XIV and rearranging.

$$(1 + 2\nu)\ \dot{\varepsilon}xx + \phi\ (1 + 2\nu)\ \varepsilon xx = \frac{\dot{\sigma}xx}{2G} + \frac{\sigma xx}{2\eta} \qquad \text{..... XV}$$

Further rearranging of equation XV will give:

$$\dot{\varepsilon}xx + \phi\ \varepsilon xx = \frac{\dot{\sigma}xx}{2G(1+2\nu)} + \frac{\sigma xx}{2\eta(1+2\nu)} \qquad \text{..... XVI}$$

This equation can be simplified by the same method as has been described for equation 3.2.11 in the case of uniaxial tension. Therefore, in the case of stress relaxation resulting equation will be:

$$\frac{\sigma xx}{\sigma^{O}xx} = \left[1 - \frac{2\phi\eta(1+2\nu)(1-\nu)}{E}\right] \text{Exp}\ \left(-\frac{Gt}{\eta}\right) + \frac{2\phi\eta(1+2\nu)(1-\nu)}{E} \qquad \text{..... XVII}$$

And for creep strain.

$$(\varepsilon xx)\text{creep} = \frac{\sigma xx(1-\nu)}{E}\left[\frac{E}{2\phi\eta(1+2\eta)(1-\nu)} - 1\right][1-\text{Exp}(-\phi t)] \quad \ldots\ldots \text{XVIII}$$

let $$C = \frac{2\phi\eta(1+2\nu)(1-\nu)}{E}$$

By equations VII and XIII, $$\frac{2\phi\eta(1+\nu)}{E} = A, \quad B = \frac{G}{\eta}$$

Hence, $$C = \frac{(1+2\nu)(1-\nu)}{(1+\nu)} \times A$$

By selecting a value of ν as 0.33

$$C = 0.8363 \times A$$

By putting value of C in equations XVII and XVIII and rearranging.

$$\frac{\sigma t}{\sigma^{o}} = 0.8363 \times A + [1-(0.8363 \times A)]\ \text{Exp}\ (-Bt) \quad \ldots\ldots \text{XIX}$$

And

$$\text{creep} = \frac{\sigma^{o}(1-0.8363A)(1-\text{Exp}(-0.8363ABt))}{0.8363(a-b\theta)\ A} \quad \ldots\ldots \text{XX}$$

$$(\because \phi = A \times B \quad \text{and} \quad \frac{E}{1-\nu} = a - b\theta)$$

Hence, for a particular temperature during a time interval Δt equation XIX and XX can be rearranged as:

$$\frac{(\sigma t)_i^{n+1}}{(\sigma^{o})_i^{n+1}} = 0.8363A_i^{n+1} + [1-(0.8363A_i^{n+1})]\ \text{Exp}\ (-B_i^{n+1}\ \Delta t) \quad \ldots\ldots \text{XXI}$$

$$(\varepsilon\text{creep})_i^{n+1} = \frac{(\sigma^{o})_i^{n+1}(1-0.8363A_i^{n+1})[1-\text{Exp}(-0.8363A_i^{n+1}B_i^{n+1}\Delta t)]}{0.8363\ (a-b\ \theta_i^{n+1})\ A_i^{n+1}}$$

$$\ldots\ldots \text{XXII}$$

APPENDIX II

Calculation of residual stresses from the results of changes in strain at the underside of a plate

The residual stresses across the thickness of the plate shown in figure II.1 may be determined by the consideration of the equilibrium of forces and moments and from the geometry of the system:

Thus from equilibrium of forces

$$\sigma_1 \Delta Z_1 + \frac{1}{2} \sigma_b Z_b - \frac{1}{2} \sigma_a Z_a = 0 \qquad \text{..... i}$$

and from equilibrium of moment

$$\sigma_1 \Delta Z_1 (Z_a + \frac{\Delta Z_1}{2}) = \frac{1}{2} \sigma_a Z_a (\frac{2}{3} Z_a) + \frac{1}{2} \sigma_b Z_b (\frac{2}{3} Z_b)$$

$$= \frac{1}{3} (\sigma_a Z_a^{\,2} + \sigma_b Z_b^{\,2}) \qquad \text{..... ii}$$

and from the geometry of the system

$$\frac{\sigma_a}{Z_a} = \frac{\sigma_b}{Z_b} \qquad \text{..... iii}$$

From i and ii by eliminating $\sigma_1 \Delta Z_1$ first and then substituting in iii

$$\frac{3}{2} (Z_a + \frac{\Delta Z_1}{2}) = \frac{\sigma_a Z_a^{\,2} + \sigma_b Z_b^{\,2}}{\sigma_a Z_a - \sigma_b Z_b} \qquad \text{..... iv}$$

or

$$\frac{3}{2} (Z_a + \frac{\Delta Z_1}{2}) = \frac{Z_a^{\,3} + Z_b^{\,3}}{Z_a^{\,2} - Z_b^{\,2}} \qquad \text{..... v}$$

but $t = Z_a + Z_b + \Delta Z_1$ vi

where t is the original thickness of the plate.

substituting and rearranging

$$Z_a = \frac{(t - \Delta Z_1)(4t - \Delta Z_1)}{6t} \quad \ldots\ldots \text{vii}$$

and $Z_b = t - Z_a - \Delta Z_1$ $\ldots\ldots$ viii

By substituting from equations vii and viii back using equations i and iii, the original stress in the first layer is given by

$$\sigma_1 = \frac{\sigma_b (t - \Delta Z_1)^2}{(2t + \Delta Z_1)\ \Delta Z_1} \quad \ldots\ldots \text{ix}$$

The stress σ_b is determined from the change in strain measured experimentally from the underside of the plate:

$$\sigma_b = \frac{E}{(1-\nu^2)} (\Delta\ \varepsilon_x + \nu\ \Delta\ \varepsilon_y) \quad \ldots\ldots \text{x}$$

when $\sigma_x = \sigma_y$

$\varepsilon_x = \varepsilon_y = \varepsilon_b$

Equation x reduces to

$$\sigma_b = \frac{E}{(1-\nu)} \Delta\ \varepsilon_b \quad \ldots\ldots \text{xi}$$

where $\Delta\ \varepsilon_b$ is the change in strain measured at the underside of the plate after the removal of the first layer. When the first layer has been removed, the stresses present in the underlying layers are modified. In order to achieve the original stress in each of the underlying layers; the measured stress as given by equation ix is adjusted to take into account the effect of the preceeding layers. In general the removal of the m^{th} layer affects the stress measured on removing the n^{th} layer by an amount:

$$\Delta_n^m = \left(\frac{\sigma_b}{Z_b}\right)_m \{ (Z_a)_m - (n-m)\ \Delta Z + \frac{\Delta Z}{2} \} \qquad \text{..... xii}$$

Thus the total residual stresses originally present in the layers can be obtained by

$$\left.\begin{aligned}
\sigma(1) &= \sigma_1 \\
\sigma(2) &= \sigma_2 - \Delta_2^1 \\
\sigma(3) &= \sigma_3 - \Delta_3^1 - \Delta_3^2 \\
\sigma(4) &= \sigma_4 - \Delta_4^1 - \Delta_4^2 - \Delta_4^3 \\
\sigma(5) &= \sigma_5 - \Delta_5^1 - \Delta_5^2 - \Delta_5^3 - \Delta_5^4 \\
\sigma(6) &= \sigma_6 \ \ldots\ldots
\end{aligned}\right\} \qquad \text{..... xiii}$$

FIGURE II.1: Stress distribution induced after an imaginary layer has been replaced on the top of the plate such that the plate is sprung back into its original shape.
(After Andrews)[7].

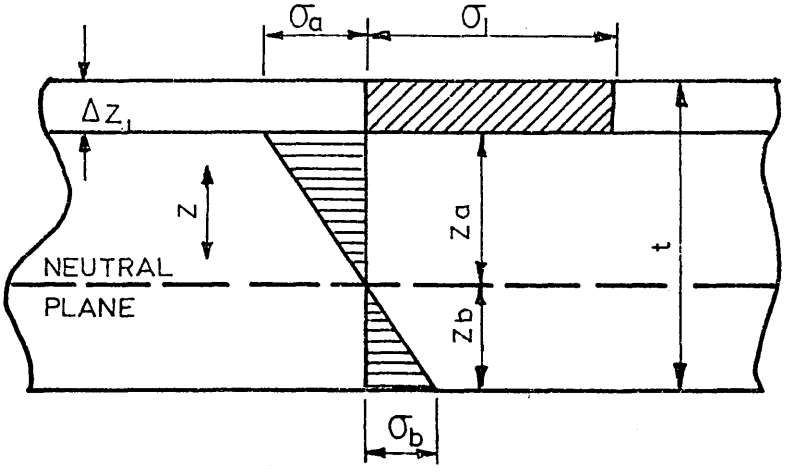
σa
σj
Δzj
z
za
t
NEUTRAL
PLANE
zb
σb

APPENDIX III

SHORT CASE STUDY

"A REPORT ON THE SELECTION OF A SUITABLE STEEL WHICH MEET THE REQUIRED LEVEL OF HARDNESS THROUGHOUT THE SECTION SIZE WITH MINIMUM STRAIN AFTER QUENCHING".

Requirement

"16 mm thick discs of a low-alloy steel are required with an as-quenched hardness of at least 450 VPN in all parts of the section. Using the data provided by the EN specifications select those alloys that meet this requirement. Hence determine which of these alloys possesses the minimum strain after quenching, making quite clear the assumptions used in the calculation. Is this considered to be the correct commerical choice for an application where residual strain is of great importance?".

1. Selection of Steels

The primary requirement is the identification of suitable steels which, under the given quench conditions, will achieve the optimum hardness (i.e. 450 VPN) throughout the 16 mm thick disc. The quenching conditions, viz: water, oil and air, are considered to identify the possible alloys, which would produce the required hardness after quenching in one of these quenchants. The information obtained from British Standards [1] for the estimation of equivalent diameter after heat treatment, and the published hardenability data [2] allowed the selection of some EN steels in the ENth series, from which the discs could be made. The selected steels for investigation are shown in table III.1, while table III.2 shows the composition and the quenching medium for these steels. The selection of a particular quenching medium for a particular

steel is based on the information from BS 5046 : 1974. Thus a 16 mm thick plate would possess a cooling rate at its centre equivalent to that attainable at the centre of a 28 mm diameter cylinder of the same material.

2. Calculation of Residual Strain

The method of calculation of the residual strain in the disc made from each selected steels as a result of quenching in the appropriate quenchant was based on the mathematical model used by Fletcher and Price[3] for EN30B steel. However, some additional assumption were made in order to apply the model to the selected steels:-

(i) The mechanical property data (i.e. Poisson's ratio, Young's modulus, stress relaxation information and the yield strength) of all the steels considered were assumed to be similar to those of EN30B (835M30) steel. The flow stress of all these steels during the course of quenching was assumed to vary with temperature in the same fashion as that of EN30B steel.

(ii) The dilatometer curves of the differnet steels were assumed to be a function of the carbon content, and the Ms and Mf temperature of the steel. The nominal carbon content, Ms and Mf temperatures and the type of quenchant used in the calculations are shown in table III.3 whereas, the dialatometric curve considered for the calculation is shown in figure III.1.

(iii) The transformation plasticity data used was the same as that for EN30B steel, but the formation of martensite (i.e. onset of the Transformation Plasticity) was dependent of the dialatometric curve and the Ms and Mf temperature of the steel involved. The transformation product in all the steels was assumed to be only martensite.

(iv) The physical property data (i.e. Density Specific heat and Thermal Conductivity) of all the steels involved was assumed to be similar to EN30B steel.

(v) The temperature dependent surface heat transfer coefficients used for the calculation in case of water and oil quenching are shown in figure III.2.

(vi) In the case of air cooled EN24 steel discs, it was assumed that thermal stresses would be negligible due to very low surface heat transfer coefficients. Therefore, the residual strain in case of air cooling was that only due to transformation of carbide and ferrite structure to martensite, as a consequence of hardening treatment.

3. Results of Residual Strain Calculation

Figure III.3 shows the calculated residual strain distribution between the surface and the centre of quenched discs at different levels beneath surface.

4. Cost Analysis

In order to achieve the optimum dimensions of the discs after quenching it is necessary to correct the change in dimensions that occurred as a result of the transformation, austenite → martensite. This would incur additional grinding costs. However, the steel with high hardenability would produce less distortions if quenched in the less drastic quench, but this would involve high material costs. Therefore, a cost analysis has been carried out in which the material cost and the post heat treatment grinding costs are considered, whereas it is assumed that machining and heat treatment costs are independent of the material from which the discs are made.

A saving in grinding costs might be possible by initially machining the discs under-size, equal to that expected distortion, so that less material would need removing after hardening. But, this would be influenced by the extent to which consistent distortion could be produced in practice.

4.1 Material Cost

Table III.4 shows the cost of various steels involved in this case study. The cost shown is of one tonne of 75 mm diameter annealed black bar of each steel. It is assumed that about 1400 discs can be made from one tonne of steel. The cost of one disc is estimated with this assumption, which is also shown in table III.4.

4.2 Grinding Cost

4.2.1 Material to be ground

The average changes in the diameters of 70 mm discs made from different steels and quenched in various quenchants are shown in table III.5. In addition to these increases in the diameters, a grinding allowance of 0.125 mm would normally be left prior to quenching. Hence, the total amount of material to be removed from the diameter would be the sum of the grinding allowance and the increase in the diameter as the result of hardening treatment, and the estimated results are shown in table III.6.

4.2.2 Time and cost for grinding operation

The following times and costs have been assumed for the grinding operation:-

- Setting up time ..... 5 mins/disc
- Roughing down to 0.05 mm over size ..... 0.05 mm/min
- Finishing of final 0.05 mm ..... 3 mins/disc
- Labour cost (one employ) £6,000/year

- Standard cost and other overheads £6/hour
- Hours available/day for work ..... 8 hours
- Days available/week for work ..... 5 days
- Weeks available/year for work ..... 48 weeks.

Number of hours available for work/year = 8 x 5 x 48 = 1920

If an efficiency of 80% is accounted for any unscheduled stoppage, then;

Effective hours/year = 0.8 x 1920

= 1536

$$\text{Labour cost/hour} = \frac{6000}{1536}$$

= £3.9

Hence,

Total grinding cost = Labour cost + overheads

= 3.9 + 6

= £9.9 per hour.

From this knowledge and the data presented in table III.6, the grinding times and hence net grinding costs for discs made from different steels have been evaluated and are presented in table III.7.

4.3 Total Cost

As already mentioned that maching cost prior to hardening and heat treatment costs are independent of the material of the discs. Therefore, the total cost of a disc considered for cost analysis purposes would be the sum of the material cost and the post heat treatment grinding cost. The total cost of each disc of different steels is presented in table III.8.

4.4 Cost Analysis for Under-Size Discs

The predicted results of distortions presented in figure III.3 indicate that the variations in the distortions from surface to centre are higher

for the materials quenched in water and are lower for oil quenched steels, whereas consistent distortions are produced in case of EN24 air cooled steel. Hence, a saving in grinding cost is possible for EN24 air cooled and all oil quenched discs, by initially maching the discs under-size to compensate the expected distortions. In table III.9 the total cost per disc for oil and air cooled undersize (prior to hardening) discs is presented.

5. Conclusion

The calculated results of distortion developed when various EN steels were quenched to achieve the required level of hardness, suggest that the level of distortion was dependent on the severity of quenchant. Thus, water quenching produced the greatest distortion and the oil quenching the least, whereas the air cooling of EN24 discs produced the strains of moderate level.

A cost analysis was carried out in which the material costs and the post heat treatment grinding costs were evaluated. The results of this analysis indicate that discs made from oil quenched EN17 would be the most economic to produce. An attempt has been made to investigate the effect of producing under-size oil and air cooled discs before hardening operation, on the total cost. In all the cases significant savings are possible.

If the cost of quenching oil, and the maintenance of quenching tank and atmosphere pollution due to oil quenching are taken into account, the production of discs from air cooled EN24 steel would be preferred, although the discs made from EN24 steel are slightly more expensive to produce than discs made from oil quenched steels. The materials that required water quenching showed poor economic performance, though the material cost of

water quenched steels was lower than oil quenched and air cooled steels. This was due to the high degree of distortion produced during quenching, and the ensuing high grinding cost.

References

1. British Standard 5046 : 1974.
2. Woolman, J. and Mottram, R.A., "The mechanical and physical properties of B.S. EN steels". Pergammon Press, London, 1966.
3. Fletcher, A.J. and Price, R.F., Metal Technology Nov: 1981 (427).
4. Lecture Notes of Module II, M.Sc. Metallurgical Process Management, S.C.P.S., 1984.

Tables

Steel Type	Maximum Equivalent Diameter		
	Water Quench	Oil Quench	Air Cool
EN16	38 mm	23 mm	-
EN17	69 mm	43 mm	4 mm
EN18	38 mm	29 mm	-
EN19	48 mm	23 mm	4 mm
EN24	>254 mm	241 mm	33 mm
EN111	44 mm	29 mm	-

TABLE III.1: Equivalent bar diameter that will produce a hardness of 450 VPN at the centre.

Steel	Composition, %						Quenching Medium
	C	Mn	Mo	Cr	Ni	Fe	
EN16	0.3/0.4	1.3/1.8	0.2/0.35	-	-	Balance	Water
EN17	0.3/0.4	1.3/1.8	0.35/0.55	-	-	"	Oil
EN18	0.35/0.45	0.6/0.9	-	0.85/1.15	-	"	Oil
EN19	0.35/0.45	0.5/0.8	0.2/0.4	0.9/1.5	-	"	Water
EN24	0.35/0.45	0.45/0.7	0.2/0.35	0.9/1.4	1.3/1.8	"	Air
EN111	0.3/0.4	0.6/0.9	-	0.45/0.75	1.0/1.5	"	Oil

TABLE III.2: Composition of steels involved.

Steel	Quenchant	%C	Ms °C	Mf °C
EN16	Water	0.35	335	120
EN17	Oil	0.35	330	154
EN18	Oil	0.40	354	100
EN19	Water	0.40	323	120
EN111	Oil	0.35	310	125

TABLE III.3: Nominal carbon content, Ms and Mf temperatures of steels involved.

Steel	Cost per tonne £	Cost per disc £
EN16	554	0.396
EN17	579	0.414
EN18	512	0.366
EN19	531	0.379
EN24	702	0.502
EN111	618	0.442

TABLE III.4: Cost of raw material (steel) used for disc manufacturing.

Steel	Average increase in Diameter after Hardening
EN16	0.217 mm
EN17	0.078 mm
EN18	0.11 mm
EN19	0.227 mm
EN24	0.114 mm
EN111	0.086 mm

TABLE III.5: Average change in diameter after quenching.

Steel	Average material to be ground off Diameter
EN16	0.342 mm
EN17	0.203 mm
EN18	0.235 mm
EN19	0.352 mm
EN24	0.239 mm
EN111	0.211 mm

TABLE III.6: Material to be ground off.

Steel	Roughing Time, mins.	Set up and finishing Time, mins.	Total grinding Time, mins.	Grinding Cost, £
EN16	5.9	8	13.9	2.294
EN17	3.1	8	11.1	1.832
EN18	3.7	8	11.7	1.931
EN19	6.1	8	14.1	2.327
EN24	3.8	8	11.8	1.947
EN111	3.3	8	11.3	1.865

TABLE III.7: Grinding cost per disc.

Steel	Material Cost £	Grinding Cost £	Total Cost £
EN16	0.396	2.294	2.69
EN17	0.414	1.832	2.246
EN18	0.366	1.931	2.297
EN19	0.379	2.327	2.706
EN24	0.502	1.947	2.449
EN111	0.442	1.865	2.307

TABLE III.8: Total cost per disc.

Steel	The extent of under sizing the diameter	Average material to be ground off diameter	Total time for grinding operation	Grinding Cost £	Material Cost £	Total Cost £
EN17	0.095%	0.137 mm	9.74 mins	1.60	0.414	2.014
EN18	0.12%	0.151 mm	10.02 mins	1.650	0.366	2.016
EN24	0.15%	0.134 mm	9.68 mins	1.597	0.502	2.099
EN111	0.095%	0.145 mm	9.9 mins	1.640	0.442	2.082

TABLE III.9: Total cost of one disc, made from different oil quenched and air cooled steels, if the discs are machined under-size prior to hardening operation.

FIGURE III.1: Dilatometric curve used in the calculation of residual strain.

FIGURE III.2: Variation of surface heat transfer coefficient used in the calculation of residual strain.

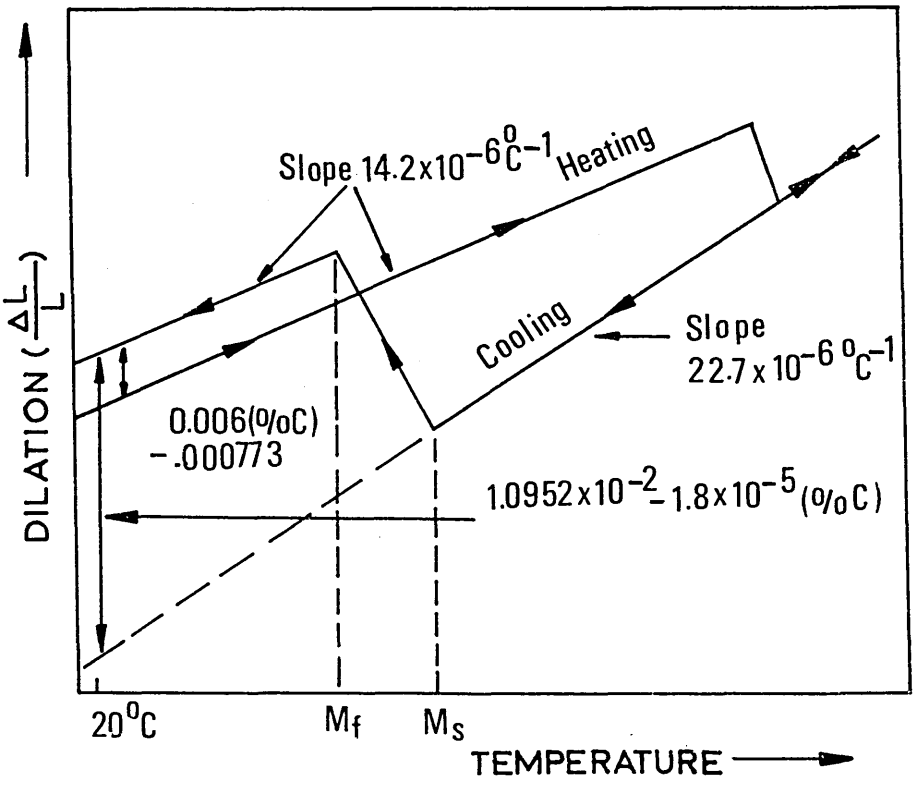
Slope 14.2x10^{-6} ^{o}C^{-1} Heating
Cooling
Slope
22.7 x 10^{-6} ^{o}C^{-1}
0.006(%oC)
-.00077
1.0952x10^{-2}-1.8x10^{-5}(%oC)
DILATION ($\frac{\Delta L}{L}$)
20^{o}C
M_f
M_s
TEMPERATURE

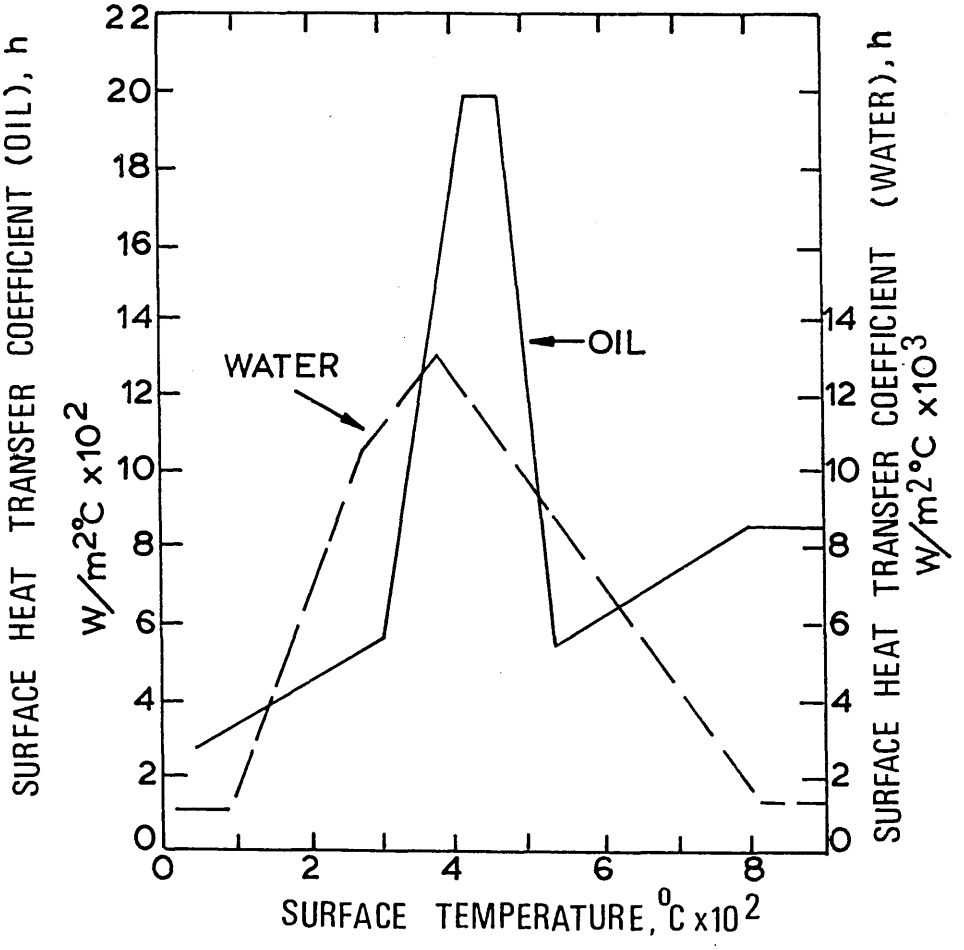
SURFACE HEAT TRANSFER COEFFICIENT (OIL), h
W/m^2°C x10^2
SURFACE HEAT TRANSFER COEFFICIENT (WATER), h
W/m^2°C x10^3
WATER
OIL
SURFACE TEMPERATURE, ^{o}C x10^2
0
2
4
6
8
10
12
14
16
18
20
22

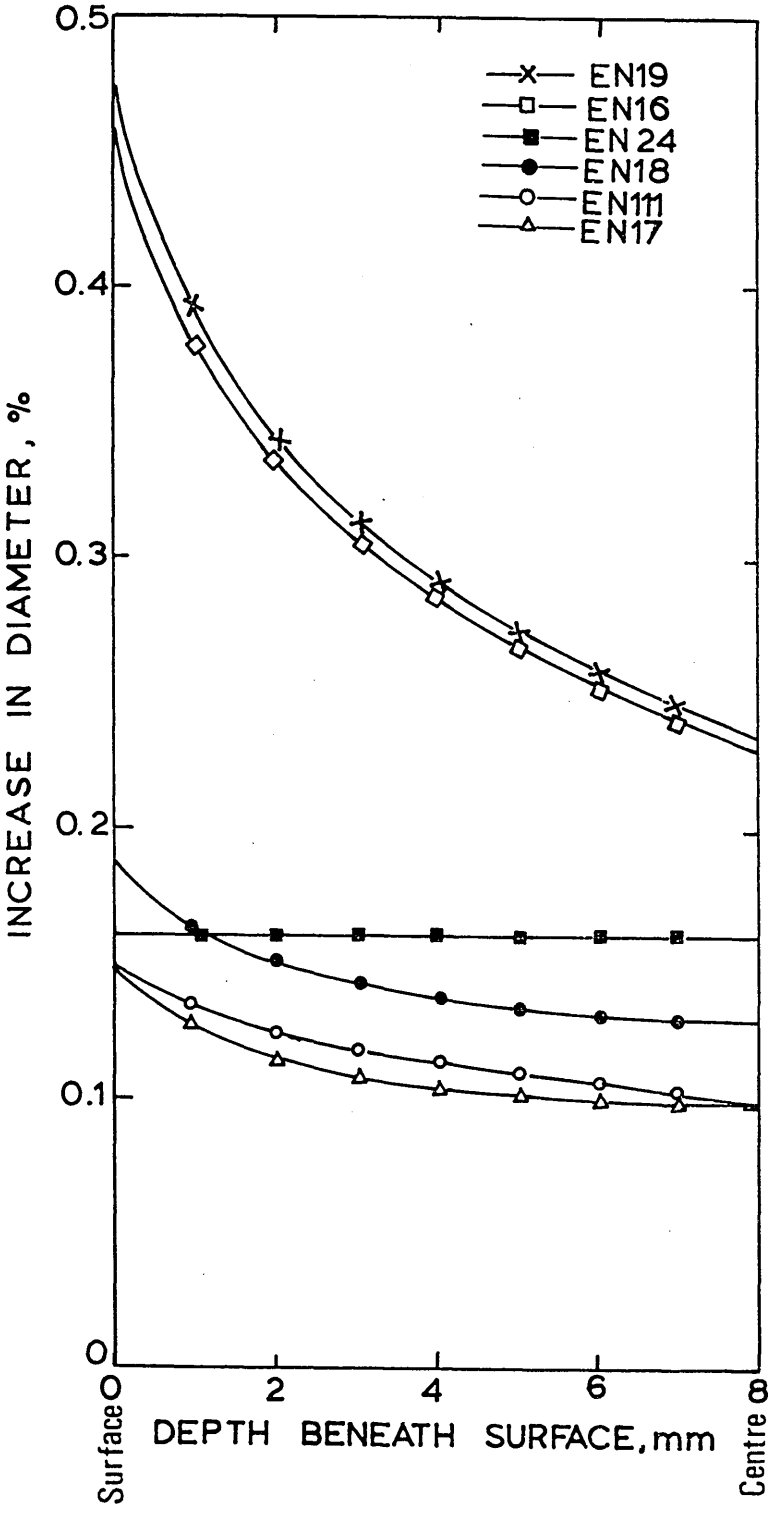
EN19
EN16
EN 24
EN18
EN111
EN17
INCREASE IN DIAMETER, %
0.5
0.4
0.3
0.2
0.1
0
0
2
4
6
8
Surface
DEPTH BENEATH SURFACE, mm
Centre